Chapter 3
Concrete Members Under Cyclic Loading

This chapter presents the mechanical behaviour:

- of the constituent materials of concrete members, namely concrete and reinforcing steel, as well as of their interaction; and
- of concrete members typical of buildings,

under cyclic loading of the type induced by strong earthquake shaking. This behaviour determines how concrete and reinforcing steel are used in concrete elements (notably, the shape and dimensions of concrete members and the shape, amount and layout of their reinforcement), for satisfactory seismic performance of the members and the structural system as a whole.

Some of the material in this chapter provides the background for detailing rules specified in Part 1 of Eurocode 8 for ductile members in new earthquake resistant buildings. These rules are derived in Chapter 5. Besides, the rules and expressions given in Part 3 of Eurocode 8 for the deformations of concrete members at yielding and at ultimate conditions are also presented here, along with their background and justification. This material is used and developed further in Chapter 4 for the modelling of concrete members in seismic response analysis and in Chapter 6 for the assessment and retrofitting of existing concrete members.

3.1 The Materials and Their Interaction

3.1.1 Reinforcing Steel

3.1.1.1 Stress-Strain Behaviour Under Cyclic Uniaxial Loading

Owing to their one-dimensional geometry, reinforcing bars are essentially subjected to uniaxial tension or compression. So, we are interested in the uniaxial σ-ε behaviour of reinforcing steel. The fundamental features of this behaviour are shown in Fig. 3.1. Yielding at the yield stress f_y is followed by the yield plateau, which is relatively short, at least in the reinforcing steels currently used in most of the world.

M.N. Fardis, *Seismic Design, Assessment and Retrofitting of Concrete Buildings*, Geotechnical, Geological, and Earthquake Engineering 8, DOI 10.1007/978-1-4020-9842-0_3,

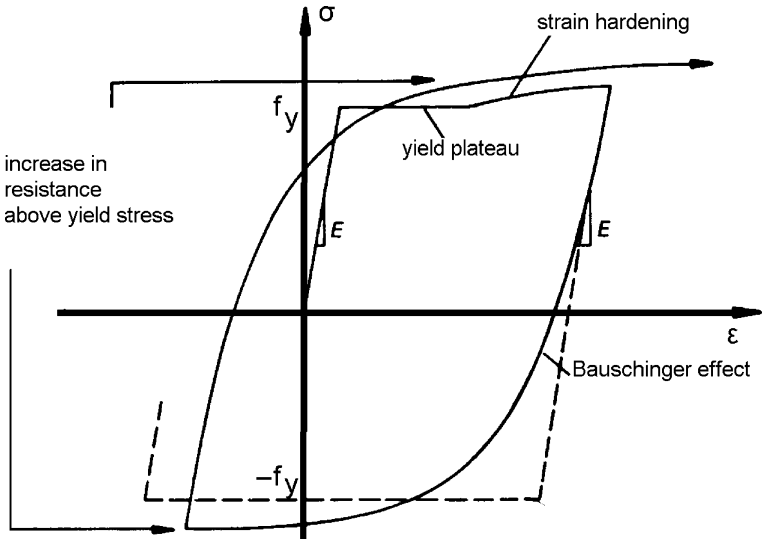

Fig. 3.1 Features of the cyclic σ-ε behaviour of reinforcing bars

Strain-hardening follows. Under monotonic loading strain-hardening leads to the maximum stress, f_t, termed tensile strength, that takes place at strain ε_{su}, which is called strain at maximum stress (or uniform elongation at failure) and is taken as the nominal ultimate strain of steel under monotonic loading.

Unloading from the yield plateau or from the strain-hardening region is initially elastic, but it gradually deviates from linearity before reaching the yield stress in monotonic compression, $-f_y$, as if the steel yielded prematurely. This is termed "Bauschinger effect". Because of it the tangent modulus of elasticity decreases from the elastic value, $E_s = 200$ GPa, to zero; but it does so gradually, not abruptly as when steel first yields in monotonic loading.

If the steel has yielded first in tension, then unloading does not lead to a yield plateau in compression. The Bauschinger effect leads to a stress that exceeds the yield stress in compression, $-f_y$. If there is a reversal of stress and strain (i.e., unloading from compression and reloading towards the original direction of loading, i.e. to tension), it leads to a σ-ε branch similar to that of the previous unloading from tension to compression. The reloading branch exceeds the yield stress f_y in first (virgin) loading and heads towards the point from where the previous reversal from tension to compression had started (previous peak stress and strain point in the current direction of loading). If loading continues past that point, it follows the σ-ε curve in monotonic loading till rupture of the bar, unless a new reversal of loading takes place towards compression.

In the unlikely case (for a bar in a concrete member) that before it yields in tension the bar yields in compression without buckling, the yield plateau takes place in compression alone (see Fig. 3.2(a)). The rest of the σ-ε behaviour is similar to the one described above, with the roles of compression and tension interchanged.

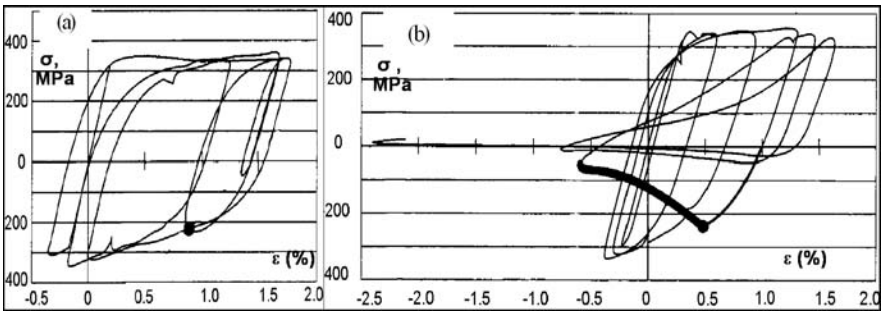

Fig. 3.2 σ-ε loops of bar that buckles in a concrete member under cyclic loading: (**a**) stress σ v real strain ε along the axis of the buckled bar; (**b**) stress v apparent strain in the original direction of the bar axis (adapted from Suda et al. (1996)). Buckling is displayed as (•)

An unloading branch from tension to compression (or vice-versa) and the following reverse branch of reloading in the opposite direction towards the point from where the first branch started, constitutes a hysteresis loop. If the second reversal (from compression to tension) occurs at a stress and strain equal and opposite to those at the first reversal (from tension to compression), the hysteresis loop is symmetric (see Fig. 3.3(a)).

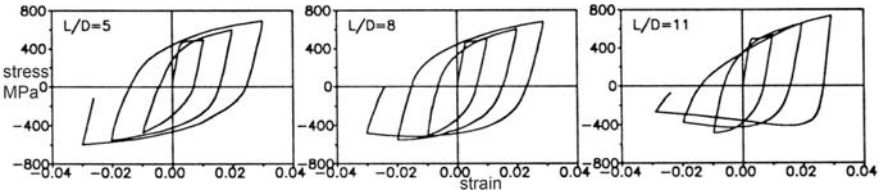

Fig. 3.3 Loops of stress vs apparent strain of bar subjected to cyclic loading with full reversal, as a function of the ratio of free bar length to diameter, *L*/*D* (Monti and Nuti 1991)

3.1.1.2 Buckling of Longitudinal Reinforcing Bars in Concrete Members Subjected to Cyclic Flexure and Its Consequences

Unless well restrained laterally – by a thick shell of sound concrete cover and/or engagement by closely spaced transverse reinforcement – a longitudinal bar in a flexural plastic hinge of a concrete member may buckle. Outward lateral pressures exerted on the bar from the bulging concrete core accelerate buckling.

As buckling entails lateral deflection of the bar, the distance between the two ends of the buckled length, *L*, shortens without any real axial shortening of the bar itself. The experimental σ-ε values in Fig. 3.2(a) show that right after buckling the mean axial strain of the bar increases algebraically: the bar axis unloads (its mean compressive stress decreases) following the σ-ε law of the material. As bending of the bar axis due to buckling shortens the distance between the ends of its buckled

length, the apparent strain of the bar along its original axis (i.e., the relative displacement of the two ends along the original axis, divided by their original distance L) decreases algebraically. Remember that what matters for the macroscopic behaviour of the member, in whose compression zone the bar belongs, is the force in the bar as a function of the average strain of the surrounding concrete, i.e. of the apparent strain of the buckled bar, not of the real one. The stress-apparent strain behaviour of a buckling bar is as shown in Fig. 3.2(b) and in Fig. 3.3(b) and (c) for bars with unrestrained length 8- or 11-times the diameter, respectively.

A longitudinal bar in a flexural plastic hinge will not buckle, unless the adjacent concrete has already disintegrated or the concrete cover is thin and weak, providing little lateral restraint. Real lateral restraint against buckling is provided only by closed ties. The effective buckling length depends on the conditions of engagement of the bar by, and the spacing and diameter of the ties. Under ideal conditions, the effective buckling length is equal to 50% of the tie spacing or of the distance of the first tie engaging the bar from the end section where the member connects to another one or to the foundation. In reality, the deflection of the bar upon buckling will extend beyond the ties engaging it and the effective buckling length will exceed the ideal value above. Ties with small diameter compared to the longitudinal bar may stretch and let the effective buckling length extend over several tie spacings (see Fig. 3.4(b)).

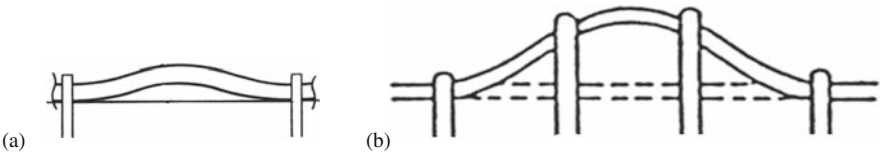

Fig. 3.4 Bar buckling over: (**a**) one; or (**b**) several tie spacings

The stress at which the bar may buckle is proportional to its Modulus and to the square of the ratio of the bar diameter to the effective buckling length. Regarding the Modulus, note that bars in concrete members subjected to seismic loading normally yield in tension before they do so in compression (see Figs. 3.5, 3.6 and 3.7 for typical seismic σ-ε histories of bars in various types of concrete members). Buckling usually takes place during a σ-ε branch of unloading from tension to compression

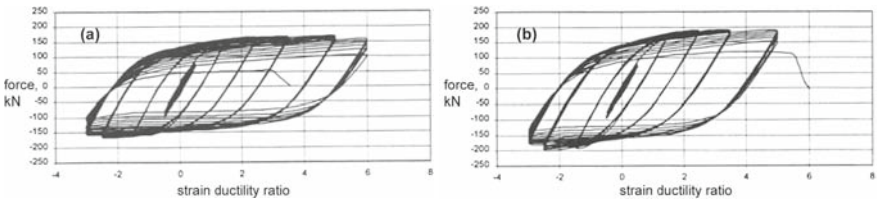

Fig. 3.5 σ-ε histories of the type induced by seismic action to column bars: (**a**) for grade S400 steel; (**b**) for S500 steel (Carvalho and Coelho 1997)

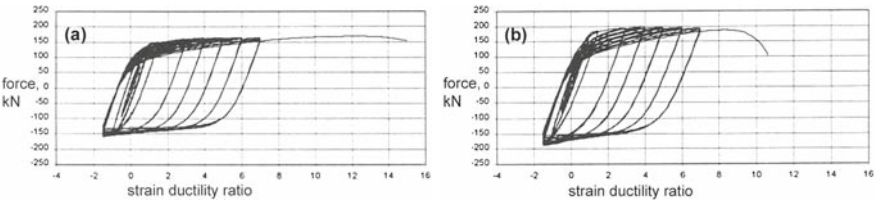

Fig. 3.6 σ-ε histories of the type induced by seismic action to bottom bars of beams: (**a**) for grade S400 steel; (**b**) for S500 steel (Carvalho and Coelho 1997)

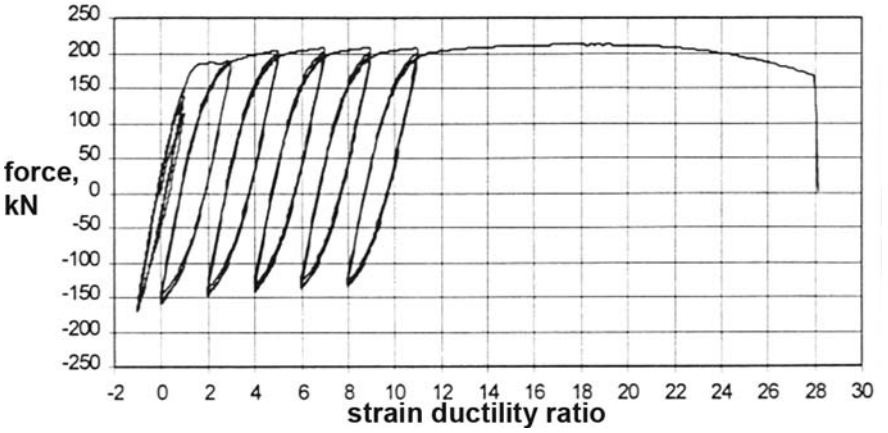

Fig. 3.7 σ-ε history of the type induced by seismic action to S500 top bars in beams (Carvalho and Coelho 1997)

that exhibits the Bauschinger effect, or in the hardening branch that follows it. So, it is not the Elastic Modulus, $E_s = 200$ GPa, that applies for the critical buckling load of the bar, but a much lower value. If bending due to buckling is considered to cause one side of the bar cross-section to unload elastically while the opposite side continues loading, then Engesser's "Reduced Modulus" or "Double Modulus" applies, which has a value between E_s and the tangent Modulus, E_t. For buckling of round bars in the strain hardening range the "Reduced Modulus" is about double the strain hardening modulus (Pantazopoulou 1998). In Shanley's alternative model for inelastic buckling the axial force in the bar is considered to keep increasing while buckling commences (as if the full bar section continues loading). So the tangent Modulus (which is much lower than Engesser's "Reduced Modulus") is considered to apply. No matter which one of the two approaches is adopted, the reduction in Modulus is such that an individual bar is predicted to buckle at a load much lower than Euler's critical load for elastic buckling.

The buckling behaviour of an individual bar compressed under force-control is different from that of a longitudinal bar in the compression zone of a flexural plastic hinge (Pantazopoulou 1998), as the latter is just one component in a highly

redundant parallel system encompassing the entire compression zone and comprising concrete and several longitudinal bars. Occurrence of buckling is very sensitive to minor differences in the lateral restraint conditions of the bar and to the pressure exerted on it by the bulging concrete. So, the longitudinal bars of the compression zone will not buckle all at the same time. Buckling of a bar takes place under conditions of deformation control and allows force redistribution to the rest of the parallel system. So, it does not have the immediate catastrophic consequences that we see, e.g., when a strut in a statically determined steel truss buckles. Normally the member will survive buckling of one or more longitudinal bars.

The immediate consequence of buckling of a compression bar in a concrete member is a drop in the lateral force resistance of the member, due to the following reasons:

- Unless it has already taken place, spalling of the shell of concrete cover will be triggered by bar buckling, as, without prior disintegration of the concrete core inside the cage of reinforcing bars, bars can buckle only outwards.
- Redistribution of the compressive force of the buckled bar brings the surrounding concrete closer to exhaustion of its compressive strength.
- A buckled bar does not contribute anymore to the confinement of the concrete core, particularly if its buckled length extends over several tie spacings. In this latter case the lateral bar deflection due to buckling stretches all ties that lie within the buckled length and reduces their own effectiveness in confining the concrete inside.

Note that in a concrete member subjected to bending the compression zone is on the concave side. So, its longitudinal bars, having their convex side inwards, would tend to buckle inwards against the concrete core. Buckling outwards would be much easier, as the concrete shell may have already spalled off, or if it hasn't, it can spall upon bar buckling. For the bar to buckle outwards, it has to overcome and reverse its inwards pre-curvature, which is unlikely. So, it is the corner bars that normally buckle first, and, as a matter of fact, they do so outwards almost at right angles to the plane of bending of the member and of the bar. For an intermediate bar to buckle, the concrete core in its immediate vicinity should be in (imminent) disintegration.

The interplay between the tendency of a compression bar in a concrete member to buckle over one or more tie spacings, the lateral pressures exerted on it by the confined concrete core and the restraint provided by the ties both against bar buckling and bulging of the confined concrete, is very complex even for monotonic loading (Pantazopoulou 1998). The phenomena are much more complex under cyclic loading, as described in the following paragraphs.

In a concrete member subjected to cyclic bending, the tension is taken exclusively by the tensile reinforcement, while the compression reinforcement shares the compressive force with the surrounding concrete. As a result, if the member is subjected to no axial load or to low axial compression, symmetric load cycles (i.e. cycles between equal and opposite values of moment M, or curvature, φ) induce in longitudinal bars asymmetric σ-ε cycles, with peak tensile strains significantly

exceeding the peak compressive ones and permanent tensile strains accumulating in the reinforcement of both sides. The σ-ε histories in Figs. 3.5, 3.6 and 3.7 are typical of what happens in concrete members subjected to cycles of constant moment amplitude but increasing deformation amplitude:

- in Fig. 3.5, for the bars of a column with symmetric reinforcement and relatively low axial load ratio, $\nu = N/A_c f_c$;
- in Fig. 3.6, for the bottom bars of an asymmetrically reinforced beam, that yield in compression in order for the crack to close at the bottom under positive (sagging) moments;
- in Fig. 3.7, in the beam's top reinforcement, which normally has larger cross-sectional area than the bottom one and never yields in compression.

In the σ-ε histories of Fig. 3.5 bar buckling may take place under conditions of tensile strain but of compressive stress in the bar. These bars, having unrestrained length six-times their diameter, indeed buckled during the last compressive half-cycle and ruptured in the following tensile half-cycle. The bars of Fig. 3.6(a) and (b) have the same geometry and mechanical properties as those of Fig. 3.5(a) and (b), respectively, but didn't buckle. They eventually broke in tension, at a strain at maximum stress not much lower than the uniform elongation, ε_{su}, of the steel in monotonic loading. Note the superior ductility of grade S400 steel over S500 in Figs. 3.5 and 3.6.

Bars seem very vulnerable to buckling during that phase of unloading-reloading when the crack is open throughout the depth of the section, owing to cyclic accumulation of tensile strains in the reinforcement of both sides, exhibited by all bars in Figs. 3.5, 3.6 and 3.7 (see also point 3 in Section 3.2.2.6). During that phase the reinforcement alone resists the compression force of the section and, in the absence of the stabilising effect of concrete, the bars of the compression zone may be considered as liable to buckling all at the same time. Fortunately, the crack may be open throughout the depth only at about the time the bending moment of the section changes sign. The likelihood of buckling during that stage is reduced by the low magnitude of compression stresses in the reinforcing bars and of the lateral pressure exerted on them by the concrete inside. Buckling may start shortly thereafter, before the surrounding concrete is fully mobilised in compression but after the bending moment increases sufficiently to build up the stress in the bar and reduce its tangent Modulus to the level necessary for buckling (see, e.g., the point where buckling occurs in Fig. 3.2(a)). It may start even later, after the outward pressure exerted on the bar and its restraining ties by the bulging concrete builds up as well.

Sometimes, but not often, bar buckling entails an immediate drop in the lateral force resistance of the member, large enough to be considered as ultimate failure.[1]

[1] A member is conventionally considered to have reached its ultimate deformation, if its (lateral) force resistance cannot increase above 80% of the maximum ever force resistance (defined as the force capacity of the member) by increasing the member's deformation, see Section 3.2.2.7.

Even when it is not, buckling of longitudinal bars in members subjected to cyclic loading may precipitate ultimate failure afterwards, by rupture in tension of the buckled bar during a subsequent half-cycle of loading, according to the following mechanism: Buckling induces in the bar additional flexural strains, positive (tensile) on one side and negative (compressive) on the other. These strains are superimposed on the axial strain of the axis of the bar (the one on the horizontal axis of Fig. 3.2(a)). The shorter the length, L, over which the bar buckles, the larger are the additional flexural strains. In all likelihood, the mean bar strain on which the flexural strains are superimposed is tensile, due to the yielding of the bar in tension before and the permanent extension it entails (cf. Fig. 3.2(a)). So, the total (mean plus flexural) strain of the extreme tensile fibres of the bar may approach, or even exceed, the uniform elongation, ε_{su}, of steel. Note that, exceedance of the rupture strain at the bar surface upon buckling is more likely in the Tempcore steels currently dominating the European market. These bars owe their superior yield and tensile strengths to quenching and tempering of their surface, which increases very much the strength of the skin but reduces its elongation at failure.[2] So, a crack may develop at the surface of the buckled bar. After reversal of the loading of the member, the bar that has buckled straightens up and – depending on the magnitude of the new half-cycle – may go into the inelastic range in tension. Then the pre-existing crack may extend through the entire cross-section, causing complete loss of the bar. If the loss of the tensile capacity of the bar causes a drop in the peak force resistance exceeding 20% of the maximum ever force resistance (see footnote 1 above), we will conventionally call this failure (or ultimate deformation) of the member.

Should the compression zone lose a large fraction of its compressive strength owing to abrupt or gradual disintegration of the concrete during load cycling, its longitudinal bars will buckle, unless they have done so already.

3.1.1.3 Time Effects on the Mechanical Behaviour of Steel

The fundamental quantities characterising a reinforcing steel, notably the yield stress, f_y, the tensile strength, f_t and the uniform elongation at rupture, ε_{su}, are measured in the lab under strain rates which are very slow compared to those induced by an earthquake. For the types of steel normally used in earthquake resistant design, namely steel grades S400–S500, it may be considered that the values of the aforementioned σ-ε parameters under monotonic loading increase with strain rate, $\dot{\varepsilon}$, by $c\ln(\dot{\varepsilon}/\ 5 \times 10^{-5})$ above those measured in the lab under quasi-static loading with $\dot{\varepsilon} = 5 \times 10^{-5}\ \mathrm{s}^{-1}$, where (CEB 1988a):

$c = 6$ MPa for f_y,
$c = 7$ MPa for f_t and
$c = 0.3\%$ for ε_{su}.

[2] Whatever effect, internal or external, increases the strength of steel, typically reduces its ductility and elongation at failure.

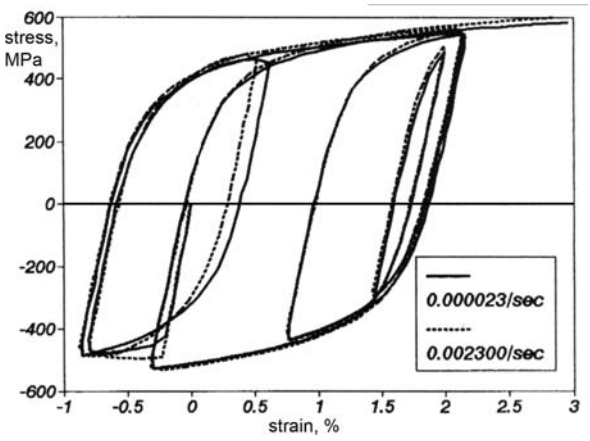

Fig. 3.8 Effect of strain rate on hysteresis loops of reinforcing steel (adapted from Restrepo-Posada et al. (1993))

Cold worked reinforcing steels, that are normally not used in earthquake resistant structures, exhibit a smaller effect of strain rate on the values of f_y and f_t than the more ductile types of steel, like those of grade S400–S500. The effect on their – anyway low – ultimate elongation is more pronounced.

Everything that has been said so far refers to monotonic loading. Figure 3.8 suggests that under cyclic loading the strain rate affects only the yield stress, leaving the subsequent σ-ε behaviour (notably the peaks of hysteresis loops) unaffected.

The strain rate is not constant during seismic loading. It is zero at peaks of the deformation, positive or negative, and attains a maximum value in-between these peaks (normally, at zero stress). The increase in strength relative to the quasi-static value is not derived from the mean strain rate during the half-cycle of the response, but from a lower value, about 15% of the peak strain rate during the response (i.e. of the strain rate attained at practically zero stress), or about 30% of the average strain rate.

3.1.1.4 Requirements on the Reinforcing Steel Used in Earthquake Resistant Construction

The steel parameters which are of prime importance for the seismic performance of concrete members are:

- the strain at maximum stress (uniform elongation at failure), ε_{su}, and
- the ratio of tensile strength to yield stress, f_t/f_y ("hardening ratio"),

of reinforcing bars. The yield stress, f_y, per se is important just for the onset of yielding of structural members, to the extent it matters for the Operational or the Immediate Occupancy performance levels and for the member stiffness to the yield point.

The importance of ε_{su} for the failure of reinforcing bars, possibly after buckling, has been noted in Sections 3.1.1.1 and 3.1.1.2. The impact of ε_{su} on the ultimate deformation of a RC member is elucidated by the relationship between the ultimate

curvature of a concrete section, φ_{su}, as controlled by rupture of the tension reinforcement, and the value of ε_{su}:

$$\varphi_{su} = \frac{\varepsilon_{su}}{(1 - \xi_{su})\, d} \tag{3.1}$$

where d is the effective depth of the section and ξ_{su} the neutral axis depth at steel rupture, normalised to d.

The hardening ratio f_t/f_y is important for several reasons. First, the higher its value, the greater is the tangent modulus of the steel bar in its strain-hardening range and the later buckling will take place. More important is the role of f_t/f_y for the control of the value of the maximum moment at the end of a member and, through it, of the extent of plastification near that end. This extent may be defined as the length of the member over which the bending moment exceeds the yield moment, M_y. If we assume that after yielding the internal lever arm at the end section stays approximately constant, then the bending moment at the end section is equal to $M = (\sigma_s/f_y)M_y$, where σ_s is the stress of the tension reinforcement there. If failure of the end section takes place due to rupture of the tension bars, at that section we have $\sigma_s = f_t$. If the bending moment diagram is approximately linear in the vicinity of the end section over a length L_s (which is equal to the moment-to-shear ratio at the end section, i.e., to the shear span), then member plastification at failure due to steel rupture extends over a length of:

$$l_{pl} = L_s \left(1 - \frac{M_y}{M_u}\right) = L_s \left(1 - \frac{f_y}{f_t}\right) \tag{3.2}$$

Therefore, the higher the value of f_t/f_y, the longer is the zone of plastification as a fraction of the shear span L_s. In turn, the longer the length of plastification, l_{pl}, the larger is the value of the chord rotation at flexure-controlled failure of the shear span (see footnote 1 in Chapter 1 and Fig. 1.4 for the definition of the chord rotation at a member end). As a matter of fact, if we assume that along the shear span, L_s, only flexural deformations take place, the ultimate chord rotation at the end of the shear span, θ_u, is derived from Fig. 3.9 as:

$$\theta_u = \varphi_y \frac{L_s}{3} + \frac{l_{pl}}{3}\left[\varphi_u \left(1 + \frac{f_y}{2f_t}\right) - \varphi_y \left(\frac{1}{2} + \frac{f_t}{f_y}\right)\right] \tag{3.3}$$

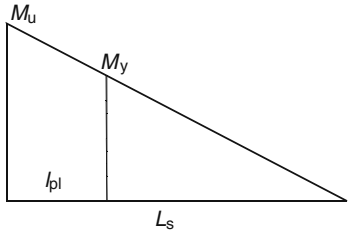

Fig. 3.9 Extent of plastification of member when the end section reaches its ultimate moment

where φ_y is the curvature at yielding of the end section and φ_u the ultimate curvature there (see Sections 3.2.2.2 and 3.2.2.4). For increasing f_t/f_y ratio, the value of the expression in brackets decreases, but not sufficiently to override the ensuing large increase in the value of l_{pl}. So, overall, the larger the hardening ratio, f_t/f_y, the greater is the flexure-controlled ultimate chord rotation at the end of the member where inelasticity takes place. As a matter of fact, if the value of f_t/f_y is close to 1.0, that of l_{pl} approaches zero and the flexure-controlled ultimate chord rotation is very low as well. For this reason, Eurocode 8 sets a lower limit to the value of the hardening ratio, f_t/f_y, of the steel to be used in ductile structures.

As emphasised in Section 1.3, current seismic design codes pursue the control of the inelastic seismic response through capacity design. The required force resistance of those regions or mechanisms intended to remain elastic is computed from equilibrium and the force capacities of the adjacent ductile regions or force-transfer mechanisms considered capable of developing large inelastic deformations. The only mechanism of force transfer entrusted to develop inelastic deformations under cyclic loading is flexure – provided that the yield moment is controlled by the tensile reinforcement and its nominal yield stress, f_{yk}. If the tensile strength of steel is much higher than its yield stress, soon after the ductile members yield their force resistance may increase well beyond the value used in the capacity design calculations. This increase may upset the balance between the force resistances of ductile and brittle mechanisms achieved through capacity design and cause the brittle mechanisms to exceed their force resistance and start developing inelastic deformations that they are not capable of. For this reason, Eurocode 8 sets an upper bound on the value of f_t/f_y of reinforcing steel to be used in ductile structures. For similar reasons, and, in addition, to ensure that the steel of any section or region will indeed yield before the concrete crushes, Eurocode 8 sets an upper limit on the ratio of the actual yield stress of the steel to the nominal value, f_{yk}.

Recognising that deformation and ductility capacity depends not only on the detailing of members, but on the inherent ductility of their materials as well, Eurocode 8 increases the ductility requirements on the steel in "critical regions" (i.e., those where inelastic deformations may take place under the design seismic action, see Section 5.1.1) of the elements of the lateral-load-resisting system (the "primary seismic" ones, see Section 4.12) with the Ductility Class, DC, as shown in Table 3.1. The limits on the hardening ratio, f_t/f_y, and the strain at maximum stress (uniform elongation at failure), ε_{su}, refer to lower 10% fractiles. The lower bound on ε_{su} is for ensuring a minimum curvature ductility and flexural deformation capacity, by preventing bar fracture prior to concrete crushing, or simply delaying it until a target flexural deformation is reached. The lower limit on f_t/f_y aims at ensuring a minimum length of the flexural plastic hinge according to Eq. (3.2). The ceiling on the values of f_t/f_y and $f_{yk,0.95}/f_{yk}$ is to limit flexural overstrength, and hence shear force demands on members and joints, as controlled by flexural yielding at the end of members, as well as the moment input from beams to columns.

Steels of class B or C according to Eurocode 2 (CEN 2004b) fulfil the conditions for the steel in DC L or M buildings. The conditions on ε_{su} and f_t/f_y of steel in DC H buildings are met only by steels of class C according to Eurocode 2.

Table 3.1 Requirements of Eurocode 8 for reinforcing steel in elements of the lateral-load-resisting system of new buildings

Ductility Class	DC L or M	DC H
5%-fractile yield strength f_{yk}	400–600 (MPa)	
95%-fractile actual yield strength $f_{yk,0.95}/f_{yk}$	–	$\leq$1.25
$(f_t/f_y)_{k,0.10}$	$\geq$1.08	$\geq$1.15
		$\leq$1.35
10%-fractile strain at maximum stress, $\varepsilon_{su,k,0.10}$	$\geq$5%	$\geq$7.5%

Strictly speaking, for buildings belonging in DC M the Eurocode 8 requirement for the use of steel of at least class B applies only to the "critical regions" at the ends of "primary seismic" elements. As in DC L buildings "critical regions" are not defined, the requirement for the use of steel of at least class B applies throughout the length of their elements. As DC M or H buildings should not in any respect be inferior in local ductility to DC L ones, the whole length of "primary seismic" elements of DC M and H buildings should have reinforcing steel of at least class B. The additional requirements on the steel of the "critical regions" of DC H buildings essentially apply:

- thoughout the entire height of "primary seismic" columns,
- in the "critical region" at the base of "primary seismic" walls, and
- in the "critical regions" near the supports of "primary seismic" beams on columns or walls (including the slab bars which are parallel to the beam and fall within the effective flange width in tension).

In practice, the Eurocode 8 requirements on reinforcing steel of "critical regions" are expected to be applied over the entire primary seismic element, including the slab it may be working with.

Thanks to its lower cost-to-strength ratio, weldability and fairly good ductility, weldable tempcore steel of type S500s has become the reinforcing steel of choice in the more seismic prone European countries since the mid-1990s. It is a surface-hardened low carbon steel with nominal yield strength of 500 MPa. It easily fulfils all Eurocode 8 requirements for DC L or M buildings, but it meets those for DC H ones (notably the lower limit on f_t/f_y) only when produced for application in moderate- or high-seismicity regions. The small quantity of S400 steel still on the market of these countries has higher strain at maximum stress, ε_{su}, and hardening ratio, f_t/f_y, both meeting easier the limit values for DC H buildings. However, the value of $f_{yk,0.95}/f_{yk}$ may exceed the maximum limit permitted for DC H. The main reason is that steels produced as S500 but failing to meet the minimum criteria on f_{yk}, are sometimes re-classified and marketed as S400.

The widest available survey of ductile steels of the type used in the seismic regions of Europe has been carried out in the early 1990s (Carvalho and Coelho 1997, Carvalho 1995, Pipa and Carvalho 1994), drawing several thousands of data from nine different European countries (Carvalho and Pipa 1994, Plumier and

Table 3.2 Outcome of surveys of steel used in seismic regions of Europe

Country of production	Spain, Portugal	Italy	Belgium, France, Germany, Italy, Luxembourg, Netherlands, Portugal, Spain	UK	Various
nominal yield strength, f_{yk} (MPa)	400	430	500	500	460
mean yield strength, f_{ym} (MPa)	496	478	571	552	530
95%-fractile of actual yield strength, $f_{yk,0.95}/f_{yk}$	*1.335*	1.19	1.23	1.165	*1.27*
mean tensile strength, f_{tm} (MPa)	598	733	663	653	618
$(f_t/f_y)_{k,0.10}$	1.15	1.44	*1.10*	*1.13*	–
$(f_t/f_y)_{k,0.90}$	1.27	*1.62*	1.23	1.23	–
mean strain at maximum stress, $\varepsilon_{su,m}$ (%)	11.8	11.6	10.4	11.7	11.1
10%-fractile of strain at max. stress, $\varepsilon_{su,k,0.10}$ (%)	9.6	9.7	8.6	9.7	–

Vangelatou 1995, Stanescu and Plumier 1993, Elnashai 1994, Calvi et al. 1994). That survey paved the way for the revision of the requirements of ENV 1998-1-3:1993 (the prestandard version of Part 1 of Eurocode 8) toward the limits in Table 3.1. The statistical outcome of that survey is compiled in Table 3.2, columns 1–5, in the form of average statistics of those steel parameters which are of interest to Eurocode 8. The last column of Table 3.2 gives also statistics of steel properties provided by the UK certification agency (Cairns 2006). All values listed in Table 3.2 meet the requirements of EN-Eurocode 8 for the reinforcement of DC L or M buildings. However, the values in italics in Table 3.2 violate the corresponding limit for the steel of DC H buildings. So, not a single one among the types of steel in Table 3.2 conformed fully to the limits placed on the steel of DC H buildings. Nevertheless, since then the steel industry in at least some European countries has developed and marketed cost-effective products that meet all Eurocode 8 limits for the steel of DC H buildings.

3.1.2 The Concrete

3.1.2.1 Concrete Under Cyclic Uniaxial Compression

Unlike reinforcing bars, which by geometry develop essentially only uniaxial stress conditions, concrete may be subjected also to biaxial or triaxial stresses. Because of its low tensile strength, concrete normally cracks at right angles to any significant tensile stresses. As a result, these stresses drop to zero. Even when there is no cracking tensile stresses are low anyway. The compressive strength and stiffness

of concrete decreases with increasing tensile stress in the transverse direction. This reduction is taken into account where relevant (see Eqs. (3.96) in Section 3.2.4.2 under *The Variable Strut Inclination Truss of the CEB/FIP Model Code 90 and Eurocode 2*). Compressive stresses in one of the three principal stress directions increase the compressive strength and stiffness in the orthogonal directions, but if the lowest of the three principal stresses is much smaller than the other two (regardless of its sign) the increase is negligible.

The prime case where multiaxiality of stresses has a major effect on the behaviour in the direction of the predominant compressive stress is when the stresses in both orthogonal directions are compressive and significant in magnitude. This is the case of confinement, Except for that case (dealt with at length in Section 3.1.2.2) and the strength reduction due to transverse tension (Eqs. (3.96) in Section 3.2.4.2 under *The Variable Strut Inclination Truss of the CEB/FIP Model Code 90 and Eurocode 2*), the multiaxiality of the stress field is neglected and the behaviour in the direction of the predominant compressive stress is considered, as if we had uniaxial compression.

The σ-ε behaviour depicted in Fig. 3.10 is typical of concrete under cyclic uniaxial compression. The energy dissipated by the material (i.e. the area enclosed by unloading-reloading hysteresis loops) is small, compared to either the deformation energy stored in the concrete at the peak of a loading cycle, or to the energy dissipated by steel under cyclic loading. Reloading σ-ε branches are directed toward the σ-ε curve in monotonic loading and follow it if reloading continues past the maximum ever previous strain value. Therefore, the monotonic σ-ε curve is the envelope and the skeleton curve of σ-ε loops under cyclic loading.

If unloading-reloading from and to a constant maximum stress equal to a large fraction of the uniaxial compressive strength, f_c, is repeated indefinitely, permanent compressive strains accumulate and the falling branch of the monotonic σ-ε envelope will ultimately be reached, signaling failure. In Fig. 3.10(b) 19 cycles at a peak stress of $0.9f_c$ suffice to reach the monotonic σ-ε curve. If the peak stress is at $0.85f_c$, 200 cycles are required for this to happen (Karsan 1968). This behaviour is characteristic of low-cycle fatigue. If the peak stress level is lower, the loading–unloading loops stabilise and the falling branch of the monotonic σ-ε curve is never reached.

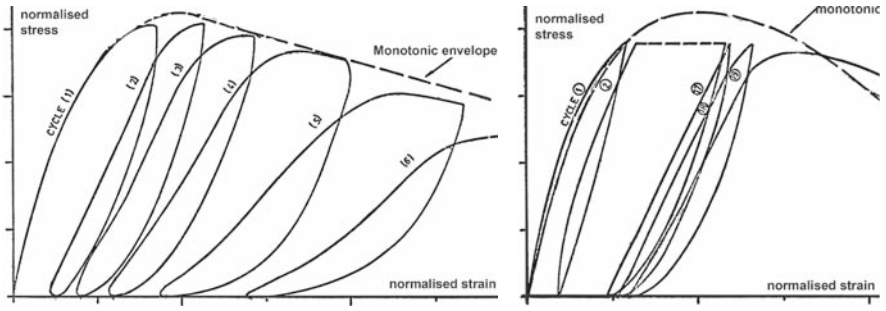

Fig. 3.10 σ-ε behaviour of concrete under cyclic uniaxial compression (adapted from Karsan (1968))

The number of stress cycles approaching the uniaxial compressive strength, f_c, in an earthquake is roughly equal to the duration of strong ground shaking divided by the predominant period of the structure. For a concrete building this number would normally be expected to be not more than 10, which means that low-cycle fatigue effects will not be important. Then, only the monotonic σ-ε behaviour of concrete in uniaxial compression is of interest.

Until a uniaxial stress of about $0.95f_c$ the Poisson ratio of concrete is approximately constant and close to 0.20. Above that stress level it increases fast, reaching a secant value of about 0.4 at ultimate strength. The underlying physical reason is that, as failure approaches, pre-existing microcracks at the interface of aggregates with the hardened cement paste extend into the latter in a direction parallel to that of the applied uniaxial compression stress and tend to join up as macro-cracks in that direction. The opening up of these macro-cracks soon leads to ultimate strength, manifesting itself as a precipitous increase in the apparent lateral strain. The volumetric contraction, which so far had been continuously increasing, starts decreasing. Right after ultimate strength it gives way to volumetric expansion (dilation). This mechanism has important implications for the enhancement of concrete strength through confinement.

3.1.2.2 Effects of Confinement on σ-ε Behaviour in Compression – Modelling

The case of prime interest in earthquake resistant design is that of concrete under the following conditions of triaxial compression:

- the stress in one principal direction, let's say direction 1, is compressive and rather high;
- the two other principal stresses, in directions 2 and 3, are compressive and about equal in magnitude, but smaller than σ_1: $\sigma_2 \approx \sigma_3 < \sigma_1$.

Such triaxial stress conditions are found in the compression zone when the concrete approaches its ultimate strength, provided that the lateral expansion that precedes its failure is restrained (Pantazopoulou 1995). Lateral restraint may come from various sources:

- tests have demonstrated that the restraint of the dilation of the compression zone of the end section of a member framing into another (a beam into a column, a column into a floor slab or a foundation element, etc.) by the volume of the surrounding concrete of the latter produces a triaxial stress condition, greatly enhancing the local strength and deformation capacity of the concrete (Takiguchi et al. 1997, Imai et al. 2005);
- closely spaced hoops or ties as transverse reinforcement restrain the lateral dilation of the concrete inside the cage of stirrups and longitudinal reinforcement (the "concrete core");
- Fibre-Reinforce Polymers (FRPs) wrapped around the member have a similar effect on the enclosed volume of concrete.

The restraint of the lateral dilation of concrete by such means is termed "confinement", and the volume of concrete affected is considered as "confined".

By opposing the large Poisson expansion arising from the opening up of internal macro-cracks parallel to the predominant compressive stress σ_1 when concrete is close to ultimate strength, a uniform pressure, $\sigma_2 = \sigma_3 = p$, at right angles to σ_1 and to these macro-cracks, increases the compressive strength in the direction of σ_1 from f_c to $f_c{}^*$ and the strain at the peak of the σ_1–ε_1 curve from $\varepsilon_{co} \approx 0.2\%$ to $\varepsilon_{co}{}^*$. The larger the lateral pressure, the greater is the enhancement of ultimate strength and of the corresponding strain. Moreover, the falling branch of the σ_1–ε_1 diagram after the peak at $f_c{}^*$, $\varepsilon_{co}{}^*$ becomes flatter with increasing value of p (i.e., confined concrete strain-softens slower). The monotonic σ_1–ε_1 curve for $p > 0$ is the envelope of the hysteresis loops under cycling loading with $p > 0$.

Several models have been proposed over the past decades for the σ-ε behaviour of confined concrete. A few of them are described here, notably those that are – for some reason or another – widely used, as well as simple models that fit well available experimental results.

The available test results for concentric compression show that the compressive strength in the direction of $\sigma_1 > \sigma_2 = \sigma_3$ increases with p as:

$$f_c^* = f_c(1 + K) \tag{3.4}$$

Eurocode 8 Part 3 (CEN 2005a) has adopted the value of K proposed in (Newman and Newman 1971).

$$K \approx 3.7 \left(\frac{p}{f_c} \right)^{0.86} \tag{3.5}$$

As shown in Fig. 3.11(a), Eq. (3.5) gives about the same result as the more complex expression fitted to data by (Elwi and Murray 1979):

$$K = 2.254 \left[\sqrt{1 + 7.94 \frac{p}{f_c}} - 1 \right] - \frac{2p}{f_c} \tag{3.6}$$

After its adoption by Mander et al. (1988), Eq. (3.6) is widely quoted and used today.

One of the earliest confinement models is the one proposed in Sheikh and Uzumeri (1982), still used in the US. It referred directly to confinement by ties. That model, gives:

$$K = a \left(7 \frac{\sqrt{2p}}{f_c} \right) \quad (p \text{ and } f_c \text{ in MPa}) \tag{3.7}$$

where a is the "confinement effectiveness factor" of the ties, given by Eqs. (3.24), (3.20), (3.21) and (3.22) in Section 3.1.2.3. The lateral pressure may be taken equal

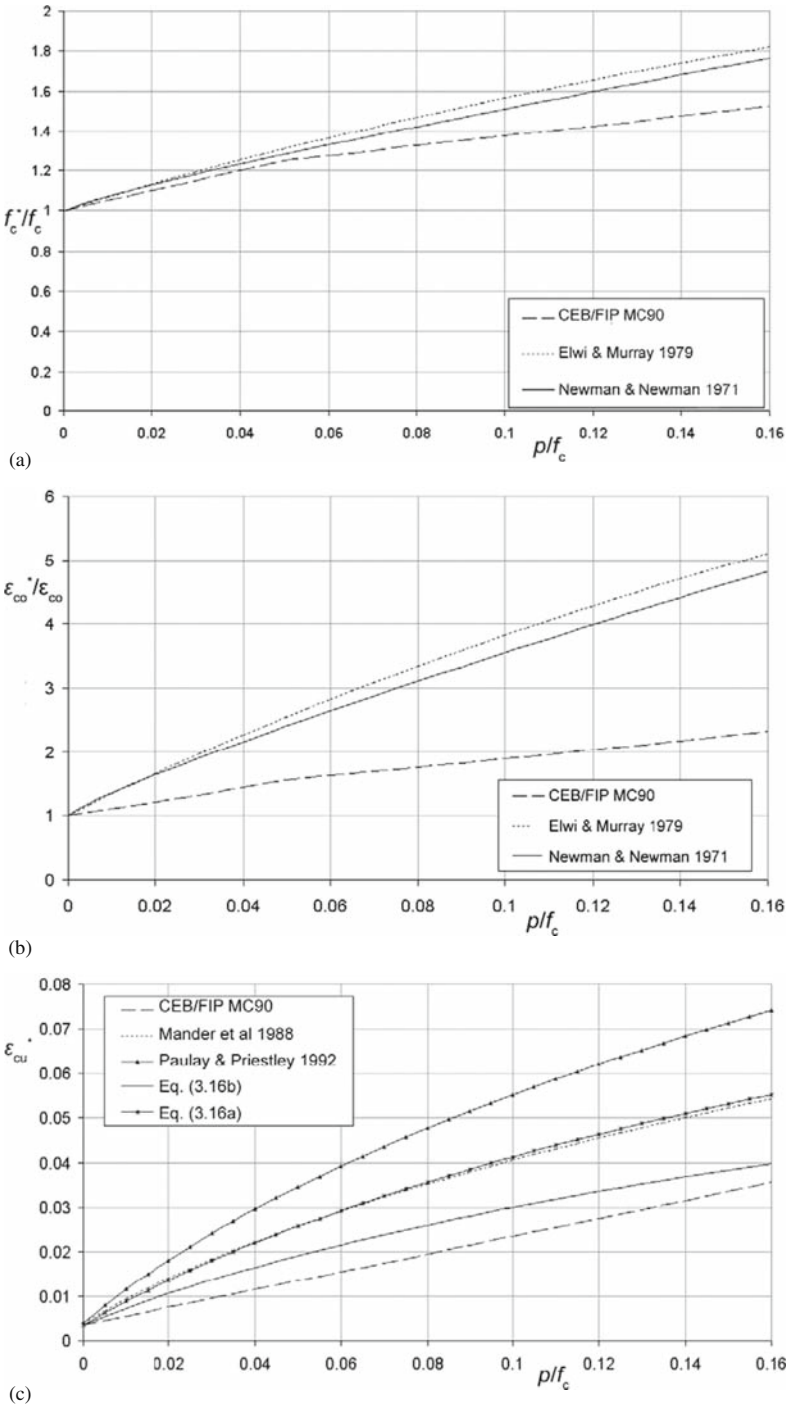

Fig. 3.11 Comparison of the predictions of various confinement models for the enhancement of concrete: (**a**) strength; (**b**) strain at maximum strength; and (**c**) ultimate strain

to $p = 0.5\rho_w f_{yw}$, where f_{yw} is the yield stress of the ties and ρ_w their volumetric ratio (ratio of the volume of stirrups to the volume of the confined core of the concrete, measured to the centreline of the perimeter stirrup) (cf. Eqs. (3.19) and (3.23)).

In Europe, the model in Model Code 90 of CEB/FIP (CEB 1991) is still in use, although it gives, in general, less enhancement of the key properties of concrete with confinement (see Fig. 3.11(a)). In that sense it is safe-sided for design. It is used mainly thanks to its adoption by Eurocode 2 (CEN 2004b). In that model the enhancement of ultimate strength and of the corresponding strain are given as:

$$f^* = \beta f_c = \min\left(1 + 5\frac{p}{f_c}; 1.125 + 2.5\frac{p}{f_c}\right) f_c \tag{3.8}$$

$$\varepsilon_{co}{}^* = \varepsilon_{co}\beta^2 \tag{3.9}$$

where β in Eq. (3.9) is the strength amplification factor in Eq. (3.8), standing for the factor (1+K) of Eq. (3.4).

If the two transverse stresses are not equal ($\sigma_2 > \sigma_3$) the value $p \approx (\sigma_2 + 4\sigma_3)/5$ may be used in Eqs. (3.5), (3.6) and (3.8). The smaller of the two transverse stresses controls confinement, implying that detailing of concrete members for earthquake resistance should aim at providing (about) the same restraint of lateral expansion in both transverse directions of the member.

Larger than the enhancement of maximum strength with confinement is the increase in the strain at maximum strength. According to Richart et al. (1928) the following expression applies (adopted also in Eurocode 8, Part 3 (CEN 2005a)):

$$\varepsilon_{co}{}^* \approx \varepsilon_{co}(1 + 5\,K) \tag{3.10}$$

Equation (3.10) gives much higher enhancement of the strain at maximum strength than Eq. (3.9) in Model Code 90 (CEB 1991) and Eurocode 2 (see Fig. 3.11(b)).

Confinement starts affecting the σ_1–ε_1 diagram only when the value of σ_1 approaches the uniaxial compressive strength of unconfined concrete, f_c. Until then, neither the tangent, nor the secant value of the elastic modulus of concrete are affected much by confinement. Note that the secant modulus from the origin to the peak of the σ_1–ε_1 diagram, i.e. the value of $f_c{}^*/\varepsilon_{co}{}^*$, drops, as the confining pressure increases. Note also that, if the ascending branch of the σ_1–ε_1 diagram is modelled as a parabolic curve (a common practice for uniaxial compression), then the initial tangent modulus is equal to $2f_c{}^*/\varepsilon_{co}{}^*$ and decreases with increasing value of p. This anomaly can be avoided by adopting – instead of the commonly used parabolic diagram – the σ_1–ε_1 relation proposed by Eurocode 2 (CEN 2004b) for use in nonlinear analysis of concrete structures. The generalised form of that relation is:

$$\frac{\sigma}{f_c^*} = \frac{\dfrac{\varepsilon}{\varepsilon_{co}^*}\left(k - \dfrac{\varepsilon}{\varepsilon_{co}^*}\right)}{1 + (k-2)\dfrac{\varepsilon}{\varepsilon_{co}^*}} \tag{3.11}$$

where:

$$k = 1.05 E_c \varepsilon_{co}{}^* / f_c^* \tag{3.12}$$

with E_c denoting the secant modulus of elasticity from the origin to a stress σ_1=0.4f_c, which is equal to $E_c = 11000 f_c{}^{0.3}$ (for E_c and f_c in MPa) according to Eurocode 2 (CEN 2004b). Equation (3.11) reduces into the simple parabolic σ_1–ε_1 diagram if k is taken equal to 2. By extension from the uniaxial compression for which it has been adopted in Eurocode 2, Eq. (3.11) may be considered to apply also along the softening branch beyond the peak at $f_c{}^*$ and ε_{co}.

In seismic design, more than the strength of concrete matters its ultimate strain – i.e. the strain beyond which concrete is considered to shed all its resistance to load and disintegrate – denoted as ε_{cu} (or $\varepsilon_{cu}{}^*$ for confined concrete). The ultimate deformation of a member (i.e. "failure") is conventionally identified with attainment of ε_{cu} at the extreme compression fibre of that section where the bending moment is largest (typically at the end section for seismic action), or of $\varepsilon_{cu}{}^*$ at the extreme fibres of the confined core. ε_{cu} is also conventionally defined as the strain at the point on the softening branch of the σ_1–ε_1 diagram where the stress, σ_1, has dropped to 0.85f_c (or to 0.85$f_c{}^*$, for $\varepsilon_{cu}{}^*$ in confined concrete). Recall that in design the flexural resistance of concrete sections is conveniently calculated assuming that the σ_1–ε_1 diagram is parabolic up to the peak stress and horizontal thereafter, until the value of ε_{cu}. The implication is that the value of ε_{cu} should be such that the softening branch of the σ_1–ε_1 diagram contributes to the maximum possible force that can develop in the compression zone with a force of $f_c b x(\varepsilon_{cu}$–$\varepsilon_{co})/\varepsilon_{cu}$, or of $f_c{}^* b^* x^* (\varepsilon_{cu}{}^* - \varepsilon_{co}{}^*)/\varepsilon_{cu}{}^*$ for confined concrete, where b and x are the width and depth of the compression zone, if rectangular, and b^*, x^* their counterparts in the confined core.

The Model Code 90 CEB/FIP model (CEB 1991), adopted by Eurocode 2 (CEN 2004b) for the design of new buildings, gives the following ultimate strain of confined concrete:

$$\varepsilon_{cu}{}^* = 0.0035 + 0.2 p / f_c \tag{3.13}$$

On the basis of test results showing that concrete confined by stirrups and subjected to concentric compression ultimately fails when concrete dilation causes the stirrups to exhaust their uniform elongation at failure, $\varepsilon_{su,w}$ and rupture, Mander et al. (1988) proposed that when the ultimate strain of confined concrete is reached, the total deformation energy stored in the stirrups until they rupture at strain $\varepsilon_{su,w}$ is equal to the gain in the total deformation energy of the confined concrete core. Assuming, for convenience, that the σ-ε diagram of the stirrup steel is horizontal (i.e. rigid-plastic) at a stress equal to f_{yw} until the failure strain of $\varepsilon_{su,w}$, the idea in Mander et al. (1988) gives: $\rho_w f_{yw} \varepsilon_{su,w} \approx f_c{}^* (\varepsilon_{cu}{}^* - \varepsilon_{cu})$, i.e.:

$$\varepsilon_{cu}{}^{*} \approx \varepsilon_{cu} + 2\varepsilon_{su,w}\frac{p}{f_c^*} \tag{3.14}$$

where the confining pressure p is taken equal to $p = 0.5\rho_w f_{yw}$, according to the discussion right after Eq. (3.7) and to Eqs. (3.19) and (3.23).

Paulay and Priestley (1992) proposed a modified form of Eq. (3.14), on the basis of test results for concentric compression (again with $p = 0.5\rho_w f_{yw}$):

$$\varepsilon_{cu}{}^{*} \approx 0.004 + 2.8\varepsilon_{su,w}\frac{p}{f_c^*} \tag{3.15}$$

Whatever has been said so far has been developed for concentrically compressed concrete and, strictly speaking, applies only there. What matters, though, for earthquake resistance is the behaviour of the extreme fibres in the confined concrete core of members subjected to cyclic bending, with or without axial load. Apart from the strain gradient (i.e. the fact that the strain is maximum at the extreme fibres, decreasing to zero towards the neutral axis), what is different from concentric compression is the target, which is the flexure-controlled ultimate deformation of the member.[3] Test results, especially in cyclic loading, show that by the time the ultimate curvature is reached, stirrups very rarely exhaust their elongation capacity and snap. Therefore, the value of $\varepsilon_{su,w}$ is not of prime importance for the confined concrete core.

If we adopt the analysis in Section 3.2.2.4 for the calculation of the ultimate curvature, φ_u, on the basis of first principles and use Eqs. (3.4), (3.5) and (3.10) for the confined concrete strength, $f_c{}^{*}$, and for the associated strain, $\varepsilon_{co}{}^{*}$, good average fitting to available experimental results on φ_u of cross-sections with rectangular compression zone and confined concrete core is achieved (with acceptable scatter) if the following expressions are used for $\varepsilon_{cu}{}^{*}$ (Biskinis 2007):

– for monotonic loading:

$$\varepsilon_{cu}{}^{*} = 0.0035 + \left(\frac{10}{h_c}\right)^2 + 0.57\frac{p}{f_c^*} \tag{3.16a}$$

– for cyclic loading:

$$\varepsilon_{cu}{}^{*} = 0.0035 + \left(\frac{10}{h_c}\right)^2 + 0.4\frac{p}{f_c^*} \tag{3.16b}$$

or, alternatively:

– for monotonic or cyclic loading:

$$\varepsilon_{cu}{}^{*} = 0.0035 + \left(\frac{1}{x_c}\right)^{3/2} + \frac{1}{3}\frac{p}{f_c^*} \tag{3.17}$$

[3] See footnote 1 in Section 3.1.1.2 for the definition of ultimate deformation (see also Sections 3.2.2.4 and 3.2.2.7).

where:

- h_c is the depth of the confined concrete core within the plane of bending (in mm);
- x_c is the neutral axis depth in the confined concrete core within the plane of bending (mm);
- the confining pressure, p, is related to the geometric ratio and to the arrangement of the confining medium (the transverse reinforcement), differently for Eqs. (3.16) or for Eq. (3.17) as specified in Section 3.1.2.3;
- the confined compressive strength, f_c^*, is given from Eqs. (3.4) and (3.5).

The "ultimate strain" of the extreme compression fibres of the unspalled section at its ultimate curvature (i.e. when the moment resistance of the unspalled section drops below 80% of the maximum previous moment resistance, see footnotes 1 and 3 of this chapter) may be determined from Eqs. (3.16) and (3.17) with $p = 0$ and the full section depth in the plane of bending, h, or the neutral axis depth x in the full concrete section, instead of h_c or x_c, respectively.

The 2nd terms in Eqs. (3.16) and (3.17) imply a size-effect, as in Bigaj and Walraven (1993) and Bosco and Debernardi (1993). Although this is a controversial issue (e.g., Alca et al. 1997), a size effect on ε_{cu} is rationalised on the basis of stability considerations of the compression zone (cf. the definition of ε_{cu} as the terminal strain of a parabolic-rectangular σ-ε diagram that reproduces the maximum possible resisting force of the compression zone).

Part 3 of Eurocode 8 (CEN 2005a) proposes the following for the ultimate strain at the extreme fibres of the confined concrete core in members under cyclic bending:

$$\varepsilon_{cu}^* = 0.004 + 0.5\frac{p}{f_c^*} \tag{3.18}$$

Equation (3.18) is meant to be used with Eqs. (3.4), (3.5) and (3.10) for f_c^* and ε_{co}^* in a package considered by Part 3 of Eurocode 8 as more accurate and representative than the confinement model of Eurocode 2, consisting of Eqs. (3.8), (3.9) and (3.13).

Figure 3.11(c) compares the outcome of Eqs. (3.16) to those of Eqs. (3.13), (3.14) and (3.15). For the purposes of this comparison, the value of $\varepsilon_{su,w}$ used in Eqs. (3.14) and (3.15) is the average in the tests to which Eqs. (3.16) have been fitted. The predictions of Eq. (3.15) are on the high side, while Eq. (3.14) seems to agree well with Eq. (3.16a) – and hence with the underlying monotonic data – but to be on the unsafe side compared to Eq. (3.16b) – and to the underlying cyclic data. The predictions of Eq. (3.18) – not shown in Fig. 3.11(c) – are half-way between those of Eqs. (3.16a) and (3.16b). Being design-oriented, Eq. (3.13) gives safe-sided estimates of the ultimate strain, but not overly so, and hence is an acceptable alternative to Eq. (3.16b) for cyclic loading.

Sections 3.2.2.4 and 3.2.2.10 elaborate further the context of Eqs. (3.16) and (3.17), notably the expressions for the ultimate curvature φ_u in which the value of ε_{cu}^* is to be used.

Note that all expressions given in the present section, except Eqs. (3.16), (3.17) and (3.18), have been fitted to concentric compression test results. The reader should be cautioned, then, for the fact that all confinement models are applied throughout the compression zone of sections subjected to bending with or without axial load, and especially to its extreme fibres. The implicit assumption there is that every point in the compression zone is laterally restrained by the surrounding volume of concrete in the same way that the perimeter stirrup and any intermediate ones restrain a section under concentric compression. Being under smaller strains than the extreme fibres, the ones immediately inwards have a lower tendency to dilate and do indeed restrain the inward dilation of the extreme fibres. However, it is rather arbitrary to assume that this restraint depends on the diameter, layout and spacing of stirrups, in exactly the same way as the outward restraint does (see next Section 3.1.2.3). Indeed, the available experimental evidence suggests they don't.

3.1.2.3 Confinement by Transverse Reinforcement

The confinement of the end section of a member by the surrounding concrete beyond the member end – i.e. by a larger column for a beam, or a large foundation element for the base of a vertical element – is neglected in design, as it refers to a single section. However, confinement of the concrete core inside the reinforcement cage by closely spaced transverse reinforcement is a key point in the detailing of concrete members for earthquake resistance.

The yield strain of reinforcing steel is about 2.5-times the lateral strain of concrete at uniaxial ultimate strength. When the uniaxial stress approaches f_c the confining steel is activated and, if in sufficient quantity, reaches its yield stress, f_{yw}, while the – by now triaxially compressed – concrete attains its enhanced ultimate strength.

Circular hoops or spirals provide the most efficient confinement. Hoops or spirals with small spacing or pitch, respectively, compared to the centreline diameter of the hoop or spiral, $D_o = 2R_o$, may be considered as a tube of thickness $t = A_{sw}/s$, where A_{sw} is the cross-section of the tie or spiral and s its spacing or pitch. (Strictly speaking, the equivalent thickness is equal to $a_s t$, where a_s is the confinement effectiveness factor given by Eqs. (3.20a) and (3.20b) and which is close to 1.0 if s/D_o is small). Reacting to the tendency of the enclosed concrete core to dilate when it approaches its ultimate strength under axial compression, the hoop or spiral will develop a tensile stress σ_s and exert on the concrete core a radial (confining) pressure, p, related to σ_s as: $p = t\sigma_s/R_o$. The confining steel reaches its yield stress, f_{yw}, while the triaxially compressed concrete attains its enhanced ultimate strength. After yielding of the confining steel, $\sigma_s = f_{yw}$, the lateral pressure p remains constant. On this basis, confinement models, like those in Section 3.1.2.2, fitted to triaxial compression tests under constant value of p are considered to apply when the lateral pressure derives from transverse reinforcement. If this reinforcement is idealised as a tube of thickness t, the value of p (normalised to the unconfined concrete strength) to be used in these confinement models is:

$$\frac{p}{f_c} = 0.5\rho_w \frac{f_{yw}}{f_c} = 0.5\omega_w \tag{3.19}$$

Where $\omega_w = \rho_w f_{yw}/f_c$ is the mechanical volumetric ratio of the confining reinforcement, defined with respect to the volume of the concrete core to the centreline of the confining hoop or spiral: $\rho_w = (2\pi R_o)A_{sw}/(\pi {R_o}^2 s) = 2A_{sw}/sR_o = 2t/R_o$.

A circular hoop or spiral exerts its confining action on the concrete it surrounds not as a uniform pressure $p = t\sigma_s/R_o$, but as a radial force per unit length of the perimeter, $2\pi R_o$. The effect of this force is dispersed within the volume of the concrete core inside the hoop or the spiral. A convenient assumption for the dispersal of the confinement force was initially proposed by Sheikh and Uzumeri (1982) and extended by Mander et al. (1988). According to this assumption, the confinement force is dispersed following parabolic arcs defined within planes through the member axis (meridional planes) and spanning from one hoop (or intersection of the spiral with the meridional plane) to the next with tangents there at $\pm 45^\circ$ to the plane of the cross-section (see Fig. 3.12(a)). Any concrete outside these parabolic arcs is assumed as unconfined, like the concrete cover outside the hoop or spiral. The entire concrete volume inside these arcs is considered as uniformly confined.

For circular hoops, the minimum confined cross-sectional area along the member is mid-way between consecutive hoops. The apex of a parabolic arc is at a distance from the chord connecting its two ends equal to $0.5(s/2)\tan\alpha$, where α is the angle of the tangent to the parabola at each end with respect to the chord of the parabolic arc. For the assumptions in Sheikh and Uzumeri (1982) and Mander et al. (1988), $\alpha = 45^\circ$. The minimum confined cross-section has a diameter equal to $2(R_o - s/4) =$

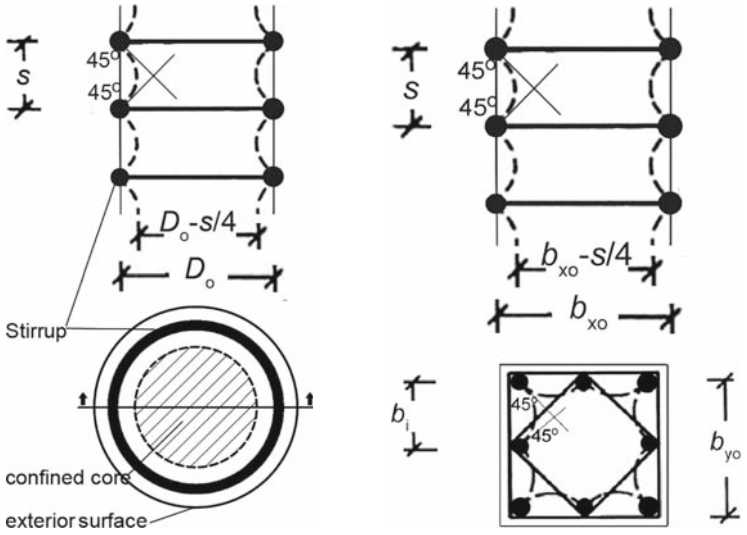

Fig. 3.12 Confined and unconfined parts over the cross-section and along a member with: (**a**) circular section and circular hoops; or (**b**) square section and multiple ties

D_o–$s/2$ and a cross-sectional area of $\pi(D_o–s/2)^2/4$, i.e. to the following fraction of the confined core defined by the centreline of the hoop:

$$a_s = \left(1 - \frac{s}{2D_o}\right)^2 \tag{3.20a}$$

If confinement is provided by a spiral, the model in Sheikh and Uzumeri (1982) and Mander et al. (1988) gives a constant confined cross-sectional area along the member. This area is circular with the ends of its diameter defined as follows:

- One end is at the apex of the parabolic arc extending between consecutive points of intersection of a meridional plane with the spiral.
- The other end is at the intersection of the same meridional plane with the spiral itself.

Then the diameter of the confined area is equal to $D_o–s/4$, where s is now the pitch of the spiral. Therefore, the confined area is equal to the following fraction of the cross-sectional area inside the centreline of the spiral:

$$a_s = \left(1 - \frac{s}{4D_o}\right)^2 \approx 1 - \frac{s}{2D_o} \tag{3.20b}$$

In rectangular sections confinement is normally provided by rectangular ties. If the centreline dimensions of the tie are b_{xo} and b_{yo} (Fig. 3.12(b)) the same reasoning gives a minimum confined cross-sectional area mid-way between consecutive ties with area equal to the following fraction of the cross-section area inside the tie centreline:

$$a_s = \left(1 - \frac{s}{2b_{xo}}\right)\left(1 - \frac{s}{2b_{yo}}\right) \tag{3.20c}$$

Circular hoops or spirals exert radial confining forces all along the perimeter. By contrast, straight stirrup legs along the perimeter do not develop any confining action, because the tendency of concrete to dilate when its stress approaches its ultimate strength causes these legs to bend outwards. The confining force exerted by a unit length of a stirrup bent to a radius of curvature equal to R is $A_{sw}\sigma_s/R$, where A_{sw} is the stirrup cross-section area and σ_s its tensile stress. This force is negligible, until eventually outwards bending of the straight stirrup leg reduces its radius of curvature, R, to a value of the order of the cross-sectional dimensions. But then it may be too late for the concrete. So, rectangular or polygonal stirrups are considered to exert concentrated confining forces on the concrete inside, only:

- at the corners, and
- wherever outwards bending of their straight legs is prevented by the hook of a cross-tie, well anchored within the concrete volume (the end hooks of intermediate single-legged cross-ties normally engage opposite sides of a perimeter tie).

Normally every stirrup corner or any intermediate point of the perimeter tie laterally restrained by a cross-tie hook engages also a longitudinal bar with much larger diameter than the stirrup itself. This bar plays an important role for the dipersal of the confining force concentrated there to the volume of the concrete core. The dispersal model in Sheikh and Uzumeri (1982) and Mander et al. (1988) is used also to separate the unconfined from the fully confined part inside the cross-section where the stirrup lies. The unconfined part is the one outside parabolic arcs connecting consecutive stirrup corners or points laterally restrained by a cross-tie hook, and the fully confined part is that inside these arcs. The apex of each parabolic arc is at a distance $b_i \tan\alpha/4$ from the chord connecting its two ends, where b_i is the length of this chord along the perimeter and α the angle between the chord and the tangent of the arc at each end, taken as $\alpha = 45^\circ$ according to Sheikh and Uzumeri (1982) and Mander et al. (1988). The area enclosed by the arc and its chord of length b_i is equal to their distance at the apex times $2b_i/3$, i.e. to ${b_i}^2/6$. So, the confined part of the cross-section at the level of a rectangular stirrup with centreline dimensions b_{xo} and b_{yo} is equal to the following fraction of the area enclosed by the centreline of the stirrup:

$$a_n = 1 - \frac{\sum {b_i}^2/6}{b_{xo} b_{yo}} \tag{3.21}$$

Circular hoops or spirals provide confinement all along their perimeter, so the counterpart of Eq. (3.21) is:

$$a_n = 1 \tag{3.22}$$

Rectangular columns or beams have a closed perimeter stirrup providing confinement only at its corners. Columns of earthquake resistant buildings designed for ductility are required by codes to have intermediate longitudinal bars engaged by a stirrup corner or cross-tie hook not further apart than a specified maximum spacing (of the order of 150–250 mm, see Table 5.2 in Chapter 5 for Eurocode 8). As a matter of fact, for buildings of Ductility Class M or H Eurocode 8 requires (for other reasons) a least one intermediate bar between adjacent corners of a column section, but does not impose engaging such bars with a cross-tie hook. Lateral restraint of intermediate bars is provided by cross-ties engaging two intermediate bars at opposite sides of the cross-section, or, more commonly in large cross-sections, by intermediate closed stirrups engaging one bar at each stirrup corner. A tensile stress $\sigma_s = f_{yw}$ in all stirrup legs and cross-ties parallel to transverse direction x (or 2) that opposes the dilatation of a concrete that approaches its ultimate strength, produces an average compressive stress σ_2 in the concrete, computed from equilibrium as: $\sigma_2 b_{yo} = (\Sigma A_{swx}/s) f_y$, i.e. $\sigma_2/f_c = \rho_x f_{yw}/f_c$, where $(\Sigma A_{swx}/s)$ is the total cross-sectional area of all stirrup legs or cross-ties per unit length of the member parallel to transverse direction x, and $\rho_x = \Sigma A_{swx}/(s b_{yo})$ the geometric ratio of transverse reinforcement in that direction. Similarly in the other transverse direction y (or 3): $\sigma_3/f_c = \rho_y f_{yw}/f_c$. If $\rho_x > \rho_y$ it is the value $p \approx (\sigma_2 + 4\sigma_3)/5$ that counts. It is simpler and safe-sided to consider that essentially the minimum of the two transverse reinforcement ratios controls confinement:

$$p/f_c \approx \min(\rho_x, \rho_y) f_{yw}/f_c = 0.5\omega_w \tag{3.19a}$$

where the volumetric ratio of confining reinforcement, ρ_w, referring to the volume of the confined concrete core inside the centreline of the perimeter stirrup, is not the real one, but that defined as:

$$\rho_w = 2\min(\rho_x, \rho_y) = 2\min(\Sigma A_{swx}/b_{yo}, \Sigma A_{swy}/b_{xo})/s \tag{3.23}$$

The mechanical volumetric ratio of confining reinforcement in Eq. (3.19a), $\omega_w = \rho_w f_{yw}/f_c$, derives from the fictitious volumetric ratio of confining reinforcement, ρ_w, given by Eq. (3.23).

Equations (3.19a) and (3.23) are similar to the one for confinement by circular hoops or spirals, Eq. (3.19), but applies only to cross-sections with stirrup legs or cross-ties parallel to the section sides. In (nearly) square columns (with $b_x \approx b_y$) with just one intermediate bar to be laterally restrained along each side, all four intermediate bars can be conveniently restrained at the same time by a diamond-shaped interior tie (Fig. 3.13 (a)). That tie enters in the calculation of ρ_x and ρ_y with its cross-sectional area A_{sw}, times $\sqrt{2}$. In that special case the value of ρ_w

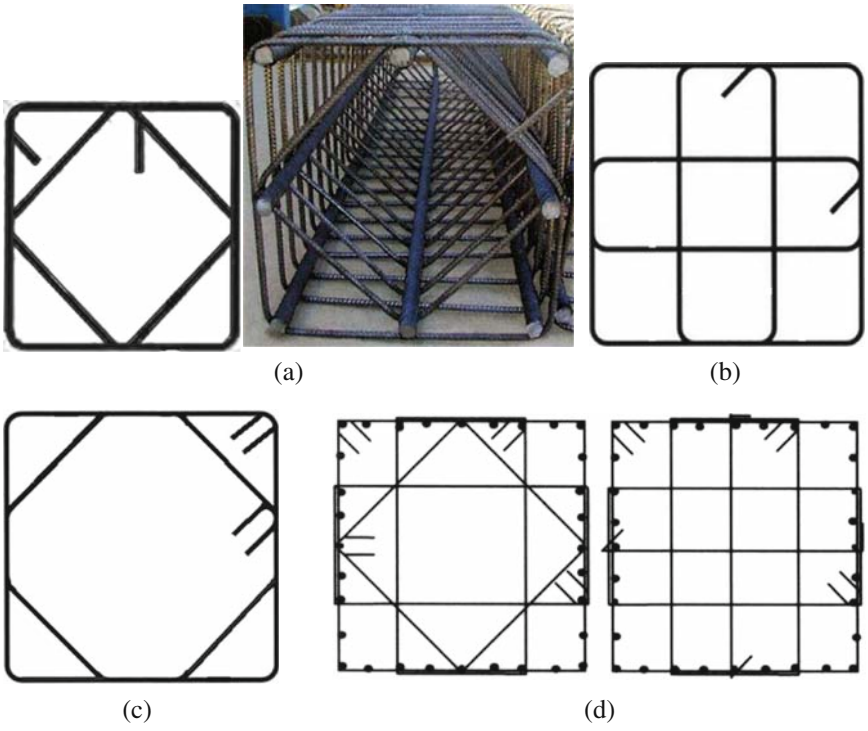

Fig. 3.13 Ties in square column engaging the four corner bars and (**a**) four mid-side bars; (**b**), (**c**) two intermediate bars per side; (**d**) three intermediate bars per side

coincides with the real volumetric ratio of confining reinforcement (volume of all tie legs, divided by the volume of confined core to the centreline of the perimeter tie). In a (nearly) square section with two intermediate bars that need lateral restraint along each side, it is cost-effective and convenient to employ a single octagonal interior tie engaging all eight intermediate bars (Fig. 3.13(c)), instead of two interior rectangular ties each engaging two pairs of intermediate bars at opposite sides of the section (Fig. 3.13(b)). The octagonal tie enters in the calculation of ρ_x and ρ_y with its cross-sectional area, A_{sw}, times $\sqrt{2}$ so, the volumetric ratio from Eq. (3.23) is slightly less than the real volumetric ratio of confining reinforcement. If all intermediate bars in a square column are laterally restrained by single-leg cross-ties, the outcome of Eq. (3.23) coincides with the real volumetric ratio of confining reinforcement. This is not the case anymore if interior rectangular ties engage each two pairs of intermediate bars at opposite sides of the section (Fig. 3.13(b) and (d)), because the legs of an interior tie on the perimeter do not count in Eq. (3.23).

Equations (3.21) and (3.22) express the confined fraction of the cross-section at the level of an individual stirrup, as a fraction of the area enclosed by the centreline of the perimeter stirrup. Equations (3.20) give the minimum confined area along the length of the member as a fraction of the confined area at the level of individual stirrups. Factors a_s and a_n may be considered as coefficients of confinement effectiveness along the member, or over the cross-section, respectively. The combined confinement effectiveness factor is the product:

$$a = a_n a_s \tag{3.24}$$

which gives the minimum confined cross-sectional area anywhere along the member, as a fraction of the area enclosed by the centreline of the perimeter stirrup or spiral (Fig. 3.12(b)).

Early work about the effect of confinement on the behaviour of concrete focused on the ultimate strength of columns under concentric compression. Under such loading the compression strength of the column is equal to that of its least confined cross section. If unconfined concrete does not exhaust its ultimate strain, ε_{cu}, before the confined concrete reaches its compressive strength, f_c^*, the ultimate compressive force of the column may be taken to be approximately equal to $(A_c + aKA_o)f_c$, where A_c is the area of the gross concrete section, A_o is the cross-sectional area enclosed by the centreline of the perimeter stirrup or spiral, a is the confinement effectiveness factor of Eq. (3.24) and K the strength enhancement factor in Eq. (3.4). It is often considered that just the concrete cover spalls-off before the confined concrete reaches its ultimate strength, f_c^*. Then the ultimate compressive load may be estimated as $aA_o f_c^*$, computed from Eq. (3.4) with the value of K multiplied times the confinement effectiveness factor of Eq. (3.24). As a matter of fact (Sheikh and Uzumeri 1982), that first introduced the concept of a confinement effectiveness factor essentially in the form of Eqs. (3.20), (3.21), (3.22) and (3.24), incorporates it in K as a multiplicative factor in Eq. (3.7).

If K is proportional to the confining pressure p (as, e.g., in the 1st term of the model of Eq. (3.8)), which in turn is proportional to the mechanical volumetric ratio of transverse reinforcement (see Eqs. (3.19) and (3.19a)), then a may multiply directly ω_w. However, this practice has been common even in models where K is nonlinear in p. In the Mander et al. (1988) model factors a_n and a_s multiply the transverse stresses σ_2 and σ_3. More specifically, for circular hoops or spirals a_s multiplies ω_w in Eq. (3.18); for rectangular ties a from Eq. (3.24) multiplies the mechanical stirrup ratios in the two transverse directions, $\omega_x = \rho_x f_{yw}/f_c$ and $\omega_y = \rho_y f_{yw}/f_c$, for the calculation of $\sigma_2/f_c = a\omega_x$, $\sigma_3/f_c = a\omega_y$. A similar approximation is common in the use of Eq. (3.5), which is also nonlinear in p. Unfortunately, this practice is carried over to the calculation of $\varepsilon_{co}{}^*$ through Eq. (3.10) and of $\varepsilon_{cu}{}^*$ through Eqs. (3.13) and (3.18). So, the common practice is to apply Eqs. (3.5), (3.6), (3.8), (3.13) and (3.18) with a value of p/f_c from Eqs. (3.19) or (3.19a) multiplied by a (which is equivalent to multiplying ω_w at the right-hand-side of Eqs. (3.19) and (3.19a) by a):

$$\frac{p}{f_c} = 0.5a\rho_w \frac{f_{yw}}{f_c} = 0.5a\omega_w \tag{3.25}$$

The same for Eqs. (3.16) and (3.17), but not for Eqs. (3.14) and (3.15).

The so resulting value of K is used then in Eqs. (3.4) and (3.10).

In earthquake resistant structures confinement is primarily of interest for the compression zone of members subjected to bending with or without axial force. A more meaningful measure of the effectiveness of confinement for a member with rectangular section subjected to bending in a plane parallel to side b_x, would involve a value of a modified as follows (see Fig. 3.14):

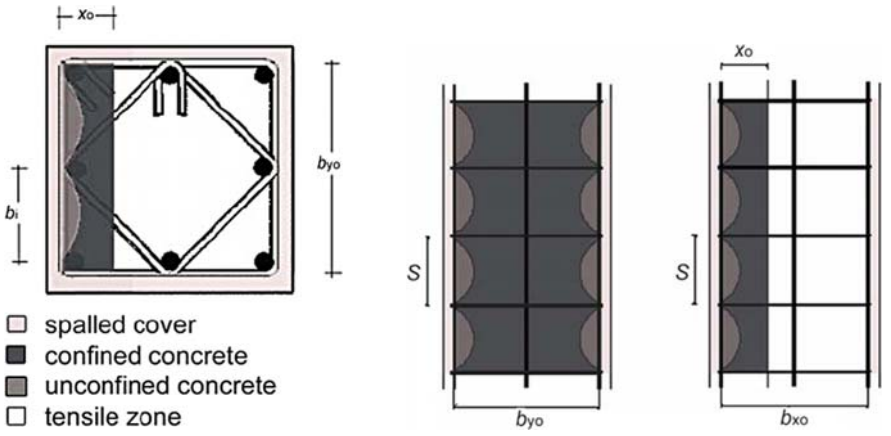

Fig. 3.14 Calculation of confinement effectiveness in the compression zone of the confined core of a member in flexure

- instead of the depth of the confined concrete core, $h_c = b_{xo}$, its neutral axis depth from the centreline of the perimeter stirrup, x_o, is used, calculated from the normalised neutral axis depth at ultimate conditions of the confined concrete core, ξ_{cu}, computed according to Section 3.2.2.4 under *Ultimate Curvature of the Confined Core, After Spalling of the Cover* and Flow Chart 3.2;
- the summation $\Sigma_i b_i^2$ in the numerator of the 2nd term of Eq. (3.21) extends over the external perimeter of the confined compression zone – i.e. from one intersection of the neutral axis with the centreline of the perimeter stirrup to the other intersection on the opposite side, excluding the neutral axis itself between these two intersection points;
- the 1st parenthesis at the right-hand-side of Eq. (3.20c) is replaced by $1–0.25s/x_o$, where s is the stirrup spacing.

The end result is a factor for the effectiveness of confinement of the compression zone:

$$a_x = \left(1 - \frac{s}{2b_{xo}}\right)\left(1 - \frac{s}{4x_o}\right)\left(1 - \frac{\sum b_i^2}{6x_o b_{yo}}\right) \tag{3.24a}$$

replacing a in Eq. (3.24).

The strong interaction between confinement of concrete and buckling of longitudinal bars, already noted in Section 3.1.1.2, is worth re-emphasising:

- Thanks to their flexural stiffness, longitudinal bars contribute to the confinement of the adjacent concrete, no matter that the model in Sheikh and Uzumeri (1982) and Mander et al. (1988) and Eqs. (3.20) and (3.21) derived from it discount this contribution. The confined concrete in turn exerts on these bars outwards pressures driving them toward buckling.
- Once they buckle outwards, longitudinal bars contribute little to confinement and to axial force resistance. Moreover, they may buckle over several tie spacings (see Fig. 3.4(b)), stretching the ties and diminishing their role for confinement. So, bar buckling may precipitate disintegration of the confined concrete core.

3.1.2.4 Confinement by FRP Wrapping

The columns of existing substandard buildings normally have widely spaced and/or poorly closed stirrups. Such stirrups provide little confinement, if at all. Confinement can be very conveniently provided a-posteriori by wrapping the end regions of columns where plastic hinges may form in Fibre-Reinforced-Polymers (FRPs) with fibres oriented (primarily) in the hoop direction of the section (see Section 6.8.3).

The lateral stress-axial strain response for the two most common Fibre-Reinforced-Polymers, notably carbon FRP (CFRP) and glass FRP (GFRP), is contrasted in Fig. 3.15(a) to that for confinement by steel. Being essentially linear-elastic, once activated by concrete that dilates after its unconfined ultimate strength

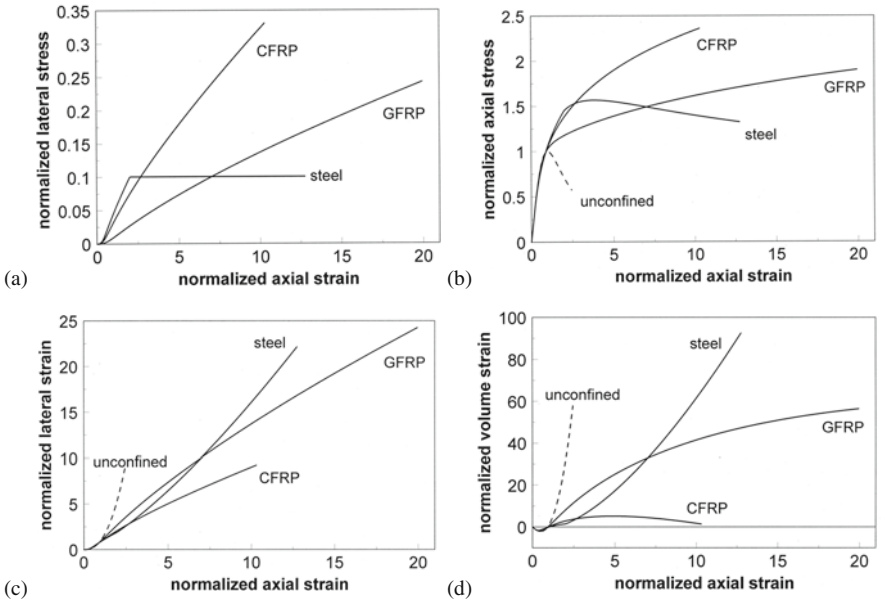

Fig. 3.15 Schematic behaviour of concrete confined with steel, CFRP or GFRP: (**a**) σ-ε curves of confining material, normalised to the yield stress and strain of steel; (**b**) axial σ-ε curves of confined concrete, normalised to the strength and the corresponding strain of unconfined concrete; (**c**) (**d**) lateral or volumetric strain v axial strain of confined concrete, normalised to the corresponding strains of unconfined concrete at ultimate strength (adapted from *fib* 2006)

is attained, the FRP provides an ever increasing confining pressure until it fractures in tension. So, unlike the σ-ε curve of concrete confined by ties which exhibits softening after the ultimate strength, those of FRP-wrapped concrete continue hardening until the FRP breaks (Fig. 3.15(b)). As shown in Fig. 3.15(c) and (d), after they yield steel ties lose effectiveness compared to CFRP, and later on to GFRP as well, in restraining the lateral and volumetric strains of concrete. As a matter of fact, as shown in Fig. 3.15(d), after the unconfined ultimate strength of concrete is exceeded, the restraint of its dilation by the large confining stiffness of CFRP can soon turn dilation into contraction (Teng and Lam 2004). Of course, for the σ-ε curve of confined concrete to be continuously ascending until rupture of the FRP, the FRP wrapping should have a minimum of tensile strength, $f_{\mathrm{fu}}t_{\mathrm{f}}$, and extensional stiffness, $E_{\mathrm{f}}t_{\mathrm{f}}$, with f_{fu} and E_{f} denoting the ultimate strength and Modulus of the FRP material and t_{f} the thickness of the FRP jacket (see Fig. 3.16 for FRP wrapping with large values of $f_{\mathrm{fu}}t_{\mathrm{f}}$ and $E_{\mathrm{f}}t_{\mathrm{f}}$). Otherwise, the confined concrete will soften after ultimate strength, as shown schematically in Fig. 3.16(b) for concrete wrapped with FRP having low values of $f_{\mathrm{fu}}t_{\mathrm{f}}$ and $E_{\mathrm{f}}t_{\mathrm{f}}$. According to Yan and Pantelides (2006, 2007), the transition from hardening to softening takes place when the value of $f_{\mathrm{fu}}t_{\mathrm{f}}/R$ drops below $0.2f_{\mathrm{c}}$.

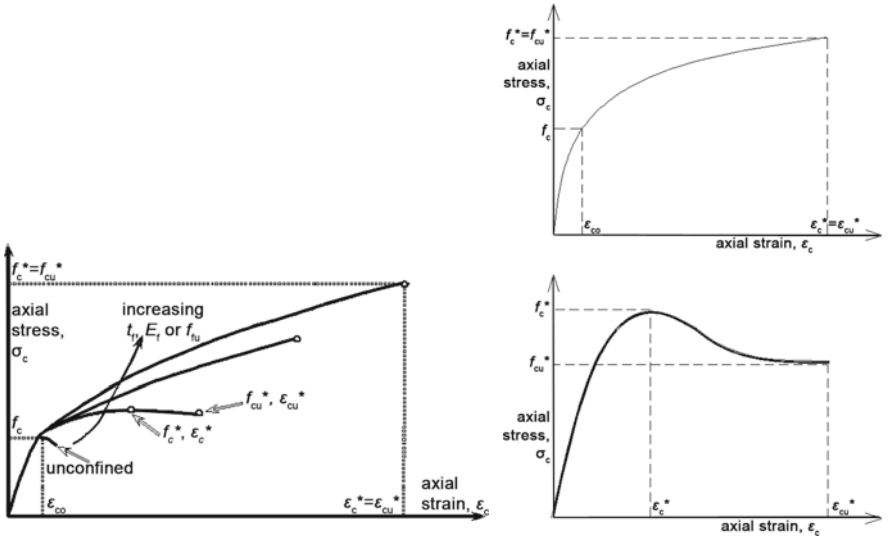

Fig. 3.16 Schematic axial σ-ε response of FRP-confined concrete (**a**) for increasing FRP strength, $f_{fu}t_f$, and stiffness, $E_f t_f$, (**b**) hardening (*top*) or softening (*bottom*) behaviour, for $f_{fu}t_f/R > 0.2f_c$ or $f_{fu}t_f/R < 0.2f_c$, respectively (adapted from Yan and Pantelides 2007)

The difference between the passive confinement offered by an elastic material, such as FRP, and an active one by a constant lateral pressure p was not recognised at the beginning. So, in the first publications that proposed and investigated the use of FRP to confine the concrete (Fardis and Khalili 1981, 1982), Eqs. (3.4) and (3.5) have been applied for the enhancement of the concrete strength. Equations (3.4), (3.7) and (3.10) were adopted for the same purpose when the subject was first revisited (Saadatmanesh et al. 1994) and later adopted in ACI Committee 440 (2002) too. All subsequent work avoided blind adoption of models of active confinement by a constant lateral pressure, p, such as those presented in Section 3.1.2.2 for concrete confined by steel ties. Models were custom-fitted, instead, to the stress-strain behaviour and the strength of FRP-confined concrete.

Research on the experimental behaviour of FRP-confined concrete under concentric compression and its modelling has been intense since the mid-1990s and will continue at least till the end of the first decade of the 20th century. In the absence of agreement within the research community about the models to be used in practice, the present section covers the subject at a greater length than warranted by its importance. Hopefully, the dust will soon settle and some of the following material will become redundant.

The ultimate strength and strain of confined concrete under concentric compression are controlled by the failure strain of the FRP in the hoop direction. It has recently emerged that the value of the effective ultimate hoop strain of the FRP, ε_{fu}, is a much more important factor for stress-strain and strength models

of FRP-confined concrete than the model itself. There is indeed strong experimental evidence that the full elongation at rupture of the FRP material, as measured in coupon tests, cannot be utilised for confinement. The FRP that confines concentrically compressed concrete fails when its hoop strain reaches a fraction of the ultimate elongation of tension coupons. In ACI Committee 440 (2002) this fraction is called efficiency factor and is given a value of 0.75 for rectangular members subjected to bending and shear (but with the value of the effective ultimate strain of FRP not to exceed 0.004), or of 1.0 for circular sections. In the light of current knowledge the values in ACI Committee 440 (2002) are high: values of the efficiency factor around 0.5 (Yan and Pantelides 2007, Toutanji et al. 2007, Fujikake et al. 2004), 0.6 (Lam and Teng 2003a,b, Tamužs et al. 2007, Tabbara and Karam 2007), or 0.85 just for AFRP (Lam and Teng 2003a,b) are more consistent with test results. It has also been found in Tabbara and Karam (2007) that models of active confinement by a constant lateral pressure, p, such as those presented in Section 3.1.2.2 for concrete confined by steel ties, can describe well the ultimate strength of FRP-confined concrete under concentric compression, provided that p is derived from the FRP geometric ratio $\rho_f = 2t_f/D$ as $p = \rho_f f_{fu}$, with the effective ultimate strength of FRP taken as $f_{fu} = E_f \varepsilon_{fu}$, where ε_{fu} is the effective, reduced ultimate hoop strain of the FRP and not the ultimate elongation of tension coupons. Finally, it has been demonstrated in Teng and Lam (2004) that σ-ε models for confined concrete agree much better to test results if they employ the measured ultimate hoop strain of the FRP, instead of a default value or the ultimate elongation of tension coupons. So, the reader should consider the statement in the second sentence of the present paragraph as well substantiated and should keep it in mind while going through the rest of this section.

The Spoelstra and Monti model in Spoelstra and Monti (1999):

$$\frac{f_c^*}{f_c} = 0.2 + 3\sqrt{\rho_f \frac{f_{fu}}{f_c}} \tag{3.26a}$$

$$\frac{\varepsilon_{cu}^*}{\varepsilon_{co}} = 2 + 1.25 \frac{E_c}{f_c} \varepsilon_{fu} \sqrt{\rho_f \frac{f_{fu}}{f_c}} \tag{3.26b}$$

applies to circular sections with diameter D, wrapped with FRP having a geometric ratio $\rho_f = 2t_f/D$ and effective ultimate strain ε_{fu}, giving an effective ultimate FRP strength $f_{fu} = E_f \varepsilon_{fu}$. Although widely quoted – notably *in fib* (2001, 2003) – the model has been recently found (Vintzileou and Panagiotidou 2007, Yan and Pantelides 2006, Tamužs et al. 2007, De Lorenzis and Tepfers 2001) to overestimate on average by about 5% the strength of confined concrete cylinders (via Eq. (3.26a)) and much more (by more than half) their ultimate strain (via Eq. (3.26b)). Moreover, it predicts that a very low level of confinement (with $\rho_f f_{fu}/f_c < 0.07$) reduces the strength below the unconfined value.

Among the widely known proposals so far, the model in Lam and Teng (2003a,b) has emerged from an independent comparison with the largest known database of FRP-confined concrete under concentric compression (Vintzileou and Panagiotidou

2007) as the most unbiased for ultimate strength and strain (with median value of experimental-to-predicted or predicted-to-experimental ratio within a few percent from 1.00), with acceptable overall scatter. Moreover, it is fairly complete: it provides the full hardening σ-ε law of circular or rectangular FRP-confined sections, giving at the limit the one of unconfined concrete. The σ-ε curve consists of a parabolic ascending branch followed by a linear one that intercepts (if extended) the stress axis at the unconfined concrete strength, f_c, and terminates to the following ultimate strength and strain point:

$$\frac{f_c^*}{f_c} = 1 + 3.3\left(\frac{b}{h}\right)^2 a_n \frac{\rho_f f_{fu}}{f_c} \tag{3.27a}$$

$$\frac{\varepsilon_{cu}^*}{\varepsilon_{co}} = 1.75 + 12\sqrt{\frac{h}{b}} a_n \frac{\rho_f f_{fu}}{f_c} \left(\frac{\varepsilon_{fu}}{\varepsilon_{co}}\right)^{0.45} \tag{3.27b}$$

The parabolic first branch merges into the linear one at the same slope $E_2 = (f_c^* - f_c)/\varepsilon_{cu}^*$ and at a strain equal to $2f_c/(E_c - E_2)$.

In Eqs. (3.27) b and h are the shorter and the longer of the two sides of the section ($b = h$ for circular sections). The confinement effectiveness factor, a_n, is given by Eq. (3.22) for circular sections and by Eq. (3.28) below for rectangular ones. On the basis of the measured hoop strains at failure of the FRP and the specimen, Lam and Teng (2003a,b) have concluded that the effective FRP ultimate strength, $f_{u,f}$, is equal to $f_{u,f} = E_f \varepsilon_{fu}$, where ε_{fu} is on average about equal to 60% of the failure strain of tensile coupons for CFRP and GFRP, or about 85% of the coupon failure strain for AFRP (for GFRP or AFRP these percentages were estimated from very limited data).

According to Lam and Teng (2003a,b), if $\rho_f f_{fu}/f_c < 0.07$, the strength enhancement in Eq. (3.27a) is neglected. However, this departure from Eq. (3.27a) may not be sufficient for the realistic description of the behaviour of concrete for low levels of FRP-confinement. In the model in Yan and Pantelides (2006, 2007) the expressions for ultimate strength and strain under hardening behaviour (i.e., for $f_{fu} t_f/R > 0.2 f_c$) are supplemented with rules for softening behaviour (with $f_{fu} t_f/R < 0.2 f_c$), namely with expressions giving both the ultimate strain point in Fig. 3.16, f_{cu}^*, ε_{cu}^*, and the peak or ultimate strength one, f_c^*, ε_c^*. That σ-ε model is more complete in this respect, but it has been fitted to limited data of tests carried out by its very proposers. So, till an independent assessment of its performance for a wider database of test results, the reader is referred to Yan and Pantelides (2006, 2007) for details.

An FRP jacket provides continuous confinement all along the length of its application around the member. So, the confinement effectiveness factor in that direction is $a_s = 1$ (cf. Eqs. (3.20) for confinement by steel ties).

Regarding the effectiveness of confinement by FRP within the section, for circular members the FRP jacket is fully effective all along the perimeter. So, the confinement effectiveness factor within the section is $a_n = 1$, as in circular steel hoops or spirals (cf. Eq. (3.22) for confinement by steel ties).

If the section is rectangular, the FRP jacket exerts confining forces only at the corners and not at all in-between (similar to a perimeter tie). Primarily to enhance the confinement effectiveness of the FRP jacket, but also to reduce stress concentrations in it at the corner that may cause premature rupture, the corner of the section is rounded into a quarter-circle of radius R before applying the FRP. Note that, when a sheet of fibre-reinforced fabric of thickness t is applied around such a corner, a strain of $\varepsilon = 0.5t/R$ is locked in at the expense of the ultimate strain capacity of the FRP. From this point of view, to achieve a target value of total tensile strength of the FRP in the circumferential direction of a rectangular section, a larger number of thin individual fibre-reinforced sheets – each with thickness t not more than a fraction of a millimetre – is preferable to fewer but thicker sheets.

In rectangular sections, confinement by the FRP jacket is fully effective right inside the rounded corners of the section. In-between the corners the parabolic arc model in Sheikh and Uzumeri (1982) and Mander et al. (1988) may be applied as in Fig. 3.17, giving in the end the following fraction of the original rectangular section as confined (CEN 2005a, *fib* 2001, 2003):

$$a_n = 1 - \frac{(b_x - 2R)^2 + (b_y - 2R)^2}{3b_x b_y} \tag{3.28}$$

The long exposé above refers exclusively to concentric compression. Strictly speaking it applies only in that case. It has been emphasised in Sections 3.1.2.2 and 3.1.2.3 that what matters for earthquake resistance is the compression zone of members subjected to cyclic flexure with or without axial load and notably the flexure-controlled ultimate deformation of the member,[4] conveniently expressed by the ultimate curvature of the section. By analogy to the development of Eqs. (3.16) and (3.17) in Section 3.1.2.2, the ultimate curvature, φ_u, is calculated from first principles according to the analysis in Section 3.2.2.4 modified to accept a parabolic-trapezoidal σ-ε curve for the confined concrete, instead of the parabolic-rectangular one used for unconfined concrete. In addition, the σ-ε model in Lam and Teng

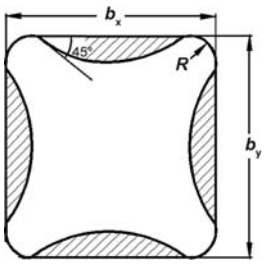

Fig. 3.17 Confinement of rectangular section by FRP jacket

[4]See footnote no. 1 in Section 3.1.1.2 for the definition of ultimate deformation (see also Section 3.2.2.7).

(2003a,b) is adopted, except that the ultimate strain, $\varepsilon_{cu}{}^*$, is determined for optimal fitting of available experimental results on φ_u of FRP-confined sections. It has been found that such a fitting is unbiased (i.e., good on average) and associated with acceptable scatter, if for cyclic loading Eq. (3.16b) is modified as follows for confinement by FRP (Biskinis and Fardis 2009):

$$\varepsilon_{cu}{}^* = 0.0035 + \left(\frac{10}{h}\right)^2 + 0.4a_n \min\left[0.5;\ \frac{\rho_f f_{u,f}}{f_c^*}\right] a_{eff\,,j} \tag{3.29}$$

where:

- h is the full section depth in the plane of bending, in mm;
- a_n is the confinement effectiveness factor of the FRP, equal to $a_n = 1$ for circular sections or given by Eq. (3.28) for rectangular ones;
- $\rho_f = 2t_f/b$ is the geometric ratio of the FRP in the direction of bending;
- $f_{fu} = E_f \varepsilon_{fu}$, with ε_{fu} as in Lam and Teng (2003a,b), i.e. about equal to 60% of the failure strain of tensile coupons; note that in Lam and Teng (2003a,b) this percentage value has been proposed only for CFRP or GFRP, while 85% was given for AFRP, but on the basis of limited test results;
- $a_{eff,j}$ is an additional effectiveness factor for the FRP jacket, expressing that its effectiveness is not proportional to the geometric ratio and stiffness of the FRP:

  - $$a_{eff,j} = 0.5\left(1 - \min\left[0.5;\ \frac{\rho_f f_{u,f}}{f_c^*}\right]\right) \quad \text{for CFRP, GFRP,} \tag{3.30a}$$
  - $$a_{eff\,,j} = 0.3\left(1 - \min\left[0.5;\ \frac{\rho_f f_{u,f}}{f_c^*}\right]\right) \quad \text{for AFRP} \tag{3.30b}$$

Section 3.2.3.10 under *Members with Continuous Bars* gives details about the outcome of the application of Eqs. (3.28), (3.29) and (3.30) for the estimation of the ultimate flexural deformation of FRP-wrapped members.

Note that, if the FRP provides relatively light confinement compared to the transverse reinforcement, the end section may survive rupture of the FRP jacket and reach subsequently a larger ultimate curvature controlled by the confined concrete core inside the stirrups, for which Section 3.1.2.2 applies.

3.1.2.5 Concrete Strength Requirements for Earthquake Resistant Buildings

Because the effect of concrete strength on member ductility and energy dissipation capacity seems to be beneficial in practically every respect (from the increase of bond and shear resistance, to the direct enhancement of deformation capacity), Eurocode 8 (CEN 2004a) sets a lower limit on the nominal cylindrical concrete strength in primary seismic elements, equal to 16 MPa (concrete class C16/20) in buildings of DC M, or 20 MPa (concrete class C20/25) in those of DC H. No upper bound is set on concrete strength, as there is no experimental evidence that the

lower apparent ductility of high strength concrete (due to which the values specified in Eurocode 2 for ε_{co} and ε_{cu} converge, from $\varepsilon_{co} = 0.002$ and $\varepsilon_{cu} = 0.0035$ for concrete class C50/60, to a single value of 0.0026 at C90/100) has any adverse effect on member ductility and energy dissipation capacity. The above lower limits on nominal concrete strength are consistent with the lowest concrete strengths currently used in buildings of the more seismic prone European countries.

3.1.3 Interaction Between Reinforcing Bars and Concrete

3.1.3.1 Cyclic Shear Transfer Along Cracks Crossed by Reinforcement

Cracks in concrete take place at right angles to the direction of a principal tensile stress. So, the crack plane is initially free of shear stresses. Owing to the change in the stress field during cyclic loading, shear stresses later develop along the crack plane. Due to such shear stresses one of the two faces of the crack tends to slip with respect to the other. Unless the shear is accompanied by stresses normal to the crack, slippage along the crack would be restrained only in the presence of reinforcing bars crossing the crack – at right angles or at an inclination. The magnitude of the slippage induced by a given shear stress (i.e., the effect of the crack on shear stiffness) and the maximum shear force that can be transferred along the crack (the shear resistance) depend on the diameter, spacing and inclination of the bars crossing the crack and the tensile stress already in them due to other reasons (i.e. at zero shear stress along the crack).

Rough cracks crossed by reinforcing bars can transfer shear by friction. In this "interface shear transfer" or "aggregate interlock" mechanism, the clamping force needed for the development of friction is provided by the reinforcing bars that cross the crack and depends on their total cross-sectional area, inclination with respect to the crack and tensile stress due to other reasons. These bars connect also the two faces of the crack as "dowels". Their effectiveness in this respect depends on their diameter (more than on their cross-sectional area) and on the minimum concrete cover in the direction of the shear stress on either side of the crack (or, if this cover is small, by the engagement of the bar acting as dowel by transverse reinforcement close to and almost parallel to the crack).

Significant shear forces can be transferred by aggregate interlock and dowel action under monotonic loading (see virgin loading branches in Figs. 3.18 and 3.19). However, both mechanisms are very sensitive to the cycling of the shear force and of the associated slip along the crack. Cycling of the slip polishes the crack faces and reduces the effectiveness of aggregate interlock. Bearing stresses under a bar acting as dowel may crush locally the concrete and open a "gap" that may need to be closed, for the bar to be re-engaged as a dowel in a subsequent load cycle. This is evident from the cyclic shear force (or stress) v slip behaviour depicted in Fig. 3.18 for aggregate interlock and in Fig. 3.19 for dowel action. In both cases (but especially for aggregate interlock) unloading-reloading loops have an inverted-S shape, with initially steep unloading and steep final reloading in the opposite direction.

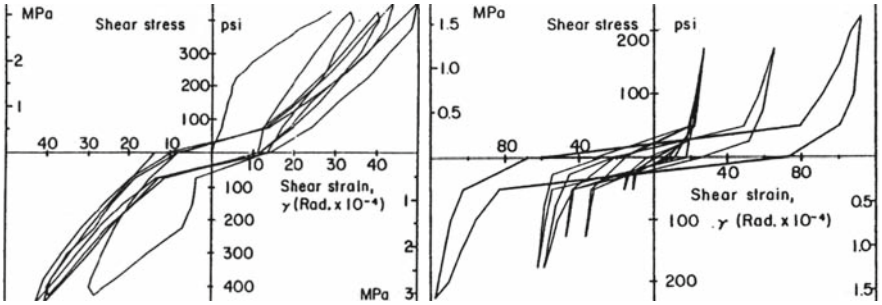

Fig. 3.18 Increase of slip in aggregate interlock for cycles of about constant shear stress amplitude, with the clamping reinforcement normal to the crack initially at: (**a**) zero tensile stress; or (**b**) 90% of yield stress (Perdikaris 1980)

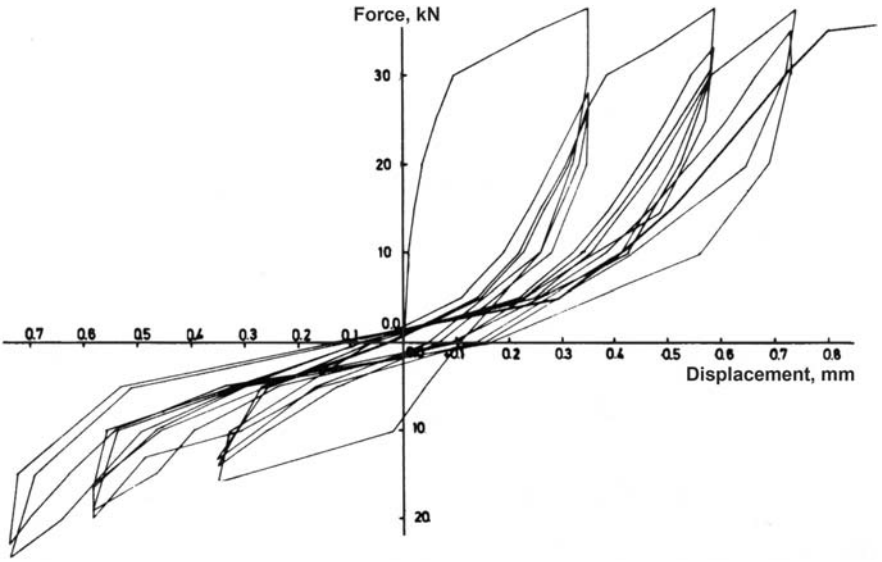

Fig. 3.19 Dowel force v slip loops for asymmetric cover of the dowel (adapted from Vintzeleou 1984)

In-between there is an intermediate phase of nearly unrestrained slippage, until hard contact of the two polished faces of the cracks resumes in the cases of Fig. 3.18, or till the bar bears against sound concrete again in that of Fig 3.18. Hysteresis loops are narrow (especially for aggregate interlock), dissipating very little energy.

Note that not only dowel action, but also shear transfer by aggregate interlock is a mechanism of concrete-steel interaction: the shear transfer by aggregate interlock is essentially a friction mechanism (Fardis and Buyukozturk 1979). For slippage to take place along a rough crack, asperities of one face have to ride over those on the opposite face. So the crack opens-up, stretching the reinforcement that crosses it.

The clamping force necessary for the friction is provided by compressive contact forces that develop between asperities of the crack faces as reaction to the tension that builds up in the reinforcement owing to the sliding and opening-up of the crack. Witness in Fig. 3.18(b) the detrimental effect of high initial tension in the clamping reinforcement on the cyclic resistance and stiffness of the aggregate interlock mechanism. Bars under high initial tension provide little clamping effect. Once they yield, almost unrestrained slippage takes place along the crack. Similar is the detrimental effect of a high tensile stress in a bar that acts as a dowel: the combination of this stress with the direct shear and bending stress due to dowel action precipitates generalised yielding of the bar in the vicinity of the crack, diminishing its resistance against further slippage. Therefore, the longitudinal bars in a plastic hinge of a concrete element, which are expected to yield during the seismic response, cannot contribute to interface shear transfer on the side.

The overall conclusion is that, under cyclic conditions the shear resistance and stiffness along cracks crossed by reinforcement degrades fast and offers practically no energy dissipation. So, one cannot rely on it for earthquake resistance.

3.1.3.2 Bond of Reinforcing Bars to Concrete

Smooth (plain) reinforcing bars were quite common until the mid-1960s (in the US) to the mid-1980s (in some European countries). Nowadays only ribbed (deformed) bars are used in concrete structures. Such bars are bonded to the surrounding concrete by bearing of their ribs against it. A characteristic parameter for the bond properties of a ribbed bar is its relative rib area, which is defined as the ratio of the projected area of the ribs on a plane normal to the bar axis to the lateral surface area of the bar – both per unit length of the bar – and is roughly equal to the rib height-to-distance ratio. A relative rib area value typical of turn-of-the-century European production is around 0.06. Doubling it to 0.12 improves the bond by just 10% (Cairns 2006). For such values of the relative rib area, bond failure along bars or laps having clear cover or clear mid-distance to the nearest anchored bar or lap less than about three bar-diameters normally is in the form of concrete splitting along planes through the axis of the bar(s), as in Figs. 3.20 and 3.21. Splitting is caused by the circumferential tensile stress that develops in the concrete due to the bursting action of the radial component of the bearing forces exerted by the ribs on the concrete. For typical configurations of the surface of the ribs, the bursting radial component is in the order of 25% of the longitudinal one (i.e., of the bond force).

Bond resistance drops rather rapidly after splitting, as the slip of the bar with respect to the surrounding concrete increases. Transverse reinforcement intercepting the potential splitting crack(s), and/or transverse pressure on the bar – be it active, due to external forces, or passive, thanks to confinement – delay splitting and reduce the drop in bond resistance it entails; they can even prevent splitting. Splitting can also be prevented if the clear cover and the clear mid-distance to the nearest anchored bar or lap are fairly large (at least three bar-diameters, for no transverse reinforcement or pressure). If in such cases bond failure ultimately takes place, it

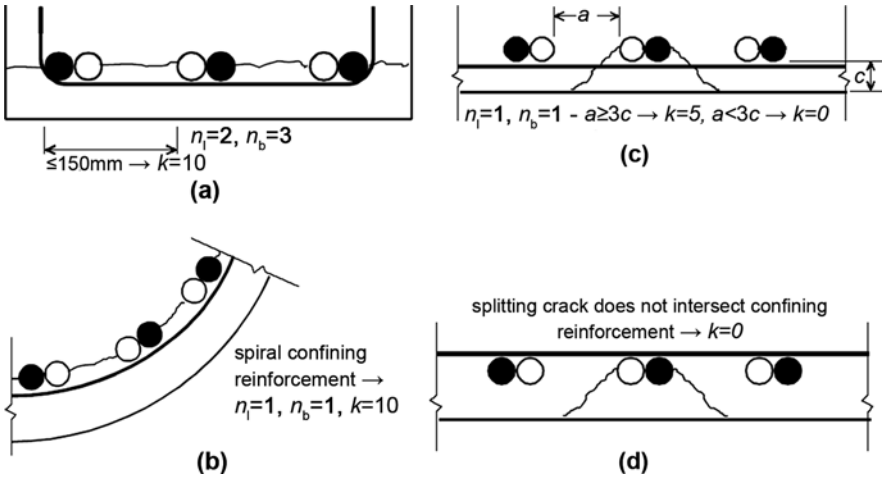

Fig. 3.20 Splitting failures of lapped bars, with definition of *k*-factor in Eq. (3.31) and of the number of bars or stirrup legs in Eq. (3.32) (adapted from Eligehausen and Lettow 2007)

has the form of bar pull-out (or -through) by shearing of the concrete around the bar or the lap, all along a surface through the tops of the ribs. This failure mode is far less brittle than by splitting: bond resistance is almost fully maintained until the bar travels nearly the full clear distance between successive ribs – about 80% of the bar diameter (Cairns 2006) – fully crushing the concrete between them.

Design codes consider bond as a uniform shear stress over the lateral surface of the bar. To determine the minimum required length of anchorages or lap splices they specify the design value of the ultimate bond stress, f_{bd}, considering it as a material property.[5] In Eurocode 2 (CEN 2004b) and hence in Eurocode 8 (CEN 2004a) as well, f_{bd} is taken as 2.25 times the design value of concrete tensile strength, $f_{ctd} = f_{ctk,0.05}/\gamma_c = 0.7 f_{ctm}/\gamma_c$, where γ_c is the partial factor for concrete and indices k, 0.05 and m to f_{ct} denote the lower characteristic and the mean value, respectively. These Eurocode 2 values of f_{bd} apply for "good" bond conditions, i.e. if the bar:

- is at an angle more than 45° to the horizontal; or
- is not more than 250 mm from the bottom of the concrete layer cast; or
- is at least 300 mm from the top surface of the concrete layer cast.

For all other positions of the bar during casting, bond conditions are considered as "poor", owing to the effects of laitance and consolidation of concrete during

[5] As we will see shortly, the concept of bond strength as a property of the concrete for given relative rib area and position of the bar with respect to casting, albeit convenient, is not representative of reality.

Fig. 3.21 Splitting cracks along corner bars due to bond

compaction. The Eurocode 2 value of f_{bd} for "poor" bond conditions is 70% of that applying under "good" conditions (CEN 2004b). So, f_{bd} is finally equal to $0.315{f_{ck}}^{2/3}$ for "good" bond conditions, or to $0.22{f_{ck}}^{2/3}$ for "poor" conditions (with f_{ck} in MPa) and for the recommended value of the partial factor for concrete $\gamma_c = 1.5$. For f_{ck} between 16 and 30 MPa, the value of f_{bd} is from 2 to 4.3 MPa under "good" bond conditions and from 1.4 to 3 MPa for "poor" conditions.

The code-specified value of f_{bd} is meant to correspond not to the real ultimate bond stress, but to the monotonic bond stress causing a slip between the bar and the surrounding concrete about equal to 0.1 mm. According to the CEB/FIP Model Code 90 (CEB 1991), the real ultimate monotonic bond stress of ribbed bars

corresponds to a slip of $s = 0.6$ mm. In unconfined concrete the ultimate bond stress in CEB (1991) is about equal to $2\sqrt{f_c}$ (units: in MPa) for "good" bond conditions, or to $\sqrt{f_c}$ for "poor" (not incorporating the partial factor γ_c). For f_c from 16 to 50, the CEB/FIP Model Code 90 ultimate bond stress ranges from 8 to 14 MPa in the former case, or from 4 to 7 MPa in the later. According to more recent results (Huang et al. 1996, Oh and Kim 2007) the ultimate monotonic bond stress along elastic ribbed bars occurs at a bond slip of about 1 mm and is higher than the CEB/FIP Model Code 90 value. In Huang et al. (1996) it was found equal to $0.45f_c$ for "good" bond conditions (i.e., between 7.2 and 22.5 MPa, for f_c from 16 to 50 MPa) and to half that value ($0.225f_c$) for "poor" conditions. In Oh and Kim (2007) the ultimate monotonic bond stress (in MPa) was found equal to $2.5{f_c}^{0.6}$ (f_c in MPa) for "good" bond conditions (i.e., between 13 and 26 MPa, for f_c from 16 to 50 MPa).

Once the bar yields, the ultimate bond stress drops by about 80%, giving in the end values of the ultimate monotonic bond stress in the range of those specified by Eurocodes 2 and 8 and incorporating a partial factor $\gamma_c = 1.5$.

Bond stress reduces gradually with increasing slip, after the real ultimate value is reached, ending up at a very low residual value of about 15% of the ultimate stress, or even less if there is little confinement.

The values quoted above for the bond resistance in unconfined concrete are for splitting failure. For bond failure by pull-out (or -through) it is considered that the above quoted ultimate stress values increase by at least 25% and the residual strength to about 40% of the ultimate stress. As noted at the beginning of this section, the slip for which the ultimate stress is retained before residual strength is reached is of the order of the bar diameter.

The slip that accompanies bond stresses is irreversible, because it is due to local micro-crushing of concrete against which the ribs of the bar bear. So, the residual slip after unloading to zero bond stress is about equal to the peak slip attained. Repeated loading, with the bond stress cycling without reversal between zero and a peak value (as in bridges due to traffic loads) produces a gradual increase in slip, similar to the accumulation of concrete strains in the right-hand part of Fig. 3.10. However, unless the cumulative slip exceeds the value of (about) 1 mm associated with the peak stress of the monotonic bond-slip curve, the ultimate monotonic bond stress is not adversely affected by any previous cycles at lower bond stress levels and is available in case of subsequent loading up to ultimate stress (Oh and Kim 2007).

The apparent conclusion from the above is that the value of the design bond stress used for the design of anchorages and splices is but a small fraction of the real ultimate stress. It is indeed about equal to the residual bond strength attained well beyond the ultimate bond strength. However, what appears under monotonic or repeated loading as a wide safety margin, is necessary in earthquake resistant structures, because reversal and full cycling of the bond stress causes a large drop in the effective bond strength and stiffness (Balázs 1991). This is evident from the test results in Fig. 3.22, showing that for constant amplitude cycling of bond stress the slip gradually increases. Hysteresis loops are narrow and pinched, dissipating very little energy. The inverted-S shape of the loops is due to:

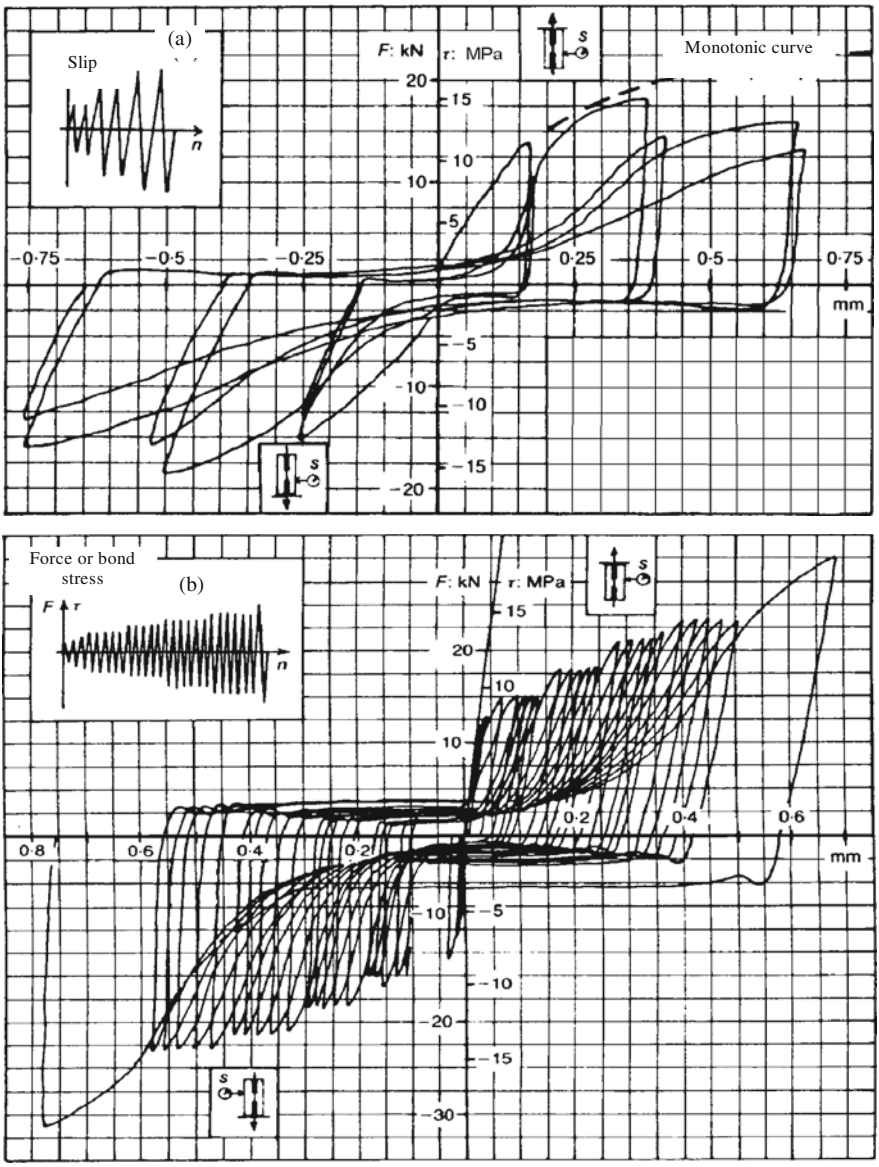

Fig. 3.22 Bond stress v slip behaviour under cyclic loading in concrete with $f_c = 25$ MPa (adapted from Balázs 1989)

- the abrupt release of the bond stress upon reversal, with no recovery of the slip;
- the almost unstrained slippage of the bar until hard contact of the ribs with sound concrete beyond the locally crushed volume of concrete, and
- the resistance of the newly contacted concrete to deformation.

Such a shape of hysteresis loops suggests that the behaviour is controlled by friction and sliding, as in aggregate interlock. The underlying mechanism is the gradual disintegration of the volume of concrete on which the ribs bear. Microcracks starting from the area of contact extend and join up with those that have formed during loading in the opposite direction.

If sufficient anchorage or lap splice length is provided, the peak bond stress demand is low and accumulation of slip as in Fig. 3.22 is limited. Moreover, seismic loading does not cause full reversals of bond stress at bar anchorages or lap splices. During the half-cycle that induces compression in the anchored or spliced bar the bond demand is reduced, as the bar shares the compressive force with the concrete around it and transfers part of its own share through bearing of its end. In buildings designed for earthquake resistance it is generally easy to keep the peak bond stress demand low, except along the length of the bar within beam-column joints. Bond stress along that length reverses fully during seismic loading, while the joint size is normally insufficient for the full anchorage length to develop (see Section 3.3.2). Moreover, the top bars of the beams framing into a joint may have yielded at its face and developed already significant inelastic deformations (see Fig. 3.7). Just inside the face of the joint tensile stresses and strains in the bar are lower, but still rather high and most likely beyond yielding. As bar slippage with respect to the surrounding concrete is equal to the integral of the steel strains along the bar (minus the normally negligible tensile strains in any still uncracked concrete), large tensile strains in the bar imply also large slippage. This in turn means that the bond stress conditions at that point of the bar will be at the tail of the monotonic bond-slip relation, where bond resistance has dropped to low values. As a result, relatively high bond stresses can develop only well inside the joint, where the concrete around the bars is well confined and can sustain high bond stress with very little slippage of the bar. So, anchorage takes place only in the core of the joint which is confined by the stirrups. Outside this core the bond is not sufficient for the reduction of the tensile stress in the bar below the yield value. For this reason, the outermost length of bars within joints, in the order of a few bar diameters, is called "yield penetration depth" (see Section 3.2.2.9 and Eqs. (3.63) there).

Implicit in the concept of ultimate bond stress as a concrete property (for given relative rib area and position of the bar with respect to casting) is the notion that the maximum force that can be transferred by bond from a bar to the surrounding concrete is equal to the ultimate bond stress times the lateral surface area of the bar within the length, l_b, available for force transfer by bond (i.e., l_b times the perimeter of the bar, πd_b). So, this force, and hence the maximum tensile stress in the bar that can be transferred by bond, are taken as proportional to l_b. Moreover, design codes consider that force transfer by bond through the concrete from the straight end of a bar to that of a nearby parallel one for lap-splicing is one-sided and hence less effective than the force transfer from the straight end of a terminating bar to the concrete. In Eurocode 2 (CEN 2004b) the loss in effectiveness ranges from 0 to 50%, if the lap-splicing of less than 25% to more than 50%, respectively, of the total cross-sectional area of the bars overlaps along the member.

In the context of the conventional wisdom above (Darwin et al. 2002a,b) overviewed several empirical expressions developed in the USA – ACI Committee 408 (2001) included – for the minimum length l_b required for full anchorage or lap-splicing of straight ribbed bars. They evaluated also these expressions on the basis of available test results on bond and anchorage. The bias (deviation in the mean) for 325 tests ranges from 12 to 24% and the coefficient of variation about the biased mean from 13 to 29%.

Against this background (Eligehausen and Lettow 2007) departed from the conventional wisdom of a maximum bar tensile stress that can be transferred by bond which is proportional to l_b and fitted a model to the largest available experimental database, comprising more than 800 tests for anchorage or lap-splicing of straight ribbed bars. According to this most complete and accurate model in the current State-of-the-Art, in "good" bond conditions the maximum possible tensile stress that such a bar can develop, f_{sm}, at a straight distance l_b from its end is about the same, no matter whether the bar is anchored or lap-spliced with a parallel bar (for clear distance of the two bars not more than $4d_b$). Its expected value is equal to:

$$f_{sm}(MPa) = 51.2 \left(\frac{l_b}{d_b}\right)^{0.55} \left(\frac{f_c(MPa)}{20}\right)^{0.25} \left(\frac{20}{\max(d_b; 20\,mm)}\right)^{0.2} \left[\left(\frac{c_d}{d_b}\right)^{1/3} \left(\frac{c_{\max}}{c_d}\right)^{0.1} + kK_{tr} + 0.2p(MPa)\right] \leq f_y \tag{3.31}$$

where:

- d_b: bar diameter;
- $c_d = \min$ [min$c$; a/2], limited in the range of d_b/2–3d_b (see Fig. 3.23),
- $c_{\max} = \max$ [max$c$; a/2], with an upper limit of $5c_d$, where:
  - min$c$ and max$c$ are the minimum and the maximum, respectively, clear cover of the anchored or lap-spliced bars (see Fig. 3.23), and
  - a is the clear distance between anchored bars or pairs of lapped bars (see Fig. 3.23);

$$K_{tr} = \frac{1}{n_b d_b} \frac{n_l A_{sh}}{s_h} \leq 0.04 \tag{3.32}$$

is the total cross-sectional area of reinforcement placed within the length l_b transverse to the axis of the anchored or lap-spliced bars and crossing the potential splitting crack, divided by $n_b d_b l_b$; in Eq. (3.32):

- n_b: number of anchored bars or pairs of lapped bars on the plane of the potential splitting crack that reaches the concrete surface;
- $n_l A_{sh}/s_h$: total cross-sectional area of legs of transverse reinforcement crossing the splitting crack, per unit length of the lapped or anchored bar;

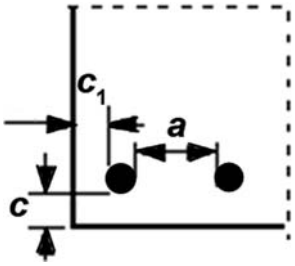

Fig. 3.23 Definition of bar distances for Eq. (3.31) ($c_d = \min[a/2; c_1; c] \geq d_b$, $c_d \leq 3d_b$, $c_{max} = \max[a/2; c_1; c] \leq 5d_b$)

Figure 3.20 shows examples of n_b and n_l from Cairns (2006).

– k = effectiveness factor, with the following values:

  - $k = 10$, if the legs of transverse reinforcement are at right angles to the splitting plane (provided that the clear distance of all anchored bars or pairs of lapped bars from the point where a leg of transverse reinforcement intersects a splitting crack is less than 150 mm, see Fig. 3.20(a)), or in circular sections with a circular perimeter tie or spiral reinforcement, where the splitting crack may either extend from the bar at right angles to the surface or develop between the bars parallel to the perimeter (Fig. 3.20(b));
  - $k = 5$, if the potential splitting extends from the bar to the surface and is crossed by a straight leg of transverse reinforcement placed within the cover, provided that the clear distance between anchored bars or pairs of lapped bars is not less than three-times the cover (Fig. 3.20(c));
  - $k = 0$, in all other cases (Fig. 3.20(c) and (d));

– p = "active" confining pressure normal to the axis of the anchored or lapped bars due to external actions (e.g., a load applied to the surface of the member) or their effects (e.g., the axial load of a column); the mean value of p across the section of the member in the plane of the bar is used.

Implicit in Eq. (3.32) is a tensile stress in the transverse reinforcement equal to the tensile strength of concrete, f_{ct}, times the ratio of Moduli, E_s/E_c. This is because the role of this reinforcement is to prevent cracking, not to make up for it. If splitting failure nonetheless does occur, the yield stress of transverse reinforcement may be mobilised to the benefit of the post-ultimate residual strength.

Equation (3.31) refers to splitting failure of bond along ribbed straight bars in tension. Its applicability is defined by the range of parameters in the tests to which it has been fitted in Eligehausen and Lettow (2007): f_c from 10 to 117 MPa, relative rib area between 0.05 and 0.07, l_b not less than $12d_b$, minimum clear cover at least $0.5d_b$ but not more than $3d_b$ and clear distance between anchored bars or pairs of lapped bars at least d_b. The coefficient of variation of the fitting is about 15%. The data show that, for given values of the parameters at the right-hand side of Eq. (3.31), the experimental value of f_{sm} is on average about 5% larger for anchored bars than for lap-splices, irrespective of the number of bars anchored or lapped at the same

location. The difference may be neglected as statistically insignificant (Eligehausen and Lettow 2007).

For the pull-out (or -through) mode of failure, Eq. (3.31) may still be applied, with the confinement terms (1st and 2nd one in the last, bracketed term) replaced by an upper limit value of 2.0.

If anchorage or lapping of ribbed bars in tension is supplemented with a hook, a bend or an anchor plate at the end, or by welding to a transverse bar, then the anchor force developed by these additional means, divided by the bar cross-sectional area is added to the right-hand-side of Eq. (3.31).

Anchorage or lapping of ribbed straight bars in compression is assisted by bar end bearing. Provided that the cover of the end in the direction of the bar axis is at least $2d_b$, the contribution of end bearing may be taken into account by adding to the right-hand-side of Eq. (3.31) the product of $3f_c$ and of the confinement term (the last, bracketed one in Eq. (3.31)) (Cairns 2006). That term can be taken equal to 2, if the bar end bears against a volume of very well confined concrete (e.g., at the tip of a column bar bearing on the top surface of the floor slab).

FRP wrapping of the member over at least the full length l_b contributes to confinement. In that case the following value of kK_{tr} may be used in Eq. (3.31) (Biskinis and Fardis 2007, 2008):

$$kK_{tr} = \frac{1}{n_b d_b}\left(\frac{k_s n_l A_{sh}}{s_h} + \frac{k_f n_f t_f E_f}{E_s}\right) \tag{3.32a}$$

where t_f: total thickness of fibre sheets in the wrapping; E_f: Modulus of the fibre material; k_s: effectiveness factor of transverse steel (the k of Eq. (3.31) and Fig. 3.20); n_f: number of FRP wraps intersected by a potential splitting crack to the surface and k_f: their effectiveness factor. For example, if the members in Fig. 3.20 are wrapped with FRP, then: for Fig. 3.20(a) $n_f = 2$, $k_f = 10$; for Fig. 3.20(b) $n_f = 1$, $k_f = 10$; for Fig. 3.20(c) and (d) $n_f = 1$ with $k_f = 5$ if $a \geq 3c$ or $k_f = 0$ if $a < 3c$.

3.1.4 Concluding Remarks on the Behaviour of Concrete Materials and Their Interaction Under Cyclic Loading

As pointed out in Section 1.3.6.1, of the two constituent materials of structural concrete, only steel is inherently ductile, with stable hysteresis loops and considerable energy dissipation capacity up to very large deformations. And that only in tension, as reinforcing bars may buckle in compression, shedding their force resistance and risking subsequent fracture. Concrete is fairly brittle, but when it is well confined it can sustain cycles of large compressive strains without appreciable drop in resistance. Confined concrete, however, cannot dissipate significant energy by itself in compressive stress cycles.

Under cyclic loading, the transfer of shear along cracks and the bond between reinforcing bars and concrete are characterised by rapid degradation of resistance

with cycling and little energy dissipation. The first of these mechanisms should not be relied upon at all, whereas bond should be kept in the elastic range, possibly through confinement.

The only way to dissipate significant energy during large amplitude deformation cycles is by combining:

- reinforcing steel in the direction where tensile internal forces and stresses are expected to develop; and
- concrete and reinforcement in the direction of compressive internal forces and stresses, provided that closely spaced ties confine the concrete and restrain the bars against buckling.

It is clear that this is feasible wherever in the member inelastic stresses and strains invariably develop in the directions where reinforcement can be conveniently placed. In essentially one-dimensional members, such as beams, columns and slender walls, it is convenient to place the reinforcement in the longitudinal and the (two) transverse direction(s). So concrete members can be designed to develop large inelastic deformations and reliably dissipate significant energy, only in their regions dominated by flexure (with or without axial load). These regions lend themselves to effective use of reinforcing bars to take up directly the tension and to restrain concrete and compression steel exactly at right angles to their compression stresses. Even there energy dissipation takes place primarily – essentially only – in the reinforcement and not in the confined concrete.

3.2 Concrete Members

This part of Chapter 3 deals with the behaviour of individual members subjected to cyclic flexure and shear of the type induced by seismic actions. Member types considered are those commonly used in earthquake resistant concrete buildings, notably prismatic members with rectangular, L- or T-section. Connections between such members are addressed at the end of the chapter.

3.2.1 The Mechanisms of Force Transfer in Concrete Members: Flexure, Shear and Bond

In prismatic concrete members, such as beams or columns, it is convenient to work with the centroidal member axis, x, and with cross-sections normal to it, and with the resultant force and moments of the normal stresses acting on the section (normal force N, bending moments M_y, M_z with respect to the centroidal principal axes y and z of the cross section, respectively) and of the shear stresses acting on it (shear forces V_y, V_z parallel to axes y, z, respectively, torsional moment T with respect to axis x). It is then convenient to distinguish the "flexural" deformations as those attributed

mainly to N, M_y and M_z and computed on the basis of the Navier-Bernoulli hypothesis of plane sections remaining plane and normal to the x axis. Shear forces cause additional ("shear") deformations, which can be computed by relaxing the Navier-Bernoulli assumption to allow cross-sections not to remain normal to the axis, while they still remain plane. Interaction effects, i.e. the influence of shear forces on flexural deformations and that of normal stress resultants on shear deformations, are important in general and cannot be neglected, especially for inelastic cyclic loading. However, if the bending moment is relatively high and the shear force low, flexural deformations not only dominate, but can also be computed in good approximation neglecting the influence of shear forces. The controlling factor is the shear span ratio, M/Vh, defined as the ratio of the shear span, $L_s = M/V$, at the end of the member where flexural yielding is expected, to the depth h of the cross-section within the plane of bending. Indeed, even within the framework of linear elasticity, the ratio of the maximum normal stress parallel to the member axis, $\sigma_{x,max} = M/W$, to the maximum value of the shear stress, $\tau_{xy,max} = 1.5V/A$, in a rectangular cross-section under uniaxial bending and shear, is equal to: $\frac{\sigma_{x,max}}{\tau_{xy,max}} = 4\frac{M}{Vh}$. So, even in the context of linear elasticity, the lower the shear span ratio, L_s/h, the more important are the shear stresses vis-à-vis the normal ones.

Beams, columns and slender walls commonly have values of shear span ratio above (about) 2.5. For such values of L_s/h the mechanisms of force transfer by flexure (i.e. through forces and stresses parallel to the member axis) or shear (i.e. via forces or stresses at right angles to the member axis) may be considered as practically uncoupled and independent. If L_s/h is less than (about) 2.5, as in squat walls or columns and in short beams, these two mechanisms of force transfer tend to merge, as the shear span itself becomes a two-dimensional element. If the member is still considered for convenience as one-dimensional, the merger of the two force transfer mechanisms is reflected in a reduction of the moment resistance due to the high shear force and of the shear capacity due to the bending moment.

In members with L_s/h above (about) 2.5, the two practically independent mechanisms of force transfer may be considered to act in series along the shear span, L_s, in the sense that:

- internal forces need to be safely transferred by both mechanisms and failure of one of the two precipitates failure of the member; and
- the overall deformations of the member are the sum of the individual (elastic or inelastic) deformations of the two mechanisms.

As a matter of fact, capacity design of members in shear (see Section 1.3.6) is based on the concept that these two mechanisms act in series, so that the overall inelastic deformations and the deformation capacity of the member can be engineered to come from the ductile flexural mechanism alone.

To the extent that the above mechanisms of force transfer require development of (tensile) stresses in reinforcing bars, they require also transfer of forces from the bars to the concrete and vice-versa through bond. Force transfer by bond is normally considered as part of the afore-mentioned two main force transfer mechanisms,

if it takes place within the shear span. It should be taken, though, as a separate force transfer mechanism in series with the other two, if it takes place along that part of the longitudinal bars extending beyond the ends of the shear span (notably into the joints with other elements). So, for the shear span of a member, L_s, a series system of the following force transfer mechanisms may be considered to develop:

i. the flexural mechanism within the shear span
ii. the shear mechanism, again within the shear span; and
iii. the development of the (mainly tensile) forces in the longitudinal reinforcement through bond beyond the end of the shear span.

The overall force capacity of the member is governed by the weakest of these three mechanisms, while the overall deformation is the sum of those of the individual ones.

In members with L_s/h below (about) 2.5, it is understood that mechanisms (i) and (ii) merge into one.

The concluding remarks of Section 3.1.4 imply that the design of a member and the detailing of its reinforcement within the member and beyond (i.e., in its anchorage zone outside the shear span), should ensure that mechanisms (ii) and (iii) will work in their elastic range, by designing mechanism (i) to have lower force capacity than the other two.

3.2.2 Flexural Behaviour at the Cross-Sectional Level

3.2.2.1 Physical Meaning and Importance of Curvature in Concrete Members

There is experimental evidence that the Navier-Bernoulli plane section hypothesis can be applied as a rough approximation to slender concrete members during practically all ranges of flexural behaviour: till and beyond concrete cracking, towards yielding of the reinforcement and even further, almost up to the ultimate deformation of the member. The plane-section hypothesis lends itself to a very convenient description of the flexural behaviour at the cross-sectional level through the relation of moment (M) to curvature (φ). It allows relating the normal strain ε to the distance y from the neutral axis as $\varepsilon = \varphi y$. Therefore, the strain of the extreme compression fibres is: $\varepsilon_c = \varphi x$, where $x = \xi d$ is the neutral axis depth; the strain of the tension reinforcement is equal to $\varepsilon_{s1} = \varphi(d–x) = \varphi(1–\xi)d$, while that of the compression reinforcement at distance d_1 from the extreme compression fibres is $\varepsilon_{s2} = \varphi(x–d_1) = \varphi(\xi–d_1/d)d$. Note that the curvature φ is the conjugate of the moment M, in the sense that the integral of $M\mathrm{d}\varphi$ gives the flexural deformation energy per unit length of the member.

The flexural behaviour of concrete members is commonly described in M–φ terms, because for monotonic loading with constant axial force N the M–φ curve can be easily established by calculation, even up to ultimate deformation. For given

geometry of the cross-section and amount and layout of the longitudinal reinforcement and for known material σ-ε laws, this is done in a stepwise manner:

- For a value of φ, the value of the neutral axis depth x is assumed, the strain distribution across the section is derived as $\varepsilon = \varphi y$ (with y measured from the trial location of the neutral axis) and the corresponding stress distribution is derived from the material σ-ε laws. Force equilibrium in the axial direction, $N = \int \sigma \, dA$, is checked and the value of x is revised, with calculations repeated until force equilibrium is satisfied.
- The value of M corresponding to this value of φ (and N) is computed from moment equilibrium: $M = \int \sigma y_{cg} dA$, where y_{cg} is the distance from the centroid of the section to which the value of M refers.
- For the next value of φ the calculations are repeated, starting the iterations with a trial value of x equal to the one for which convergence to the value of N has been achieved in the previous step.

This approach can be used to construct cyclic M–φ relations for a given history of imposed curvatures, provided that the complete cyclic σ-ε relations of the materials are known, including the rules applying after reversal of loading from any (σ, ε) point.

Owing to its computational convenience, curvature is an appealing and very popular measure of flexural deformations. However, in concrete members loaded beyond cracking, the curvature loses its physical meaning. The reason is that concrete cracking, and later on cover spalling, bar buckling and concrete crushing, are all of discrete nature. For this reason, in concrete members curvature is commonly defined – and experimentally measured – as the relative angle of rotation $\Delta\theta$ of two neighbouring sections, divided by their distance, Δx. This distance is not infinitesimal but finite and should be of the order of:

- the typical distance of two adjacent flexural cracks, if the behaviour prior to yielding is of interest, or
- the length over which concrete is expected to spall or crush and reinforcing bars may buckle or even break.

The resulting value of $\varphi = \Delta\theta/\Delta x$ is a mean curvature that corresponds to the mean moment within Δx. In experiments, values of Δx in the range of $h/2$–h are commonly selected.

3.2.2.2 Moment-Curvature Relation up to Yielding Under Uniaxial Bending with Axial Force

Cross-Sections with Rectangular Compression Zone

Until concrete cracks the M–φ relation is linear, with slope M/φ equal to the rigidity, $E_c I_t$, of the uncracked transformed section, i.e. of a concrete section in which any reinforcing bar of cross-sectional area $A_{s,i}$ has been replaced by an equiv-

alent concrete area, $\alpha A_{s,i}$, where $\alpha = E_s/E_c$ is the ratio of Moduli of the two materials. A flexural crack forms at the cracking moment M_{cr} (which is equal to $M_{cr} = (f_{ctm}+N/A_t)I_t/y_t$, where N is the axial force – positive for compression – A_t is the cross-sectional area of the transformed section and y_t the distance of the extreme tension fibres from the centroid). The rigidity of the cross-section drops abruptly then, remaining practically constant until the section finally yields.

The members of concrete buildings typically have rectangular, T-, L-, H- or U-section (in beams monolithically connected with the slab, or in walls or columns with non-rectangular section). If the compression zone of a non-rectangular section falls within a single rectangular part of the section, the compression zone is rectangular. This is the case considered here. The next section addresses cases with a T-, L- or U-shaped compression zone.

If section yielding is identified with yielding of the tension steel, the yield curvature is:

$$\varphi_y = \frac{f_{yL}}{E_s\left(1-\xi_y\right)d} \tag{3.33a}$$

with f_{yL} denoting the yield stress of the longitudinal bars and ξ_y the neutral axis depth at yielding (normalised to the section effective depth, d), given by:

$$\xi_y = \left(\alpha^2 A^2 + 2\alpha B\right)^{1/2} - \alpha A \tag{3.34}$$

in which $\alpha = E_s/E_c$ denotes the ratio of elastic moduli (steel-to-concrete) and A, B are given from Eqs. (3.35a) (Panagiotakos and Fardis 2001a):

$$A = \rho_1 + \rho_2 + \rho_v + \frac{N}{bdf_y}, \quad B = \rho_1 + \rho_2\delta_1 + \frac{\rho_v\left(1+\delta_1\right)}{2} + \frac{N}{bdf_y} \tag{3.35a}$$

where ρ_1 and ρ_2 are the ratios of the tension and compression reinforcement and ρ_v is the ratio of "web" reinforcement (i.e. of the reinforcement which is – almost – uniformly distributed between the tension and the compression steel). The area of any diagonal bars, times the cosine of their angle with respect to the member axis, is added to the reinforcement area included in ρ_1 and ρ_2. All steel ratios are normalised to bd. Further in Eq. (3.35a), b is the width of the compression zone, N the axial load (with compression taken as positive) and $\delta_1 = d_1/d$, where d_1 is the distance of the centre of the compression reinforcement from the extreme compression fibres.

Sometimes members with high axial load ratio, $\nu = N/A_c f_c$, exhibit apparent yielding as a distinct downwards curving of the moment-curvature diagram of the end section, owing to significant nonlinearity of the concrete in compression before the tension steel yields. A simple way to treat such apparent yielding is by identifying it with exceedance of a certain strain at the extreme compression fibres, while still considering both steel and concrete as linear-elastic till that point. The test results on members yielding under high axial load ratio suggest the following value for this "elastic strain limit" (Panagiotakos and Fardis 2001a):

$$\varepsilon_c \approx \frac{1.8 f_c}{E_c} \tag{3.36}$$

Then apparent yielding of the member takes place at a curvature:

$$\varphi_y = \frac{\varepsilon_c}{\xi_y d} \approx \frac{1.8 f_c}{E_c \xi_y d} \tag{3.33b}$$

where the neutral axis depth at yielding, ξ_y (again normalised to the section effective depth, d), is still given by Eq. (3.34), but this time with A, B from Eqs. (3.35b):

$$A = \rho_1 + \rho_2 + \rho_v - \frac{N}{\varepsilon_c E_s b d} \approx \rho_1 + \rho_2 + \rho_v - \frac{N}{1.8\alpha\, b d f_c}, \quad B = \rho_1 + \rho_2 \delta_1 + \frac{\rho_v (1 + \delta_1)}{2} \tag{3.35b}$$

The lower of the two φ_y values from Eqs. (3.33a) or (3.33b) is the yield curvature. Then the yield moment, M_y, can be computed from equilibrium of the (plane) section as:

$$\frac{M_y}{b d^3} = \varphi_y \left\{ E_c \frac{\xi_y^2}{2} \left(\frac{1 + \delta_1}{2} - \frac{\xi_y}{3} \right) + \frac{E_s (1 - \delta_1)}{2} \left[\left(1 - \xi_y\right) \rho_1 + \left(\xi_y - \delta_1\right) \rho_2 + \frac{\rho_v}{6} (1 - \delta_1) \right] \right\} \tag{3.37}$$

It is noted that, by the time a strong earthquake shakes a building, practically every end section of its beams, columns or walls are already cracked, owing to the gravity loads combined with stresses due to the restrained shrinkage or thermal strains or other imposed deformations. Normally such previous stresses are not sufficient to cause cracking of columns and walls having significant axial load. However, the construction joint at the base of these members in each storey and often at the top as well (at the beam soffit) have little cohesion and will readily open in an earthquake. So, concrete members may be considered as already cracked at the time of the earthquake and their M –φ diagram may be taken as linear up to yielding.

Sections with T Compression Zone

T-, L-, H-, U- or hollow rectangular sections are considered here to have a compression flange with constant width and thickness, b and t, respectively, and total thickness of the webs b_w. The bending moment is about an axis parallel to the flange and induces compression in it. Equations (3.34) and (3.35) may still be applied, but if the outcome of Eq. (3.34) (significantly) exceeds the ratio of the flange thickness to the effective depth: $\xi_y > t/d$, the neutral axis falls in the web and the compression zone has T-, L- or U-shape. The neutral axis depth and the moment at yielding

may then be obtained from an extension of the analysis in the previous sub-section *Cross-Sections with Rectangular Compression Zone*, under the same assumptions and yield criteria. The tension, the compression and the web reinforcement are again normalised to bd, to give ratios ρ_1, ρ_2 and ρ_v, respectively. The counterparts of Eqs. (3.35) are (Biskinis 2007, Biskinis and Fardis 2007):

– For section yielding because of yielding of the tension steel:

$$\begin{aligned} A &= \frac{b}{b_w}\left(\rho_1+\rho_2+\rho_v+\frac{N}{bdf_y}\right)+\frac{1}{\alpha}\frac{t}{d}\left(\frac{b}{b_w}-1\right), \\ B &= \frac{b}{b_w}\left(\rho_1+\rho_2\delta_1+0.5\rho_v\left(1+\delta_1\right)+\frac{N}{bdf_y}\right)+\frac{1}{2\alpha}\left(\frac{t}{d}\right)^2\left(\frac{b}{b_w}-1\right) \end{aligned} \tag{3.38a}$$

– For section yielding when the strain limit of Eq. (3.36) is reached at the extreme compression fibres:

$$\begin{aligned} A &= \frac{b}{b_w}\left(\rho_1+\rho_2+\rho_v-\frac{N}{\varepsilon_c E_s bd}\right)+\frac{1}{\alpha}\frac{t}{d}\left(\frac{b}{b_w}-1\right), \\ B &= \frac{b}{b_w}\left(\rho_1+\rho_2\delta_1+0.5\rho_v\left(1+\delta_1\right)\right)+\frac{1}{2\alpha}\left(\frac{t}{d}\right)^2\left(\frac{b}{b_w}-1\right) \end{aligned} \tag{3.38b}$$

Equations (3.33) and (3.34) still apply, but the yield moment should be computed from the following counterpart of Eq. (3.37) (Biskinis 2007, Biskinis and Fardis 2007):

$$\frac{M_y}{bd^3}=\varphi_y\left\{\begin{array}{l} E_c\left[\frac{\xi_y^2}{2}\left(\frac{1+\delta_1}{2}-\frac{\xi_y}{3}\right)\frac{b_w}{b}+\left(1-\frac{b_w}{b}\right)\left(\xi_y-\frac{t}{2d}\right)\left(1-\frac{t}{2d}\right)\frac{t}{2d}\right]+ \\ \frac{E_s\left(1-\delta_1\right)}{2}\left[\left(1-\xi_y\right)\rho_1+\left(\xi_y-\delta_1\right)\rho_2+\frac{\rho_V}{6}\left(1-\delta_1\right)\right] \end{array}\right\} \tag{3.39}$$

Note that Eqs. (3.38) and (3.39) degenerate into Eqs. (3.35) and (3.37) respectively, if b_w equals b.

Comparison with Experimental Results and Empirical Expressions for the Curvature

The outcome of Eqs. (3.37) and (3.39), with φ_y computed according to the two sub-sections above: *Cross-Sections with Rectangular Compression Zone* or *Sections with T Compression Zone*, has been compared in Biskinis (2007) to the "experimental yield moment", estimated as the moment at the corner of a bilinear M–θ (moment-chord rotation) curve fitted to the envelope of the measured M–θ

hysteresis loops, taking into account P–Δ effects. The data come from tests of about 2050 beam/columns, 125 rectangular walls or 155 members with T-, H-, U- or hollow rectangular section, all with shear span ratio and reinforcement such that there were no flexure-shear interaction effects (see Section 3.2.5). The "experimental yield moment" exceeds the prediction of Eqs. (3.37) and (3.39) by an average factor of: 1.025, 1.015 or 1.075 for beams/columns, rectangular walls or members with T-, U- or hollow rectangular section, respectively (Biskinis 2007). The reason for the difference is that the corner of a bilinear M–θ curve that envelops the measured hysteresis loops expresses global yielding of the member and hence is slightly past the point where the extreme tension steel or compression fibres of the end section "yield". The factor of 1.025, 1.015 or 1.075 should be applied, as correction factor, also to the value of φ_y obtained from Eqs. (3.33) for beams/columns, rectangular walls or members with T-, U- or hollow rectangular section, respectively. The coefficient of variation of the test-to-prediction ratio for M_y is equal to 16.3, 14.8 and 12.6% for beams/columns, rectangular walls or members with T-, U- or hollow rectangular section, respectively (Biskinis 2007). Test-to-test variability and natural scatter of material properties (e.g., of the yield stress of specimen rebars with respect to reported values from few coupons, or of the concrete strength relative to the reported mean values from test cylinders or cubes, etc.) or of geometric parameters (e.g., of the effective depth to the tension or compression reinforcement, etc.) correspond to a coefficient of variation of experimental-to-predicted M_y values of about 5% (Biskinis 2007). The rest of the scatter is due to model uncertainty. Assuming statistical independence, the corresponding coefficient of variation of the test-to-prediction ratio for M_y is about equal to the values quoted above reduced by just 1%.

The comparison above refers to members with ribbed bars. Bond along smooth (plain) bars may not be sufficient for full mobilisation of their yield strength at "apparent yielding" at the section of maximum moment. This may explain why the mean and median of the test-to-prediction ratio in about 40 tests of beam/columns with such bars is about 0.95.

The literature contains also experimental data on the yield curvature, φ_y, "measured" as relative rotation between the section of maximum moment and a nearby one, divided by the distance between the two sections. In some of them measured relative rotations include also the effect of reinforcement pull-out from its anchorage zone beyond the section of maximum moment. Because:

- the "experimental yield moment", $M_{y,exp}$, is established more accurately in a test than the "measured" yield curvature, and
- the relation between φ_y and M_y, Eqs. (3.37) and (3.39), is well established, as based on equilibrium and plane section analysis,

it is preferable to consider as "experimental yield curvature", $\varphi_{y,exp}$, the value derived from the "experimental yield moment", $M_{y,exp}$, by inverting Eq. (3.37) or (3.39). The theoretical yield curvature from Eqs. (3.33), (3.34), (3.35) and (3.38), times the correction factor of 1.025, 1.015, or 1.075 for beams/columns, rectangular

walls or members with T-, U- or hollow rectangular section, respectively, may be considered to predict the $\varphi_{y,exp}$ with a median test-to-prediction ratio of 1.0 and a coefficient of variation equal to that of the test-to-prediction ratio for M_y, i.e. 12.5–16%.

The following expressions have also been fitted to $\varphi_{y,exp}$ (Biskinis 2007):

– for beams or columns:

$$\varphi_y \approx \frac{1.54 f_{yL}}{E_s d} \tag{3.40a}$$

– for rectangular walls:

$$\varphi_y \approx \frac{1.34 f_{yL}}{E_s d} \tag{3.40b}$$

– for T-, U- or hollow rectangular sections:

$$\varphi_y \approx \frac{1.47 f_{yL}}{E_s d} \tag{3.40c}$$

or alternatively:

– for beams or columns:

$$\varphi_y \approx \frac{1.75 f_{yL}}{E_s h} \tag{3.41a}$$

– for rectangular walls:

$$\varphi_y \approx \frac{1.44 f_{yL}}{E_s h} \tag{3.41b}$$

– for T-, U- or hollow rectangular sections:

$$\varphi_y \approx \frac{1.57 f_{yL}}{E_s h} \tag{3.41c}$$

Being empirical, Eqs. (3.40) and (3.41) predict $\varphi_{y,exp}$ without any bias (i.e., with median value of 1.0 for the ratio test-to-prediction). However, as important parameters (e.g., the axial load level and the ratios and layout of longitudinal reinforcement) are neglected, these expressions give a larger coefficient of variation of the test-to-prediction ratio than Eqs. (3.33) (3.34), (3.35) and (3.38): 17.5, 18.4 and 16.2% for Eqs. (3.40a), (3.40b) and (3.40c), respectively, or 29.2, 17.9 and 17.9% for Eqs. (3.41a), (3.41b) and (3.41c) (Biskinis 2007).

3.2.2.3 Fixed-End Rotation Due to Bar Pull-Out from the Anchorage Zone Beyond the Section of Maximum Moment – Value at Yielding

If there is complete symmetry of the member and its loading with respect to the section of maximum moment (as at mid-span of a beam subjected to symmetric loading), or if the longitudinal reinforcement is anchored by welding right next to this cross-section, there is no slippage (pull-out) of the longitudinal reinforcement from the region beyond the section of maximum moment. However, such slippage takes place from the anchorage of longitudinal bars within a joint or footing where the member frames, contributing to the transverse deflections of the entire shear span by a rigid-body rotation, θ_{slip}. The effect of this rotation is included in the measurement of transverse deflections and of chord-rotations of a test specimen with respect to the base or the joint into which it frames.

If s denotes the slippage of the tension reinforcement from its anchorage beyond the section of maximum moment, θ_{slip} is equal to $\theta_{slip} = s/(1–\xi)d$, where ξ is the neutral axis depth, normalised to the effective depth, d. The value of s is equal to the sum of:

- the slip of the bar with respect to the surrounding concrete at the far end of its straight embedment length (which is non-zero only if there is a hook, bend or anchor plate at that end, in which case the slip there is equal to the local deformation of the concrete due to the contact pressure under the hook, bend or anchor plate); plus
- the elongation of the bar between the far end of its straight embedment length and the section of maximum moment of the member.

Note that the value of M at the section of maximum moment is roughly proportional to the force in the tension reinforcement and that this force is the resultant of bond stresses along the anchorage length. So, the $M–\theta_{slip}$ relation reflects the bond-slip behaviour with its strongly pinched shape of the hysteresis loops. To the extent that the total chord-rotation θ is due to θ_{slip}, the apparent flexibility of the member increases and the shape of the overall $M–\theta$ loops includes certain pinching.

Fixed-end rotation due to bar pull-out equals the slip from the anchorage zone divided by the depth of the tension zone, $(1–\xi)d$ (Fig. 3.24). Assuming that bond stresses are uniform over a length l_b of the tension bars beyond the end section, the stress increases linearly along l_b from zero at the end of the bar to the bar elastic steel stress at the end section of the member, σ_s. Bar slippage from its anchorage equals $0.5\sigma_s l_b/E_s$. The ratio σ_s/E_s to $(1–\xi)d$ is the curvature, φ. The length l_b is proportional to the force in the bar, $A_s\sigma_s$, divided by its perimeter, πd_b (i.e. to $d_{bL}\sigma_s/4$ where d_{bL} is the mean tension bar diameter) and inversely proportional to bond strength, i.e., in good approximation, to $\sqrt{f_c}$. Setting at yielding of the end section: $\varphi = \varphi_y$, taking the mean bond stress in MPa along l_b equal to f_c(MPa) (which is about 50% or 40% of the bond stress corresponding to a slip equal to $s = 0.6$ mm of about $2\sqrt{f_c}$ in unconfined or confined concrete, respectively, for "good" bond conditions according

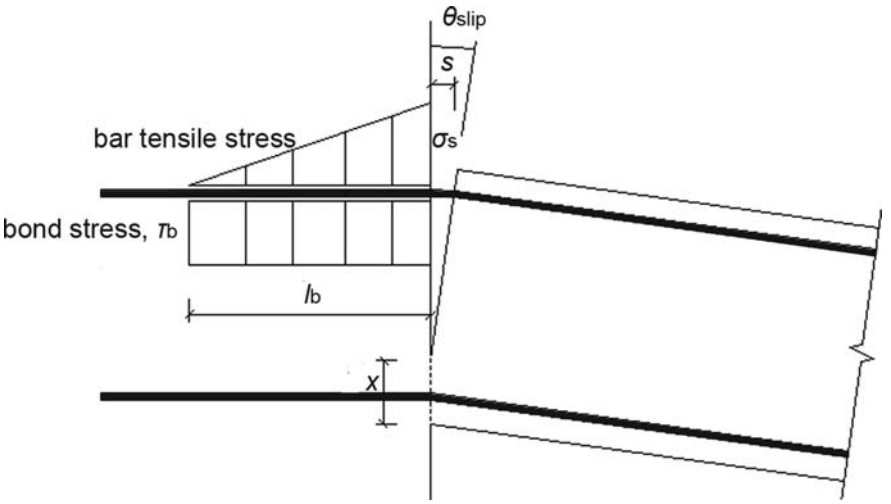

Fig. 3.24 Fixed-end rotation, θ_{slip}, due to slippage of longitudinal bars from their anchorage within a joint in which the member frames

to CEB (1991)) and setting for simplicity $\sigma_s = f_{yL}$ (even when φ_y is obtained from Eq. (3.33b)), the "fixed-end rotation" of the end section at yielding is:

$$\theta_{y,slip} = \frac{\varphi_y d_{bL} f_{yL}}{8\sqrt{f_c}} \qquad (f_{yL} \text{ and } f_c \text{ in MPa}) \tag{3.42}$$

Equation (3.42) has been calibrated to about 160 cases in the literature where curvature was measured as relative rotation between the section of maximum moment and a nearby one, divided by the distance between the two sections, including the effect of reinforcement pull-out from its anchorage zone beyond the section of maximum moment (including a few cases where the rigid-body rotation due to bar pull-out, θ_{slip}, was directly measured). The ratio of the (experimental) yield curvature from the measured relative rotations including the effect of pull-out from the specimen base, to the theoretical one from Eqs. (3.33) (3.34), (3.35) and (3.38) times the correction factor of 1.025, 1.015 or 1.075, plus the value from Eq. (3.42) divided by the gauge length over which relative rotations are measured, does not exhibit any systematic effect of the gauge length in these 160 cases and has a median value of 1.00 and a coefficient of variation of 33.9% (Biskinis 2007).

3.2.2.4 Ultimate Curvature of Sections with Rectangular Compression Zone Under Uniaxial Bending with Axial Force

Definitions and Assumptions

The ultimate curvature φ_u of a section is commonly (and conventionally) identified with a distinct change in the pattern of the moment-curvature response:

– In monotonic loading, with a noticeable drop of the moment resistance after the peak (at least 20% of the maximum resistance).
– In cycling loading, with an abrupt and distinct reduction of the reloading slope, or of the area of the hysteresis loops, or of the peak moment of the cycle, compared to those of the preceding cycle(s). Such abrupt degradation phenomena are typically associated with a drop in the maximum possible resisting moment of at least 20% of the maximum ever resisting moment. Whenever such abrupt and distinct degradation phenomena cannot be identified, the conventional rule of a maximum possible resisting moment less than 80% of the maximum ever moment resistance is used to define the ultimate deformation. Section 3.2.2.7 discusses in more detail this conventional definition of ultimate deformation.

The calculation of φ_u can be based on a plane section analysis but with nonlinear σ-ε laws, described below under (i) and (ii).

A section will reach its ultimate condition under increasing deformations when one of the following takes place:

a. The tension reinforcement reaches its ultimate elongation, ε_{su}, and ruptures. This gives an ultimate curvature equal to:

$$\varphi_{su} = \frac{\varepsilon_{su}}{(1 - \xi_{su})\, d} \tag{3.43}$$

where ξ_{su} is the neutral axis depth (normalised to d) when the ultimate curvature of the section is attained due to steel rupture.[6] This case is the subject of the sub-section below titled *Failure of the Full Section Due to Rupture of Tension Reinforcement Before Spalling of the Concrete Cover*.

b. The compression zone disintegrates and sheds (most of) its compressive force. This takes place when the concrete of the extreme compression fibres reaches its ultimate strain, ε_{cu}, giving an ultimate curvature of:

$$\varphi_{cu} = \frac{\varepsilon_{cu}}{\xi_{cu} d} \tag{3.44}$$

This case is dealt with in the sub-section below on *Curvature at Spalling of the Concrete Cover*.

Depending on:

– the value of the axial load on the section,
– the amount and location of longitudinal bars, and
– the confinement of the compression zone by transverse reinforcement, etc.,
– failure mode (a) or (b) may take place either:

[6] Equation (3.43) has already appeared in Section 3.1.1.4 as Eq. (3.1).

1. before, or at spalling of the unconfined concrete cover, i.e. at the level of the full section (sub-sections *Failure of the Full Section Due to Rupture of Tension Reinforcement Before Spalling of the Concrete Cover* and *Curvature at Spalling of the Concrete Cover*), or
2. in the confined core, after spalling of the unconfined concrete cover (sub-section *Ultimate Curvature of the Confined Core, After Spalling of the Cover*); then Eqs. (3.43) and (3.44) are applied with: the effective depth of the full section, d, replaced by that of the confined core, d_c; the neutral axis depth, ξ, referring to the confined core and normalised to d_c; and the ultimate strain of confined concrete, $\varepsilon_{cu}{}^*$, used in Eq. (3.44) in lieu of ε_{cu}.

The following σ-ε laws of the materials are adopted here:

1. Unconfined concrete has a parabolic σ-ε law up to the ultimate strength of f_c and the corresponding strain, ε_{co}. Beyond that point the σ-ε law is horizontal until a strain $\varepsilon_c \leq \varepsilon_{cu.}$[7] Then the compression zone contributes to the axial compressive force with a force equal to $\xi(bdf_c)(1-\varepsilon_{co}/3\varepsilon_c)$.
2. The σ-ε law of reinforcing steel is elastic-perfectly plastic at relatively low strains, as those at section ultimate conditions due to crushing of the concrete (failure mode (b) above). At the large steel strains accompanying section failure due to steel rupture (failure mode (a)), the steel is considered to strain-harden after the yield plateau at the yield stress f_y. Strain-hardening is linear, starting from the yield stress f_y at a strain ε_{sh}, till the ultimate strength f_t of steel at an elongation of ε_{su}. The σ-ε parameters (f_y, $\varepsilon_y = f_y/E_s$, ε_{sh}, f_t, ε_{su}) of tension, compression and web reinforcement are indexed by 1, 2 or v, respectively.

The ultimate curvature of sections with rectangular compression zone is computed according to the multi-step procedure of sub-sections *Failure of the Full Section Due to Rupture of Tension Reinforcement Before Spalling of the Concrete Cover, Curvature at Spalling of the Concrete Cover*, *Ultimate Curvature of the Confined Core, After Spalling of the Cover* and Flow Charts 3.1 and 3.2. Symbols used in the analysis are:

- $\nu = N/bdf_c$: axial load ratio, positive for compression;
- $\omega_1 = \rho_1 f_{y1}/f_c$, $\omega_2 = \rho_2 f_{y2}/f_c$, $\omega_v = \rho_v f_{yv}/f_c$: mechanical reinforcement ratios of tension, compression and web reinforcement, respectively, with ρ_1, ρ_2, ρ_v normalised to bd;
- $\delta_1 = d_1/d$: the distance of compression reinforcement from the extreme compression fibres, (normalised to d).

[7] This is the σ-ε law used in CEN (2004b) and CEB (1991) for the calculation of the resistance of cross-sections.

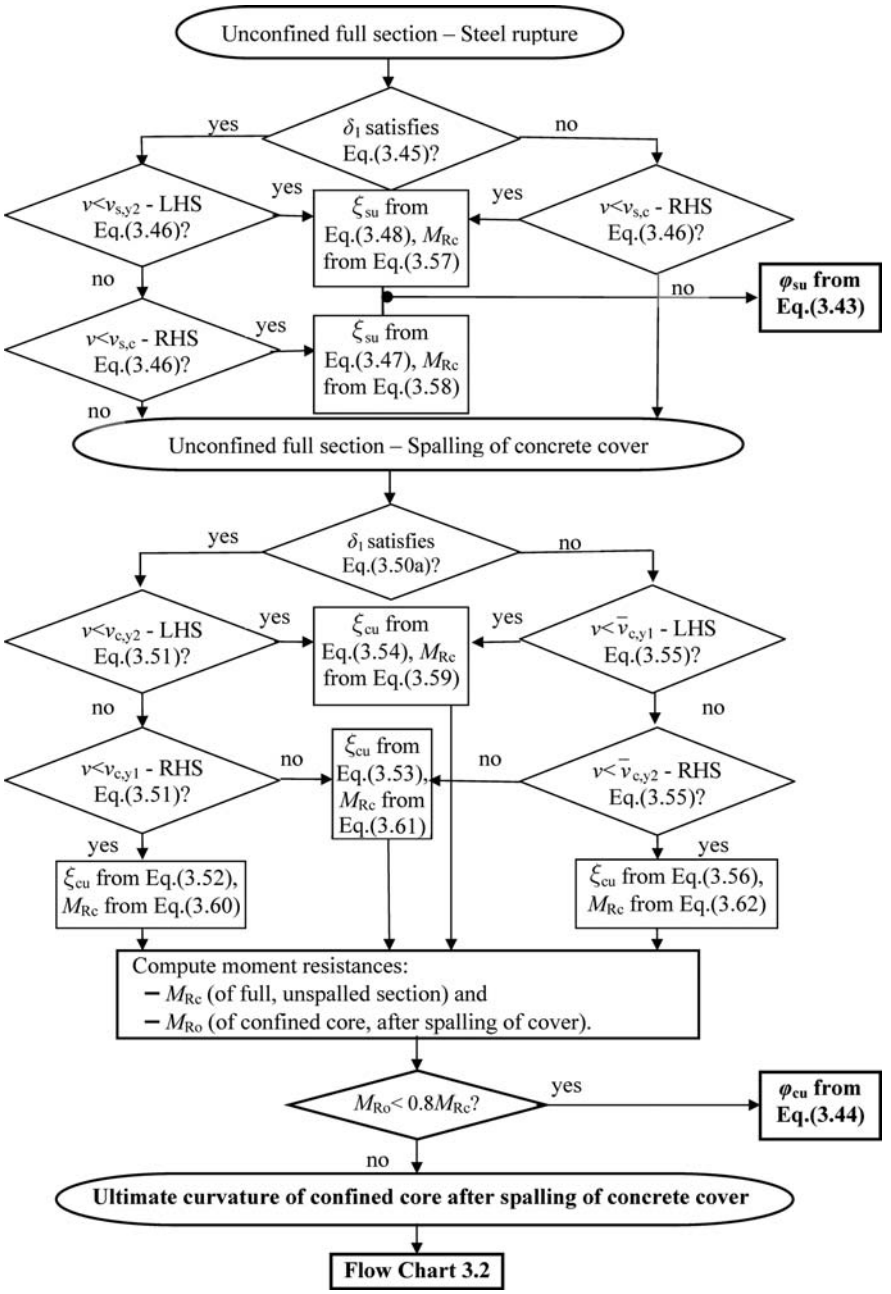

Flow Chart 3.1 Calculation of ultimate curvature for the full section before spalling of the concrete cover (LHS: left-hand-side, RHS: right-hand-side)

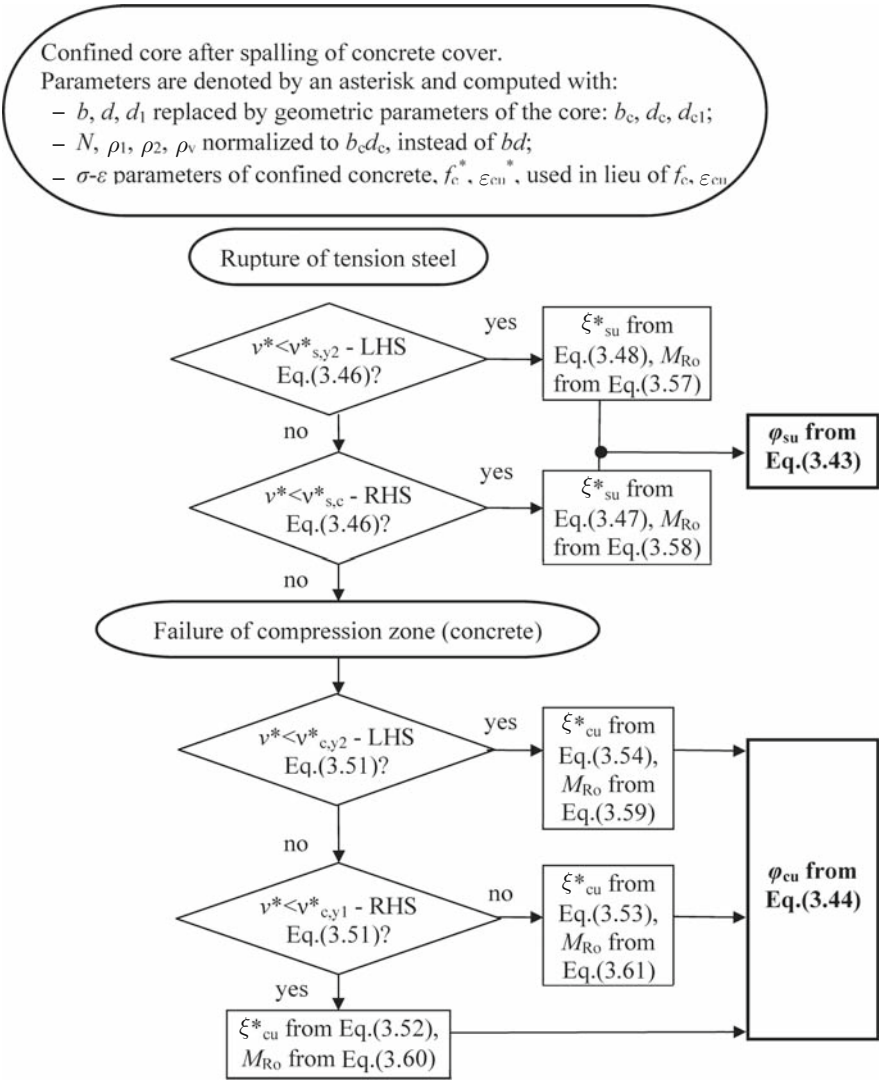

Flow Chart 3.2 Calculation of ultimate curvature for the confined core of the section after spalling of the concrete cover

Section 3.2.2.4 applies also to sections with more than one rectangular parts in two orthogonal directions, with the width b taken as that of the section at the extreme compression fibres, provided that the so-computed depth $x = \xi d$ of the compression zone does not exceed the other dimension (depth) of the rectangular part to which b belongs.

Failure of the Full Section Due to Rupture of Tension Reinforcement Before Spalling of the Concrete Cover

Failure of the full section by rupture of the tension reinforcement at an elongation of ε_{su} takes place before the extreme fibres of the concrete cover reach the crushing strain of unconfined concrete, ε_{cu}, if the neutral axis depth (normalised to d) ξ is: $\xi < \varepsilon_{cu}/(\varepsilon_{cu}+\varepsilon_{su})$. Such a failure may also occur before yielding of the compression reinforcement, if ξ satisfies the inequality: $\xi < (\varepsilon_{y2}+\varepsilon_{su}\delta_1)/(\varepsilon_{y2}+\varepsilon_{su})$. So, the full section may fail by steel rupture after yielding of the compression reinforcement, if the distance of the compression reinforcement from the extreme compression fibres, $\delta_1 = d_1/d$ (normalised to d), meets the condition:

$$\delta_1 \leq \frac{\varepsilon_{cu} - \varepsilon_{y2}}{\varepsilon_{cu} + \varepsilon_{su}} \tag{3.45}$$

If Eq. (3.45) is satisfied and the axial load ratio, ν, fulfills the inequality:

$$\begin{aligned} &\frac{\delta_1\varepsilon_{su} + \varepsilon_{y2} - (1-\delta_1)\frac{\varepsilon_{co}}{3}}{\varepsilon_{su1} + \varepsilon_{y2}} + \omega_2 - \omega_1\frac{f_{t1}}{f_{y1}} - \frac{\omega_v}{\varepsilon_{su1} + \varepsilon_{y2}} \\ &\left[\varepsilon_{su1} - \varepsilon_{y2} + \frac{1}{2}(\varepsilon_{su1} - \varepsilon_{shv})\left(1 + \frac{f_{tv}}{f_{yv}}\right)\right] \equiv \nu_{s,y2} \leq \nu \leq \\ &\nu_{s,c} \equiv \frac{\varepsilon_{cu} - \frac{\varepsilon_{co}}{3}}{\varepsilon_{cu} + \varepsilon_{su1}} + \omega_2 - \omega_1\frac{f_{t1}}{f_{y1}} - \frac{\omega_v}{(1-\delta_1)(\varepsilon_{su1} + \varepsilon_{cu})} \\ &\left[\delta_1(\varepsilon_{su1} + \varepsilon_{cu}) - (\varepsilon_{su1} - \varepsilon_{cu}) + \frac{1}{2}(\varepsilon_{su1} - \varepsilon_{shv})\left(1 + \frac{f_{tv}}{f_{yv}}\right)\right] \end{aligned} \tag{3.46}$$

failure of the full section by rupture of the tension reinforcement takes place with the compression reinforcement already beyond yielding. Then, plane-sections analysis gives the following value of ξ_{su} to be used in Eq. (3.43):

$$\xi_{su} \approx \frac{(1-\delta_1)\left(\nu + \omega_1\frac{f_{t1}}{f_{y1}} - \omega_2 + \frac{\varepsilon_{co}}{3\varepsilon_{su}}\right) + \left(1 + \delta_1 + \frac{1}{2}\left(1 - \frac{\varepsilon_{shv}}{\varepsilon_{su1}}\right)\left(1 + \frac{f_{tv}}{f_{yv}}\right)\right)\omega_v}{(1-\delta_1)\left(1 + \frac{\varepsilon_{co}}{3\varepsilon_{su1}}\right) + \left(2 + \frac{1}{2}\left(1 - \frac{\varepsilon_{shv}}{\varepsilon_{su1}}\right)\left(1 + \frac{f_{tv}}{f_{yv}}\right)\right)\omega_v} \tag{3.47}$$

If the condition of Eq. (3.45) is met, but the axial load ratio, ν, is less than the limit value $\nu_{s,y2}$ defined at the left-hand-side (LHS) of Eq. (3.46), then the full section fails by steel rupture not only before spalling of the concrete cover but also before the compression reinforcement yields. In that case, the value of ξ_{su} for use in Eq. (3.43) is the positive root of the equation:

$$\left[1+\frac{\varepsilon_{co}}{3\varepsilon_{su}}+\frac{\omega_v}{2(1-\delta_1)}\left(1+\frac{f_{tv}}{f_{yv}}\left(1-\frac{\varepsilon_{shv}}{\varepsilon_{su1}}\right)+\frac{\varepsilon_{shv}-3\varepsilon_{yv}}{\varepsilon_{su1}}-\frac{\varepsilon_{su1}}{\varepsilon_{yv}}\right)\right]\xi^2$$
$$-\left[1+\nu+\frac{2\varepsilon_{co}}{3\varepsilon_{su}}+\omega_1\frac{f_{t1}}{f_{y1}}+\omega_2\frac{\varepsilon_{su1}}{\varepsilon_{y2}}+\frac{\omega_v}{(1-\delta_1)}\left(1+\frac{f_{tv}}{f_{yv}}\left(1-\frac{\varepsilon_{shv}}{\varepsilon_{su1}}\right)\right.\right.$$
$$\left.\left.+\frac{\varepsilon_{shv}-3\varepsilon_{yv}}{\varepsilon_{su1}}-\delta_1\frac{\varepsilon_{su1}}{\varepsilon_{yv}}\right)\right]\xi+\left[\nu+\frac{\varepsilon_{co}}{3\varepsilon_{su}}+\omega_1\frac{f_{tv}}{f_{yv}}+\omega_2\delta_1\frac{\varepsilon_{su}}{\varepsilon_{y2}}\right.$$
$$\left.+\frac{\omega_v}{2(1-\delta_1)}\left(1+\frac{f_{tv}}{f_{yv}}\left(1-\frac{\varepsilon_{shv}}{\varepsilon_{su1}}\right)+\frac{\varepsilon_{shv}-3\varepsilon_{yv}}{\varepsilon_{su1}}-\delta_1^2\frac{\varepsilon_{su1}}{\varepsilon_{yv}}\right)\right]=0 \tag{3.48}$$

If Eq. (3.45) is met and the axial load ratio, ν, exceeds the limit value $\nu_{s,c}$ defined at the right-hand-side (RHS) of Eq. (3.46), spalling of the concrete cover when its outermost fibres reach the crushing strain of unconfined concrete, ε_{cu}, will precede rupture of the tension reinforcement, but will take place with the compression reinforcement already beyond yielding. Then the procedure in sub-section *Curvature at Spalling of the Concrete Cover* should be followed.

If the condition of Eq. (3.45) is not met, the limit value $\nu_{s,y2}$ defined at the left-hand-side of Eq. (3.46) is greater than the limit value $\nu_{s,c}$ given by the right-hand-side of that inequality. The implication is that the compression reinforcement will already have yielded, when the tension reinforcement ruptures before spalling of the concrete cover. Then, if the axial load ratio, ν, is less than the limit value $\nu_{s,c}$ at the left-hand-side of Eq. (3.46), the value of ξ_{su} to be used in Eq. (3.43) is still the positive root of Eq. (3.48). If, by contrast, the axial load ratio, ν, exceeds the limit value $\nu_{s,c}$, the concrete cover will spall before the tension reinforcement ruptures, but with the compression reinforcement already beyond yielding. The procedure in sub-section *Curvature at Spalling of the Concrete Cover* should be followed in that case.

Curvature at Spalling of the Concrete Cover

When the outermost fibres reach the crushing strain of unconfined concrete, ε_{cu}, and the concrete cover spalls, the moment resistance of the section drops – be it temporarily. To see what happens after cover spalling, the following moment resistances should be computed:

- the moment resistance of the full unspalled section, neglecting any effect of confinement on the concrete properties, M_{Rc},
- the moment resistance of the confined core of the section (conventionally defined to the centreline of the perimeter stirrup), after spalling of the concrete cover, M_{Ro}.

The moment capacity of the confined core, M_{Ro}, is determined on the basis of the strength f_c^* and ultimate strain ε_{cu}^* of confined concrete and of the dimensions b_c, d_c, d_{c1} of the confined core; d_c and d_{c1} are obtained by subtracting from d or d_1, respectively, the sum of the cover and of half the diameter of transverse reinforcement; b_c is obtained by subtracting twice this sum from b.

$$\text{If}: \quad M_{\text{Ro}} \leq 0.8 M_{\text{Rc}} \tag{3.49a}$$

spalling of the concrete cover can be taken as the ultimate condition of the section. Then, the ultimate curvature is given by Eq. (3.44), where the value of the neutral axis depth, ξ_{cu} (normalised to d), may be determined from Eqs. (3.52), (3.53), (3.54) or (3.56).

If $\xi < \varepsilon_{\text{cu}}/(\varepsilon_{\text{cu}}+\varepsilon_{\text{y1}})$, then the tension steel has already yielded by the time the extreme compression fibres reach the crushing strain of unconfined concrete ε_{cu}.

When ε_{cu} is reached at the outermost compression fibres, the compression steel will still be elastic if $\xi < \delta_1 \varepsilon_{\text{cu}}/(\varepsilon_{\text{cu}}-\varepsilon_{\text{y2}})$. By contrast, if $\xi > \delta_1 \varepsilon_{\text{cu}}/(\varepsilon_{\text{cu}}-\varepsilon_{\text{y2}})$ the compression steel will be beyond yielding at crushing of the extreme compression fibres. It follows from this and the previous paragraph that a range of ξ values exists for which both the tension and the compression reinforcement have yielded before ε_{cu} is reached at the extreme compression fibres, provided that $\varepsilon_{\text{cu}}/(\varepsilon_{\text{cu}}+\varepsilon_{\text{y1}}) > \delta_1 \varepsilon_{\text{cu}}/(\varepsilon_{\text{cu}}-\varepsilon_{\text{y2}})$, i.e. if:

$$\delta_1 \leq \frac{\varepsilon_{cu} - \varepsilon_{y2}}{\varepsilon_{cu} + \varepsilon_{y1}} \tag{3.50a}$$

If Eq. (3.50a) is not met, there can never be a range of ξ values for which both the tension and the compression reinforcement yield before the crushing strain of concrete is reached at the outermost compression fibres. Instead, a range of ξ values exists where both the tension and the compression reinforcement will still be elastic when the extreme compression fibres reach a strain of ε_{cu}. This latter situation does not lend itself to ductile behaviour of the cross section. In the sequel, two distinct cases are considered:

i. Equation (3.50a) is satisfied, or
ii. The following condition is fulfilled instead:

$$\delta_1 > \frac{\varepsilon_{cu} - \varepsilon_{y2}}{\varepsilon_{cu} + \varepsilon_{y1}} \tag{3.50b}$$

Case i is considered first, as more common in practice (and more desirable too).

Values of ξ between $\varepsilon_{\text{cu}}/(\varepsilon_{\text{cu}}+\varepsilon_{\text{y1}})$ and $\delta_1 \varepsilon_{\text{cu}}/(\varepsilon_{\text{cu}}-\varepsilon_{\text{y2}})$ correspond to the following range of values for the axial load ratio, ν:

$$\begin{aligned} &\omega_2 - \omega_1 + \frac{\omega_v}{1-\delta_1}\left(\delta_1 \frac{\varepsilon_{cu} + \varepsilon_{y2}}{\varepsilon_{cu} - \varepsilon_{y2}} - 1\right) + \delta_1 \frac{\varepsilon_{cu} - \frac{\varepsilon_{co}}{3}}{\varepsilon_{cu} - \varepsilon_{y2}} \equiv \nu_{c,y2} \leq \nu < \\ &\nu_{c,y1} \equiv \omega_2 - \omega_1 + \frac{\omega_v}{1-\delta_1}\left(\frac{\varepsilon_{cu} - \varepsilon_{y1}}{\varepsilon_{cu} + \varepsilon_{y1}} - \delta_1\right) + \frac{\varepsilon_{cu} - \frac{\varepsilon_{co}}{3}}{\varepsilon_{cu} + \varepsilon_{y1}} \end{aligned} \tag{3.51}$$

Within this range the value of ξ_{cu} to be used in Eq. (3.44) is:

$$\xi_{cu} = \frac{(1-\delta_1)(\nu+\omega_1-\omega_2)+(1+\delta_1)\omega_v}{(1-\delta_1)\left(1-\frac{\varepsilon_{co}}{3\varepsilon_{cu}}\right)+2\omega_v} \tag{3.52}$$

For values of ν greater than the limit value $\nu_{\mathrm{c,y1}}$ defined at the right-hand-side of Eq. (3.51) the extreme compression fibres reach the crushing strain of concrete, $\varepsilon_{\mathrm{cu}}$, after yielding of the compression reinforcement, but with the tension reinforcement elastic. Then the value of ξ_{cu} to be used in Eq. (3.44) is the positive root of the equation:

$$\left[1-\frac{\varepsilon_{co}}{3\varepsilon_{cu}}-\frac{\omega_v}{2(1-\delta_1)}\frac{\left(\varepsilon_{cu}-\varepsilon_{yv}\right)^2}{\varepsilon_{cu}\varepsilon_{yv}}\right]\xi^2+\left[\omega_2+\omega_1\frac{\varepsilon_{cu}}{\varepsilon_{y1}}-\nu+\frac{\omega_v}{1-\delta_1}\left(\frac{\varepsilon_{cu}}{\varepsilon_{yv}}-\delta_1\right)\right]\xi$$
$$-\left[\frac{\omega_1}{\varepsilon_{y1}}+\frac{\omega_v}{2\,(1-\delta_1)\,\varepsilon_{yv}}\right]\varepsilon_{cu}=0 \tag{3.53}$$

Finally, if ν is less than the limit value $\nu_{\mathrm{c,y2}}$ defined at the left-hand-side of Eq. (3.51), the outermost compression fibres reach the strain $\varepsilon_{\mathrm{cu}}$ after the tension reinforcement yields, but with the compression reinforcement still elastic. In that case the value of ξ_{cu} to be used in Eq. (3.44) is the positive root of the equation:

$$\left[1-\frac{\varepsilon_{co}}{3\varepsilon_{cu}}+\frac{\omega_v}{2(1-\delta_1)}\frac{\left(\varepsilon_{cu}+\varepsilon_{yv}\right)^2}{\varepsilon_{cu}\varepsilon_{yv}}\right]\xi^2-\left[\nu+\omega_1-\omega_2\frac{\varepsilon_{cu}}{\varepsilon_{y2}}+\frac{\omega_v}{1-\delta_1}\left(1+\frac{\varepsilon_{cu}\delta_1}{\varepsilon_{yv}}\right)\right]\xi$$
$$-\left[\frac{\omega_2}{\varepsilon_{y2}}-\frac{\omega_v\delta_1}{2\,(1-\delta_1)\,\varepsilon_{yv}}\right]\varepsilon_{cu}\delta_1=0 \tag{3.54}$$

Case ii, where Eq. (3.50b) is fulfilled, is not so desirable. Fortunately it is rare in practice, as the right-hand-side of Eqs. (3.48) is in the order of 0.15–0.2, implying that the compression steel is at a distance to the extreme compression fibres of over 15–20% of the section depth, which is uncommon. At any rate, if Eq. (3.50b) is met, for values of the axial load ratio between $\overline{\nu}_{\mathrm{c,y1}}$ and $\overline{\nu}_{\mathrm{c,y2}}$, in Eq. (3.55), both the tension and the compression reinforcement are still elastic by the time the extreme compression fibres reach the crushing strain of concrete:

$$\frac{\omega_2}{\varepsilon_{y2}}\left((1-\delta_1)\varepsilon_{cu}-\delta_1\varepsilon_{y1}\right)-\omega_1+\frac{\omega_v}{2\varepsilon_{yv}}\left(\varepsilon_{cu}-\frac{1+\delta_1}{1-\delta_1}\right)+\frac{\varepsilon_{cu}-\frac{\varepsilon_{co}}{3}}{\varepsilon_{cu}+\varepsilon_{y1}}\equiv\overline{\nu}_{c,y1}\le\nu<$$
$$\overline{\nu}_{c,y2}\equiv\omega_2-\frac{\omega_1}{\varepsilon_{y1}}\frac{(1-\delta_1)\varepsilon_{cu}-\varepsilon_{y2}}{\delta_1}+\frac{\omega_v}{\delta_1\varepsilon_{yv}}\left(\frac{1+\delta_1}{1-\delta_1}\varepsilon_{y2}-\varepsilon_{cu}\right)+\delta_1\frac{\varepsilon_{cu}-\frac{\varepsilon_{co}}{3}}{\varepsilon_{cu}-\varepsilon_{y2}} \tag{3.55}$$

Within this range of ν the value of ξ_{cu} to be used in Eq. (3.44) is the positive root of:

$$\left[1-\frac{\varepsilon_{co}}{3\varepsilon_{cu}}\right]\xi^2-\left[\nu-\left(\frac{\omega_1}{\varepsilon_{y1}}+\frac{\omega_2}{\varepsilon_{y2}}+\frac{\omega_v}{(1-\delta_1)\varepsilon_{yv}}\right)\varepsilon_{cu}\right]\xi \\ -\left(\frac{\omega_1}{\varepsilon_{y1}}+\frac{\delta_1\omega_2}{\varepsilon_{y2}}+\frac{\omega_v(1+\delta_1)}{2(1-\delta_1)\varepsilon_{yv}}\right)\varepsilon_{cu}=0 \tag{3.56}$$

For values of ν greater than the limit value $\overline{\nu}_{c,y2}$ defined at the right-hand-side of Eq. (3.55) the extreme compression fibres reach the crushing strain of concrete after yielding of the compression reinforcement, but with the tension reinforcement still elastic. The value of ξ_{cu} to be used in Eq. (3.44) is the positive root of Eq. (3.53) above. If, by contrast, ν is less than the limit value $\overline{\nu}_{c,y1}$ defined at the left-hand-side of Eq. (3.55), the extreme compression fibres reach a strain of ε_{cu} after yielding of the tension reinforcement, but with the compression reinforcement still elastic. In that case the value of ξ_{cu} to be used in Eq. (3.44) is the positive root of Eq. (3.54).

The expressions above for ξ (i.e., Eqs. (3.47), (3.48), (3.52), (3.53), (3.54) and (3.56)) are derived from the equivalence of the normal stress resultant on the section to the axial force N. The plane sections hypothesis and the nonlinear σ-ε laws outlined in points (i) and (ii) at the end of sub-section *Definitions and Assumptions* are also used. Equation (3.52) is derived below for illustration, with the tension reinforcement not considered to go into strain-hardening.

Because the tension and the compression reinforcement are both past yielding, their joint contribution to the axial compressive force is equal to $(A_{s2}–A_{s1})f_y=(\omega_2–\omega_1)bdf_c$. For a neutral axis depth equal to ξd the web reinforcement, taken as uniformly distributed over a length $(1–\delta_1)d$ between the compression and tension steel, contributes to the axial compression with a force of $[(\omega_v bdf_c)/(1–\delta_1)][(\xi–\delta_1)–(1–\xi)]=(\omega_v bdf_c)(2\xi–1–\delta_1)/(1–\delta_1)$. Equilibrium gives: $\nu=\frac{N}{bdf_c}=\omega_2-\omega_1+\frac{\omega_v(2\xi-1-\delta_1)}{1-\delta_1}+\left(1-\frac{\varepsilon_{co}}{3\varepsilon_{cu}}\right)\xi$, from which Eq. (3.52) is derived.

Ultimate Curvature of the Confined Core, After Spalling of the Cover

If

$$M_{Ro}>0.8M_{Rc} \tag{3.49b}$$

then the confined core of the section recovers from spalling of the concrete shell around it. It ultimately fails either by rupture of the tension reinforcement or by disintegration of the extreme compression fibres of the core itself.

The analysis in sub-sections *Definitions and Assumptions*, *Failure of the Full Section Due to Rupture of Tension Reinforcement Before Spalling of the Concrete Cover* and *Curvature at Spalling of the Concrete Cover* applies for the calculation of the ultimate curvature of the confined core after spalling of the cover, provided that:

- dimensions b, d and d_1 are replaced by b_c (equal to b minus the diameter of transverse reinforcement and twice the cover), d_c (equal to d minus the cover and half the diameter of transverse reinforcement) and d_{c1} (equal to half the diameter of transverse reinforcement plus half that of longitudinal bars), respectively;
- N, ρ_1, ρ_2, ρ_v are normalised to $b_c d_c$, instead of bd, and
- the σ-ε parameters of confined concrete, f_c^*, ε_{cu}^*, are used, in lieu of f_c, ε_{cu}.

Note that d_{c1} is small compared to d_1 above. So, the conditions of Eqs. (3.45) and (3.50a) are always met in the confined core. Then, only Eqs. (3.46), (3.47), (3.48), (3.51), (3.52), (3.53) and (3.54) in sub-sections *Failure of the Full Section Due to Rupture of Tension Reinforcement Before Spalling of the Concrete Cover* and *Curvature at Spalling of the Concrete Cover* are meaningful for the ultimate curvature of the confined core.

3.2.2.5 Moment Resistance of Concrete Sections with Rectangular Compression Zone

The moment resistance of the confined core and of the unspalled section, M_{Ro}, M_{Rc}, respectively, for use in Eqs. (3.49), may be estimated as uniaxial moment resistances of concrete sections with rectangular compression zone, through dimensioning tools (tables, diagrams, analytical expressions or computer codes) available for the Ultimate Limit State of such sections under uniaxial bending with axial force. When such design tools are utilised, the actual (or expected) value of material strengths should be used, instead of the design values:

- for reinforcing steel, use f_{ym} or f_y in lieu of $f_{yd}=f_{yk}/\gamma_s$;
- for concrete, instead of $f_{cd}=f_{ck}/\gamma_c$, the value f_{cm} or f_c should be used before spalling and the value f_{cm}^* or f_c^* for the confined concrete core after spalling (for M_{Ro}); if the design tools used include a reduction factor on f_{cd} due to long term or other effects, e.g. a reduction factor of 0.85, this factor should be removed by using the value $f_c/0.85$ or $f_c^*/0.85$ for f_{cd}.
- for the moment corresponding to rupture of the tension reinforcement at the full section before spalling (and to the ultimate curvature φ_{su}), or at the confined core afterwards (and to φ_{su}^*), the cross-sectional area of tension reinforcement should be taken equal to $A_{s1}f_t/f_y$ (i.e., ω_1 should be multiplied by f_t/f_y).

As an alternative, the flexural resistance may be calculated analytically, as described below for M_{Rc} (see also Flow Charts 3.1 and 3.2). The value of M_{Ro} can be calculated similarly, using the geometric and strength parameters of the confined core.

For failure of the section due to rupture of the tension steel (i.e., when the axial load ratio, ν, is less than the minimum of the limit values $\nu_{s,y2}$, $\nu_{s,c}$ defined in Eq. (3.46) of sub-section *Failure of the Full Section Due to Rupture of Tension Reinforcement Before Spalling of the Concrete Cover*), we consider first the usual

case when Eq. (3.45) is met. Then, for ν less than the limit value $\nu_{s,y2}$ defined at the left-hand-side of Eq. (3.46), the compression reinforcement is elastic while the tension reinforcement is at ultimate strength. With ξ given by Eq. (3.48), the moment resistance of the section is:

$$\begin{aligned}\frac{M_{Rc}}{bd^2 f_c} &= (1-\xi)\left[\frac{\xi}{2} - \frac{\varepsilon_{co}}{3\varepsilon_{su1}}\left(\frac{1}{2} - \xi + \frac{\varepsilon_{co}}{4\varepsilon_{su1}}(1-\xi)\right)\right] \\ &+ \frac{(1-\delta_1)}{2}\left(\omega_1 \frac{f_{t1}}{f_{y1}} + \omega_2 \frac{\xi - \delta_1}{1-\xi}\frac{\varepsilon_{su1}}{\varepsilon_{y2}}\right) \\ &+ \frac{\omega_v}{6(1-\delta_1)}\left\{\left[1 - \delta_1 + \xi\left(1 - \frac{\varepsilon_{yv}}{\varepsilon_{su1}}\right)\right]\left[1 + \frac{\varepsilon_{su1}}{\varepsilon_{yv}}\left(\frac{\xi - \delta_1}{1-\xi}\right)\right]\right. \\ &\left[\frac{1-\delta_1}{2} - (1-\xi)\frac{\varepsilon_{yv}}{\varepsilon_{su1}}\right] + \left[\frac{2(1-\delta_1)}{3} - \left(1 - \frac{\varepsilon_{shv}}{\varepsilon_{su1}}\right)(1-\xi)\right] \\ &\left.\left(1 - \frac{\varepsilon_{shv}}{\varepsilon_{su1}}\right)\left(\frac{f_{tv}}{f_{yv}} - 1\right)(1-\xi)\right\}\end{aligned} \tag{3.57}$$

If, by contrast, ν satisfies Eq. (3.46), the compression reinforcement is beyond yielding but not yet in strain-hardening. Then, with ξ from Eq. (3.47), the section moment resistance is:

$$\begin{aligned}\frac{M_{Rc}}{bd^2 f_c} &= (1-\xi)\left[\frac{\xi}{2} - \frac{\varepsilon_{co}}{3\varepsilon_{su1}}\left(\frac{1}{2} - \xi + \frac{\varepsilon_{co}}{4\varepsilon_{su1}}(1-\xi)\right)\right] \\ &+ \frac{(1-\delta_1)}{2}\left(\omega_1 \frac{f_{t1}}{f_{y1}} + \omega_2\right) + \frac{\omega_v}{1-\delta_1}\left\{(\xi - \delta_1)(1-\xi) - \frac{1}{3}\left(\frac{(1-\xi)\,\varepsilon_{yv}}{\varepsilon_{su1}}\right)^2\right. \\ &\left.+ \left[\frac{(1-\delta_1)}{4} - \left(1 - \frac{\varepsilon_{shv}}{\varepsilon_{su1}}\right)\frac{1-\xi}{6}\right]\left(1 - \frac{\varepsilon_{shv}}{\varepsilon_{su1}}\right)\left(\frac{f_{t1}}{f_{y1}} - 1\right)(1-\xi)\right\}\end{aligned} \tag{3.58}$$

If Eq. (3.45) is not met, but the axial load ratio, ν, is still less than the limit value $\nu_{s,c}$ defined at the right-hand-side of Eq. (3.46), the compression reinforcement is still elastic while the tension reinforcement is at ultimate strength. Then the moment resistance of the section is again given by Eq. (3.57), with ξ from Eq. (3.48).

For section failure due to concrete crushing (i.e., for axial load ratio, ν, greater than the minimum of the limit values $\nu_{c,y2}$, $\overline{\nu}_{c,y1}$ defined at the left-hand-side of Eqs. (3.51) and (3.55), respectively, in sub-section *Curvature at Spalling of the Concrete Cover*), we consider first the case of Eq. (3.50a) being met. Then, if ν is less than the limit value $\nu_{c,y2}$ at the left-hand-side of Eq. (3.51), the compression reinforcement is elastic while the tension reinforcement is beyond yielding but not yet in strain-hardening. With ξ given by Eq. (3.54), the moment resistance of the section is:

$$\frac{M_{Rc}}{bd^2 f_c} = \xi\left[\frac{1-\xi}{2} - \frac{\varepsilon_{co}}{3\varepsilon_{cu}}\left(\frac{1}{2} - \xi + \frac{\varepsilon_{co}}{4\varepsilon_{cu}}\xi\right)\right] + \frac{(1-\delta_1)}{2}\left(\omega_1 + \omega_2\frac{\xi-\delta_1}{\xi}\frac{\varepsilon_{cu}}{\varepsilon_{y2}}\right) + \frac{\omega_v}{4(1-\delta_1)}\left[\xi\left(1+\frac{\varepsilon_{yv}}{\varepsilon_{cu}}\right) - \delta_1\right]\left[1+\frac{\varepsilon_{cu}}{\varepsilon_{yv}}\left(\frac{\xi-\delta_1}{\xi}\right)\right]\left[1-\frac{\delta_1}{3} - \frac{2}{3}\xi\left(1+\frac{\varepsilon_{yv}}{\varepsilon_{cu}}\right)\right] \tag{3.59}$$

If ν satisfies Eq. (3.51), the tension and the compression reinforcement are both beyond yielding but not in strain-hardening. The moment resistance of the section is then:

$$\frac{M_{Rc}}{bd^2 f_c} = \xi\left[\frac{1-\xi}{2} - \frac{\varepsilon_{co}}{3\varepsilon_{cu}}\left(\frac{1}{2} - \xi + \frac{\varepsilon_{co}}{4\varepsilon_{cu}}\xi\right)\right] + \frac{(1-\delta_1)(\omega_1+\omega_2)}{2} + \frac{\omega_v}{1-\delta_1}\left[(\xi-\delta_1)(1-\xi) - \frac{1}{3}\left(\frac{\xi\varepsilon_{yv}}{\varepsilon_{cu}}\right)^2\right] \tag{3.60}$$

with ξ given by Eq. (3.52). If, by contrast, ν exceeds the limit value $\nu_{c,y1}$ at the right-hand-side of Eq. (3.51), the tension reinforcement is elastic while the compression reinforcement is beyond yielding but not in strain-hardening. With ξ from Eq. (3.53) the moment resistance is:

$$\frac{M_{Rc}}{bd^2 f_c} = \xi\left[\frac{1-\xi}{2} - \frac{\varepsilon_{co}}{3\varepsilon_{cu}}\left(\frac{1}{2} - \xi + \frac{\varepsilon_{co}}{4\varepsilon_{cu}}\xi\right)\right] + \frac{(1-\delta_1)}{2}\left(\omega_1\frac{1-\xi}{\xi}\frac{\varepsilon_{cu}}{\varepsilon_{y1}} + \omega_2\right) + \frac{\omega_v}{4(1-\delta_1)}\left[1-\xi\left(1-\frac{\varepsilon_{yv}}{\varepsilon_{cu}}\right)\right]\left[1+\frac{\varepsilon_{cu}}{\varepsilon_{yv}}\left(\frac{1-\xi}{\xi}\right)\right]\left[\frac{1}{3} - \delta_1 + \frac{2}{3}\xi\left(1-\frac{\varepsilon_{yv}}{\varepsilon_{cu}}\right)\right] \tag{3.61}$$

We consider next the rare case when Eq. (3.50b) is met. If ν is less than the limit value $\overline{\nu}_{c,y1}$ at the left-hand-side of Eq. (3.55), the compression reinforcement is elastic and the tension reinforcement is beyond yielding but not strain-hardening yet. The moment resistance of the section is given by Eq. (3.59), with ξ from Eq. (3.54). If ν satisfies Eq. (3.55), the entire reinforcement of the section is elastic and the moment resistance is:

$$\frac{M_{Rc}}{bd^2 f_c} = \xi\left[\frac{1-\xi}{2} - \frac{\varepsilon_{co}}{3\varepsilon_{cu}}\left(\frac{1}{2} - \xi + \frac{\varepsilon_{co}}{4\varepsilon_{cu}}\xi\right)\right] + \frac{(1-\delta_1)\varepsilon_{cu}}{2\xi}\left((1-\xi)\frac{\omega_1}{\varepsilon_{y1}} + (\xi-\delta_1)\frac{\omega_2}{\varepsilon_{y2}}\right) + \frac{\omega_v(1-\delta_1)^2}{12\xi}\frac{\varepsilon_{cu}}{\varepsilon_{yv}} \tag{3.62}$$

with ξ from Eq. (3.56). If ν exceeds the limit value $\overline{\nu}_{c,y2}$ defined at the right-hand-side of Eq. (3.55), the tension reinforcement is elastic and the compression

reinforcement is beyond yielding but not in strain-hardening. The moment resistance of the section is given by Eq. (3.61), with ξ from Eq. (3.53).

Equations (3.57), (3.58), (3.59), (3.60), (3.61) and (3.62) are derived from moment equilibrium of the normal stresses acting on the section with respect to its centroid, taken to be at mid-distance between the tension and the compression reinforcement. The plane section hypothesis and the nonlinear σ-ε laws outlined in points (i) and (ii) at the end of sub-section *Definitions and Assumptions* are used also. As an illustration, the derivation of Eq. (3.60) is given below, with the tension reinforcement not considered to be in strain-hardening.

The tension and compression longitudinal reinforcement, with mechanical ratios ω_1 and ω_2, each at a distance $h/2–d_1=(d–d_1)/2$ to the centroid of the section, contribute to its moment resistance a moment of $(\omega_1+\omega_2)bd^2f_c(1–\delta_1)/2$. When the strain of the outermost compression fibres is equal to ε_{cu}, the "web" reinforcement, distributed between ω_1 and ω_2 and having mechanical ratio ω_v, contributes to the flexural resistance a moment about the centroid of the section equal to $\omega_v bd^2f_c/(1–\delta_1)[(\xi–\delta_1)(1–\xi)–(\xi f_y/E_s\varepsilon_{cu})^2/3]$. With respect to the same point and for a parabolic-rectangular σ-ε diagram, the compression zone contributes a moment equal to $bd^2f_c\xi[(1–\xi)/2–(1/2–\xi+\xi\varepsilon_{co}/4\varepsilon_{cu})(\varepsilon_{co}/3\varepsilon_{cu})]$. Adding all three contributions, Eq. (3.60) is obtained.

3.2.2.6 Flexural Behaviour Until Failure Under Cyclic Loading

Let's consider the following load history, which is quite commonly part of the load history applied in experimental studies of the cyclic behaviour of concrete members:

- reversal of loading into unloading at a value of curvature φ_r past flexural yielding;
- continuation of unloading into reloading in the opposite direction, up to a curvature of about $-\varphi_r$[8];
- new unloading from $-\varphi_r$ towards the original direction of loading, until and past the peak curvature reached in the previous cycle, φ_r;
- new unloading from a peak curvature greater than φ_r.
- The experimental behaviour is shown in:
- Fig. 3.25 for a rectangular section with symmetric reinforcement and zero axial load;
- Fig. 3.26 for a rectangular beam with less reinforcement at the bottom (corresponding in Fig. 3.26 to negative moment) than at the top and zero axial load.

Measured curvatures in these two figures do not include the effect of bar pull-out from the anchorage zone beyond the end section. Figure 3.26 is typical of a frame beam, which at the face of the column usually has greater top reinforcement than

[8]Symmetric deflection cycles, i.e. from a deflection δ_r to $-\delta_r$; as commonly applied on test specimens, produce almost but not quite symmetric curvature cycles at the member end where yielding takes place.

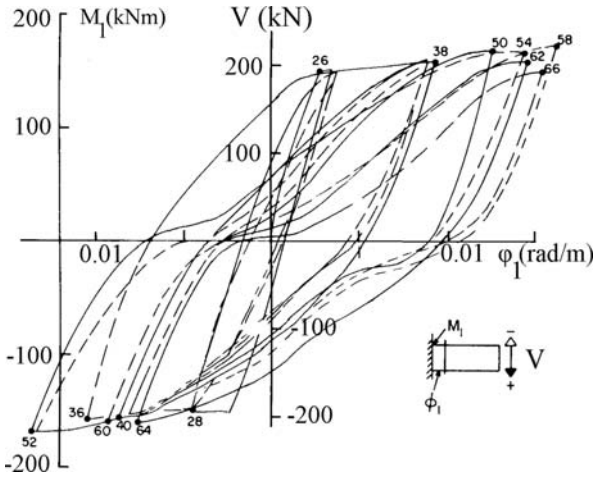

Fig. 3.25 Experimental M-(mean) φ curves of symmetrically reinforced member in cyclic bending (Ma et al. 1976)

at the bottom. In an actual beam the cross-section is not rectangular, but T or L, with different effective flange width in tension or compression. As pointed out in Sections 1.3.4 and 2.2.1, in beams integral with the slab the effective flange width increases with increasing end moment and deformation, especially after the yielding of the longitudinal bars placed within the width of the web mobilises the strength and stiffness of the flange and spreads the nonlinearity into the slab further away from the web.

In both cases the cyclic behaviour exhibits the following features:

1. In the monotonic branch before any unloading (i.e., during primary or virgin loading) flexural cracking is followed by a gradual softening of the response. If the reinforcement is concentrated near the extreme tension and compression fibres of the section, yielding of the tension bars shows up as a rather abrupt softening of the overall moment-curvature response. After yielding the resisting moment keeps increasing, initially because the reduction of the neutral axis depth due to the large post-yield elongation of the tension reinforcement increases the internal lever arm, and then because strain hardening of the tension bars starts. When the concrete cover spalls at a compressive strain equal to the ε_{cu}-value of unconfined concrete, the resisting moment drops momentarily. Depending on the magnitude of its strains, the compression steel will most likely yield at that point and may not contribute further to the increase of the resisting moment. These effects are usually more than offset by the increase of the strength and stiffness of the core concrete effected by the mobilisation of confinement.
2. During unloading from the post-yield branch of the primary loading curve, the unloading stiffness is initially high, about equal to the ”elastic” (post-cracking) stiffness. The unloading branch gradually softens, especially as the applied

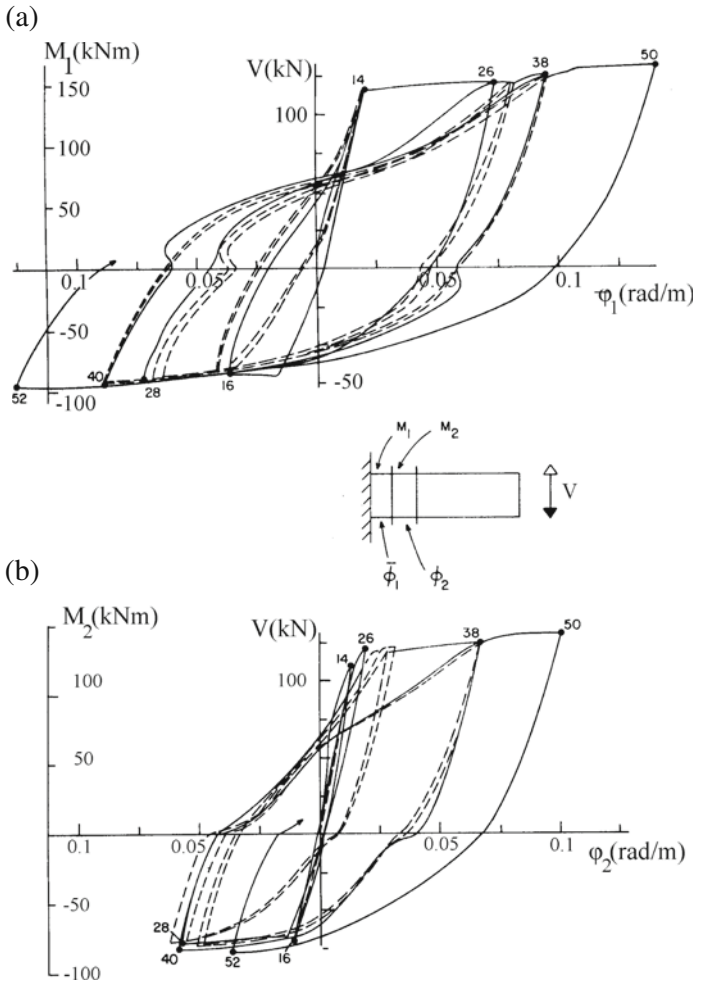

Fig. 3.26 Experimental M–(mean) φ curves of asymmetrically reinforced member in cyclic bending: (**a**) next to the member end; (**b**) a short distance from the member end (Ma et al. 1976)

moment approaches zero. Overall, and throughout the unloading branch until the horizontal axis, $M = 0$, the unloading slope is less than the "elastic" secant stiffness to the yield-point, M_y/φ_y and decreases with increasing value of the peak curvature where unloading started, φ_r. This reduction is part of the so-called "stiffness degradation", which is a characteristic feature of the cyclic flexural behaviour of concrete members. When the applied moment becomes zero, there is a significant residual deformation, mainly due to the permanent inelastic strains locked in the tension bars and to the residual slip between the bars and the concrete. Owing to this residual slip, at zero applied moment the cracks remain open.

3. Right after the applied moment changes sign, the slope ("stiffness") of the branch of loading in the opposite direction ("reloading") considerably decreases. The reduction in stiffness is due to the fact that, when the applied moment changes sign, the crack is open throughout the depth of the section, including the (new) compression side. The reason is that the bars of that side – now in compression – have previously yielded in tension and have a certain plastic elongation locked-in. So, the applied moment is resisted only by the force couple of the tension and compression reinforcement. So long as the steel couple alone resists the moment, the M–φ diagram resembles that of the σ-ε diagram of steel in cyclic loading, including the Bauschinger effect for yielding in the opposite direction (cf. Fig. 3.1 in Section 3.1.1.1). Moreover, the slope (tangent stiffness) of the M–φ diagram is considerably less than the slope of unloading to the horizontal axis. For the crack to close at the (newly) compressed side and for the concrete to be activated again there, the compression reinforcement needs to develop compressive stresses sufficiently large to suppress its (plastic) tensile strains (or to buckle). Once this takes place, the crack closes and the slope (tangent stiffness) of the reloading branch increases again, tending to a roughly constant value, which is maintained until the previous maximum curvature, φ_r, in the current direction of (re)loading is reached. As a result, the unloading-reloading branch has an inverted-S shape. If the section is symmetrically reinforced with all the reinforcement concentrated at the two ends of the section,[9] the shape of unloading-reloading branches resembles an inverted-S for both directions of loading (cf. Fig. 3.25) The inverted-S shape of one or both unloading-reloading branches produces hysteresis loops that are "pinched" at the middle. In sections with asymmetric reinforcement, i.e. with $\rho_1+\rho_v > \rho_2$ as in Fig. 3.26, the unloading-reloading branch exhibits a clear pinching only when reloading takes place from a state with the less reinforced side (that with ratio ρ_2) in tension towards one with this reinforcement in compression. Being less than that of the other side, this reinforcement yields soon in compression, allowing the crack to close at the compression side. For reloading in the reverse direction, with the more heavily reinforced side (that with ratio ρ_1) going from tension to compression, the reinforcement of the opposite side (with ratio ρ_2) is not sufficient to drive the reinforcement with the large ratio (ρ_1) to yielding in compression. This delays closure of the through-depth crack. As shown in Fig. 3.7, at the more heavily reinforced side of the section compressive strains are relatively low and the concrete is not heavily stressed, because the reinforcement there can resist the full compression force even without yielding. So, in asymmetrically reinforced sections, unloading-reloading branches have the shape of an inverted-S only when reloading takes place in the direction towards the larger

[9] If a large fraction of the reinforcement is distributed between the top and the bottom of the section, e.g., along the two sides that are parallel to the plane of bending, as in large columns or walls, most, if not all, of this reinforcement is normally in tension, because the compression zone is limited to (much) less than half of the effective section depth. So, the tension reinforcement is always more than the compression reinforcement and can easily drive it to yielding and beyond.

moment resistance. Reloading in the reverse direction always takes place at a lower stiffness, namely that developed by the steel couple alone. This stiffness is the same as the initial reloading stiffness in the reverse direction, before the concrete is engaged in compression and the tangent stiffness increases. An external compressive force on the section helps close the crack on the compression side and reduces the length of the branch exhibiting low stiffness. Large axial compression does not let the crack remain open throughout the depth. Then the stiffness along the unloading-reloading branch decreases steadily and smoothly.

If the continuation of unloading into (re)loading in the reverse direction happens to be a first-time post-elastic loading in that direction, it may be considered as virgin loading. The softening that follows the stiffening at the end of the pinching (due to yielding of the bars at the side currently in tension) is more gradual than during first loading in the original direction, because the bars now yielding in tension have in all likelihood yielded in compression previously and exhibit the Bauschinger effect. The same effect causes the bars on the compression side, that have previously yielded in tension, to start yielding early and gradually, contributing to the gradual softening of reloading. After the yielding of both the tension and the compression bars is complete, the moment-curvature response in further loading is like primary post-elastic loading in the current loading direction, as affected by possible spalling of the concrete cover on the newly compressed side and by strain-hardening of the steel bars on the side newly in tension.

4. In addition to the degradation of resistance with increasing lateral displacements, which is due to the increased deformations imposed on concrete and steel, cycling of the deformations per se even at constant amplitude normally causes degradation of strength with respect to the envelope provided by the primary loading curve. The sources of this ”strength degradation” are many. First, alternating opening and closing of cracks causes degradation of strength and stiffness of the concrete in compression, because small shear sliding, flaking off or debris accumulation along a crack prevents its faces from returning to even and full contact. Second, cyclic deterioration of the bond-slip behaviour along the bars (cf. Fig. 3.22) gradually increases the crack width and reduces the tension-stiffening effect (i.e. the activation of the concrete in tension around the bar). Third, apart from the gradual deterioration with cycling of the shear behaviour per se (i.e., of aggregate interlock, dowel action, etc.), the transfer of the shear force by dowel action along open full-depth cracks when the steel couple alone resists the applied moment, causes concrete splitting along the longitudinal bars (the “dowels”) and subsequent further bond deterioration and stiffness degradation, or even spalling of the concrete cover and deterioration of both flexural strength and stiffness. Well designed and detailed members exhibit little degradation of strength with cycling. Moreover, for constant amplitude cycling of either force or deflection, the deterioration is noticeable between the 1st and the 2nd cycle but diminishes almost to zero thereafter, leading to very stable hysteretic behaviour. Lack of such stabilisation is a sign of imminent failure under

cyclic loading. Increasing the transverse steel reduces strength degradation with cycling, as it enhances confinement. However, increasing the longitudinal steel seems to increase also the degradation of strength and stiffness with cycling, because the concrete, which is the main source of the degradation, becomes more critical.

Besides the absence of strong pinching in reloading towards the direction of the lower moment resistance, the prime difference of the cyclic flexural behaviour between the cases of symmetric (Fig. 3.25) and asymmetric cross-section and reinforcement (Fig. 3.26) is in the stiffness and strength exhibited by the envelope (and primary loading) curve in the two directions of bending, positive or negative.

3.2.2.7 Failure of Members Under Cyclic Flexure

Flexural damage is physically concentrated in the end region of the member and entails one or more of the following (see Fig. 3.27 for examples):

- spalling of the concrete cover, often extending to disintegration of the concrete core inside the reinforcement cage;
- buckling of reinforcing bars (especially of the corner ones);
- rupture of one or more reinforcing bars.

Members detailed for earthquake resistance normally do not fail abruptly under cyclic loading. Their failure in flexure is typically gradual, governed by the progressive deterioration of the compression zone. Damage starts with spalling of the cover concrete and normally continues with buckling of the bars that lose their lateral support and finally with disintegration of the core concrete. Lightly reinforced members may fail suddenly by fracture of one or more tension bars. Such a fracture often takes place at a minute crack in the bar caused by buckling during the previous half-cycle. The reduction in moment resistance caused by a bar fracture shows up in the moment-curvature response as an abrupt drop in the moment, often considered as failure. When there are no such clear signals of failure, the member may be considered to have failed if, from a certain point on, the pattern of the response changes. For example, when, during constant amplitude cycling the peak force drops disproportionately from one cycle to the next ("strength decay"), compared to previous cycles at the same or smaller deformation amplitude. Another example is an entire hysteresis loop that tilts or shrinks relative to the previous ones. The column in Fig. 1.2(b) exhibits both these features during the last cycles of the response. Such changes in the macroscopic behaviour signify a marked loss of stiffness, strength or energy dissipation capacity and may be taken to signal failure. Examples in this chapter include Fig. 3.5(a) and (b) (for reinforcing bars), the shear failures of specimens No. 1, 3 and 4 in Fig. 3.36(a), the ductile shear failure in Fig. 3.38(c) and (f) and the subassembly failure in Fig. 3.46(c).

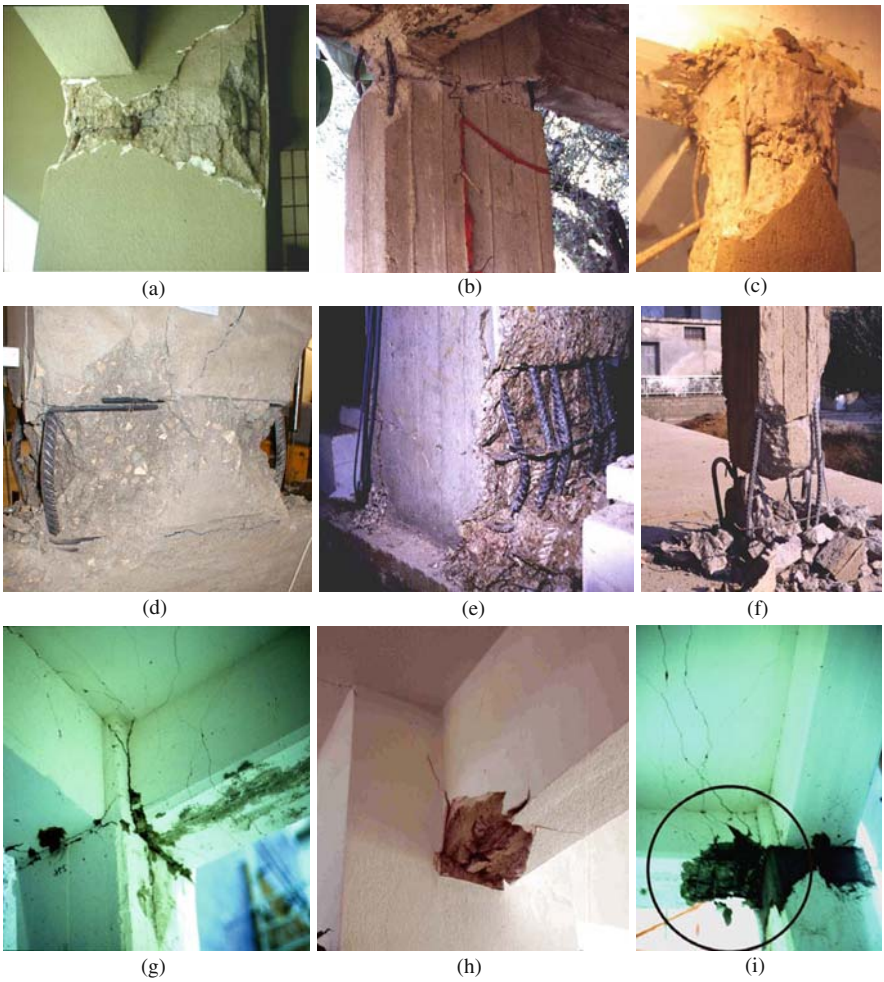

Fig. 3.27 Examples of flexural damage or failure in the lab or in the field: (**a**), (**b**) horizontal crack at column top, concrete spalling at the corners, buckling of corner bars; (**c**) complete loss of cover, partial disintegration of concrete and buckling of bars in horizontal zone near the column top; (**d**) full loss of cover, partial disintegration of concrete and buckling of bars in horizontal zone just above column base; (**e**) loss of cover, partial disintegration of concrete core and bar buckling, with tie opening-up on one side of a column above the base; (**f**) full disintegration of concrete and buckling of bars in a lapping region at floor level; (**g**) through-depth cracking near the support of a T-beam with extension of the cracks into the slab at the top flange; (**h**) local crushing of concrete and bar buckling at the bottom of a T-beam; (**i**) disintegration of concrete and bar buckling at the bottom of a T-beam, with through-depth flexural cracks extending into the slab at the top flange (See also Colour Plate 7 on page 721)

No matter whether the loss of strength, stiffness or energy dissipation capacity is abrupt or gradual, a conventional definition of member failure under cyclic loading is necessary. A definition covering both the abrupt and the gradual change in the force-deformation response has been proposed in French and Schultz (1991) and Saatcioglou (1991). According to it, failure is taken to occur when it is not possible to increase the force resistance above 80% of the maximum resistance attained during the test, even though the imposed deformation keeps increasing. In the examples of Figs. 1.2(b), 3.5(a) and (b), 3.36 (no. 1, 3 and 4), 3.38(c) and (f) and 3.46(c), the conventional identification of failure with a 20%-drop in post-ultimate resistance coincides with a rather abrupt change in the cyclic force-deformation response. By contrast, the column of Fig. 1.2(c), the material behaviour in Figs. 3.3(right), 3.6(b) and 3.10 and the subassembly in Fig. 3.46(b), exhibit a very gradual deterioration of peak resistance with cycling and failure can be defined only conventionally (as the 20% drop in post-ultimate resistance).

If the qualitative definition of failure as a change in the hitherto pattern of behaviour is applied to monotonic loading, then failure may be identified with the peak force resistance (ultimate strength, see Fig. 1.2(a) and monotonic conclusion of the tests in Figs. 3.6(a) and (b), 3.7 and 3.36(b) (specimen No. 8)). On the other hand, identification of failure with inability to increase the force resistance above 80% of its hitherto peak value, coincides with the frequently used convention of identifying failure under monotonic loading with a force point on the falling branch of the force-deformation response at 80% of the ultimate strength. In Figs. 1.2(a), 3.6(b) and 3.7, the drop in post-peak resistance by at least 20% is clearly meaningful as failure.

If the section and the reinforcement are symmetric, flexural damage (in a cyclic test or in the field during an earthquake) is also nearly symmetric at the two sides of the section. In an asymmetric cross-section the two sides may experience different failure modes under cyclic loading. Failure with the stronger side in tension is typically gradual, with progressive disintegration of the weaker compression side and crushing of the concrete there. Failure with the weaker side in tension may be abrupt, owing to fracture of the steel bars there, possibly after buckling in a previous half-cycle. Often steel fracture on the weaker side is preceded by a significant drop in strength (called, conventionally or not, failure) during a half-cycle with the stronger side in tension. So, under displacement-controlled cyclic load histories, failure of asymmetric sections typically occurs with the stronger side under tension.

3.2.2.8 Effect of Axial Force on the Cyclic Flexural Behaviour

If the axial load ratio, $\nu = N/A_c f_c$, is low, zero or negative (tensile) and the compression zone is well confined, repetition of a full cycle between equal and opposite values of peak curvature produces fairly stable hysteresis loops, with no degradation of the peak resistance from cycle to cycle.

Some axial compression on the cross-section helps close the cracks in the final phase of unloading and the first stage of reloading in the reverse direction, by promoting yielding in compression of the bars that have previously yielded in tension

and now go into compression. As a result, never during the loading cycle are the cracks open through the section depth or is the applied moment carried by the steel couple alone. So, the moment-curvature behaviour does not exhibit strong pinching of the loops. However, high axial compression has adverse effects on the behaviour, especially if the normalised axial force, ν, approaches the value at balance load (which coincides with $\nu_{c,y1}$, defined at the right-hand-side of Eq. (3.51) if the condition of Eq. (3.50a) is met, or with $\overline{\nu}_{c,y1}$, defined at the left-hand-side of Eq. (3.55), if it is not). For high axial compression the compression zone may disintegrate with cycling and the peak resistance may drop from cycle to cycle, giving shallower and narrower hysteresis loops. Failure then may be abrupt, unless the concrete core is very well confined.

The axial load in frame columns does not always stay constant during the seismic response. The seismic overturning moment produces an axial force (mainly) in the exterior columns, compressive on the "leeward" side of the building, tensile on the "windward" one (see Eq. (2.13) in Section 2.2.1.5). Seismic axial forces are largest at the bottom storey. The variation of axial compression during the cyclic response may significantly affect the column inelastic behaviour, so long as the column stays below its balance load,[10] as described below.

An increase in the axial compression increases the yield and ultimate moments (cf. Eqs. (3.37), (3.39), (3.57), (3.58), (3.59), (3.60), (3.61) and (3.62)), the ordinates of the envelope curve of the hysteresis loops under cyclic loading, and the stiffness in virgin loading, unloading and reloading, as the larger neutral axis depth increases the contribution of concrete to the flexural resistance and stiffness. By contrast, when the axial compression decreases, all its strength and stiffness properties decrease. So, a history of symmetric displacement cycles with variation of the axial force during the cycle produces asymmetric hysteresis loops, with strength and stiffness distinctly higher in the direction of increasing axial compression (that of negative moments in Fig. 3.28) than in the opposite one (for positive moments in Fig. 3.28). Therefore, during the seismic response the "leeward" exterior columns exhibit an increase in stiffness (increasing momentarily their share in the seismic shear) and yield moment. The "windward" exterior columns exhibit the reverse effects.

So long as the response is elastic, the seismic axial force in the columns varies in proportion both to the column moment and to the column deformation. This proportionality does not apply anymore, once plastic hinging and inelastic response start developing in the frame. So long as the column end section of interest is still in the elastic range, its seismic axial force will vary less than proportionally to the column moment and deformation. In the post-yield range of the column end section, and provided that the mechanism developing in the frame is closer to the beam-sway type (cf. Fig. 1.3(b)–(e)), the column's seismic axial force will keep varying with the column deformation (not the moment) but again less than proportionally to it. If a soft-storey type of mechanism tends to form (as in Fig. 1.3(a)), the column's

[10] If the value of the axial force varies around the column balance load, there is no clear-cut effect of this variation on the column flexural behaviour.

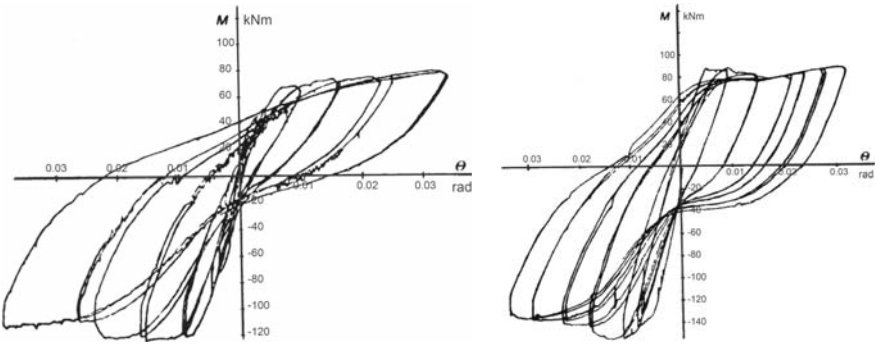

Fig. 3.28 Moment-chord rotation response of column with axial force varying in proportion: (**a**) to the moment; (**b**) to the deformation (adapted from CEB 1996a)

seismic axial force will stay essentially constant during post-yield primary loading but vary again with the column moment during unloading or reloading.

Tests on columns with the axial load varying about its mean value in proportion to the moment (Abrams 1987) demonstrate (Fig. 3.28(a)) that the effect of axial load on post-elastic stiffness in virgin loading or reloading shows up gradually, accelerating the softening in that direction of loading in which the axial compression decreases with increasing moment (i.e., for positive moments in Fig. 3.28(a)) but reducing it for loading in the opposite direction (toward negative moments in Fig. 3.28(a)), even to the point of producing an overall stiffening effect. An axial force that varies with the applied moment will remain essentially constant after column yielding. The different final values of axial force for the two directions of loading just cause different yield moments in these directions. The post-yield behaviour follows closely the envelope associated with the corresponding constant axial force value.

If the axial load varies about its average value in proportion to the deformations (Fig. 3.28(b)), yielding in the direction of decreasing axial force (i.e., for positive moments in Fig. 3.28(b)) is followed by a drop in the moment resistance, as this decreases with decreasing axial load (Abrams 1987). In the other direction of loading (towards negative moments in Fig. 3.28(b)), the increase of axial load with the post-yield deformation increases the yield moment further, showing up initially as an apparent but significant increase in the post yield stiffness. However, this post yield stiffening is soon followed by a strength decay, which may eventually lead to failure.

No matter whether the axial force varies with the moment or with the deformation, failure by rupture of the tension steel (Section 3.2.2.4 under *Failure of the Full Section Due to Rupture of Tension Reinforcement Before Spalling of the Concrete Cover*) is reached sooner for decreasing axial compression, while that by concrete crushing (Section 3.2.2.4 under *Curvature at Spalling of the Concrete Cover*) happens earlier for increasing axial load. As the ultimate curvature is much lower for the latter failure mode than for the former, the "leeward" exterior columns typically fail before the "windward" ones.

3.2.2.9 Fixed End-Rotation at Member Ultimate Curvature, Due to Bar Pull-Out from the Anchorage Zone Beyond the Section of Maximum Moment

If the anchorage of the longitudinal bars beyond the member end is insufficient, it will fail, normally by pull-out. Such a failure may well pre-empt yielding of these bars and flexural yielding of the member's end section. It will certainly prevent that section from developing its full moment resistance, Eqs. (3.57), (3.58), (3.59), (3.60), (3.61) and (3.62). Figure 3.29 shows examples of wide residual cracks at the ends of beams with short bar anchorage in corner joints, suggesting very large fixed-end rotations there during the response. In concrete buildings with well designed and detailed members, anchorage failures of this type do not take place. Instead, the fixed-end rotation due to bar pull-out from the anchorage zone will keep increasing from its value at yielding of the end section, Eq. (3.42), while the member heads towards its ultimate flexural deformation.

Strain hardening of the tension bars at the section of maximum moment does not increase markedly the bond stress demand along their anchorage past that section. The increase of the fixed-end rotation from yielding till the ultimate flexural deformation is due to penetration of inelastic strains into the initial part of the anchorage length of these bars (see Section 3.1.3.2). Bar anchorage beyond this "yield penetration length", $l_{y,p}$, remains intact and the fixed-end rotation produced by bar pull-out from the anchorage zone is still given by Eq. (3.42). However, steel elongation along the "yield penetration length" shows up as additional slippage of the tension bars at the section of maximum moment. If these bars are perfectly-plastic along the yield

Fig. 3.29 Pull-out of beam bars from short anchorage in corner joint has produced fixed-end rotation during the response and wide residual cracks (See also Colour Plate 8 on page 722)

penetration length, their strain is practically constant along that length and equal to the steel strain, ε_s, at the section of maximum moment. It produces then an additional slippage of $\varepsilon_s l_{y,p}$ and an additional fixed-end-rotation, $\Delta\theta_{u,slip} = \varphi_u l_{y,p}$, by the time of the ultimate curvature, φ_u, of the end section. If the tension bars are considered as linearly strain-hardening all along the yield penetration length, their strain may be taken to increase linearly along that length from the yield strain, ε_y, to the value ε_s at the section of maximum moment. In that case we have: $\Delta\theta_{u,slip} = (\varphi_y+\varphi_u)l_{y,p}/2$.

Biskinis (2007) used about 465 measurements of relative rotations near the end of the member at the time of member ultimate deformation, 120 of which included the fixed-end rotation due to reinforcement pull-out. On the basis of these tests the additional fixed-end rotation between yielding and ultimate curvature can be inferred as equal to:

– for cyclic loading:

$$\Delta\theta_{u,slip} = 5.5 d_{bL} \varphi_u \tag{3.63a}$$

– for monotonic loading:

$$\Delta\theta_{u,slip} = 9.5 d_{bL} \varphi_u \tag{3.63b}$$

or

– for cyclic loading:

$$\Delta\theta_{u,slip} = 10 d_{bL} \left(\varphi_y + \varphi_u\right)/2 \tag{3.63c}$$

– for monotonic loading:

$$\Delta\theta_{u,slip} = 16 d_{bL} \left(\varphi_y + \varphi_u\right)/2 \tag{3.63d}$$

A slightly better fit to the data is achieved with Eqs. (3.63c) and (3.63d) than with Eqs. (3.63a) and (3.63b): the coefficient-of-variation is 45.5% v 47.5%.

Note, in this connection, that according to Eurocode 8 (CEN 2004a) the anchorage length of beam or column bars in beam-column joints of DC H buildings should be measured starting 5-bar-diameters inside the joint for reasons of yield penetration. This length is quite consistent with Eq. (3.63a).

The value of φ_u in Eqs. (3.63) is calculated according to Section 3.4.4.2, using Eqs. (3.4), (3.5), (3.10), (3.16) or (3.17), (3.20), (3.21), (3.22), (3.23), (3.24) and (3.25) for the properties of concrete, including the confined core, as well as Eqs. (3.64) of Section 3.2.2.10 for the strain at which the tension bars rupture.

3.2.2.10 Experimental Ultimate Curvatures and Comparison with Predictions for Various Confinement Models

The most important parameters in the approach of Section 3.2.2.4 for the calculation of ultimate curvature, φ_u, are the ultimate strain of concrete, confined or not, and the available elongation of the tension reinforcement.

Equations (3.16) or (3.17) in Section 3.1.2.2 give the ultimate strain of concrete, confined or not, to be used together with Eqs. (3.4), (3.5), (3.10), (3.20), (3.21), (3.22), (3.23), (3.24) and (3.25) for the prediction of ultimate curvature. Biskinis (2007) has developed Eqs. (3.16) and (3.17) on the basis of about 465 measurements of relative rotations near the end of the member at the time of member ultimate deformation. About 120 of these measurements included fixed-end rotation due to reinforcement pull-out and were corrected for its effect using Eqs. (3.63). The first two terms of Eqs. (3.16) and (3.17) have been derived from 65 cases with almost no confinement, where the ultimate curvature had been reached at spalling of the concrete cover. The resulting predictions for φ_u give a test-to-prediction ratio with a median of 0.925 and a coefficient-of-variation of 55.5%. The 3rd term in Eqs. (3.16) and (3.17) has been derived from 105 monotonic and about 80 cyclic tests that reached ultimate curvature by crushing of the confined concrete core. The resulting φ_u-values give a test-to-prediction ratio with median of 1.02 or 0.99 and a coefficient-of-variation of 51.9% or 52.6%, for these monotonic or cyclic tests, respectively. Finally, about 115 monotonic and 100 cyclic tests, reported or inferred to have reached ultimate curvature by rupture of the tension reinforcement, lead to the conclusion that the available elongation of tension reinforcement at ultimate curvature is on average equal to the following fraction of the nominal bar strain at maximum stress, $\varepsilon_{su,nominal}$, as obtained from coupon tests of the bars (Biskinis 2007, Biskinis and Fardis 2009):

– for monotonic loading:

$$\varepsilon_{su,mon} = (7/12)\varepsilon_{su,nominal} \tag{3.64a}$$

– for cyclic loading:

$$\varepsilon_{su,cy} = (3/8)\varepsilon_{su,nominal} \tag{3.64b}$$

The adverse effect of cyclic loading on steel bars (e.g., surface cracking upon buckling, etc.) is the main reason for the large difference of $\varepsilon_{su,cy}$ from $\varepsilon_{su,nominal}$, in Eq. (3.64b). By contrast, the prime reason for the (smaller, albeit significant) difference of $\varepsilon_{su,mon}$ from $\varepsilon_{su,nominal}$ in Eq. (3.64a) is not mechanical but statistical, similar to the well known statistical size effect that decreases strength with increasing specimen size. The 115 monotonic tests that reached ultimate curvature by rupture of the tension reinforcement had from 1 to 20 tension bars (on average 5). Unlike the cyclic test results, which do not exhibit a statistically significant effect of the number of bars on $\varepsilon_{su,cy}$, the monotonic ones show clearly that when the number of

bars increases, the actually available elongation of tension reinforcement, $\varepsilon_{su,mon}$, decreases. This is consistent with control of failure by the minimum value of ε_{su} among the bars. Normally, the probability distribution of the minimum value of ε_{su} among N bars is taken to follow a Type I extreme value distribution of the smallest values. The parameters of that probability distribution depend on the functional dependence of the lower tail of the underlying distribution of the value of ε_{su} of the individual bars, on ε_{su}. A reasonable form of dependence is an exponential of the negative of an increasing function of the deviation of ε_{su} from its mean value, taken as $\varepsilon_{su,nominal}$ (Benjamin and Cornell 1970). If that function is taken proportional to $(\varepsilon_{su}-\varepsilon_{su,nominal})^2$, the mode (i.e., most likely value) of the minimum value of ε_{su} among N bars is a linear function of $\sqrt{lnN}$ (Benjamin and Cornell 1970). Then, as Eq. (3.64a) corresponds to an average of 5 tension bars in the 115 monotonic tests with rupture of tension reinforcement, it can be generalised as follows:

– For monotonic loading:

$$\varepsilon_{su,mon} = \left(1 - \frac{1}{3}\sqrt{\ln N_{b,tension}}\right)\varepsilon_{su,nominal} \tag{3.64c}$$

where $N_{b,tension}$ is the number of bars in the tension zone. Equation (3.64c) gives $\varepsilon_{su,mon} = \varepsilon_{su,nominal}$ if $N_{b,tension} = 1$ and $\varepsilon_{su,mon} \approx (7/12)\varepsilon_{su,nominal}$ for the average value of $N_{b,tension} = 5$ in the tests. When Eqs. (3.64c) and (3.64b) are used, the test-to-prediction ratio for φ_u has a median of 1.00 or 1.01 and a coefficient-of-variation of 44.8% or 34.7%, for these monotonic or cyclic tests, respectively.

Overall, in about 465 ultimate curvature values derived from measurements of relative rotation, the test-to-prediction ratio for φ_u has a median of 0.995 and a coefficient-of-variation of 49.8% (or 1.01 and 0.985, and 53.2 and 44.6% separately for monotonic and cyclic loading, respectively) (Biskinis 2007). Natural and test-to-test variability contributes to the scatter a coefficient of variation of about 18.5% in practically identical specimens. After subtracting this source of the scatter, model uncertainty corresponds to a coefficient of variation equal to the values quoted above, reduced by 3.3% for the larger values to 5.2% for the smaller ones. The overall statistics, as well as those for the individual failure modes, are slightly worse if the ultimate concrete strain is given by a single expression, Eq. (3.17), both for monotonic and cyclic loading, instead of the two different ones of Eqs. (3.16).

After correcting the "experimental" value of φ_u for any fixed-end rotation due to reinforcement pull-out from its anchorage beyond the section of maximum moment according to Eqs. (3.63), its magnitude does not exhibit any systematic effect of the gauge length over which the relative rotation had been measured (Biskinis 2007).

Notwithstanding the large scatter, the above statistics demonstrate that φ_u-values based on Eqs. (3.4), (3.5), (3.10), (3.16), (3.17) and (3.64) agree much better with test results than the φ_u-values obtained from alternative well known or widely used models, namely:

a. From the model in informative Annex A of Part 3 of Eurocode 8 (CEN 2005a). According to it, the ultimate strain of longitudinal reinforcement, ε_{su}, to be used for cyclic loading can be taken equal to the following values, higher than those of Eq. (3.64b):

   - the lower limit values specified in Eurocode 2 (CEN 2004b) for the 10%-fractile strain at maximum force, ε_{uk}, if the steel class is A or B (for class B, this is the minimum value for DC L or M in Table 3.1 of Section 3.1.1.4); and
   - 6% for steel class C (i.e., steel meeting the requirements for DC H in Table 3.1 of Section 3.1.1.4).

   According to CEN (2005a), the parameters of confined concrete, including the effect of confinement, may be obtained either:

   i. from Eqs. (3.4), (3.5), (3.10) and (3.18), or
   ii. from Eqs. (3.8), (3.9) and (3.13) (i.e., according to CEN (2004b) and CEB (1991)).

   For confinement model (i) the test-to-prediction ratio of φ_u has a median of 1.04 or 0.94 and coefficient-of-variation of 67.2% or 47.3% for monotonic or cyclic loading, respectively. Overall (for monotonic and cyclic loading) the median is 0.985 and the coefficient-of-variation 62.9%.
   For confinement model (ii) the median and the coefficient-of-variation of the test-to-prediction ratio of φ_u is 1.37 or 1.3, and 70.6% or 51.3% for monotonic or cyclic loading, respectively, and overall (monotonic and cyclic) 1.33 and 65.6% (Biskinis 2007). If the ultimate strain of steel, ε_{su}, is taken from Eqs. (3.64) instead, the median improves to 1.39, 1.14 and 1.27, for monotonic, cyclic loading and overall (monotonic and cyclic), respectively, without a significant increase of the scatter.

b. From Mander et al. (1988) and Paulay and Priestley (1992) regarding confinement, i.e., from Eqs. (3.4), (3.6) and (3.10) and either Eq. (3.14) (Mander et al. 1988), or Eq. (3.15) (Paulay and Priestley 1992) for the ultimate strain of confined concrete.
   Best average agreement of these models with tests is obtained if the ultimate strain of longitudinal reinforcement, ε_{su}, is taken according to Part 3 of Eurocode 8 (CEN 2005a). Then the ultimate strain model of Eq. (3.14) (Mander et al. 1988) gives a median of 1.015 or 1.155 for the test-to-prediction ratio of φ_u and a coefficient-of-variation of 71.5% or 52.4%, for monotonic or cyclic loading, respectively, and overall a median ratio of 1.035 and a coefficient-of-variation of 64.5%. If the ultimate strain model of Eq. (3.15) (Paulay and Priestley 1992) is used instead, the test-to-prediction ratio of φ_u has a median of 0.95 or 0.89 and a coefficient-of-variation of 74.5% or 53% for monotonic or cyclic loading, respectively. Overall the median is 0.925 and the coefficient-of-variation 68.4%.
   When the ultimate strain of longitudinal reinforcement, ε_{su}, is taken from Eqs. (3.64), the ultimate strain model of Eq. (3.14) (Mander et al. 1988) gives

for the test-to-prediction ratio of φ_u a median equal to 0.895 or 0.945, and a coefficient-of-variation of 78.3% or 44.2%, for monotonic or cyclic loading, respectively, and a median of 0.92 and a a coefficient-of-variation of 68.3% overall. If the ultimate strain model of Eq. (3.15) (Paulay and Priestley 1992) is used instead, the test-to-prediction ratio of φ_u has a median of 0.87 or 0.835 and a coefficient-of-variation of 84.2% or 47.1%, for monotonic or cyclic loading, respectively. Overall the median is 0.835 and the coefficient-of-variation 75.1%.

3.2.2.11 Curvature Ductility Factor

Equations (1.1) and (1.2) in Section 1.2 relate:

- the behaviour factor q by which the elastic force demand on the structure as a whole is divided, in order to obtain the design force (base shear) that the system should be designed to resist at the ULS, to
- the global (lateral) displacement ductility factor, μ_δ, of the system, defined as ratio of the displacement demand at the top or at the point of application of the resultant lateral force, to the displacement at the same point at global yielding (i.e., at the corner of an elastoplastic curve fitted to the force displacement response)

The importance of μ_δ arises from its relation with q through Eqs. (1.1) and (1.2).

As noted in Section 1.3 with reference to Fig. 1.3, if the plastic mechanism of the response is known, member deformation demands (conveniently expressed as chord rotation demands at member ends, see Figs. 1.3 and 1.4) can be related to the global displacement demand on the building and evaluated from it. Accordingly, these member deformation demands are also normalised to the corresponding value at yielding of the member (i.e., to θ_y, if the chord rotation θ is used), i.e. as member deformation (e.g. chord rotation) ductility factors (e.g. $\mu_\theta = \theta/\theta_y$). This practice is extended to the curvature of sections, for which the curvature ductility factor is defined as $\mu_\varphi = \varphi/\varphi_y$.

There is always a demand value for any ductility factor, deriving from the seismic action, and a supply value, characterising the corresponding deformation capacity (at ultimate deformation) of the section, member or system. The demand value of the curvature ductility factor is:

$$\mu_\varphi = \frac{\varphi}{\varphi_y} \tag{3.65a}$$

and its supply (or available) value is:

$$\mu_{\varphi u} = \frac{\varphi_u}{\varphi_y} \tag{3.65b}$$

where φ_y can be obtained according to Section 3.2.2.2 and φ_u from Section 3.2.2.4, using Eqs. (3.16) or (3.17) in Section 3.1.2.2 for the ultimate strain of concrete, confined or not, together with Eqs. (3.4), (3.5), (3.10), (3.20), (3.21), (3.22), (3.23), (3.24) and (3.25), as well as Eq. (3.64) for the available elongation of the tension reinforcement

The importance of μ_φ derives mainly from the possible link of its available value from Eq. (3.65b) to a supply value of the member chord rotation ductility factor, μ_θ. The link is via Eq. (3.71) in Section 3.2.3.4 and certain approximations. In the end it relates μ_φ to μ_δ and hence to q through Eqs. (1.1) and (1.2) (see Section 5.1, Eqs. (5.1) and (5.2)).

3.2.3 Flexural Behaviour at the Member Level

3.2.3.1 Chord Rotations from Member Tests

The chord rotation at a member end has been introduced in Section 1.3 with reference to Figs. 1.3 and 1.4. The chord rotations $\theta_A = \int_{x_A}^{x_B} \varphi(x)(x_B - x)dx / (x_B - x_A)$, $\theta_B = \int_{x_A}^{x_B} \varphi(x)(x_A - x)dx / (x_B - x_A)$ at the two ends A and B of a member are the angles between the chord connecting the ends in the deformed configuration of the member and the normal to the cross-section at A and B, respectively. The relative rotation θ_{AB} of these two sections is: $\theta_{AB} = \int_{x_A}^{x_B} \varphi(x)dx = \theta_A - \theta_B$.

The chord rotation at a member's end is the most important and convenient deformation measure for concrete members, for the following reasons:

- Both in the elastic and inelastic range, chord rotations at member ends are equal to the nodal rotations there, after subtracting the rigid-body displacements of the member axis. Therefore, it is in terms of them that the stiffness or flexibility relation of the member is formulated in member-type models (see Sections 4.10.1.2 and 4.10.1.4). For example, in the elastic range the moments at ends A and B are derived from the chord rotations there as: $M_A = (2EI/L)(2\theta_A+\theta_B)$, $M_B = (2EI/L)(2\theta_B+\theta_A)$. The chord rotations due to flexure determine the distribution of bending moments along the full length of the member.
- Unlike curvatures, which lack physical meaning and are hard to measure experimentally, deflections are reliably measured or controlled. So, test results, mostly from single- or double-cantilever specimens, are typically presented as a lateral force-deflection diagram, F–δ, at the point of application of the lateral load and reflect the overall load-displacement response of the specimen. Normally the deflection δ is at the end B of the shear span, $L_s = M/V$, and is measured with respect to the original axis of the specimen, which coincides with the normal to the section A of maximum moment. The F–δ diagram can be translated into an end moment-chord rotation (or "drift") diagram, M–θ, of the member, by multiplying the shear force by L_s and dividing δ by L_s. Such a diagram refers to the

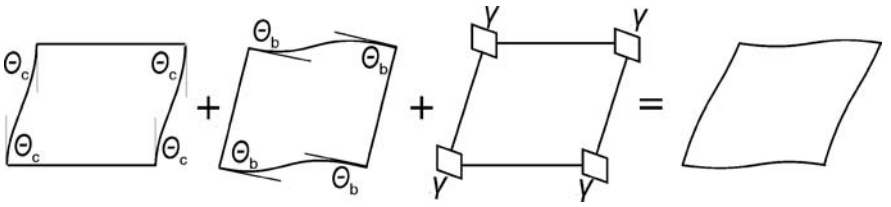

Fig. 3.30 Contribution of chord rotations of columns and beams to the angular distortion of a frame bay

entire shear span and is closely linked to its length. Note that it is the deflection at point B (where the load is applied) with respect to the tangent at the section A of maximum moment, that gives the chord-rotation at A, θ_A.

– The angular distortion of a frame bay with beams and columns in skew symmetric bending ($\theta_A = \theta_B$) is equal to the sum, $\theta_c + \theta_b$, of the chord rotations of a column and a beam around the bay, plus the (average) shear distortion of the joint panel, γ (Fig. 3.30). In design for earthquake or wind, damage to non-structural elements filling the frame panel, such as partition walls, etc., is limited by limiting this angular distortion, usually termed drift angle or drift ratio. The term "drift" is also used for the chord rotation in single- or double-cantilever member tests.

Tests are the main source of information for the cyclic behaviour of concrete members up to failure. Recall that energy dissipation and inelastic action should take place mostly in the beams, which should be weaker than the columns they frame into. In buildings beams are normally subjected to uniaxial bending with practically zero normal force, whereas columns, in general, may be subjected to biaxial bending with axial force. So, most of the experimental research on the cyclic behaviour of reinforced concrete members has addressed the simplest case of uniaxial flexure without axial force. However, although in practice only beams are subjected to uniaxial bending and zero axial force, in most tests the specimen has rectangular cross-section and symmetric reinforcement, as in columns. There are few tests on specimens with T-section and asymmetric reinforcement. But even in them another source of asymmetric behaviour is missing: the shear span is maintained constant during testing, whereas in a beam carrying gravity loads and belonging in a frame subjected to seismic loading the shear span varies during the response. It is minimum, and hence the effect of shear on behaviour is greatest, when the moment and the shear due to the seismic loading act in the same sense as those due to gravity loads (i.e., introducing tension to the top flange).

In the most common test setup the specimen cantilevers from a large concrete base and is subjected to a cyclic lateral force at the tip under displacement control. Then the shear span is the distance of the point of application of the force to the top of the base. In another setup, more representative of frame members (especially of columns), the specimen is fixed against rotation at both ends and subjected to skew symmetric counter-flexure. Then the shear span is half the specimen

length. In both setups there is slippage (partial pull-out) of the longitudinal bars from their anchorage in the concrete block(s) at the end(s) of the specimen, that macroscopically shows up as "fixed-end rotation" of the member's end section(s) (see Sections 3.2.2.3 and 3.2.2.9). In yet another setup the specimen is a simply supported beam subjected to cyclic deflections at mid-span. The symmetry with respect to the section of maximum moment in principle prevents slippage of the reinforcement towards either side of that section. This is essentially a test of two specimens simultaneously, namely of the two halves. From a certain point on during the test symmetry is destroyed by unavoidable differences in the behaviour of the two halves (with one of them reaching ultimate strength or deformation before the other), the mid-span section rotates and deflection measurements there become difficult to use and interpret.

3.2.3.2 Member Chord Rotation at Flexural Yielding of the End Section in Uniaxial Loading

Of interest is the drift ratio of the shear span of a member, L_s, at yielding of the end section of the shear span. This is the chord rotation at the yielding end, θ_y.

"Tension stiffening", i.e., the contribution of the concrete in tension between cracks to stiffness, is relatively small in members with longitudinal reinforcement ratios as high as those typical of members designed for earthquake resistance. Moreover, this contribution depends heavily on the bond along the bars between the cracks, which degrades with cyclic loading. So, as the member has normally been subjected to one or more elastic load cycles by the time its end section yields, the (anyway small) effect of concrete in tension on the overall flexural deformations of the member at yielding is negligible. Therefore, the part of the chord rotation at yielding which is due to purely flexural deformations is: $\theta_y = \varphi_y L_s/3$.

Inclined cracking and shear deformations along the shear span increase the magnitude of θ_y. Diagonal cracking near the yielding end of the member spreads yielding of the tension bars up to the point where the first diagonal crack from the end section intersects them (Fig. 3.31). This is the "shift rule" in dimensioning of the tension reinforcement for the Ultimate Limit State in bending with axial force. According to it the value of the force in the tension reinforcement is shifted from the section to which it corresponds on the basis of the moment and axial force diagrams, to one where the moment is lower (i.e. further away from the member end). The shift is due to diagonal cracking and its magnitude depends on the inclination of the diagonal cracks to the member axis and on the amount of transverse reinforcement. However, usually a default value is taken for the shift equal to the internal lever arm, z. Such a shift increases the value of θ_y which is theoretically due to flexural deformations, from $\varphi_y L_s/3$ to about $\varphi_y(L_s+z)/3$.[11] Of course, such an increase would not take place

[11] Strictly speaking the increase is to a value of $\varphi_y[(L_s-z)(1-z/L_s)(1+0.5z/L_s)/3+z(1-0.5z/L_s)]$, but the difference from $\varphi_y(L_s+z)/3$ is practically insignificant.

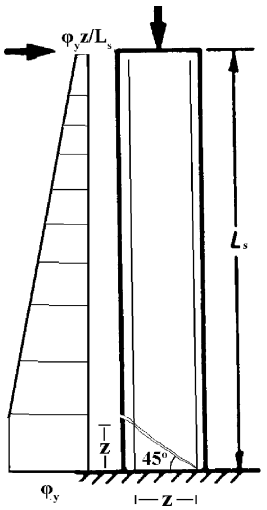

Fig. 3.31 Shift of yielding of tension reinforcement along the member due to diagonal cracking (Biskinis 2007)

unless diagonal cracking precedes flexural yielding at the end section. So, the term z should be added to L_s only if the shear force that causes diagonal cracking, V_{Rc}, is less than the shear force at flexural yielding of the end section, $V_{My} = M_y/L_s$.

Any fixed-end rotation due to reinforcement pull-out from its anchorage zone beyond the yielding end contributes to θ_y with the fixed-end-rotation, $\theta_{y,slip}$, from Eq. (3.42). However, the sum of $\varphi_y L_s/3$ (or $\varphi_y(L_s+z)/3$ if there is diagonal cracking) and of the fixed-end-rotation (if any) from Eq. (3.42) on average falls short of the "experimental" chord rotation at flexural yielding, taken at the corner of a bilinear M–θ curve fitted to the envelope of the experimental M–θ hysteresis loops, including P–Δ effects (cf. Section 3.2.2.2 under *Comparison with Experimental Results and Empirical Expressions for the Curvature*). The shortfall can be empirically corrected via the 2nd term of Eqs. (3.66), fitted to "experimental" chord rotations at flexural yielding of members with shear span ratio and reinforcement such that there are no flexure-shear interaction effects on yielding (see Section 3.2.5) (Biskinis 2007, Biskinis and Fardis 2004):

– For beam/columns with rectangular section (about 1560 tests):

$$\theta_y = \varphi_y \frac{L_s + a_V z}{3} + 0.0014\left(1 + 1.5\frac{h}{L_s}\right) + a_{sl}\frac{\varphi_y d_{bL} f_y}{8\sqrt{f_c}} \tag{3.66a}$$

– For walls (rectangular or not) and hollow rectangular members (about 250 tests):

$$\theta_y = \varphi_y \frac{L_s + a_V z}{3} + 0.0013 + a_{sl}\frac{\varphi_y d_{bL} f_y}{8\sqrt{f_c}} \tag{3.66b}$$

where:

- φ_y in the 1st term is the "theoretical" yield curvature from Eqs. (3.33), (3.34), (3.35) and (3.38) times the correction factor of 1.025, 1.015 or 1.075, for beams/columns, rectangular walls, or members with T-, U-, H- or hollow rectangular section, respectively;
- a_v is a zero-one variable:
  - $a_v = 0$, if $V_{Rc} > V_{My} = M_y/L_s$, with V_{Rc} taken here from Eurocode 2 (CEN 2004b), Eq. (3.67);
  - $a_v = 1$, if $V_{Rc} \leq V_{My} = M_y/L_s$;
- z is the length of the internal lever arm, taken as:
  - $z = d–d_1$ in beams, columns, or members with T-, H-, U- or hollow rectangular section, and:
  - $z = 0.8h$ in walls with rectangular section.
- a_{sl} is a zero-one variable:
  - $a_{sl} = 1$ if slippage of longitudinal bars from the anchorage zone beyond the end section is possible, or
  - $a_{sl} = 0$ if slippage is not possible.
- as in Eq. (3.42), f_y and f_c in the last term are in MPa.

The shear force at diagonal cracking of the member, V_{Rc}, is taken here equal to the shear resistance of members without shear reinforcement, given in Eurocode 2 (CEN 2004b) as:

$$V_{R,c} = \left\{ \max \left[180\,(100\rho_1)^{1/3}\,,\ 35\sqrt{1+\sqrt{\frac{0.2}{d}}}\,f_c^{1/6} \right] \left(1+\sqrt{\frac{0.2}{d}}\right) f_c^{1/3} + 0.15\frac{N}{A_c} \right\} b_w d \tag{3.67}$$

With ρ_1 denoting the tension reinforcement ratio and the axial load N taken positive for compression (but if N is tensile, then $V_{R,c} = 0$), Eq. (3.67) gives the value of $V_{R,c}$ in kN when b_w (width of the web) and d are in m, f_c is in MPa and N in kN.

Annex A of Part 3 of Eurocode 8 (CEN 2005a) has adopted an earlier version of Eqs. (3.66a) and (3.66b) (Biskinis and Fardis 2004) with a coefficient of 0.13 instead of 1/8 = 0.125 in the 3rd term and with Eq. (3.66b) applicable only to walls and its 2nd term replaced by $0.002[1–0.125L_s/h]$. It has also adopted an alternative form of these expressions where the pullout of tensile reinforcement at the yielding end section, $0.5f_y l_b/E_s$, has been translated to fixed-end rotation by dividing it by the distance between the tension and the compression bars in the section, $(d–d_1)$, instead of the depth of the tension zone at yielding, $(1–\xi_y)d$ (Biskinis 2007, Biskinis and Fardis 2004). The 3rd term of the alternative expressions uses $\varepsilon_y d_{bL} f_y/[6(d–d_1)\sqrt{f_c}]$ (with $\varepsilon_y = f_y/E_s$ being the yield strain of longitudinal bars) instead of $\varphi_y d_{bL} f_y/(8\sqrt{f_c})$. This

alternative fits the data almost as well as Eqs. (3.66), but is probably easier to apply in that the 3rd term is independent of φ_y, whose calculation is harder and more prone to errors.

Equations (3.66) give a median of 1.01 or 0.995 for the test-to-prediction ratio of θ_y, and a coefficient-of-variation of 32.1% or 33.7%, for beams/columns or walls/hollow rectangular members, respectively. Natural and test-to-test variability contributes to the scatter a coefficient of variation of about 10% in practically identical specimens. The rest of the scatter is mainly due to model uncertainty and corresponds to coefficients of variation equal to the values above reduced by about 1.5%. The variants of Eqs. (3.66a) and (3.66b) adopted in Part 3 of Eurocode 8 (CEN 2005a) (with the value 0.13 used in the 3rd term instead of 1/8) give as good or even slightly better fit to the data.

The comparison above refers to tests with ribbed bars. In about 20 tests of beam/columns with smooth (plain) bars the mean or the median of the test-to-prediction ratio are about 0.98. So, the poorer bond along such bars does not seem to increase member deformations at yielding.

A prime use of the prediction of θ_y from Eqs. (3.66) is for the calculation of the effective member stiffness at incipient yielding from Eq. (3.68) in Section 3.2.3.3. So, the fitting of Eqs. (3.66) to the experimental values of θ_y aims at accuracy in the median, as much for θ_y, as for the effective stiffness at yielding from Eq. (3.68) in Section 3.2.3.3. So, any mismatch in the median between the experimental and the predicted values of θ_y should not be seen independently of the median agreement or mismatch between the effective stiffness from Eq. (3.68) and the test values.

3.2.3.3 Effective Stiffness of Members at Incipient Yielding: Importance and Estimation

A fundamental simplification underlying the provisions of force-based seismic design using elastic forces reduced by the behaviour factor q is that the global inelastic response of the structure to monotonic lateral forces is bilinear, close to elastic-perfectly-plastic. Then, the stiffness used in the elastic analysis should correspond to the stiffness of the elastic branch of such a bilinear global force-deformation response. So, the full elastic stiffness of uncracked concrete in the analysis is not the proper value to use. Eurocode 8 (like US codes) requires concrete buildings be designed using in the seismic analysis stiffness values for members that take into account the effect of cracking and correspond to the initiation of yielding of the reinforcement (secant stiffness to the yield-point). Unless more accurate modelling is used, Eurocode 8 follows US codes in allowing to derive that stiffness from 50% of the uncracked gross section rigidity, $E_c I_c$, neglecting the effect of reinforcement.

Within the force- and strength-based seismic design philosophy of current seismic design codes, a high estimate of the effective stiffness gives safe-sided results, as it increases the period(s) and therefore the corresponding spectral acceleration(s) and design forces. The use of $0.5E_cI_c$ serves exactly that purpose, as the experimental secant stiffness of concrete members at incipient yielding is generally much

lower. Only the lateral drifts and the P–Δ effects computed from these overly high stiffness values may be (seriously) underestimated. As a matter of fact, Eurocode 2 (CEN 2004b) specifies as follows the effective stiffness for the calculation of 2nd-order effects in concrete structures:

- as equal to the stiffness $E_s I_s$ of the section reinforcement with respect to the centroid of the section, plus the minimum of $0.2E_c I_c$ and $0.3\nu E_c I_c$ (where $\nu = N/A_c f_c$ is the axial load ratio),
- $0.3E_c I_c$ if the reinforcement ratio exceeds 1% (although its exact value is not known in this stage of the design).

Clause 10.11.1 of ACI (2008) specifies the effective stiffness for the magnification of moments in compression members and frames due to 2nd-order effects as follows:

- $0.35E_c I_c$ for beams and cracked walls,
- $0.70E_c I_c$ for columns and uncracked walls,
- $0.25E_c I_c$ for flat plates or slabs.

Clause 10.12.3 of ACI (2008), by contrast, gives the following effective stiffness for the calculation of moment magnification due to 2nd-order effects in non-sway frames:

- the stiffness $E_s I_s$ of the reinforcement with respect to the centroid of the section, plus $0.2E_c I_c$ (i.e., as in the Eurocode 2 rule, except that the fraction of $E_c I_c$ is not taken as $0.3\nu = 0.3N/A_c f_c$, if this value is smaller than 0.2); or
- $0.2E_c I_c$, as a simpler approximation.

Note that, using in the analysis a low-side estimate of effective stiffness increases 2nd-order effects, which is safe-sided in the context of design for non-seismic actions, as with Eurocode 2 or Clause 10 of the ACI 318 code.

As elaborated in Chapter 6, seismic assessment and retrofitting of existing buildings is nowdays fully displacement-based, with direct or indirect verification of member deformation capacities against the inelastic deformation demands. So it needs a relatively accurate estimation of inelastic deformation demands throughout the structure, which in turn requires realistic values of the effective cracked stiffness of concrete members at yielding. The use of a member stiffness of $0.5E_c I_c$ for displacement-based seismic assessment and retrofitting of existing structures is unsafe: member seismic deformation demands will be seriously underestimated.

The most realistic estimate of the effective elastic stiffness of the shear span, $L_s = M/V$, in a bilinear force-deformation model of a concrete member under monotonic loading, is the secant stiffness of the shear span to the member yield-point:

$$EI_{eff} = \frac{M_y L_s}{3\theta_y} \tag{3.68}$$

where M_y is the yield moment in the bilinear M–θ model of the shear span and θ_y the chord rotation at the yielding end, both by calculation (from Sections 3.2.2.2 and 3.2.3.2, respectively).

The "experimental effective stiffness" at member yielding is obtained by using experimental values of M_y and θ_y in Eq. (3.68). Its ratio to the value obtained from Eq. (3.68), using the M_y and θ_y values from Sections 3.2.2.2 and 3.2.3.2, respectively, has a median of 1.01 or 0.99 and a coefficient of variation of 32.3% or 47.1% for beams/columns, or walls/hollow rectangular members, respectively. Natural and test-to-test variability contributes to the scatter with a coefficient of variation of about 10% in practically identical specimens. If Eqs. (3.66a) and (3.66b) are replaced by their variants in Part 3 of Eurocode 8 (CEN 2005a) for the calculation of θ_y, the agreement with the data is almost the same (Biskinis 2007, Biskinis and Fardis 2004). These comparisons refer to tests with ribbed bars. In about 20 tests of beam/columns with smooth (plain) bars the mean test-to-prediction ratio of the secant stiffness to yield point is about 1.03, implying that the poorer bond along these bars does not seem to adversely affect the member stiffness.

The specimens in the large database used for the calibration of the expressions for M_y and θ_y in Sections 3.2.2.2 and 3.2.3.2, have "experimental effective stiffness" at member yielding on average equal to 22% or 15% of the stiffness of the uncracked gross section, $E_c I_c$, for beams/columns, or walls and members with hollow rectangular section, respectively. The coefficients of variation of the experimental effective stiffness with respect to this average are about twice the values from the application of Eq. (3.68).

For Eq. (3.68) to be applied using the values of M_y and θ_y, the amount and layout of the longitudinal reinforcement should be known. In displacement-based seismic assessment of existing buildings this information is available before the analysis. If it is not, as in displacement-based seismic design of new structures, a purely "empirical effective stiffness" would be more convenient, if it is expressed in terms of geometric, etc., characteristics of the member known before dimensioning its reinforcement. The following expression has been fitted in Biskinis (2007) to the "experimental effective stiffness" at member yielding:

$$\frac{\mathrm{EI_{eff}}}{\mathrm{E_c I_c}} = a\left(0.8 + \ln\left[\max\left(\frac{L_s}{h};\, 0.6\right)\right]\right)\left(1 + 0.048\ \min\left(50\,MPa;\, \frac{N}{A_c}\right)\right) \tag{3.69}$$

where N/A_c is in MPa, and

- $a = 0.081$ for columns;
- $a = 0.10$ for beams;
- $a = 0.115$ for rectangular walls; and
- $a = 0.09$ for members with T-, U-, H- or hollow rectangular section.

Equation (3.69) refers to the – common in practice – case where slip of the longitudinal bars from their anchorage beyond the member's end section is physically possible ($a_{sl} = 1$ in Eqs. (3.66)). If it isn't (i.e., if $a_{sl} = 0$ in Eqs. (3.66)), the effective stiffness increases by one-third, i.e. the values above should be multiplied by 4/3.

Being purely empirical, Eq. (3.69) achieves a median of 1.00 for the test-to-prediction ratio. However, neglecting the dependence of effective stiffness on the amount and layout of longitudinal reinforcement increases the scatter: the coefficient of variation of the test-to-prediction ratio is 37.6, 58.7 and 42.6%, for beams/columns, rectangular walls and members with T-, U-, H- or hollow rectangular section, respectively. More serious than the larger scatter is the lack-of-fit of Eq. (3.69) with respect to the amount of longitudinal reinforcement. Equation (3.69) has been fitted to a database of mainly seismically detailed members, with total reinforcement ratio between 0.1 and 7% (2% on average) and tension reinforcement ratio between 0.1 and 4.8% (on average 0.9%). So it overpredicts the experimental value by 10% on average for members with reinforcement ratio at the lower end of the range and underpredicts it by 40% on average at the upper end.

One would expect the empirical effective stiffness to be a decreasing function of $d_{bL}f_y/(h\sqrt{f_c})$, which is proportional to the last term in Eqs. (3.66) and is known before dimensioning of the longitudinal reinforcement if its diameter has been chosen. However, the increase of the "experimental effective stiffness" with the tension reinforcement ratio – which does not appear in Eq. (3.69) and is proportional to the square of d_{bL}/h– fully masks its dependence on $d_{bL}f_y/(h\sqrt{f_c})$ in the cases when slip from the anchorage beyond the member's end takes place.

3.2.3.4 Flexure-Controlled Ultimate Chord Rotation Under Uniaxial Loading: Calculation from Curvatures and the Plastic Hinge Length

The ultimate condition in terms of deformations is commonly defined conventionally, as described in Sections 3.2.2.4 and 3.2.2.7 for the ultimate curvature. The ultimate chord rotation occurs at the same time as the ultimate curvature and is defined similarly.

The most common model for the ultimate chord rotation at the member end (let's say A) where the moment is maximum (Fig. 3.32) uses the yield and ultimate curvatures at section A and assumes that at ultimate conditions the plastic part of the curvature is constant and equal to $\varphi_u - \varphi_y$ over a length L_{pl} next to the end section at A. This means that the real distribution of plastic curvatures, which is nearly triangular over the length of plastification l_{pl}, is replaced by a uniform plastic curvature over a shorter length $L_{pl} \approx 0.5l_{pl}$. L_{pl} is called "plastic hinge length" and is a conventional quantity. The plastic rotation that has developed in the plastic hinge length by the time the ultimate condition is reached is equal to $\theta_{pl,u} = (\varphi_u - \varphi_y)L_{pl}$. It takes place with respect to the centre of the plastic hinge length and produces a plastic part of the deflection at the end B of the shear span equal to $\theta_{pl}(L_s - L_{pl}/2)$. If the entire deflection at B is attributed to flexure, its elastic part is equal to $\varphi_y {L_s}^2/3$. Therefore, the ultimate chord rotation at end A is equal to $\theta_A = \delta_B/L_s$, i.e. to:

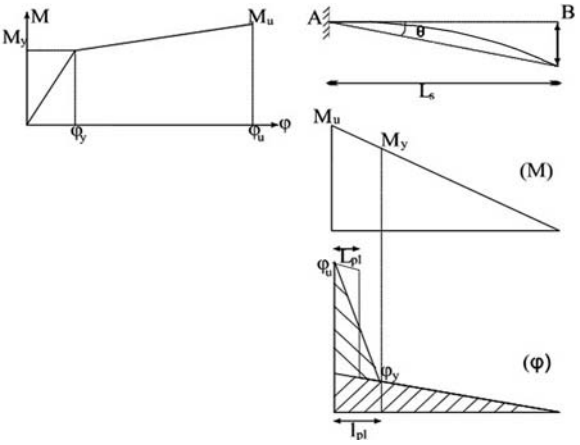

Fig. 3.32 Actual plastification length, l_{pl} and plastic hinge length L_{pl} in the shear span

$$\theta_u = \varphi_y \frac{L_s}{3} + \left(\varphi_u - \varphi_y\right) L_{pl} \left(1 - \frac{L_{pl}}{2L_s}\right) \tag{3.70a}$$

A variant of Eq. (3.70a) may give the chord rotation at end A, θ, when the curvature φ at A is between yielding and ultimate:

$$\theta = \varphi_y \frac{L_s}{3} + \left(\varphi - \varphi_y\right) L_{pl} \left(1 - \frac{L_{pl}}{2L_s}\right) \tag{3.70b}$$

If the behaviour is postulated to be purely flexural, the chord rotation at yielding equals $\theta_y = \varphi_y L_s/3$. So, the chord rotation ductility factor, $\mu_\theta = \theta/\theta_y$, is linked to the curvature ductility factor of the end section of the shear span, $\mu_\varphi = \varphi/\varphi_y$, as:

$$\mu_\theta = 1 + \left(\mu_\phi - 1\right) \frac{3L_{pl}}{L_s} \left(1 - \frac{L_{pl}}{2L_s}\right) \approx \frac{3L_{pl}}{L_s} \mu_\phi \tag{3.71}$$

The formulation in Eqs. (3.70) and (3.71) offers the following advantages:

- it represents a mechanical and physical model (inelasticity is considered as lumped in the plastic hinge and uniformly spread within the plastic-hinge length), and
- φ_y and φ_u can be expressed through plane section analysis in terms of cross-section and material properties, as in Sections 3.2.2.2 and 3.2.2.4, respectively.

This formulation normally deals indirectly with any effects of shear, bond-slip, etc., through L_{pl}, which is not a physical but a conventional quantity, such that Eq. (3.70a) is satisfied when the ultimate deformation is attained.

Notwithstanding its mechanical and physical appeal, the real criterion for the value of Eq. (3.70a) is its ability to predict the experimental ultimate drift ratio or chord rotation, θ_u. Empirical expressions for L_{pl} needed to this end cannot be developed independently of the models used for the other variables in Eq. (3.70a), notably for φ_u and φ_y. To maintain the apparent rationality of Eq. (3.70a), priority should be given to models based on rational mechanics. A natural choice for φ_y is the model in Section 3.2.2.2, based on first principles and calibrated for good average agreement with test results. Regarding φ_u, a good choice is the model in Section 3.2.2.4 (also based on first principles) in conjunction with the proposals developed/calibrated in Section 3.2.2.10 on the basis of a large volume of test data. Those proposals include the use of the confinement model of Eqs. (3.4), (3.5), (3.10), (3.16) or (3.17) and of the ultimate steel strain, ε_{su}, from Eqs. (3.64).

A better overall fit of Eq. (3.70a) to the data on θ_u is possible, if the chord at yielding, θ_y, from Eqs. (3.66) in Section 3.2.3.2 is used in lieu of the flexural term, $\varphi_y L_s/3$, alone. Besides, to recognise the contribution of the fixed-end rotation due to bar pull-out from the anchorage zone beyond the end of the member where failure takes place, we should add to the right-hand-side of Eq. (3.70a) the fixed-end rotation that takes place between yielding and ultimate curvature of the end section, from Eqs. (3.63) in Section 3.2.2.9. The final expression is:

$$\theta_u = \theta_y + a_{sl}\,\Delta\theta_{u,slip} + (\varphi_u - \varphi_y) L_{pl} \left(1 - \frac{L_{pl}}{2L_s}\right) \tag{3.72}$$

The 1st term in Eq. (3.72) is the chord rotation at yielding from Eqs. (3.66). The 2nd one is the fixed-end rotation from yielding to ultimate due to bar slippage from the anchorage zone beyond the member end where flexural failure takes place. It may be calculated from Eqs. (3.63), with $a_{sl} = 0$ if bar slippage from the anchorage zone beyond the member end is not physically possible, or with $a_{sl} = 1$ if it is (cf. 3rd term in Eqs. (3.66)). The 3rd term is the plastic deformation of the flexural plastic hinge.

The same empirical expression for L_{pl} cannot fit both the monotonic and the cyclic data. Best among the possible simple expressions for L_{pl} seem to be a linear combination of the shear span, L_s, and of the section depth, h. Under the conditions outlined above for the calculation of φ_y, φ_u, θ_y, the following expressions provide optimal overall fit to θ_u at flexural failure of rectangular beams, columns and walls and for members with T-, H-, U- or hollow rectangular section, in monotonic or cyclic loading (about 300 or 1050 tests, respectively):

– if the ultimate concrete strain is given by the two separate expressions of Eqs. (3.16) for monotonic and cyclic loading (Biskinis 2007):

  • for monotonic loading, regardless of detailing for earthquake resistance:

$$L_{pl,mon} = h\left(1.1 + 0.04 \min\left(9; \frac{L_s}{h}\right)\right) \tag{3.73a}$$

- for cyclic loading, but with member detailing for earthquake resistance:

$$L_{pl,cy} = 0.2\,h\left(1 + \frac{1}{3}\min\left(9; \frac{L_s}{h}\right)\right) \tag{3.73b}$$

– if the ultimate concrete strain is given by the same expression for monotonic and cyclic loading, Eq. (3.17):

- for monotonic loading, regardless of detailing for earthquake resistance:

$$L_{pl,mon} = h\left(1.2 + 0.04\min\left(9; \frac{L_s}{h}\right)\right) \tag{3.74a}$$

- for cyclic loading, but with member detailing for earthquake resistance:

$$L_{pl,cy} = 0.2\,h\left(1 + \frac{3}{8}\min\left(9; \frac{L_s}{h}\right)\right) \tag{3.74b}$$

If Eqs. (3.16) and (3.73) are used, the test-to-prediction ratio of Eq. (3.72) has a median of 1.00 and coefficient of variation of 66.8, 44.8 and 51.7%, for monotonic, cyclic loading and overall (monotonic and cyclic), respectively. Better overall agreement is achieved if Eqs. (3.17) and (3.74) are used instead of Eqs. (3.16) and (3.73): the median of the test-to-prediction ratio is also 1.00 and the coefficient of variation 65.6, 43.5 and 50.5%, for monotonic, cyclic loading and overall (monotonic and cyclic), respectively. Besides, the median is 1.07 and 1.03 for the sub-groups of rectangular walls and members with T-, H-, U- or hollow rectangular section, compared to medians of 1.08 and 1.05 for these two sub-groups if Eqs. (3.16) and (3.73) are used. Natural and test-to-test variability contributes to the scatter a coefficient of variation of about 18% in practically identical specimens. After subtracting this source of scatter, the coefficient of variation due to model uncertainty is equal to the values quoted above, reduced by 2.5% for the larger of these values to 3.5% for the smaller ones. But even after this reduction, the variance of the cyclic data with respect to Eq. (3.72) is still about 80% of their total variance if Eqs. (3.16) and (3.73b) are used, or about 75% of its value if Eqs. (3.17) and (3.74b) are applied. The picture is only slightly better for the monotonic data.

Well known or widely used alternatives for the plastic hinge length can be evaluated on the basis of the data used for the fitting of Eqs. (3.73) and (3.74). Each expression for L_{pl} is applied here as proposed in its source, i.e., with its accompanying models for the calculation of φ_{u} and Eq. (3.70a) (or variations thereof) instead of Eq. (3.72), as slippage of reinforcement from its anchorage zone is reflected by a separate term in these expressions for L_{pl}, in lieu of the 2nd term at the right-hand-side of Eq. (3.72).

I. The first two expressions evaluated here are those given in Annex A of Part 3 of Eurocode 8 (CEN 2005a) for cyclic loading of members detailed for earthquake

resistance. According to CEN (2005a) these expressions are meant to be used in Eq. (3.70a), but with the full expression for θ_y from Eqs. (3.66) instead of the flexure-only yield term, $\varphi_y L_s/3$. The ultimate steel strain values specified in CEN (2005a) for the calculation of φ_u have been given at the end of Section 3.2.2.10 under point (a). A different expression is given in CEN (2005a) for L_{pl}, for each one of the two alternative concrete confinement models in CEN (2005a):

i for the model of Eqs. (3.4), (3.5), (3.10) and (3.18):

$$L_{pl} = \frac{L_s}{30} + 0.2\,h + a_{sl}\frac{0.11 d_{bL} f_{yL}}{\sqrt{f_c}} \qquad (f_{yL} \text{ and } f_c \text{ in MPa}) \qquad (3.75)$$

ii. for the model of Eqs. (3.8), (3.9) and (3.13) (i.e., according to CEN (2004b), CEB (1991)):

$$L_{pl} = 0.1 L_s + 0.17\,h + a_{sl}\frac{0.24 d_{bL} f_{yL}}{\sqrt{f_c}} \qquad (f_{yL} \text{ and } f_c \text{ in MPa}) \qquad (3.76)$$

Options (i) and (ii) produce a median test-to-prediction ratio for θ_u in over 1000 cyclic tests of rectangular beams, columns, walls and members with T-, H-, U- or hollow rectangular section under cyclic loading equal to 0.90 and 0.79, respectively. The corresponding coefficients of variation are 52.5 and 62.1% (Biskinis 2007). The poorer performance of option (ii) (which includes also a certain lack of fit for high experimental values of θ_u) is mainly due to its serious handicap in the prediction of ultimate curvature (see Section 3.2.2.10, point (a)).

II. The other model evaluated here is the widely used and quoted expression (Paulay and Priestley 1992):

$$L_{pl} = 0.08 L_s + a_{sl}(0.22 d_{bL} f_{yL}) \qquad (f_{yL} \text{ in MPa}) \qquad (3.77)$$

It is used in Eq. (3.70a), along with the σ-ε models and parameters for the calculation of φ_u outlined at the end of Section 3.2.2.10 under point (b), namely:

- the two concrete confinement models in Mander et al. (1988) and Paulay and Priestley (1992) and
- the two ultimate steel strain options for which the ultimate curvature predictions resulting from the above confinement models have been evaluated at the end of Section 3.2.2.10 under point (b), namely:

  a. the ultimate steel strain in Annex A of Part 3 of Eurocode 8 (CEN 2005a) and described in Section 3.2.2.10, point (a); this is the strain used in the evaluation above pertaining to Part 3 of Eurocode 8 (CEN 2005a), for both options (i) and (ii); or
  b. the values from Eqs. (3.64) in Section 3.2.2.10; used also above in the calculation of θ_u from Eq. (3.72) together with Eqs. (3.73) and (3.74) and the concrete ultimate strain models of Eqs. (3.16) and (3.17), respectively.

The confinement model in Mander et al. (1988) combined with options (a) or (b) for steel give a median test-to-prediction ratio for θ_u in over 1000 cyclic tests of rectangular beams, columns, walls or members with T-, H-, U- or hollow rectangular section equal to 0.96 or 1.14, respectively. The corresponding coefficient of variation is 74.9% or 65.5% (Biskinis 2007). The median and the coefficient of variation of the test-to-prediction ratio for the confinement model in Paulay and Priestley (1992) used with options (a) or (b) for steel are 0.83 or 1.035 and 83.6% or 70.9%, respectively (Biskinis 2007). These four options give a median test-to-prediction ratio for the approximately 300 monotonic tests between 1.7 and 1.85.

Note that, for all options considered in I and II above the variance of the cyclic data with respect to Eq. (3.72) is not less than their total variance, even after removing the contribution of natural and test-to-test variability from the scatter. So, none of these options seems to be of much value for the prediction θ_u.

3.2.3.5 Flexure-Controlled Ultimate Chord Rotation Under Uniaxial Loading: Empirical Calculation

The scatter of the predictions of Eq. (3.72), used together with Eqs. (3.73) and (3.74) and the corresponding ultimate concrete strains, Eqs. (3.16) and (3.17), respectively, is significant. Even larger is that of Eq. (3.70a), used together with Eqs. (3.75), (3.76) and (3.77) and the corresponding concrete confinement and steel ultimate strain models. In view of this, purely empirical expressions for the chord rotation at flexural failure, θ_u, have been developed in Panagiotakos and Fardis (2001a). That work has shown:

- that θ_u depends on whether loading to failure is monotonic or fully-reversed (cyclic), but is rather insensitive to the number of major deflection cycles preceding failure;
- that monotonic test data should be distinguished from the cyclic, but used together in regressions for θ_u, as complementary: monotonic tests in the literature cover many members with asymmetric reinforcement and/or less ductile steel, but few walls or members with T-, H-, U- or hollow rectangular section and no diagonally reinforced elements; the reverse applies for the available cyclic tests;

As a follow up and improvement over (Panagiotakos and Fardis 2001a), a larger databank of test results has been used in Biskinis (2007) and Biskinis and Fardis (2004, 2007) to develop three alternative – and almost equivalent – expressions for the chord rotation at flexure-controlled failure, θ_u, of members with rectangular compression zone and detailing for earthquake resistance (including the use of continuous ribbed bars for the longitudinal reinforcement). The first one, Eq. (3.78a), is for the total ultimate chord rotation, θ_u. Equations (3.78b) and (3.78c) by contrast separate θ_u into its elastic component, θ_y, given by Eqs. (3.66), and the plastic one, $\theta_u{}^{pl} = \theta_u - \theta_y$.

$$\theta_u = a_{st}(1 - 0.43a_{cy})\left(1 + \frac{a_{sl}}{2}\right)(1 - 0.42a_{w,r})\left(1 - \frac{2}{7}a_{w,nr}\right)(0.3^{\nu})$$
$$\left[\frac{\max\,(0.01;\,\omega_2)}{\max\,(0.01;\,\omega_1)}f_c\right]^{0.225}\left[\min\left(9;\,\frac{L_s}{h}\right)\right]^{0.35}25^{\left(\frac{a\rho_s f_{yw}}{f_c}\right)}1.25^{100\rho_d} \tag{3.78a}$$

$$\theta_u = \theta_y + \theta_u^{pl} = \theta_y + a_{st}^{pl}(1 - 0.52a_{cy})$$
$$\left(1 + \frac{a_{sl}}{1.6}\right)(1 - 0.44a_{w,r})\left(1 - \frac{a_{w,nr}}{4}\right)(0.25)^{\nu}\left(\frac{\max(0.01;\,\omega_2)}{\max(0.01;\,\omega_1)}\right)^{0.3}$$
$$f_c^{0.2}\left[\min\left(9;\,\frac{L_s}{h}\right)\right]^{0.35}25^{\left(\frac{a\rho_s f_{yw}}{f_c}\right)}1.275^{100\rho_d} \tag{3.78b}$$

$$\theta_u = \theta_y + \theta_u^{pl} = \theta_y + a_{st}^{hbw}(1 - 0.525a_{cy})$$
$$(1 + 0.6a_{sl})\left(1 - 0.052\max\left(1.5;\min\left(10,\,\frac{h}{b_w}\right)\right)\right)(0.2)^{\nu}$$
$$\left[\frac{\max(0.01;\,\omega_2)}{\max(0.01;\,\omega_1)}\min\left(9;\,\frac{L_s}{h}\right)\right]^{\frac{1}{3}}f_c^{0.2}25^{\left(\frac{a\rho_s f_{yw}}{f_c}\right)}1.225^{100\rho_d} \tag{3.78c}$$

where:

a_{st}, $a^{pl}{}_{st}$, $a^{hbw}{}_{st}$: coefficients for the steel type: $a_{st} = a^{pl}{}_{st} = 0.0185$ and $a^{hbw}{}_{st} = 0.022$ for ductile hot-rolled or heat-treated (Tempcore) steel; $a_{st} = 0.0115$, $a^{pl}{}_{st} = 0.009$ and $a^{hbw}{}_{st} = 0.0095$ for cold-worked steel;

a_{cy}: zero-one variable for the type of loading, equal to $a_{cy} = 0$ for monotonic loading and to $a_{cy} = 1$ for cyclic loading;

a_{sl}: zero-one variable for slip, equal to $a_{sl} = 1$ if there is slip of the longitudinal bars from their anchorage beyond the section of maximum moment, or to $a_{sl} = 0$ if there is not (cf. Eqs. (3.66) and (3.72));

$a_{w,r}$: zero-one variable for rectangular walls, $a_{w,r} = 1$ for rectangular walls, $a_{w,,r} = 0$ otherwise;

$a_{w,nr}$: zero-one variable for non-rectangular walls, $a_{w,nr} = 1$ for walls with T-, H-, U- or hollow rectangular section and $a_{w,nr} = 0$ for other members;

$\nu = N/bhf_c$, with b = width of compression zone, N = axial force, positive for compression;

$\omega_1 = (\rho_1+\rho_v)f_{yL}/f_c$: mechanical reinforcement ratio of tension and "web" longitudinal reinforcement;

$\omega_2 = \rho_2 f_{yL}/f_c$: mechanical reinforcement ratio of compression longitudinal reinforcement;

f_c: uniaxial (cylindrical) concrete strength (MPa);

$L_s/h = M/Vh$: shear span ratio at the section of maximum moment;
$\rho_s = A_{sh}/b_w s_h$: ratio of transverse steel parallel to the loading direction;
f_{yw}: yield stress of transverse steel;
a: effectiveness factor for confinement by transverse reinforcement from Eq. (3.24) (using Eqs. (3.20c) and (3.21));
ρ_d: steel ratio of diagonal reinforcement in each diagonal direction.
b_w: width of one web, even in cross-sections with one or more parallel webs (for Eq. (3.78c) which distinguishes walls and members with T-, H-, U- or hollow rectangular section only through the aspect ratio, h/b_w, of each web).

Annex A of Eurocode 8, Part 3 (CEN 2005a) has adopted the special case of Eqs. (3.78a) and (3.78b) for cyclic loading ($a_{cy} = 1$) and slippage of the longitudinal bars from their anchorage beyond the section of maximum moment ($a_{sl} = 1$), but with a different value of the coefficient multiplying $a_{w,r}$ for walls: 0.40, in lieu of 0.42 or 0.44.

The dependence of θ_u on h/b_w according to Eq. (3.78c) suggests that the lower ultimate deformation of non-rectangular walls and mainly of rectangular ones, compared to beams or columns with more compact section, may be due to lateral instability.

Equations (3.78b) and (3.78c) can be extended more easily than Eq. (3.78a) to variations of the standard case of unretrofitted members with continuous longitudinal bars. Lap-splicing of longitudinal bars within the plastic hinge region (see Section 3.2.3.9) and/or wrapping of the end region with an FRP jacket (see Section 3.2.3.10) affect differently the elastic and the plastic part of the ultimate chord rotation and should be accounted for accordingly.

For the subsets of 300 monotonic and 1040 cyclic tests available, as well as overall, each one of Eqs. (3.78) give a median test-to-prediction ratio for θ_u of (effectively) 1.00. The coefficient of variation of the test-to-prediction ratio in the monotonic tests is 53.3%. In the 1040 cyclic tests the corresponding values are 37.4, 37.3 and 38%. For the overall 1340 monotonic or cyclic tests the coefficient of variation of the test-to-prediction ratio is 42.4%. For the subgroup of 62 rectangular walls, Eq. (3.78a), (3.78b) or (3.78c) give a median test-to-prediction ratio of 1.00 and a coefficient of variation of 33.6, 33.1 and 37.5%. For 55 members with T-, H-, U- or hollow rectangular section, either Eq. (3.78a) or (3.78b) give a median test-to-prediction ratio of 1.00 and coefficients of variation of 33 and 31.5%, while Eq. (3.78c) gives a median of 1.07 and a coefficient of variation of 28.6%.

Although Eqs. (3.78) give a fairly uniform scatter throughout the full range of all independent variables, they underpredict high values of θ_u, especially for monotonic loading, and overpredict low ones. They share this lack of fit with any model in Section 3.2.3.4 based on curvatures and the plastic hinge length. In all cases Eqs. (3.78) give a less biased and more accurate estimate of θ_u than anyone of the models in Section 3.2.3.4. The scatter of the test-to-prediction ratio is much less, notably not much larger than that of Eqs. (3.66) for the chord rotation at yielding, and not unduly large compared to the contribution of the natural or test-to-test variability, which gives a coefficient of variation of about 18% for θ_u of practically

identical specimens. After subtracting this source of scatter, the coefficient of variation due to model uncertainty is equal to the values quoted above, reduced by about 3% for the larger of these values to 5% for the smaller ones. After this reduction, the variance of the cyclic data with respect to Eqs. (3.78a), (3.78b) or (3.78c) is 36.5%, 41.5% or 41%, respectively of their total variance. The corresponding variances of the monotonic data values are 43, 44.5 and 46%, respectively. So, Eqs. (3.78) perform better than any of the models in Section 3.2.3.4.

The few data for members without detailing for earthquake resistance (e.g., not closed stirrups), but with continuous ribbed (deformed) longitudinal bars, show that their chord rotation at flexure-controlled failure may be obtained by the following modification of Eqs. (3.78) (Biskinis 2007):

$$\theta_{u,old} = \theta_{u,Eq.(3.78a)} / 1.2, \text{ or} \tag{3.79a}$$

$$\theta_{u,old} = \theta_y + \theta^{pl}_{u,Eq.(3.78b) \text{ or } Eq.(3.78c)} / 1.2 \tag{3.79b}$$

Annex A of Eurocode 8, Part 3 (CEN 2005a) has adopted a version of Eqs. (3.79) with factor $1/1.2 = 0.833$ replaced by 0.825.

For about 50 cyclic tests of members without detailing for earthquake resistance but with continuous ribbed longitudinal bars, Eq. (3.79a) and (3.79b) (the latter with $\theta_u{}^{pl}$ from Eq. (3.78c)) give a median of 1.00 for the test-to-prediction ratio and a coefficient of variation of 30.8%. The corresponding values for Eq. (3.79b) with $\theta_u{}^{pl}$ from Eq. (3.78b) are 0.99 and 32.2% (Biskinis 2007). The Eurocode 8-Part 3 versions give medians higher than the above by 0.01.

Few (about 30) available cyclic tests of members without detailing for earthquake resistance and continuous smooth (plain) longitudinal bars suggest the following expression for the chord rotation at flexure-controlled failure, giving a median of 1.00 and a coefficient of variation of 32.7% for the test-to-prediction ratio:

$$\theta_{u,smooth} = 0.95\,\theta_{u,Eq.(3.79)} \tag{3.80}$$

3.2.3.6 Member Axial Deformations Due to the Flexural Response

When the curvature increases from zero to φ, the axial strain at mid-depth of a section changes by:

$$\Delta\varepsilon_o = |\varphi|(0.5 - \xi)d \tag{3.81}$$

If the axial load on the cross-section is zero or low (as in beams or in walls, respectively), the neutral axis depth, normalised to the effective depth d as ξ, is less than 0.5. It may even become negative during the phase of the response when the cracks are open through the depth and the steel couple alone resists the applied moment. Because ξ increases with increasing axial force ratio, ν, the higher the value of ν, the lower is the additional elongation (as a comparison between

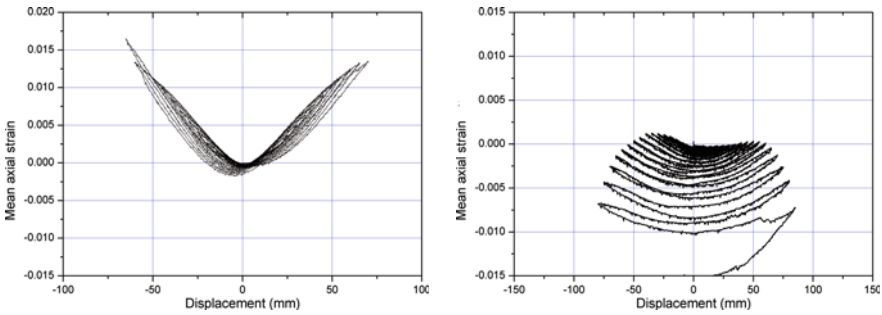

Fig. 3.33 Axial strain at section mid-depth due to cycling of the lateral displacement: (**a**) column with low axial force that does not fail; (**b**) column with high axial load ultimately failing in bending

Fig. 3.33(a) and (b) shows). If ν exceeds the balance load, the value of ξ exceeds 0.5 and the axial strain at mid-depth of the cross-section turns into shortening.

At each displacement cycle an axial *extension* normally accompanies the development of curvature, regardless of the sign of curvature. Except during the phase when cracks are open through the depth, the value of ξ is approximately constant along the member and the total additional axial displacement between two sections A and B of the member is equal to:

$$\Delta\delta_x = \int_l \Delta\varepsilon_o \, dx = (0.5 - \xi)d \int_l |\varphi| dx = (0.5 - \xi)\theta_{AB} d \tag{3.82}$$

where θ_{AB} is the relative rotation of sections A and B.[12] Equation (3.82) shows that the maximum additional axial extension takes place when relative rotation attains its peak value and is proportional to it.

The axial extension given by Eqs. (3.81) and (3.82) is additional to any axial deformation that may exist during the "neutral" part of the loading cycle, i.e. when the section curvature, φ, is (about) zero. At that stage through-depth cracks may be open and the total axial strain at mid-depth of the section, ε_o, is the average of the permanent strains locked in the tension and the compression reinforcement. These permanent strains are normally tensile (see the values of strain in Figs. 3.5, 3.6 and 3.7 at zero stress, after several load cycles). In beams, or in columns and walls with low axial load, the tensile strain at mid-depth of the section may be significant in magnitude and increase in a ratcheting manner during cycling of the deflection (see evolution of axial displacements at the bottom left diagram of Fig. 3.34). In columns, after the cover spalls, the concrete core partially disintegrates and/or vertical bars buckle, the mean compressive stress of the concrete increases and normally turns the axial strain, ε_o, at section mid-depth during the "neutral" part of the loading cycle from extension to shortening. Axial shortening accelerates as failure due to cyclic

[12] If moments and curvatures change sign between sections A and B, θ_{AB} is not the angle between the tangent to the member axis at these two sections, but the sum of the absolute values of relative rotations between section A and the point of inflection and between the point of inflection and section B.

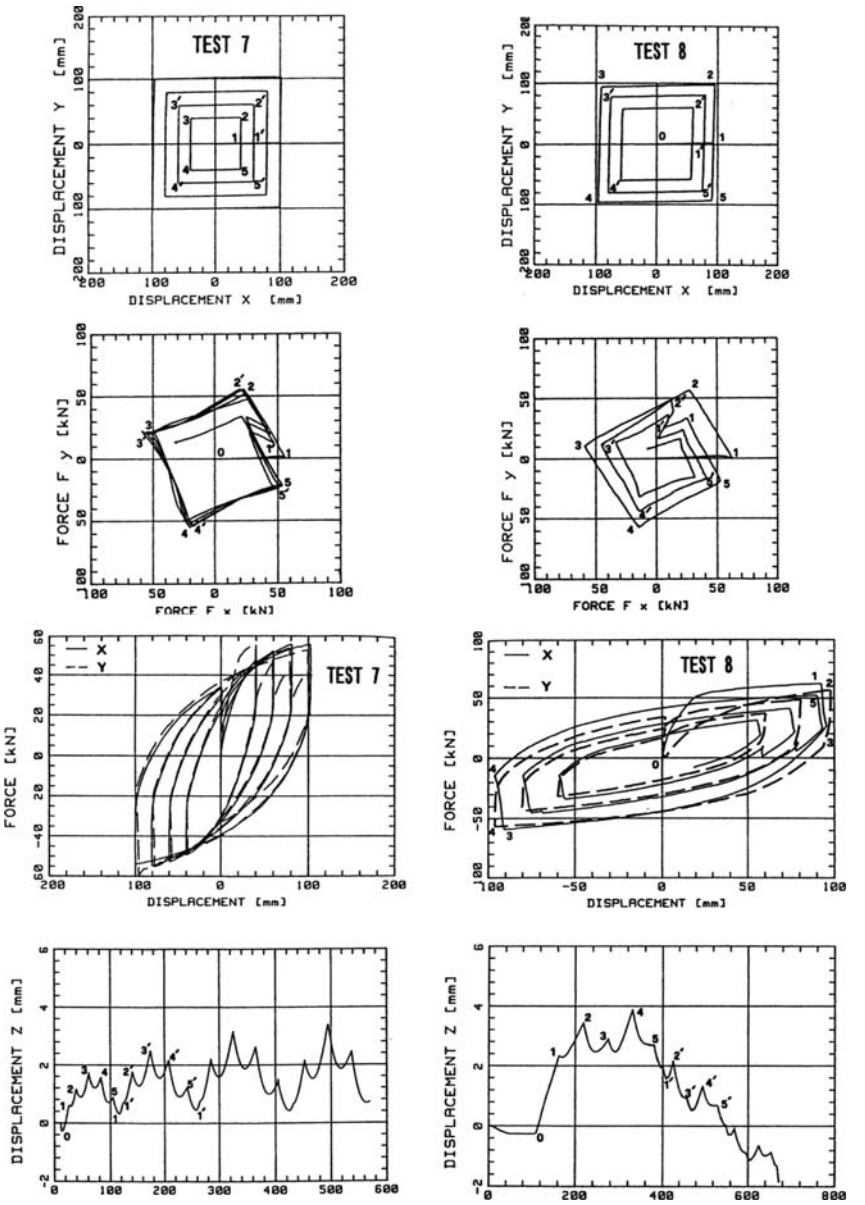

Fig. 3.34 Column biaxial deflection paths (**a**), (**b**), resulting biaxial force paths (**c**), (**d**), force-deflection loops in the two lateral directions (**e**), (**f**), evolution of axial displacement (**g**), (**h**) (Bousias 1993)

loading approaches (Fig. 3.33(b)). So, what has started as accumulation of tensile axial strains at the axis of the column may at the end of the cyclic load history revert into net shortening (see evolution of axial displacements at the bottom right diagram of Fig. 3.34). Moreover, if the axial load ratio ν has intermediate values (e.g., above 0.2), from the very beginning of the cyclic loading the ratcheting axial strain at mid-depth of the column section, ε_o, during the "neutral" part of the loading cycle is shortening instead of elongation (Fig. 3.33(b)).

Unlike the axial strain of Eq. (3.81) that may refer to the full length and produces a net axial elongation at the peak of the lateral displacement cycle according to Eq. (3.82), ratcheting axial strains that develop during the "neutral" (low-displacement) part of the load cycle according to the previous paragraph take place only within the plastic hinge. Therefore, their overall effect on the length of the member is normally smaller than the additional net elongation of Eq. (3.82) at the peaks of the cyclic lateral displacement history.

There is another facet of the coupling between flexural and axial behaviour, notably the effect of the variation of axial force on flexural deformations: for constant moment, the reduction of flexural deformation due to an increase in the axial compression is less than its increase due to an axial force reduction by the same amount. So, cycling of the axial force causes a ratcheting increase of flexural deformations. Their cumulative magnitude is significant in comparison to the residual flexural deformations due to cycling of the moment itself (Bousias et al. 1992, 1995). The build-up of flexural deformations due to an axial force that varies concurrently with the bending moments amounts to a gradual, albeit significant, apparent degradation of flexural stiffness.

According to Eq. (3.82) walls with large effective depth, d, develop large net elongation at the centroid of the section concurrently with the peaks of their lateral displacements response. We have seen in Section 2.2.2.4 that the effects of such elongation on the response and performance of wall or wall-equivalent dual systems are beneficial.

Compared to walls, columns have much shorter effective depth, d, and larger values of ξ. So, the peaks of their lateral displacement response are accompanied by small additional elongation according to Eq. (3.82). This additional elongation brings about an increase in the axial compression of those columns that have larger size (effective depth, d), smaller ξ-value (i.e., lower axial load ratio, ν) and/or larger deformation response (relative rotation between sections, θ_{AB}) than the other columns, especially their neighbouring ones. The increase in axial compression of these columns will be counterbalanced by a reduction in the others, effected through shear forces in the beams connecting the columns in the 3D frame structural system. Although small, the increase in axial compression is detrimental for the performance of large, lightly loaded columns with the larger deformation response, as it reduces their ultimate flexural deformation. By contrast, the net shortening of the columns with fairly heavy axial load (with axial load ratio well above 0.2), or of any column that approaches its ultimate deformation capacity, has a beneficial effect, as it causes part of the axial load to be transferred – via shear forces in the beams – to other columns of the system.

Beams have about the same effective depth, d, as columns but much smaller ξ-values. So, the additional net elongation according to Eq. (3.82) accompanying the peaks of their flexural response is larger. The columns into which a beam frames restrain this axial extension through shear forces translated into a compressive axial force in the beam. This compressive force will not only tend to reduce its axial extension, but will also affect its flexural behaviour, increasing its stiffness and strength, etc.

The three paragraphs above have pointed out the coupling between the flexural and the axial behaviour of the members of real frames or dual structural systems. This coupling is not taken into account explicitly in practical seismic design. To account for it in a nonlinear seismic response analysis, a member model should capture not only the flexural behaviour, but also the axial one, including its coupling with the flexural response. Fibre models, described in Section 4.10.1.2, have this capability.

3.2.3.7 Flexural Behaviour Under Cyclic Biaxial Loading

The behaviour of axially loaded concrete members under biaxial moment histories is important, as in general the seismic response of columns in concrete frames is in three dimensions (3D). Biaxial flexure reduces the moment resistance in any of the two principal directions of bending and increases cyclic strength degradation compared to uniaxial loading. By contrast, the beams of 3D frame systems are subjected to uniaxial flexure and do not suffer from the adverse effects of biaxial loading. So, biaxial column moments and the 3D response work against strong-column/weak-beam behaviour and reduce the effectiveness of the relevant criterion, Eq. (1.4), applied separately in two orthogonal horizontal directions in 3D frames.

Test results on axially loaded members under biaxial bending moment histories are limited. So, as the manner in which the histories of bending moments in the two orthogonal directions are combined adds considerably to the complexity of the problem, current knowledge of the inelastic behaviour of columns under biaxial cyclic moments is well behind our understanding of their behaviour in uniaxial cyclic flexure with axial load.

The available test results point to the conclusion that after flexural yielding there is strong coupling of the behaviour in the two orthogonal directions of bending. The M–φ and M–θ response in one of these directions is affected by the magnitude and the history of the moment and/or deformation in the orthogonal direction. The main effects of this coupling on the M–φ and M–θ behaviour in each of the two orthogonal directions of bending are the following:

1. The apparent resistance and stiffness in each individual direction decrease, owing to a concurrent deformation in the orthogonal direction. So, the moment component required to maintain a given deformation in the same direction drops (Fig. 3.34). Similarly, the moment increment necessary for an increment in deformation decreases. Ratcheting flexural deformations in the direction of a moment

component that is maintained constant are induced by cycling of the deformation in the orthogonal direction (Bousias 1993, Bousias et al. 1992, 1995).

2. The hysteretic energy dissipation increases, as hysteresis loops in each individual direction become broader (e.g., when the peak resistance in a cycle drops under constant deformation in its own direction, owing to an increase in moment and deformation in the orthogonal direction, Fig. 3.34). If the response is described in terms of a path in the 2D space of the two components of bending moment and the concurrent path in the 2D space of the two deformation components, the deformation vector always trails the moment vector by a "phase lag", ψ (Fig. 3.34). The increase in hysteretic energy dissipation due to the coupling of the two components can be expressed as an equivalent viscous damping ratio equal to $\sin\psi$ (Bousias et al. 1992, 1995). The "phase lag", ψ, increases with inelasticity, i.e. with the magnitude of the post-yield excursion, especially when column failure is imminent.
3. The deformation capacity in each individual direction decreases. When a flexure-controlled ultimate deformation is reached (i.e., when the resultant of the two moment components cannot increase above 80% of the peak moment resultant reached so far during the biaxial response) the individual deformation components are lower than they would had been, if flexure-controlled ultimate deformation were attained by uniaxial loading in the corresponding lateral direction.

Effects no. 1 and 3 are adverse, but effect no. 2 is beneficial.

The additional axial extension accompanying biaxial flexural deformations roughly follows Eqs. (3.81) and (3.82) in Section 3.2.3.6 and is independent of the direction of the lateral displacement. The same applies for the ratcheting axial strains (extension for low values of axial load ratio, shortening for medium or high ones) that accumulate due to cycling of the deflections. The axial displacements at the bottom of Fig. 3.34 increase in a ratcheting manner during cycling of the lateral displacement. At the diagram on the right the axial extension turns at the end of the load history to shortening as failure due to cyclic loading approaches.

Loading along the diagonal of the cross-section may be considered as simultaneous equal biaxial loading parallel to the sides of the section. When presented in terms of moment and deformation components along the sides of the cross-section, the behaviour appears to give a reduced (by about $\sqrt{2}$) strength and stiffness compared to uniaxial loading and accordingly reduced energy dissipation. If presented, however, in terms of the resultant moment and deformation along the single direction of loading, hysteresis loops are similar to those in uniaxial loading, with about the same or even sometimes enhanced strength and energy dissipation capacity. This applies in general for any loading in a single transverse direction oblique to the sides of the section.

Except when the axial load varies near the balance load, the variation of the axial force with both components of the biaxial moment/deformation affects the flexural response in both lateral directions as in the uniaxial case. When the axial compression increases, the instantaneous resistance and stiffness increase, strength decay with cycling accelerates and deformation capacity is reduced. Reduction of the

axial compression has the opposite effects. Variation of the axial load only with one component of the moment/deformation affects the resistance, stiffness and cyclic strength decay, mainly in the corresponding lateral direction.

3.2.3.8 Flexural Yielding and Flexure-Controlled Ultimate Chord Rotation Under Cyclic Biaxial Loading

Test results of columns under cyclic biaxial bending with axial force are sparse, owing to the practical difficulties of such testing. Yielding in such tests may be identified with the corner of a bilinear M–θ envelope of the experimental monotonic M–θ curve or of the M–θ hysteresis loops, separately for each one of the two directions of bending, y and z. The so-determined components, $M_{\mathrm{yy,exp}}$ and $M_{\mathrm{yz,exp}}$, of the experimental yield moment in 35 flexure-dominated biaxial tests in which yielding had taken place under biaxial loading, have been compared with the components of the biaxial moment resistance. These components have been computed from plane-section analysis, using an elastic-perfectly plastic σ-ε law for the reinforcing bars (at their exact location in the section) and a parabolic-rectangular one for the concrete, up to a compressive strain of 0.0045 at one corner of the cross-section.[13] Both of the so-computed components of moment resistance gave a mean test-to-prediction ratio of 1.0, which is better than what has been achieved for uniaxial bending in Section 3.2.2.2, where section yielding was identified with yielding of the extreme tension bars or with a fixed concrete strain at the extreme compression fibres for linear-elastic concrete in compression. This confirms that the corner of a bilinear M–θ envelop of the measured hysteresis loops, expressing overall section yielding is slightly past yielding of the extreme corner bar or compression fibre.

The uniaxial chord rotations in the two directions of bending, $\theta_{\mathrm{yy,uni}}$, $\theta_{\mathrm{yz,uni}}$, have also been computed from Eqs. (3.66) for these 35 biaxial tests. The experimental values at section yielding, $\theta_{\mathrm{yy,exp}}$, $\theta_{\mathrm{yz,exp}}$, give ratios $\theta_{\mathrm{yy,exp}}/\theta_{\mathrm{yy,uni}}$ and $\theta_{\mathrm{yz,exp}}/\theta_{\mathrm{yz,uni}}$ that on average exceed by a little more than 10% a circular interaction diagram of the form:

$$\left(\frac{\theta_{yy,\mathrm{exp}}}{\theta_{yy,uni}}\right)^2 + \left(\frac{\theta_{yz,\mathrm{exp}}}{\theta_{yz,uni}}\right)^2 = 1 \tag{3.83}$$

The prime role of θ_{y} is for the calculation of the effective stiffness to yield point via Eq. (3.68). Using the values of $M_{\mathrm{yy,exp}}$, $\theta_{\mathrm{yy,exp}}$, and $M_{\mathrm{yz,exp}}$, $\theta_{\mathrm{yz,exp}}$ at the corner of a bilinear envelope M–θ of the experimental monotonic M–θ curve or of the M–θ hysteresis loops, 35 pairs of the "experimental" effective stiffness have been

[13] Except for the value of the terminal strain, these assumptions are the same as those made for the calculation of the uniaxial moment resistance in Section 3.2.2.5. The computed components of the biaxial moment resistance were found to be fairly insensitive to the precise value of this limit strain.

computed from Eq. (3.68), separately in each direction of bending, y or z. They have been compared to:

i. the corresponding effective stiffness computed from Eq. (3.68) separately from $M_{yy,uni}$, $\theta_{yy,uni}$ and $M_{yz,uni}$, $\theta_{yz,uni}$, using the uniaxial yield moment from Section 3.2.2.2 and the chord rotation at yielding from Eq. (3.66), and
ii. the "empirical" effective stiffness from Eq. (3.69),

in the transverse direction, y or z, of interest (Biskinis 2007). The test-to-prediction ratios suggest that the "experimental" effective elastic stiffness in each one of the two directions is about 10% less, on average, than the uniaxial theoretical effective stiffness calculated in (i), i.e. theoretically from Eq. (3.68). By contrast, it exceeds by about 7% the "empirical effective stiffness" in (ii). These trends are opposite and hence inconclusive. However, as the theoretical effective stiffness is more reliable and unbiased than the "empirical" one, the limited test results may be considered to suggest that biaxial loading reduces slightly the effective elastic stiffness in each one of the two directions of loading.

Biaxial tests carried to flexure-controlled failure are also few (about 35). The components of chord rotation along the sides of the section at ultimate in these tests, $\theta_{uy,exp}$ and $\theta_{uz,exp}$, may be normalised to the corresponding ultimate chord rotations in uniaxial loading from:

(a) the semi-empirical procedure of Section 3.2.3.4 (i.e. Eqs. (3.72) and (3.73), together with curvatures according to Sections 3.2.2.4 and 3.2.2.10); and
(b) the purely empirical procedure of Section 3.2.3.5 and Eqs. (3.78).

The test-to-prediction ratio exceeds, on average, the circular interaction diagram:

$$\left(\frac{\theta_{uy,\mathrm{exp}}}{\theta_{uy,uni}}\right)^2 + \left(\frac{\theta_{uz,\mathrm{exp}}}{\theta_{uz,uni}}\right)^2 = 1 \tag{3.84}$$

by about 5% if the uniaxial ultimate chord rotations are calculated according to Eqs. (3.72) and (3.73), etc. or by about 16% if Eqs. (3.78) in Section 3.2.3.5 are used instead (Biskinis 2007, Bousias et al. 2002). Therefore, Eq. (3.84) is safe-sided for the verification of the ultimate chord rotations under biaxial bending, with uniaxial ultimate chord rotations estimated according to Sections 3.2.3.4 or 3.2.3.5.

3.2.3.9 Members with Ribbed Longitudinal Bars Lap-Spliced in the Plastic Hinge Region

Effect of Lap-Splicing on the Yield Properties

It is still common in many parts of the world – including Europe – to lap-splice all vertical bars of columns or walls at floor levels, for convenience of bar fixing.

The seismic parts of the US follow nowadays the good practice of splicing longitudinal bars of vertical elements outside their end regions where plastic hinges may develop. But even there, short lap splices at floor levels are typical of vertical members in existing substandard construction, adversely affecting their resistance and cyclic deformation capacity.

Provided that the lap length is sufficient (i.e., greater than the value giving $f_{sm} = f_y$ in Eq. (3.31) of Section 3.1.3.2, or greater than the limit value in Eq. (3.85) below), the yield moment and the moment resistance of columns with ribbed (deformed) longitudinal bars lapped starting at the column base is clearly higher than in similar members with continuous longitudinal bars (Biskinis and Fardis 2004, Fardis et al. 2005, Bousias et al. 2005a,b). This is thanks to end bearing of a compression bar stopping at the base section against the very well confined concrete beyond (i.e., the concrete at the top of a footing or at the face of 3D joint, etc.), which seems sufficient for the build-up of a compressive stress in that bar almost as high as in its companion bar in the lap that continues beyond the end section. Compatibility of longitudinal strains between these two bars and the concrete surrounding them near the member's end section contributes to this effect. The measured yield moment of such columns compares better with the outcome of Eq. (3.37) in Section 3.2.2.2 under *Cross-Sections with Rectangular Compression Zone* (after correction with the calibration factors given in Section 3.2.2.2 under *Comparison with Experimental Results and Empirical Expressions for the Curvature*), if in the calculation of M_y both bars in any pair of lapped compression bars count towards the compression reinforcement ratio within the lap splice.

The measured secant stiffness to the yield-point is also higher than in a similar member with continuous longitudinal bars. It compares better with the outcome of Eq. (3.68) in Section 3.2.3.3, if in Eq. (3.68):

i. the value of M_y is based on the yield curvature, φ_y, calculated from Eqs. (3.33), (3.34), (3.35) and (3.36) in Section 3.2.2.2 under *Cross-Sections with Rectangular Compression Zone*, including in the compression reinforcement ratio both bars of any pair of lapped bars in the compression zone, and
ii. θ_y is calculated from Eqs. (3.66) with the 1st and 3rd terms there based on the value of φ_y in (i) above and with the 2nd term multiplied by the ratio of the yield moment M_y modified for the lap splicing, to the value of M_y outside the lap splice; moreover, to determine whether $a_V = 1$ in the 1st term of Eqs. (3.66), $L_s V_{Rc}$ is compared to the value of M_y accounting for the effect of lapping.

The recommendations above, adopted also in Part 3 of Eurocode 8 (CEN 2005a), refer to lapped bars in compression. Regarding the lapped tension bars, Eqs. (3.31) and (3.32) in Section 3.1.3.2 may be applied for their maximum possible stress to be used in the calculation of M_y and φ_y. If this is done for over 100 tests on members with rectangular or hollow rectangular section and ribbed bars lapped starting at the section of maximum moment, the test-to-prediction ratio for the yield moment has a median of 0.995 and a coefficient of variation of 11.7% (Biskinis and Fardis 2007). Equations (3.66) may also be applied for the chord rotation at yielding according

to rule (ii) of the previous paragraph. Then, the test-to-prediction ratio of the chord rotation at yielding in over 80 tests has a median of 1.04 and a coefficient of variation of 20.5%. The corresponding statistics for the secant stiffness to the yield-point are 0.935 and 25.4%.

A simpler rule has been proposed in Biskinis and Fardis (2004, 2007) for the maximum possible stress of lapped tension bars and adopted in Part 3 of Eurocode 8 (CEN 2005a). According to it, if the straight lap length, l_o, is less than a minimum value of lap length, $l_{oy,min}$, required for the full transfer of the yield stress of a lapped bar in tension to the continuing one, M_y and φ_y should be calculated with the yield stress of the tension bars, f_{yL}, multiplied by $l_o/l_{oy,min}$. The value of $l_{oy,min}$ is given by the following expression (Biskinis and Fardis 2004, 2007, CEN 2005a):

$$l_{oy,\min} = \frac{0.3 d_{bL} f_{yL}}{\sqrt{f_c}} \qquad (f_{yL} \text{ and } f_c \text{ in MPa}) \tag{3.85}$$

where d_{bL} and f_{yL} are the mean diameter and the yield stress of longitudinal bars, respectively. Again, Eqs. (3.66) are applied for the chord rotation at yielding according to rule (ii) above (Biskinis and Fardis 2004, 2007, CEN 2005a). The test-to-prediction ratio for the so-computed yield moment has a median of 1.00 and a coefficient of variation of 11.6%, that for the chord rotation at yielding a median of 1.05 and a coefficient of variation of 19.9% and the one of the secant stiffness to the yield-point a median of 0.935 and a coefficient of variation of 25.6%. Note that, if $l_o \geq l_{oy,min}$, the value of M_y from Eq. (3.37) and of the secant stiffness to the yield-point from Eq. (3.68) increase owing to the lapping. If $l_o < l_{oy,min}$, both M_y and the secant stiffness to the yield-point decrease with decreasing l_o.

There is very little experimental information about members with short anchorage of the longitudinal bars beyond the end section. Section 3.1.3.2 has pointed out, though, that Eq. (3.31) applies equally well either to a single ribbed bar with straight anchorage length l_b or to two bars lap-spliced over the same length. On this basis, M_y, φ_y and θ_y at an end section with insufficient anchorage length l_b of its longitudinal bars beyond the end section may be estimated applying the rules above for the calculation of the tensile stress in the tension bars, using l_b instead of l_o.

Effect of Lap-Splicing on the Flexure-Controlled Ultimate Deformation

A column with ribbed vertical bars lapped starting at its base exhibits higher flexure-controlled ultimate deformation than a similar one with continuous vertical bars, provided that the lapping is at least equal to a certain minimum lap length, $l_{ou,min}$, given by the following expression (Biskinis and Fardis 2004, 2007), adopted also in Part 3 of Eurocode 8 (CEN 2005a):

$$l_{ou,\min} = \frac{d_{bL} f_{yL}}{\left(1.05 + 14.5 a_{l,s} \frac{\rho_s f_{yw}}{f_c}\right) \sqrt{f_c}} \qquad (f_{yL},\ f_{yw},\ f_c \text{ in MPa}) \tag{3.86}$$

where:

– ρ_s is the ratio of the transverse steel parallel to the plane of bending, and

$$a_{l,s} = (1 - 0.5s_h/b_o)(1 - 0.5s_h/h_o)n_{restr}/n_{not}, \tag{3.87}$$

with

- s_h: stirrup spacing,
- b_o, h_o: dimensions of the confined concrete core to the hoop centreline,
- n_{tot}: total number of lapped longitudinal bars along the perimeter of the section and
- n_{restr}: number of lapped bars which are engaged by a stirrup corner or a cross-tie.

To reflect this finding, the ultimate curvature or chord rotation, monotonic or cyclic, calculated according to the pertinent models in Sections 3.2.2.4, 3.2.3.4 and 3.2.3.5, should include in the compression reinforcement ratio both bars of any pair of lapped bars in the compression zone.

Tests to flexural failure of rectangular members with ribbed longitudinal bars lap-spliced starting at the section of maximum moment suggest that the flexure-controlled ultimate deformation decreases with decreasing lap length, l_o, if $l_o < l_{ou,min}$. With the effect of lapping on the chord rotation at yielding, θ_y, quantified according to the sub-section above on the *Effect of Lap-Splicing on the Yield Properties*, it is convenient to compute the ultimate chord rotation as the sum of the so-modified value of θ_y plus a plastic part, ${\theta_u}^{pl}$, appropriately reduced owing to the short lapping, $l_o < l_{ou,min}$. There are two approaches for the estimation of the reduced value of ${\theta_u}^{pl}$:

(i) The empirical approach of Section 3.2.3.5. The available test results suggest that ${\theta_u}^{pl}$ decreases linearly with l_o, if $l_o < l_{ou,min}$; ${\theta_u}^{pl}$ may be taken equal to the last term at the right-hand-side of Eqs. (3.78b) or (3.78c) times $l_o/l_{ou,min} \leq 1$, with $l_{ou,min}$ from Eq. (3.86) (Biskinis and Fardis 2004, 2007, CEN 2005a). In about 75 tests to flexure-controlled ultimate deformation the test-to-prediction ratio of the so-computed ultimate chord rotation, θ_u, has a median of 1.065 and a coefficient of variation of 36.4% if the un-reduced value of ${\theta_u}^{pl}$ is taken from Eq. (3.78b), or a median of 1.045 and a coefficient of variation of 35.9% if Eq. (3.78c) is used instead.

(ii) The approach of Section 3.2.3.4, based on curvatures and the plastic hinge length. In that case, the yield curvature, φ_y, entering the calculation may be modified according to the sub-section above on the *Effect of Lap-Splicing on the Yield Properties* for the effect of lap-splicing. The only other modification is in the calculation of φ_u. There, in addition to including in the compression reinforcement ratio both lapped compression bars in any pair, if the lap length, l_o, is shorter than the value of $l_{ou,min}$ from Eq. (3.86), the maximum elongation

of the extreme tension bars at ultimate conditions due to steel rupture should be reduced to:

$$\varepsilon_{su,l} = \left(1.2\frac{l_o}{l_{ou,\min}} - 0.2\right)\varepsilon_{su} \geq \frac{l_o}{l_{oy,\min}}\frac{f_{yL}}{E_s} \tag{3.88}$$

where ε_{su} is given by Eq. (3.64c) or (3.64b) for monotonic or cyclic loading, respectively, and $l_{oy,min}$, $l_{ou,min}$ are given by Eqs. (3.85) and (3.86), respectively. In about 75 tests to flexure-controlled ultimate deformation the test-to-prediction ratio of the so-computed ultimate chord rotation, θ_u, has a median of 1.005 and a coefficient of variation of 35.2%, i.e., better than in approach (i) above.

There are very few cyclic tests of columns without detailing for earthquake resistance and smooth (plain) hooked bars lapped starting at the base (just 7 tests to the author's knowledge, all with $l_o \geq 15d_{bL}$). They suggest the following modification of Eq. (3.80) for the chord rotation at flexure-controlled failure:

$$\theta_{u,\text{smooth-lapped}} = \frac{10 + \min\left(\frac{l_o}{d_{bL}}; 40\right)}{50}\theta_{u,Eq.(3.80)} \tag{3.80a}$$

giving a median of 1.0 and a coefficient of variation of 28% for the test-to-prediction ratio.

3.2.3.10 Effect of FRP Wrapping of the Plastic Hinge Region on Flexural Behaviour

Members with Continuous Bars

Flexural yielding of the member's end section is normally associated with yielding of the tension reinforcement and is insensitive to what happens at the compression zone unless the axial load is high. The experimental yield moment of members having the plastic hinge region wrapped with FRP nonetheless exceeds on average the value calculated according to Section 3.2.2.2. This exceedance is not fully redressed when the confined concrete strength, f_c^*, estimated from Eq. (3.27a) in Section 3.1.2.4, is used instead of the unconfined value, f_c: the test-to-prediction ratio of the so-estimated yield moment in 180 FRP-wrapped members has a median of 1.065 (in lieu of 1.025 for beams or columns without FRP wrapping, see Section 3.2.2.2 under *Comparison with Experimental Results and Empirical Expressions for the Curvature*) and a coefficient of variation of 19.6% (Biskinis and Fardis 2009). So, a calibration factor of 1.065 should be applied on the values of the yield moment and curvature, M_y, φ_y, obtained from 1st principles according to Section 3.2.2.2 using the confined concrete strength, f_c^*, in lieu of f_c. The correction factor of 1.065 should be applied also on the 1st (flexural) term of Eqs. (3.66) for the chord rotation at apparent yielding, θ_y, of members with FRP-wrapped ends. By doing so,

the test-to-prediction ratio of θ_y in about 135 FRP-wrapped members has a median of 0.995 and a coefficient of variation of 37.8% (Biskinis and Fardis 2009). If the so-computed values of M_y and θ_y are used in Eq. (3.68), the test-to-prediction ratio of the secant stiffness to the yield-point of these FRP-wrapped test specimens has a median of 1.055 and a coefficient of variation of 28.7% (Biskinis and Fardis 2009).

FRP-wrapping is often applied to retrofit members that have suffered serious damage during an earthquake (ranging from yielding to ultimate deformation), of course after repair of the damage. Repair followed by FRP-wrapping fully re-instate the yield moment of the damaged member: the mean and the median of the test-to-prediction ratio of the yield moment of 20 FRP-wrapped pre-damaged columns do not deviate significantly from those of the undamaged ones. By contrast, repair and FRP-wrapping cannot redress the effect of previous damage on the effective flexural stiffness to yielding (as controlled by the chord rotation at yielding, θ_y): the result of Eq. (3.68) has been found to exceed the secant stiffness to the yield-point of 20 FRP-wrapped pre-damaged columns by about 30% on average (Biskinis and Fardis 2009).

If the plastic hinge region is wrapped with FRP its ultimate flexural deformation is enhanced, primarily thanks to the confinement of the compression zone and the increase of the concrete ultimate strain there. As a matter of fact, Eqs. (3.29) and (3.30) in Section 3.1.2.4 for the ultimate strain of concrete under cyclic loading have been fitted to ultimate curvature data in about 35 tests of rectangular FRP-wrapped columns (Biskinis and Fardis 2009). In that case the ultimate curvature, φ_u, is calculated from first principles according to the analysis in Section 3.2.2.4, modified to accept a parabolic-trapezoidal σ-ε curve for the confined concrete – as in Lam and Teng (2003a,b) – instead of the parabolic-rectangular one of unconfined concrete. Equations (3.29) and (3.30) used together with the (Lam and Teng 2003a,b) confined strength model, Eq. (3.27a), give an average test-to-prediction ratio of 1.01 for φ_u with a coefficient of variation of 27.5%.[14] If the so-computed ultimate curvature, φ_u, is used in Eq. (3.72) of Section 3.2.3.4 together with the value of L_{pl} from Eq. (3.73) (fitted to members without FRP wrapping under cyclic loading), the test-to-prediction ratio of θ_u in about 95 tests of members with FRP wrapping has a median of 0.995 and a coefficient of variation of 34.6% (Biskinis and Fardis 2009). In another 18 members that had suffered certain damage by testing before been repaired, FRP-wrapped and re-tested, Eqs. (3.72) and (3.73) give a median test-to-prediction ratio of 0.985 and a coefficient of variation of 23.1%. If the columns that had been FRP-wrapped after been damaged and repaired are put together with the virgin ones, the overall median of the test-to-prediction ratio is 0.995 and the coefficient of variation 33.4%.

---

[14] If the Lam and Teng Eq. (3.27b) is used for $\varepsilon_{cu}{}^*$ instead of Eqs. (3.29) and (3.30), the ultimate curvature of the FRP-wrapped member is underpredicted by a factor of about 2.3. So, notwithstanding any adverse effect of the cycling, the FRP that confines the extreme compression fibres seems to be put under lower demands by cyclic bending than by the condition of monotonic concentric compression for which Eq. (3.27b) has been developed, a condition inducing a uniformly large strain to the FRP all around the section.

It has been proposed in Biskinis and Fardis (2004) and adopted by Eurocode 8, Part 3 (CEN 2005a) to extend to members with FRP wrapping the purely empirical model for θ_u, Eqs. (3.78) in Section 3.2.3.5, by adding the term $a_f \rho_f f_{f,e}/f_c$ to the exponent of the 2nd term from the end to include the effect of confinement by the FRP, where:

- $\rho_f = 2t_f/b_w$ is the geometric ratio of the FRP parallel to the loading direction,
- a_f is the confinement effectiveness factor of the section by the FRP, given by Eq. (3.28) where it is denoted by a_n, and
- $f_{f,e}$, is the effective stress of the FRP:

$$f_{f,e} = \min\left(f_{fu,nom};\ \varepsilon_{u,f} E_f\right)\left(1 - \min\left[0.5;\ 0.7\min\left(f_{fu,nom};\ \varepsilon_{u,f} E_f\right)\frac{\rho_f}{f_c}\right]\right) \tag{3.89}$$

with $f_{fu,nom}$ and E_f denoting the nominal strength and the Elastic modulus of the FRP and $\varepsilon_{u,f}$ being a limit strain, equal to:

- $\varepsilon_{u,f} = 0.015$ for CFRP or AFRP; and
- $\varepsilon_{u,f} = 0.02$ for GFRP.

With this modification Eqs. (3.78) give a median for the test-to-prediction ratio in about 95 tests of FRP-wrapped members equal to 1.10 and a coefficient of variation of 31.8%. In 18 members that had been FRP-wrapped and re-tested after been pre-damaged by testing and repaired, the modification of Eqs. (3.78) on the basis of Eq. (3.89) gives a median test-to-prediction ratio of 0.925 and a coefficient of variation of 24%. If all FRP-wrapped columns, virgin and pre-damaged/repaired are lumped together, the overall median of the test-to-prediction ratio is 1.09 and the coefficient of variation is 31.5%.

The proposal above has been improved as follows (Biskinis and Fardis 2009): the term added to the exponent of the 2nd term from the end of Eqs. (3.78) to reflect effective confinement by the FRP is:

$$\left(a\frac{\rho f_u}{f_c}\right)_{f,eff} = a_f \min\left[1.0;\ \min\left(f_{fu,nom};\ \varepsilon_{u,f} E_f\right)\frac{\rho_f}{f_c}\right] \left(1 - 0.4\min\left[1.0;\ \min\left(f_{fu,nom};\ \varepsilon_{u,f} E_f\right)\frac{\rho_f}{f_c}\right]\right) \tag{3.90}$$

where the limit strain is always equal to $\varepsilon_{u,f} = 0.015$. With this modification Eqs. (3.78) give a median test-to-prediction ratio in about 95 tests of FRP-wrapped virgin members equal to 1.06 and a coefficient of variation of 31.3%.

An even better fit to those tests is achieved (median test-to-prediction ratio of 1.035 and coefficient of variation of 31.2%) if the FRP-confinement term added to the exponent of the 2nd term from the end of Eqs. (3.78) is based on the effective FRP strength of the model in Lam and Teng (2003a,b): $f_{fu,L\&T} = E_f \varepsilon_{fu}$, with ε_{fu} about

equal to 60% of the failure strain of tensile coupons.[15] The resulting alternative to Eq. (3.90) is:

$$\left(a\frac{\rho f_u}{f_c}\right)_{f,eff} = a_f c_f \min\left[0.4;\ \frac{\rho_f f_{fu,L\&T}}{f_c}\right]\left(1 - 0.5\min\left[0.4;\ \frac{\rho_f f_{fu,L\&T}}{f_c}\right]\right) \tag{3.91}$$

where $c_f = 1.8$ for CFRP and $c_f = 0.8$ for GFRP or AFRP.

In the 18 members that were FRP-wrapped and re-tested after been pre-damaged by testing and repaired, Eqs. (3.78) modified on the basis of Eqs. (3.90) or (3.91) give a median test-to-prediction ratio of 0.925 or 0.945, and a coefficient of variation of 24% or 26%, respectively. If all FRP-wrapped columns, virgin and pre-damaged/repaired are lumped together, the overall median of the test-to-prediction ratio of Eqs. (3.78) modified on the basis of Eqs. (3.90) or (3.91) is 1.045 or 1.03, respectively, and the coefficient of variation is about 31%.

Note that the last term in each one of Eqs. (3.89), (3.90) and (3.91) reflects the experimentally documented reduced effectiveness of FRP-wrapping when larger amounts of FRP are used.

It has been suggested above that previous damage does not have a statistically significant effect on the ultimate chord rotation of FRP-wrapped members predicted from Eqs. (3.72), (3.73) and (3.74) and using in Eq. (3.72) an ultimate curvature, φ_u, from:

- first principles, according to the analysis in Section 3.2.2.4 modified to use a parabolic-trapezoidal σ-ε curve for confined concrete – as in the (Lam and Teng 2003a,b) model for confinement by FRP – instead of a parabolic-rectangular one,
- the (Lam and Teng 2003a,b) model for the confined strength, Eq. (3.27a), and
- Equations (3.29) and (3.30) for the ultimate strain of FRP-confined concrete under cyclic loading.

That conclusion is not corroborated by the comparisons of the predictions of Eqs. (3.78), modified with the help of Eqs. (3.89), (3.90) and (3.91). Although the data are not sufficient for a statistically meaningful conclusion, previous damage seems to reduce by 10–15% the ultimate chord rotation predicted by Eqs. (3.78) as modified on the basis of Eqs. (3.89), (3.90) or (3.91). The predictions are on the safe side for members that are intact when wrapped with FRP and slightly on the unsafe side for previously damaged ones.

Members with Lap-Spliced Ribbed Bars

What has been said in the sub-section above on *Effect of Lap-Splicing on the Yield Properties* regarding the effect of lap-splicing on the yield moment and the member

[15] As noted in Section 3.1.2.4, in Lam and Teng (2003a,b) this percentage value is proposed only for CFRP or GFRP, and 85% is given for AFRP, but on the basis of few test results.

secant stiffness to the yield-point still applies if the end region(s) of the member is wrapped with FRP. The only difference is in the calculation of the maximum possible stress of lapped tension bars, where the effect of the FRP wrapping should be taken into account. Provided that the wrapping extends over at least the full length of the lap, M_y and φ_y may be calculated with the maximum possible stress of the lapped tension bars from Eq. (3.31), using there Eq. (3.32a) (see Section 3.1.3.2). In about 30 tests on members of rectangular section, having their ribbed bars lapped and FRP wrapping applied starting at the section of maximum moment, the test-to-prediction ratio for the so-computed yield moment is on average equal to 1.13 and its coefficient of variation is 8.8%. The corresponding statistics for the chord rotation at yielding are 1.17 and 18% and for the member secant stiffness to the yield-point 1.00 and 18.8%, respectively.

Section 3.2.3.9 under *Effect of Lap-Splicing on the Yield Properties* has presented a simpler alternative to the use of Eq. (3.31) to account for the effect of lapping of ribbed bars on the yield properties of members without FRP wrapping. In that alternative the yield stress of lapped tension bars, f_{yL}, is multiplied by $l_o/l_{oy,min} \leq 1$ (Biskinis 2007, Biskinis and Fardis 2004, 2007, CEN 2005a). The extension of that rule to members with FRP wrapping all along the length of the lap splice entails just a reduction by one-third of the minimum length given by Eq. (3.85):

For FRP wrapping:

$$l_{oy,\min} = \frac{0.2 d_{bL} f_{yL}}{\sqrt{f_c}} \qquad (f_{yL} \text{ and } f_c \text{ in MPa}) \tag{3.85a}$$

This simplification, proposed in (Biskinis 2007, Biskinis and Fardis 2004, 2007) and adopted in Part 3 of Eurocode 8 (CEN 2005a), gives for the test-to-prediction ratio of the yield moment in about 30 tests an average of 1.06 and a coefficient of variation of 11.4% (Biskinis and Fardis 2009). The corresponding statistics for the chord rotation at yielding are 1.085 and 16.6% and for the member secant stiffness to the yield-point 1.005 and 18.2%, respectively.

The approach of Section 3.2.3.9 under *Effect of Lap-Splicing on the Flexure-Controlled Ultimate Deformation* for the effect of lap-splicing of ribbed longitudinal bars on the member's flexure-controlled ultimate deformation can be extended to members with FRP wrapping all along the lap-splicing. In a way similar to that approach, the ultimate chord rotation, θ_u, is expressed as the sum of the chord rotation at yielding, θ_y, plus a plastic part, $\theta_u{}^{pl}$. The effect of FRP-wrapping on θ_y is estimated according to the paragraph above. Regarding the effect on $\theta_u{}^{pl}$, approach (i) in Section 3.2.3.9 under *Effect of Lap-Splicing on the Flexure-Controlled Ultimate Deformation*, based on the empirical ultimate chord rotation of Section 3.2.3.5, takes $\theta_u{}^{pl}$ as equal to the last term at the right-hand-side of Eqs. (3.78b) or (3.78c) times $l_o/l_{ou,min} \leq 1$, with $l_{ou,min}$ from Eq. (3.86) (Biskinis 2007, Biskinis and Fardis 2007, CEN 2005a). For the extension of that approach to members with FRP wrapping all along the region with the lap-splice, recall the three approaches presented in the sub-section above on *Members with Continuous Bars* for the empirical estimation of $\theta_u{}^{pl}$ of members with continuous bars and FRP wrapping:

1. The one proposed in (Biskinis 2007, Biskinis and Fardis 2004, 2007) and adopted in Eurocode 8, Part 3 (CEN 2005a), uses Eq. (3.89) in the calculation of the effect of confinement by the FRP. Its natural extension, also proposed in (Biskinis 2007, Biskinis and Fardis 2007) and adopted in CEN (2005a), is to calculate $l_{ou,\min}$ via the following modification of Eqs. (3.86) and (3.87):

$$l_{ou,\min} = \frac{d_{bL} f_{yL}}{\left(1.05 + 14.5 \frac{4}{n_{tot}} a_f \frac{\rho_f f_{f,e}}{f_c}\right) \sqrt{f_c}} \qquad (f_{yL},\ f_{f,e},\ f_c \text{ in MPa}) \qquad (3.92)$$

where $f_{f,e}$ comes from Eq. (3.89) and n_{tot} denotes the total number of lapped longitudinal bars along the perimeter of the section, out of which only the four corner ones are confined by the FRP ($n_{restr} = 4$ in Eq. (3.87)). Note that, θ_u^{pl} before its reduction due to the lap splice is calculated from Eqs. (3.78b) or (3.78c) with the exponent of the 2nd term from the end reflecting confinement by the steel ties as well as by the FRP (i.e., the term $a_f \rho_f f_{f,e}/f_c$ is added). By contrast, confinement of lapped bars by the FRP alone and not by the steel ties is taken into account in Eq. (3.92). Thirty members with lap-spliced ribbed bars and FRP-wrapping cyclically tested to flexure-controlled ultimate deformation have mean test-to-prediction ratio for the so-computed ultimate chord rotation, θ_u, equal to 0.965 or 0.95, and a coefficient of variation of that ratio of 26.6% or 27.2%, if the un-reduced value of θ_u^{pl} is taken from Eq. (3.78b) or (3.78c), respectively (Biskinis and Fardis 2009).
2. The improvement of the approach in (Biskinis 2007, Biskinis and Fardis 2004, 2007, CEN 2005a) as proposed in Biskinis and Fardis (2009), namely the use of Eq. (3.90) for the FRP-confinement term. The natural extension of that approach, also presented in Biskinis and Fardis (2009), is to modify Eqs. (3.86) and (3.87) for $l_{ou,\min}$ as follows:

$$l_{ou,\min} = \frac{d_{bL} f_{yL}}{\left(1.05 + 14.5 \frac{4}{n_{tot}} \left(a \frac{\rho f_u}{f_c}\right)_{f,eff}\right) \sqrt{f_c}} \qquad (f_{yL},\ f_{f,u},\ E_f,\ f_c \text{ in MPa}) \qquad (3.93)$$

with $(a\rho f_u/f_c)_{f,eff}$ from Eq. (3.90). Again the value of θ_u^{pl} before the reduction due to the lap splice is calculated from Eq. (3.78b) or (3.78c) accounting for confinement by the steel ties and by the FRP through the exponent of the 2nd term from the end (i.e., adding there the term $(a\rho f_u/f_c)_{f,eff}$ from Eq. (3.90)), while Eq. (3.93) accounts only for confinement of lapped bars by the FRP but not by the steel ties. In 30 cyclic tests of members with lap-spliced ribbed bars and FRP-wrapping the test-to-prediction ratio of the so-computed ultimate chord rotation, θ_u, is on average equal to 0.925 or 0.91, and has a coefficient of variation of 28.4% or 28.9%, if the un-reduced value of θ_u^{pl} is taken from Eq. (3.78b) or (3.78c), respectively (Biskinis and Fardis 2009).
3. The further modification of the approach, in order to use in the FRP-confinement term the effective FRP strength of the Lam and Teng (2003a,b) model: $f_{fu,L\&T} = E_f \varepsilon_{fu}$, with ε_{fu} about equal to 60% of the failure strain of tensile coupons. This

modification uses Eq. (3.90) for the FRP-confinement term in the calculation of θ_u^{pl} for members with continuous bars and FRP wrapping. It is extended to members with lap-spliced bars by using in Eq. (3.93) the value of $(a\rho f_u/f_c)_{f,eff}$ from Eq. (3.91). The test-to-prediction ratio of the so-computed value of θ_u in 30 cyclic tests of members with lap-spliced ribbed bars and FRP-wrapping is on average equal to 0.98 or 0.965, if the un-reduced value of θ_u^{pl} is taken from Eq. (3.78b) or (3.78c), respectively, and has a coefficient of variation of 30.6% (Biskinis and Fardis 2009).

So, although with the approach in (Biskinis 2007, Biskinis and Fardis 2004, 2007, CEN 2005a) modified as in 2 and 3 above the accuracy of the predictions of θ_u improves for members with continuous bars and FRP wrapping, it deteriorates if the bars inside the wrapping are lap-spliced.

In approach (ii) of Section 3.2.3.9 under *Effect of Lap-Splicing on the Flexure-Controlled Ultimate Deformation* the limit strain of steel for the calculation of the ultimate curvature of members without FRP wrapping (used in the estimation of the ultimate chord rotation from the plastic hinge length according to Section 3.2.3.4) is corrected for the effect of lap-splicing according to Eq. (3.88). On the other hand, the ultimate curvature of FRP-wrapped members with continuous bars may be calculated according to the 3rd paragraph of the sub-section above on *Members with Continuous Bars*: from (a) the analysis in Section 3.2.2.4 modified to use a parabolic-trapezoidal σ-ε curve for the confined concrete (as in the (Lam and Teng 2003a,b) model), instead of the parabolic-rectangular one of unconfined concrete, (b) the (Lam and Teng 2003a,b) confined strength model and (c) the ultimate strain of FRP-confined concrete under cyclic loading given by Eqs. (3.29) and (3.30) in Section 3.1.2.4. If the tension bars are lapped inside the FRP wrapping their limit strain may be taken from Eq. (3.88), but using there the value of $l_{ou,min}$ for FRP-wrapped members from Eq. (3.93). In that expression the value of $(a\rho f_u/f_c)_{f,eff}$ should be the one from Eq. (3.91), consistent with the (Lam and Teng 2003a,b) model applied for the FRP-confined concrete in the calculation of φ_u. If this is done, the test-to-prediction ratio of θ_u in 30 cyclic tests of members with lap-spliced ribbed bars and FRP-wrapping is on average equal to 1.42 and has a coefficient of variation of 25.7%. Therefore, if the more "fundamental" approach for the ultimate chord rotation is extended to FRP-wrapped members with lapped bars, it gives worse predictions than the versions 1–3 of the empirical approach presented in the paragraphs above.

3.2.3.11 Effect of Bonded Prestressing Tendons on the Cyclic Flexural Behaviour

Prestressing of long span beams or girders can be used to advantage in concrete buildings. However, the scope of current seismic design codes, including Eurocode 8 (CEN 2004a), does not include prestressed elements that are part of the lateral-load-resisting system ("primary seismic" elements in Eurocode 8, see Section 4.12). The exclusion is implicit. It comes from the fact that code rules on design and detailing

for ductility of beam ends where plastic hinges are expected to form apply only to reinforced concrete beams. A notable exception is the CEB Seismic Model Code (CEB 1985) that includes a few clauses warning against the use of unbonded tendons in "primary" members (except in partially prestressed beams with 80% of their flexural resistance coming from ordinary reinforcement and with prestressing tendons placed only within the mid-third of the section depth) and against placing tendon anchorages in beam-column joints next to potential plastic hinges. CEB (1985) also limits the neutral axis depth in potential plastic hinges of prestressed beams at the moment resistance to less than 20% of the section depth (to avoid brittle failure of the compression zone) and asks for a 25% margin between cracking and ultimate moments of any prestressed section.

Concrete buildings designed for energy dissipation according to current codes may include prestressed girders, provided that they, as well as the columns connected to them, are not taken to be part of the lateral-load-resisting system, i.e., they are considered and designed as "secondary seismic" elements in the Eurocode 8 terminology (see Section 4.12). According to Eurocode 8 (CEN 2004a) this implies that the total lateral stiffness of all frames in the building that include prestressed girders does not exceed 15% of the lateral stiffness of the system of "primary seismic" elements. As a matter of fact, it is sensible to consider the columns supporting prestressed girders as "secondary seismic", because normally the weak-beam/strong-column capacity design rule of Eq. (1.4) cannot force plastic hinging in girders with size typical of prestressed ones. Another option is to design concrete buildings having prestressed girders for Ductility Class L and a value of the behaviour factor q not higher than 1.5 (as recommended in Eurocode 8 only for low seismicity regions).

Note that, at least in buildings, prestressing is primarily – if not exclusively – used in long span horizontal elements for resistance against gravity loads. So tendons are placed eccentric in the member section, on the side where gravity moments induce tension. Eccentric tendons normally do not enhance the ductility and deformation capacity of plastic hinges, particularly at beam supports under hogging moments that induce tension to the top flange, where the tendons are located. Under such moments the beam section at the face of the column soon reaches its deformation capacity, owing either to the low ultimate strain of prestressing steel (compared to ordinary reinforcement) or to crushing of the concrete at the narrow bottom flange. So, a less eccentric placement of tendons at beam supports and a larger quantity of ductile ordinary reinforcement at both flanges may be appropriate, for the plastic hinges at the ends of prestressed beams to develop significant ductility and deformation capacity.

Conventional wisdom in seismic design and codification is against prestressing members expected to develop plastic hinges, because compression due to prestressing is thought to place additional demands on the compression zone, reducing the flexural deformation capacity. Recent tests, however, have demonstrated the beneficial effect of prestressing on the cyclic behaviour of bridge piers: ultimate deformation increases with prestressing and residual displacements decrease (Sakai et al. 2006, Inoue and Tanabe 2006).

So, prestressing of bridge piers has received considerable attention in the draft code of the Japan Prestressed Concrete Engineering Association for performance-based seismic design of prestressed concrete bridges (JPCEA 2002).

The international literature contains very few cyclic tests on prestressed members, mainly with square section and concentric prestressing. Their results are compared below to the predictions of the models proposed in previous sections, after appropriate modifications.

In the application of the model in Section 3.2.2.2 for the calculation of the yield moment and curvature of prestressed members with rectangular compression zone, any bonded tendons that are near the extreme tension fibres are included in the ratio of tension reinforcement, ρ_1, after weighing the cross-sectional areas of any reinforcement near the outermost tension fibres by the corresponding yield stress. The same weighing is applied for the determination of the centroid of the tension reinforcement. Bonded tendons and non-prestressed reinforcement in the compression zone and the web are elastic at yielding of the section. So, their cross-sectional areas may be added without any weighing by the yield stress.

There are two alternatives for considering the effect of prestressing:

1. Prestress is considered as part of the actions, as in Serviceability Limit States:

   – the action effects due to prestress are taken from the elastic analysis; in isostatic (statically determinate) systems prestressing induces an axial force equal to the total prestressing force, P (positive for compression) and a bending moment equal to P times the eccentricity of the mean tendon, and
   – bonded tendons are considered as an integral part of the section, working elastically up to their available yield stress, which is equal to their full yield stress, $f_{0.01}$, minus the initial stress in the tendon, σ_p.

2. The prestress is considered as part of the resistance: This is how bonded tendons that yield are normally considered at the Ultimate Limit States:

   – bonded tendons that yield are taken to contribute to the resistance as an integral part of the section, working in the plastic range with their full yield stress, $f_{0.01}$;
   – bonded tendons that have not yielded are considered as in case (1) above, i.e.:

     • they are taken to induce in the section an axial force and a bending moment equal to the force and moment resultant of their prestressing, and
     • they are considered to work elastically as an integral part of the section up to their available yield stress, $f_{0.01}$–σ_p.

For either one of the two alternative considerations (1) and (2) above, the model in Section 3.2.2.2 underestimates by 13.5% on average the yield moment, M_y, of concentrically prestressed members. More important, Eq. (3.66) overestimates the chord rotation at yielding, by 11% on average when prestress is taken as part of the actions and by almost 50% when it is considered as part of the resistance. The scatter of the predictions for chord rotations at yielding is large. These differences are

carried over to the calculation of the secant stiffness to the yield-point through Eq. (3.68). Its average test-to-prediction ratio is 1.50 if prestress is taken as part of the actions and about 2.0 when it is considered as part of the resistance! The empirical secant stiffness to the yield-point from Eq. (3.69) does not improve the predictions.

In view of the very small sample size, the magnitude of underestimation of the yield moment of concentrically prestressed members by the models for non-prestressed members is considered as acceptable. The same could be said for the overestimation of the chord rotation at yielding, but only when prestress is taken as part of the actions. These deviations, however, accumulate into a more significant underestimation of the secant stiffness to the yield-point through Eq. (3.68), which borders the unacceptable. It seems that the effects of the suppression of cracking by the prestress along part of the member is not fully captured by considering an axial force equal to the total prestressing force, P. Taking the prestress as part of the resistance, or using the empirical secant stiffness to the yield-point, Eq. (3.69), give very poor predictions both for the chord rotation at yielding and for the secant stiffness to it.

The three versions of Eqs. (3.78) underestimate the flexure-controlled cyclic ultimate chord rotation, θ_u, of five concentrically prestressed specimens by 7.5–8.5% on average (with a coefficient of variation of the test-to-prediction ratio from 8.5 to 12.5%). The concentrically prestressed specimens may have exceeded the expecations of a formula fitted to conventionally reinforced members, because their tendons are always in tension and do not buckle under cyclic loading. For this reason, it seems appropriate to apply Eq. (3.72), based on the ultimate curvature, φ_u, from Sections 3.2.2.4 and 3.2.2.10 and the plastic hinge length from Eq. (3.73b), with the limit strain of tendons taken from Eq. (3.64a), for monotonic loading that does not cause buckling of the tendons. However, the cyclic ultimate chord rotation in the five tests is still underestimated by 9% on average (and with a coefficient of variation of the test-to-prediction ratio of 35.5%).

Note that bending moments nowhere enter in the application of Eqs. (3.78) and (3.72). So, if the prestress is taken as part of the resistance, there is no way to take into account the bending moment induced by the bonded tendons that have not yielded. Therefore, in the calculations of θ_u the prestress has been taken as part of the action, even though bonded tendons close to the extreme tension fibres had yielded before the ultimate flexural failure.

The very limited available test data suggest that concentric prestressing is beneficial for the flexure-controlled cyclic ultimate chord rotation, θ_u. Moreover, the recentring effect of concentric prestressing reduces the residual deformations, and therefore damage, no matter whether the conventionally defined flexure-controlled chord rotation capacity, θ_u, has been exceeded or not. If this capacity is not exceeded, a member without any ordinary non-prestressed reinforcement and with only concentric prestressing returns to about zero residual deformations. If there is a combination of non-prestressed and prestressed reinforcement, the residual deformation may be considered to decrease in proportion to the contribution of prestressing (in percent) to the yield moment of the section, i.e. to the ratio $M_y(A_p=0)/M_y$, where $M_y(A_p=0)$ is the yield moment for presumed zero cross-sectional area of prestressed reinforcement in the section.

3.2.4 Behaviour of Members Under Cyclic Shear

3.2.4.1 Introduction: Brittle vs. Ductile Shear Behaviour

If it precedes flexural yielding, ultimate failure of concrete members in shear occurs at relatively low deformations and is associated with a large drop in lateral load resistance. So, it is considered as a "brittle" failure mode. Figure 3.35 depicts characteristic shear failures of columns or walls in past earthquakes. A shear failure of a stair flight acting as an inclined wall has been shown in Fig. 2.13(a).

Often concrete members that first yield in flexure may, under cyclic loading, ultimately fail in a mode showing strong and clear effects of shear: diagonal cracks are prominent and their width and extent increase during cycling, despite the gradual drop of peak force resistance with cycling of the load. At the same time, phenomena which are associated with flexure (e.g., a single wide crack at right angles to the member axis at the section of maximum moment, disintegration of the compression zone and/or buckling of longitudinal bars next to that section) may not be so pronounced in such cases. By contrast, these phenomena (often including rupture of a longitudinal bar) grow in magnitude when flexure-controlled ultimate deformation approaches, while any diagonal cracks that may have formed initially decrease in width and may even disappear owing to the drop of the force resistance with load cycling after the flexure-controlled ultimate strength. Failure in shear under cyclic loading after initial flexural yielding is termed "ductile shear" failure (Kowalsky and Priestley 2000). It occurs only under cyclic loading, because shear strength degrades faster with load cycling than flexural strength. It is normally associated with diagonal tension and yielding of the web reinforcement, rather than with web crushing by diagonal compression.

The left-hand-side of Fig. 3.36 (Yoshimura et al. 2004) shows force-drift hysteresis loops of three columns with high longitudinal reinforcement ratio, ρ_{tot}, and low transverse steel ratio, ρ_w, failing in brittle shear before yielding in flexure. Their right-hand-side companions have sufficiently low values of ρ_{tot} to first yield in flexure and then fail in "ductile shear" (the upper two columns) or in flexure (that at the lower right corner).

Dimensioning of concrete members against brittle shear failure is a familiar subject, covered in current codes and standards for the design of concrete structures under non-seismic action effects that increase monotonically until ultimate strength. Relevant models are reviewed in the Section 3.2.4.2. Shear design of members in new earthquake-resistant concrete buildings and seismic evaluation of existing elements in substandard ones should also consider the reduction of shear resistance with cyclic loading below the monotonic value.

Several mechanisms may explain the degradation of shear strength during cyclic loading:

1. The degradation of dowel action with cycling of the shear (see Section 3.1.3.1) and with the accumulation of inelastic strains in the longitudinal bars.
2. The development of flexural cracks through the depth of the member and the ensuing decreased contribution of the compression zone to shear resistance.

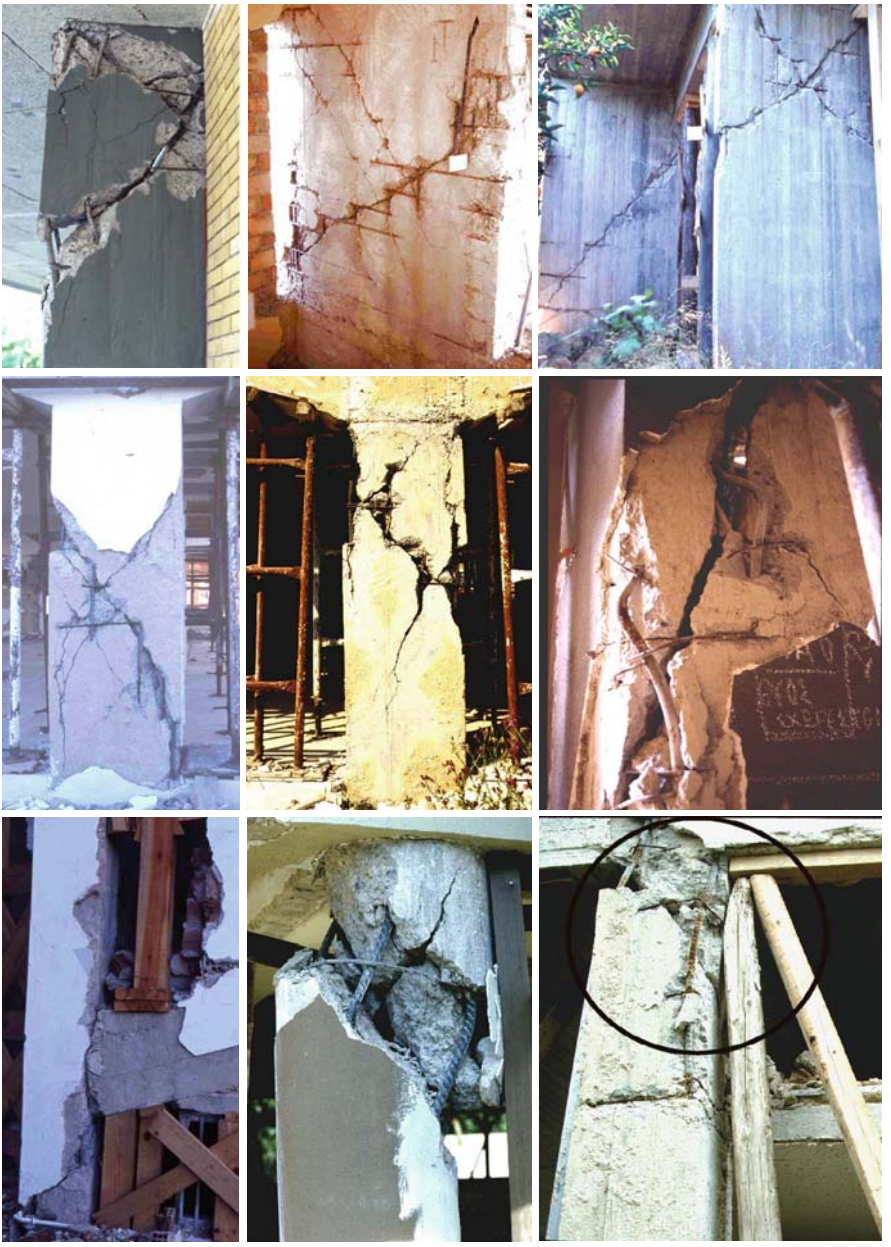

Fig. 3.35 Shear failures of columns or walls (See also Colour Plate 9 on page 723)

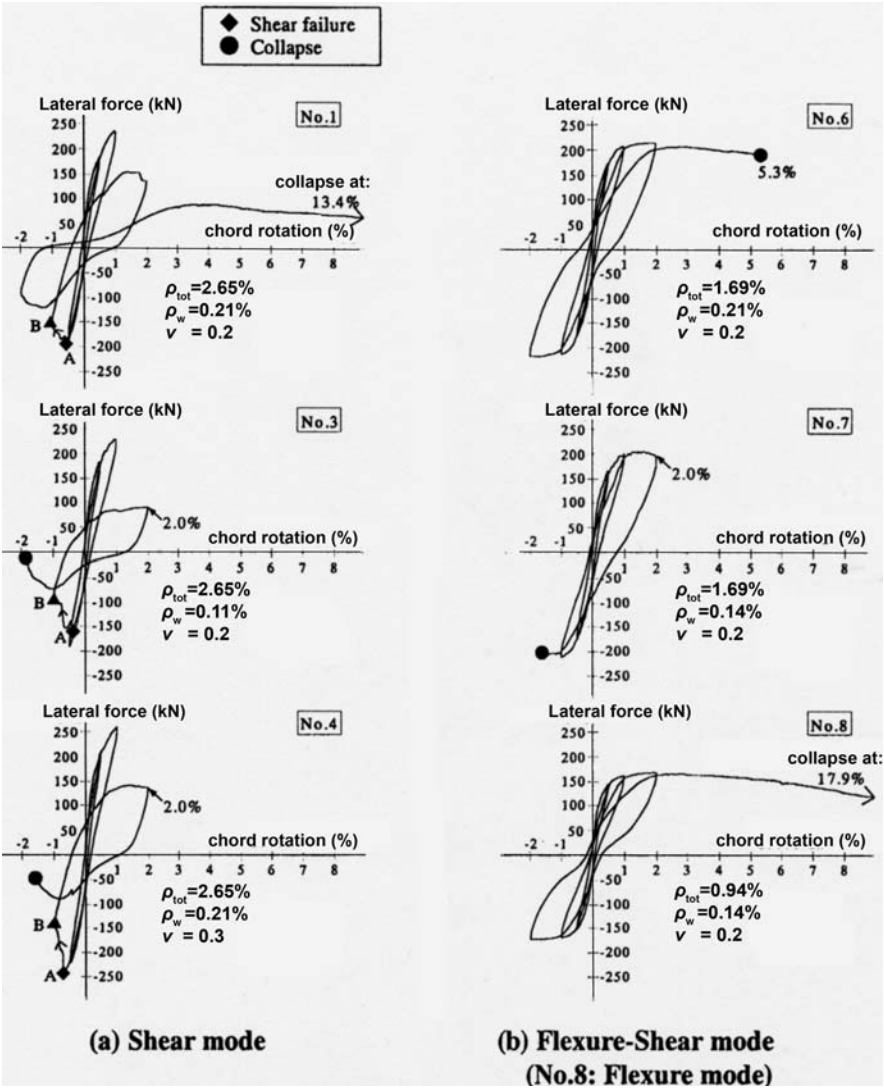

Fig. 3.36 Shear force-chord rotation behaviour for: (**a**) brittle shear; and (**b**) "ductile shear" or flexural behaviour (adapted after Yoshimura et al. 2004)

3. The reduction of aggregate interlock along diagonal cracks, as their interfaces are ground and become smoother with cycling; in addition, the cracks open up owing to bond slippage and accumulation of inelastic strains in the stirrups crossing the cracks.
4. The softening of concrete in diagonal compression due to accumulation of transverse tensile strains.

The degradation of shear strength during cyclic loading is normally associated with diagonal tension and yielding of the web reinforcement, rather than with diagonal compression failure in the web. It has by now prevailed to quantify this failure mode in terms of a shear resistance, V_R, (as this is governed by web reinforcement according to the well-established Mörsch-Ritter truss analogy) that decreases with increasing (displacement) ductility ratio under cyclic loading (Kowalsky and Priestley 2000, Moehle et al. 2001, Ascheim and Moehle 1992). The contributions to shear strength decay listed above as 1–3 have to do with the contribution of concrete to shear resistance, i.e. with the term V_c normally added to the contribution of transverse steel according to a 45°-truss analogy, V_w. Degradation mechanisms no. 3 and 4 involve also, be it indirectly, the contribution of transverse steel to shear resistance, reflected in V_w.

Naturally the cyclic degradation of shear resistance is larger within flexural plastic hinges, as it is there that:

- flexural cracks extend into wide and intersecting diagonal cracks,
- the compression zone suffers more damage and decreases in size,
- longitudinal bars develop inelastic strains, or even buckle, and lose most of their effectiveness in dowel action, and
- (at the end section) the compression zone supports the diagonal strut of the truss mechanism of shear resistance.

Consequently, the decay of shear strength with cycling takes place mainly in concrete members that develop flexural plastic hinges before exhausting their shear resistance. Therefore, the phenomenon is normally expressed quantitatively as a reduction of shear strength with cyclic inelastic deformations, until the so-reduced shear strength, V_R, becomes less than the shear force corresponding to flexural yielding, $V_y = M_y/L_s$. The member deformation where this takes place may be considered as its deformation capacity, as governed by shear.

An alternative way to describe the phenomenon might be to consider that the member develops a relatively ductile failure mode in shear after initially yielding in flexure, but that its ultimate cyclic deformation capacity is less than in an – otherwise similar – member with higher shear resistance but ultimately failing in flexure. Such an approach might allow direct quantification of member cyclic deformation capacity as governed by shear without recourse to a force-based criterion. However, owing to:

- the lack of rational models for the ultimate deformation of concrete elements as controlled by “ductile shear” failure, and
- the scarcity of sufficient data for the development of purely empirical alternatives,

the models proposed so far for the description of ultimate shear failure due to cyclic deformations beyond flexural yielding use force-based criteria as outlined in the previous paragraph and described in detail in Section 3.2.4.3. These criteria

employ empirical corrections of the truss analogy model of shear resistance, to incorporate the effect of cyclic degradation.

The experimental results in Fig. 3.37 (Ma et al. 1976) are typical of the evolution of shear phenomena under cyclic loading. They refer to a T-beam with $L_s/h = 3.9$ subjected to symmetric cycles of tip deflection in sets of three cycles of the same amplitude. Figure 3.37(a) displays the moment-(mean) curvature loops measured over a length of $d/2$ next to the beam end section. Figure 3.37(b) presents the corresponding loops of shear force v mean shear strain up to a distance $0.3d$ from the end section. Diagonal cracking occurred at a shear force of 50 kN (point A in Fig. 3.37(c)). It is only after that stage that the stirrups were activated and shear strains started developing. After flexural yielding of the end section, shear strains grew rapidly with deflection cycles, although the peak force of the cycles remained almost the same. As a matter of fact, shear strains increased from the 1st to the 3rd cycle of each set of three cycles, while the corresponding peak curvatures of the cycle decreased (cf Fig. 3.37(a) and (b)). The gradual increase of shear strains during cycling accelerated the activation of the stirrups, driving the one monitored in Fig. 3.37(c) to yielding. Witness the small stress of that particular stirrup (about 25% of its yield stress) at the time the end section first yielded.

Similar is the behaviour of the 3-storey barbelled wall in Fig. 3.38 (Wang et al. 1975). It is reminded that walls are considered to resist flexure with the two well-confined and heavily reinforced section edges, while the web in-between resists the shear. The vertical bars in the web play of course a role for the behaviour and resistance of the wall in flexure (see term ρ_v in Eqs. (3.35), (3.37), (3.38) and (3.39) and ω_v in Eqs. (3.57), (3.58), (3.59), (3.60), (3.61) and (3.62)). Moreover, if the shear capacity provided by the web reinforcement is exhausted, the boundary elements at the two ends of the section may contribute to shear resistance via the dowel action of their large diameter bars, or, even, by acting themselves as big dowels. Notwithstanding the presumed distinct and uncoupled roles of the web and of the two boundary elements, flexural yielding at the base of the wall's 1st or 2nd storey (see Fig. 3.38(a), or (b), respectively) triggers the onset of significant inelastic shear deformations over the entire 1st or 2nd storey, respectively (see Fig. 3.38(c) and (d)). Ultimate failure of that wall took place in shear at the 1st storey, while the moment-curvature response in the 1st and 2nd storeys was very stable (see Fig. 3.38(a) and (b)). Besides the gradual degradation of shear resistance due to inelastic cyclic deformations, Figs. 3.37(b) and 3.38(c), (d) display the shape of force-deformation loops typical of shear behaviour. Unlike the ones in flexure in Figs. 3.25, 3.26, 3.28, 3.34, 3.37(a), 3.38(a) and (b), the loops in Figs. 3.37(b) and 3.38(c), (d), become almost flat upon unloading to zero force and remain so until a steep but late increase in stiffness while the wall reloads in the reverse direction. The end result is a narrow and inverted-S V-γ loop, with very little energy dissipation.

The inverted- S shape of the V-γ loop derives from the following mechanism: Because of dislodgement of aggregates along the diagonal cracks and of inelastic strains in stirrups that have yielded in tension, diagonal cracks do not close immediately after reversal of the shear force. Significant reverse shear deformation needs

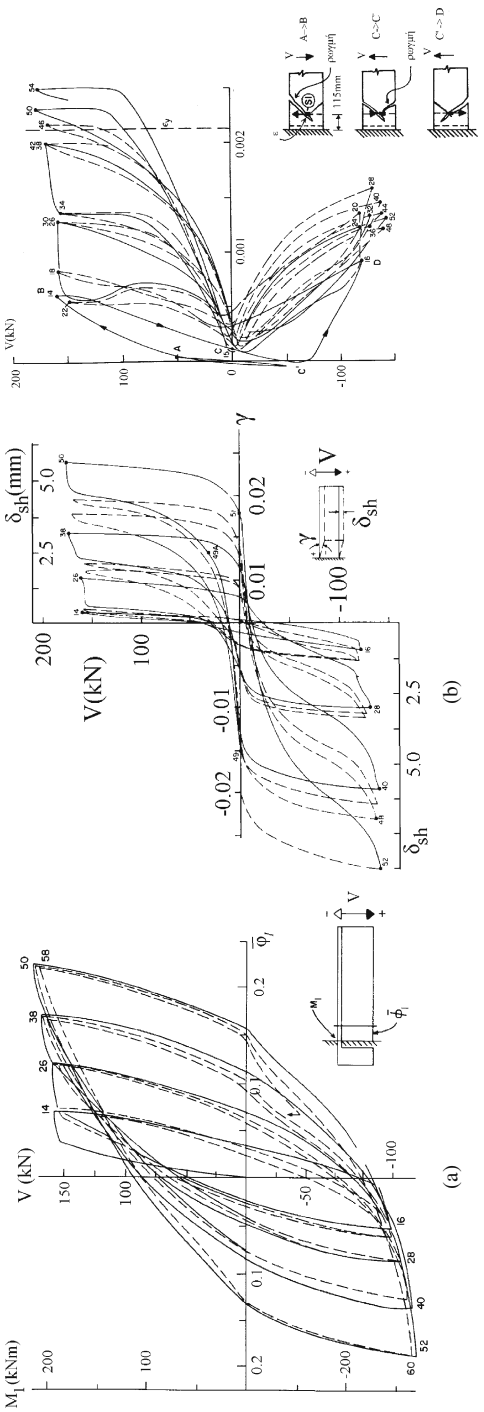

Fig. 3.37 T-beam under cyclic loading: (**a**) M-φ loops next to the end section; (**b**) V-γ loops in plastic hinge region; (**c**) loops of shear force V vs stirrup strain (adapted from Ma et al. 1976)

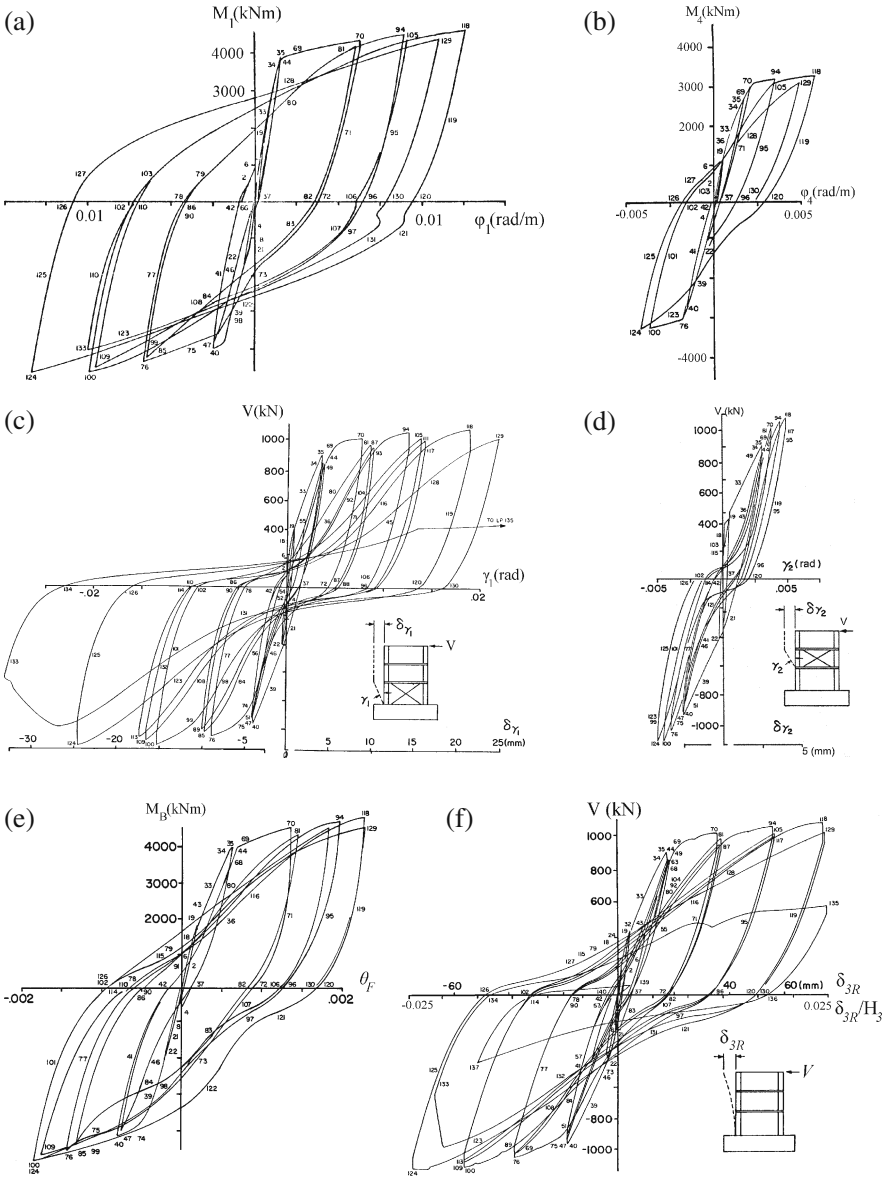

Fig. 3.38 3-storey wall (adapted from Wang et al. 1975): (**a**), (**b**): *M*-φ loops next to the base of 1st and 2nd storey; (**c**), (**d**): *V*-γ loops over 1st and 2nd storey; (**e**) loops of base moment vs fixed-end rotation due to bar pull-out from the anchorage in the footing; (**f**) base shear vs. top deflection

to be applied, to suppress the inelastic tensile strains in the stirrups and force the cracks to fully close and develop compressive stresses normal to their face. Especially when their geometric ratio, ρ_w, is low, stirrups present little stiffness until the crack closes. When that happens, a steep increase in stiffness takes place.

The small energy dissipation capacity of the shear mechanism of force transfer in cyclic loading and the steady accumulation of inelastic shear deformations in constant-amplitude cycling of the shear force suggest that the behaviour in shear does not possess the stability and dissipation capacity required for ductile behaviour under cyclic loading. Moreover, ultimate failure in shear takes place either by propagation of diagonal cracks into the compression zone, causing its disintegration, or by diagonal web crushing in compression. In both cases failure is abrupt and catastrophic and cannot be prevented or mitigated by confinement. For all these reasons, shear should be confined in the elastic region. Capacity design rules in shear aim at exactly that. For the same reason, what is primarily of interest for concrete members in shear is their cyclic shear resistance and not their (anyway small) inelastic shear deformations.

3.2.4.2 Fundamental Models for Shear Resistance in Monotonic Loading

The Variable Strut Inclination Truss of the CEB/FIP Model Code 90 and Eurocode 2

CEB/FIP Model Code 90 (CEB 1991) and Eurocode 2 (CEN 2004b) have adopted for shear resistance the variable strut inclination truss model – strictly speaking, a model with variable angle of inclination, δ,[16] of the compression stress field in the web with respect to the member axis. According to this model (Walraven 2002), a concrete member with:

- longitudinal reinforcement, typically concentrated at two "chords" at the ends of the section, and
- reinforcement transverse to the axis, with geometric ratio ρ_w

equilibrates a shear force V through a statically determinate "truss" mechanism comprising:

1. a compressive stress field in the concrete, at an angle δ to the member axis; equilibrium gives the compression stress in the concrete as: $\sigma_c = 2V/(b_w z \sin 2\delta)$;
2. a tensile stress in the transverse reinforcement equal to $V\tan\delta/(\rho_w b_w z)$, where b_w is the width of the web and z is the internal lever arm between the two "chords"; this stress amounts to a tension force per unit length of the member equal to $V\tan\delta/z$;
3. a tension force of $V\cot\delta$ in the longitudinal reinforcement.

Diagonal cracking first takes place at about 45° to the member axis. At that time the compression stress field is parallel to the cracks and at an angle to the member axis $\delta \approx 45°$. So long as the web has sufficient strength to resist the compres-

[16] The symbol δ is used here instead of the symbol θ normally used for the angle of inclination, to avoid confusion with chord rotations.

sive stress field, the member can sustain yielding of the transverse reinforcement at its yield stress, f_{yw}, and develop a further increased shear resistance at a steadily decreasing inclination of the new cracks and of the compression field, δ, with respect to the member axis:

$$V_{R,s} = \rho_w b_w z f_{yw} \cot\delta \tag{3.94}$$

Shear resistance increases with the rotation of the compression field, until either one of the following possibilities takes place:

i. The tension chord yields, as its tensile force increases owing both to the increase of the loading and the decrease of the inclination δ. If the member is also subjected to a bending moment, M, and an axial force N (positive for compression), and the longitudinal reinforcement is concentrated at two "chords" at the ends of the section, the force in the tension chord is: $M/z + 0.5(V\cot\delta - N)$. The shear force at yielding of a tension chord with cross-sectional area A_{s1} and yield stress f_{yL} is:

$$V_{R,L} = 2\left(A_{sl} f_{yL} - M/z + N/2\right)\tan\delta \tag{3.95}$$

ii. The web concrete fails in diagonal compression, as the compressive stresses in the web also increase owing both to the reduction of δ and the increase of V. Note that the compressive strength of concrete at an angle δ to the member axis is less than its uniaxial compressive strength, f_c, because of the tensile stresses and strains in the orthogonal direction (namely those associated with yielding of the transverse reinforcement and the tensile stresses in the concrete between adjacent diagonal cracks). The reduced strength of concrete is taken equal to nf_c,[17] with:

$$n = 0.6\left(1 - \frac{f_c(MPa)}{250}\right) \quad \text{in Eurocode 2 (CEN 2004b) or Model Code 90 (CEB 1991)} \tag{3.96a}$$

$$n = 0.7\left(1 - \frac{f_c(MPa)}{200}\right) \quad \text{in the AIJ Guidelines (AIJ 1994)} \tag{3.96b}$$

So, the shear resistance at diagonal compression failure of the web is:

$$V_{R,\max} = 0.5 b_w z (n f_c) \sin 2\delta \tag{3.97}$$

According to Eq. (3.94), a low value of δ gives less transverse reinforcement, as the shallower crack intersects and activates more stirrups. According to Eq. (3.95),

[17] The symbol n is used here instead of the symbol v used in both Eurocode 2 and CEB/FIP Model Code 90, to avoid confusion with the normalised axial force $v = N/A_c f_c$.

however, it is more demanding for the chords in tension and, according to Eq. (3.97), for the inclined compression stress field as well.

The shear resistance normally attains its maximum value when the web concrete fails in diagonal compression, while the transverse reinforcement has already yielded (case ii above). The condition $V_{\mathrm{R,s}} = V_{\mathrm{R,max}}$ gives the following lower limit for the inclination angle, δ (Walraven 2002):

$$\sin\delta = \sqrt{\frac{\omega_w}{n}},\ \tan\delta = \sqrt{\frac{\frac{\omega_w}{n}}{1-\frac{\omega_w}{n}}} \tag{3.98}$$

where $\omega_{\mathrm{w}} \equiv \rho_{\mathrm{w}} f_{\mathrm{yw}}/f_{\mathrm{c}}$ is the mechanical ratio of transverse reinforcement. At this limit value of δ the dimensionless shear resistance is:

$$\upsilon_R = \frac{V_R}{b_w z f_c} = \sqrt{\omega_w(n-\omega_w)} \tag{3.99}$$

Although less common than case ii, case i above may also lead to shear failure. The condition $V_{\mathrm{R,s}} = V_{\mathrm{R,L}}$ gives the following limit value of δ:

$$\tan\delta = \sqrt{\frac{\omega_w}{2(\omega_1-\mu)+\nu}} \tag{3.100}$$

where $\omega_1 \equiv A_{\mathrm{s1}} f_{\mathrm{yL}}/(b_{\mathrm{w}} z f_{\mathrm{c}})$ is the mechanical ratio of tension reinforcement and $\mu \equiv M/(b_{\mathrm{w}} z^2 f_{\mathrm{c}})$, $\nu \equiv N/(b_{\mathrm{w}} z f_{\mathrm{c}})$ are the dimensionless bending moment and axial force, respectively (using in all normalisations the internal lever arm, z, in lieu of the effective depth). At this value of δ the dimensionless shear resistance is:

$$\upsilon_R = \frac{V_R}{b_w z f_c} = \sqrt{\omega_w(2(\omega_1-\mu)+\nu)} \tag{3.101}$$

Even less common is a failure mode where the tension chord yields first, followed by diagonal compression failure of the web concrete while the transverse reinforcement stays elastic. The condition $V_{\mathrm{R,max}} = V_{\mathrm{R,L}}$ gives the following upper limit for δ:

$$\cos\delta = \sqrt{\frac{2(\omega_1-\mu)+\nu}{n}},\ \tan\delta = \sqrt{\frac{n-2(\omega_1-\mu)-\nu}{2(\omega_1-\mu)+\nu}} \tag{3.102}$$

and a dimensionless shear resistance of:

$$\upsilon_R = \frac{V_R}{b_w z f_c} = \sqrt{(n-2(\omega_1-\mu)-\nu)(2(\omega_1-\mu)+\nu)} \tag{3.103}$$

The variable strut inclination truss model is rational, transparent and consistent with the strut-and-tie approach for the Ultimate Limit State (ULS) design of

two-dimensional concrete regions (including discontinuities of geometry, supports and regions with concentrated forces). So there is smooth transition between such regions and adjacent prismatic ones. Accordingly, in Europe it is the basis of the provisions for calculation of shear resistance of concrete members at the ULS. The designer is allowed to choose the value of δ in the range:

– in Eurocode 2 (CEN 2004b):

$$0.4 \leq \tan\delta \leq 1 \,(22^\circ \leq \delta \leq 45^\circ); \tag{3.104a}$$

– in the CEB/FIP Model Code 90 (CEB 1991):

$$1/3 \leq \tan\delta \leq 1 (18^\circ \leq \delta \leq 45^\circ) \tag{3.104b}$$

Eurocode 2 and CEB/FIP Model Code 90 consider that a compressive axial force, N, contributes to shear resistance according to the following mechanism. Shear force goes together with bending moments. In the common case of a column in counter-flexure, the axial force N will be equilibrated at the two end sections by concrete compressive stress blocks that develop at opposite ends of these two sections.[18] The axial force N is transferred, therefore, from the compressive stress block at one end section to that at the other end via a diagonal compression strut (Fig. 3.39(a), left). The component of the strut force parallel to the column axis is equal to N, while the component transverse to the axis is equal to $V_N = N(z_1+z_2+d_1-d)/L$ where z_1 and z_2 are the internal lever arms at the two end sections, $d_1 = h-d$ and L is the clear column length. This internal force is in the opposite sense with respect to the acting (external) shear force. So, it can be considered as the contribution of the diagonal compression strut to the shear resistance of the column. In the common case that the two ends have about the same acting moment and cross section reinforcement, this contribution is: $V_N = N(h-x)/L$ where x is the neutral axis depth of the end sections at flexural yielding (computed as $x = \xi_y d$, with ξ_y from Section 3.2.2.2). The rest of the shear force, $V-V_N$, is resisted by the internal truss mechanism with a (variable) strut inclination δ (Fig. 3.39(a), right). The normal stress component $\sigma = N/b_w(h-x)$ in the strut acts together with the compression field of the truss, which is equal to $2(V-V_N)/(b_w z \sin 2\delta)$ and is at an angle δ to the column axis.

As shown in Fig. 3.40, for monotonic loading the variable strut inclination truss model gives a safe-side bound of test results on beams failing by diagonal compression of the web after yielding of the transverse reinforcement (Walraven 2002). In Fig. 3.40(b) the beneficial effect of the (compressive) prestressing force on shear resistance is taken into account at the same time as the adverse effect of the superposition of the normal stress component in the strut due to prestress with the

[18] Being symmetrically reinforced, each end section will resist the bending moments there through approximately equal and opposite forces in the two "chords", that produce no net contribution to N.

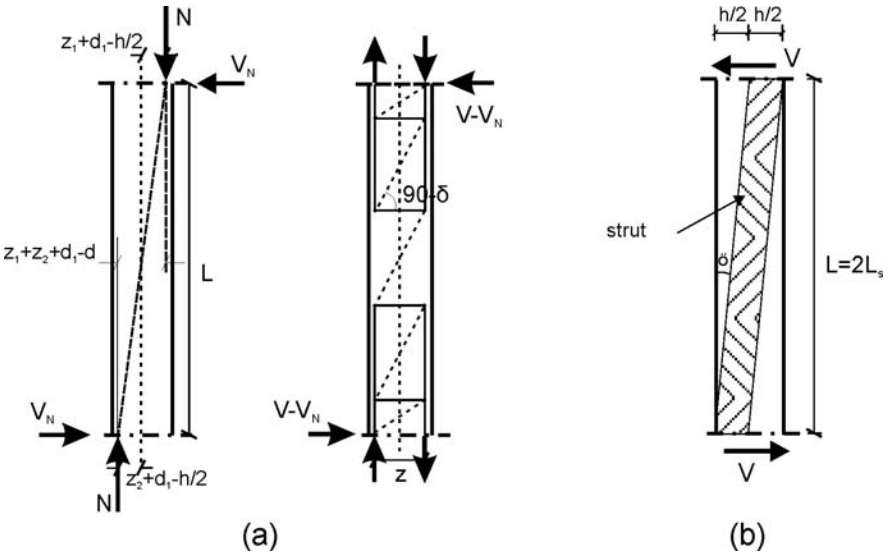

Fig. 3.39 Shear resistance model: (**a**) according to (CEB 1991); (**b**) according to (AIJ 1994)

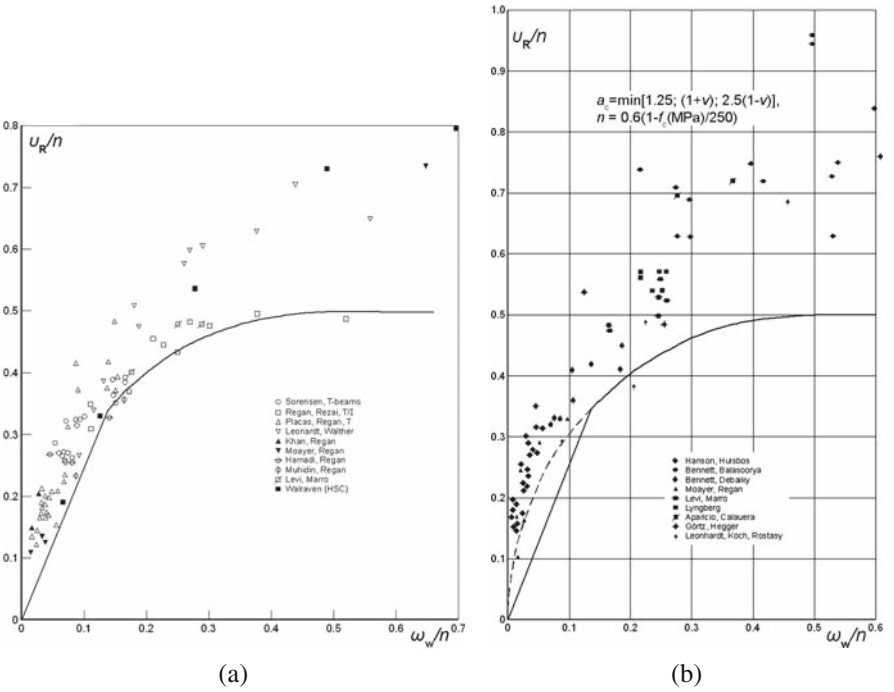

Fig. 3.40 Comparison of Eq. (3.99), subject to the limits of Eq. (3.104a), to monotonic shear resistance data: (**a**) reinforced beams with rectangular or T-section; (**b**) prestressed T- or I-beams (Walraven 2002)

compression field of the truss, by multiplying the shear resistance at diagonal compression failure in the web by the following empirical factor given in Eurocode 2:

$$a_c = \min[1.25;\ (1 + \nu);\ 2.5(1 - \nu)] \tag{3.105}$$

where ν is the normalised axial compression, in this case due to the prestress: $\nu = P/A_c f_c$.

The variable strut inclination approach is a generalisation of the classical Mörsch-Ritter truss, where $\delta = 45^\circ$. The 45°-truss is still the basis for shear design in the US (ACI 2008). In such an approach, transverse reinforcement is dimensioned to take a tensile force per unit length along the member axis equal to $(V–V_c)/z$, instead of the value $V\tan\delta/z$ of the variable strut inclination truss model. The V_c term replaces the increase in the contribution of stirrups to shear strength, $V_{R,s}$, according to Eq. (3.94) as the strut inclination decreases from $\delta = 45^\circ$ to a lower value. It is considered as the "concrete contribution to shear resistance". Its physical basis is claimed to be the contributions to the truss model of shear resistance of:

- the uncracked compressive zone;
- aggregate interlock along open diagonal cracks (considered at an angle $\delta = 45^\circ$);
- dowel action of the longitudinal bars; and
- the tensile strength of concrete between diagonal cracks.

As it is not feasible to quantify the contribution of each one of the above four mechanisms in terms of the corresponding parameters, the V_c term is just the difference between:

- the experimentally measured shear resistance, and
- the contribution of transverse reinforcement calculated from Eq. (3.94) with $\delta = 45^\circ$, plus any contribution of the axial force N.

So the value of V_c is commonly given by empirical or semi-empirical expressions in terms of all other parameters that seem to significantly affect shear resistance. Recall in this connection the Eurocode 2 empirical expression, Eq. (3.67), for the shear resistance of concrete members without shear reinforcement, V_{Rc}.

The Truss Plus Diagonal Strut Model of the AIJ Guidelines

The approach of the Guidelines of the Architectural Institute of Japan (AIJ 1994) for the shear resistance of concrete members under cyclic loading is the most fundamental in all codes or standards for earthquake-resistant design of concrete structures. In this approach shear resistance is taken as the sum of contributions from two mechanisms:

- a "variable strut inclination" truss, as in Eurocode 2 (CEN 2004b) and Model Code 90 (CEB 1991); and

– a diagonal strut between the two end sections of the member, considered in skew symmetric bending (i.e. with length L twice the shear span L_s).

The contribution of the truss mechanism to shear resistance is considered to be controlled by the transverse reinforcement according to Eq. (3.94). A compression field at an angle δ to the member axis equal to: $\sigma_c = 2V_w/(b_w z \sin 2\delta) = \rho_w f_{yw}/\sin^2\delta$ is necessary, to support this contribution to shear resistance. The stress σ_c uses up part of the reduced diagonal concrete strength, nf_c (see Eqs. (3.96) for the reduction factor n). Neglecting the different orientations of the diagonal strut and of the compression field of the truss mechanism, the effective compressive strength available to the diagonal strut is $nf_c - \rho_w f_{yw}/\sin^2\delta$. The AIJ Guidelines assume the diagonal strut to take up half of the cross-sectional depth h in the direction of the shear force, no matter the width of the compression zone due to flexure. The strut inclination with respect to the member axis, ϕ, is such that:

$$\tan\phi = \sqrt{\left(\frac{2L_s}{h}\right)^2 + 1} - \frac{2L_s}{h} \approx h/4L_s. \tag{3.106}$$

In the end the maximum compressive force that the diagonal strut can develop has a component transverse to the member axis equal to $0.5 b_w h(nf_c - \rho_w f_{yw}/\sin^2\delta)\tan\phi$, which is the strut contribution to shear resistance. Therefore, the total shear resistance is:

$$V_R = \rho_w f_{yw} b_w z \cot\delta + 0.5 b_w h[nf_c - \rho_w f_{yw}(1 + \cot^2\delta)]\tan\phi \tag{3.107}$$

An upper limit is set for the value of $\cot\delta$, equal to the smallest of the three values:

– $\cot\delta \le 2\ (\delta \ge 26.5)^\circ$ (3.108a)

for a positive term in brackets in Eq. (3.107):

– $\cot\delta \le \sqrt{(nf_c/\rho_w f_{yw} - 1)}$ (3.108b)

– $\cot\delta \le z(h\tan\phi) \approx 4\zeta L_s/h$ (3.108c)

(with $\zeta = z/h$), which gives the maximum possible shear resistance from Eq. (3.107).

The effect of inelastic cyclic deformations on the shear strength of plastic hinge regions is taken into account:

– by replacing the limit of Eq. (3.108a) with:

$$\cot\delta \le \max(1;\ 2 - 50\theta_{pl}) \tag{3.108d}$$

– by reducing the value of n from Eq. (3.96b) to:

$$n = 0.7\left(1 - \frac{f_c(MPa)}{200}\right)\max\left(0.25;\ 1 - 15\theta_{pl}\right) \tag{3.109}$$

where θ_{pl} is the plastic hinge rotation: $\theta_{\mathrm{pl}} = (\mu_\theta - 1)\theta_{\mathrm{y}}$, with μ_θ denoting the demand value of the displacement or chord rotation ductility factor.

3.2.4.3 Models of Cyclic Resistance in Diagonal Tension After Flexural Yielding

At pointed out in Section 3.2.4.1, after flexural yielding the shear strength degrades in the plastic hinge with increasing cyclic inelastic deformations. It has also been noted that this phenomenon is normally expressed quantitatively as a reduction of shear strength with cyclic inelastic deformations, until the so-reduced shear strength, V_{R}, drops below the value of shear force corresponding to flexural yielding, $V_{\mathrm{y}} = M_{\mathrm{y}}/L_{\mathrm{s}}$.

Several models have been proposed for the cyclic decay of the strength of concrete members for diagonal tension failure (Kowalsky and Priestley 2000, Moehle et al. 2001, Ascheim and Moehle 1992, Biskinis et al. 2004). They all recognise a contribution of transverse reinforcement to shear resistance, V_{Rs}, and a separate concrete contribution, V_{c}.

The "Revised UCSD model" model in Kowalsky and Priestley (2000) has been developed on the basis of 18 circular columns that failed in shear after yielding in flexure. Predictions also compare well to the strength of 20 circular columns yielding and failing in shear and are compatible with the strength of 9 circular columns failing in flexure.

As in the CEB/FIP Model Code 90, the model in Kowalsky and Priestley (2000) includes the contribution of the column axial force to shear resistance as a distinct mechanism, giving a shear resistance:

$$V_R = N\frac{h-x}{2L_s} + \sqrt{f_c}k\left(\mu_\theta\right)\min\left(1.5,\ \max\left(1;\ 3 - \frac{L_s}{h}\right)\right) \\ \min\left(1;\ 0.5 + 20\rho_{tot}\right)(0.8A_c) + V_{Rs}\ \text{(units: MN, m)} \tag{3.110}$$

where:

– ρ_{tot} is the total ratio of longitudinal steel, reflecting in this case dowel action,
– A_{c} is taken equal to $\pi {D_{\mathrm{c}}}^2/4$ (with D_{c}: diameter of concrete core inside the hoops),
– h is the depth of the cross-section (equal to the diameter D in circular sections),
– N is the axial load (positive for compression),
– x is the neutral axis depth at flexural yielding ($x = \xi_{\mathrm{y}} d$, with ξ_{y} from Section 3.2.2.2), and
– $L_{\mathrm{s}}/h = M/Vh$ is the shear span ratio at the member end, reflecting the arch mechanism of shear resistance.

Shear strength degradation due to cyclic deformations of the shear span up to a chord rotation ductility ratio μ_θ[19] is taken into account through the coefficient $k(\mu_\theta)$ in the concrete term V_c:

$$k(\mu_\theta) = \frac{1.07 - 0.115\mu_\theta}{3} \quad , 0.05 \le k(\mu_\theta) \le 0.28 \tag{3.111}$$

Equations (3.110) and (3.111) have been developed for circular columns with the contribution of transverse steel, V_{Rs}, taken as:

$$V_{Rs} = \frac{\pi}{2}\frac{A_{sw}}{s_h} f_{yw}(D - x - c)\cot\delta \tag{3.112}$$

where A_{sw} denotes the cross-sectional area of a circular hoop, s_h its spacing and c its concrete cover. In the "revised UCSD model" the truss inclination is taken as: $\delta = 30^\circ$.

Although originally developed for columns with circular section, Eqs. (3.110) and (3.111) are often applied to rectangular sections as well, using for V_{Rs} Eq. (3.94) with $z = d–x$, $\delta = 30^\circ$, and replacing the term $0.8A_c$ by $b_w d$ (where b_w is the width of the web and d the effective depth). In that case it overestimates the shear resistance of rectangular columns by about 20%, of rectangular walls by about 10% and of non-rectangular walls or hollow rectangular piers by about 30% (Biskinis 2007, Biskinis et al. 2004).

In the most recent one of the family of models by Moehle and co-workers for rectangular columns (Moehle et al. 2001), the contribution of axial compression to shear resistance is accounted for in the V_c term and not as a separate mechanism (cf. 1st term in Eq. (3.110)). More important, the reduction of shear strength with cyclic deformation is considered to affect both the V_{Rs} and the V_c terms, which are multiplied by the same coefficient $k(\mu_\theta)$ (Moehle et al. 2001):

$$V_R = k(\mu_\theta)(V_c + V_{Rs}) \; ; \quad V_c = 0.5\sqrt{f_c}\left(\sqrt{1 + \frac{N}{0.5\sqrt{f_c}A_c}}\right)A_c\frac{d}{L_s} \quad \text{(units: MN, m)} \tag{3.113a}$$

$$k(\mu_\theta) = 1.15 - 0.075\mu_\theta, \; 0.7 \le k(\mu_\theta) \le 1.0 \tag{3.113b}$$

where $A_c = b_w d$, for cross-sections with rectangular web of width b_w and effective depth d. The part of the V_c term multiplied by d/L_s in Eq. (3.113a) is the product of the gross section area and the principal tensile stress at diagonal cracking, computed on the basis of a postulated concrete tensile strength of $0.5\sqrt{f_c}$. For beams, rectangular columns, rectangular walls or barbelled, T-, H- or hollow rectangular sections the contribution of transverse reinforcement, V_{Rs}, is taken from Eq. (3.94), with

[19] In members the chord rotation ductility factor, μ_θ, is the same as the displacement ductility factor.

$\delta = 45^\circ$, as in the classical Ritter-Mörsch truss analogy. In circular columns $V_{R,s}$ may in this case be taken from Eq. (3.112), but with $\delta = 45^\circ$ and (D–x–c) replaced by (D–2c).

Equations (3.113) agree well, on average, with the experimental results on rectangular columns, but underestimate the shear resistance of circular ones by almost 20% and of rectangular walls by about 10%, while it overestimates that of non-rectangular walls or hollow rectangular piers by about 15% (Biskinis 2007, Biskinis et al. 2004).

Note that in Eqs. (3.110) and (3.111) the V_c term is constant and equal to 18% of its value for zero ductility demand, when the value of μ_θ exceeds 8. According to Eq. (3.113b), it is for values of μ_θ above 6 that the entire shear resistance V_R attains its minimum value of 70% of that for zero ductility demand. The difference in the limiting value may be attributed to:

- the reduction of the entire shear resistance with increasing μ_θ in Eq. (3.113a), whereas only one term out of three is taken to decrease with increasing μ_θ in Eqs. (3.110) and (3.111); and
- the relative small magnitude of the only term that decreases with μ_θ in Eq. (3.110), owing to the adoption of a value $\delta = 30^\circ$ for the truss inclination δ in Eqs. (3.94) and (3.112).

In both models above, μ_θ is derived from the experimental θ_y, which is not known a-priori in practical applications. This may be considered as a weakness.

The models proposed in (Biskinis et al. 2004, Biskinis and Fardis 2004, Biskinis 2007) and adopted in Part 3 of Eurocode 8 (CEN 2005a) are based on the largest database of cyclic tests of members failing by diagonal tension after yielding in flexure: 70 circular columns, 192 rectangular beams/columns, 12 rectangular walls and 26 hollow rectangular piers or non-recangular walls. The range of important parameters in these tests are:

- $\nu = N/A_c f_c$: –0.01–0.85;
- L_s/h: 0.5–6;
- ρ_{tot}: 0.55–5.5%;
- f_c: 13–113 MPa;
- μ_θ: 1.0–9.5.

In these models the resistance in diagonal tension, V_R, is taken a function of $\mu_\theta^{pl} = (\mu_\theta – 1)$, computed as the ratio of the plastic part of the chord rotation at ductile shear failure (: total chord rotation minus experimental yield value) to the yield chord rotation, θ_y, from Eqs. (3.66), instead of the experimental θ_y. In this way μ_θ^{pl} is not affected by the flexibility of the base of some test specimens, which increases the measured pre-yield deflection but affects very little the post-elastic deformations of the specimen itself. Similar to Eq. (3.110) of Kowalsky and Priestley (2000), the axial compression N is taken to affect shear resistance according to the CEB/FIP Model Code 90 (CEB 1991), but the effect of axial tension is neglected. As in Eqs.

(3.110) and (3.113a), $\sqrt{f_c}$ appears in the V_c term, reflecting the tensile strength of concrete.

In the first one of two models only the V_c term is taken to degrade with inelastic cyclic displacements (cf. Eq. (3.110)). With units: MN, m, this model is:

$$V_R = \frac{h-x}{2L_s} \min\left(N;\ 0.55A_c f_c\right) + 0.16\left(1 - 0.095\min\left(5;\ \mu_\theta^{pl}\right)\right) \max(0.5,\ 100\rho_{tot})\left(1 - 0.16\min\left(5;\ \frac{L_s}{h}\right)\right)\sqrt{f_c}A_c + V_{Rs} \tag{3.114a}$$

In the other model both V_c and the contribution of V_{Rs} degrade with cyclic μ_θ :

$$V_R = \frac{h-x}{2L_s} \min\left(N;\ 0.55A_c f_c\right) + \left(1 - 0.05\min\left(5;\ \mu_\theta^{pl}\right)\right) \left[0.16\max(0.5;\ 100\rho_{tot})\left(1 - 0.16\min\left(5;\ \frac{L_s}{h}\right)\right)\sqrt{f_c}A_c + V_{Rs}\right] \tag{3.114b}$$

V_{Rs} is taken with $\delta = 45^\circ$ and as for Moehle et al. (2001): in circular columns from Eq. (3.112) with (D–x–c) replaced by (D–2c) and for all other sections from Eq. (3.94).

Both Eqs. (3.114a) and (3.114b) agree very well with the data and are practically equivalent as far as scatter is concerned. Their test-to-prediction ratio in 300 cyclic tests to diagonal tension failure has median of 0.995 and coefficients of variation of 15.5% or 14.6%, respectively. For comparison, the median test-to-prediction ratio for Eqs. (3.110) or (3.113) is 0.83 or 1.015, respectively, and the coefficient of variation of both is about 25%.

Equations (3.114) are also in good agreement with three cyclic tests on prestressed specimens, failing by diagonal tension after flexural yielding. In this calculation the prestress can only be taken as part of the actions, even though bonded tendons near the extreme tension fibres may yield, when the member's end section yields before ultimate failure in shear. The prestress cannot be taken as part of the resistance, because bending moments nowhere enter in this calculation and hence the bending moment induced by the bonded tendons that have not yielded cannot be taken into account.

According to Eqs. (3.114), beyond $\mu_\theta = 6$ there is no further decay of shear strength. For $\mu_\theta > 6$ the V_c term in Eq. (3.114a) assumes a constant value equal to 52.5% of that at $\mu_\theta = 1$. In Eq. (3.114b) for $\mu_\theta > 6$ the sum of V_c and V_{Rs} attains a constant value of 75% that at $\mu_\theta = 1$.

Equations (3.110), (3.111), (3.112), (3.113) and (3.114) can be conveniently used to assess whether a member that initially yields in flexure may ultimately fail in shear by diagonal tension at a cyclic deformation less than that at failure by flexure. In principle, they can also be inverted to estimate the cyclic deformation capacity of members failing by diagonal tension after flexural yielding: by setting the shear resistance V_R equal to the shear force, M_y/L_s, at flexural yielding, solving for μ_θ

and estimating the shear-controlled chord rotation capacity as μ_θ times θ_y, from Eqs. (3.66). However, the sensitivity of V_R to μ_θ is not sufficiently large to allow using this force-based criterion to predict the deformation capacity as controlled by shear. So, the predictive capability of the inverted procedure is poor (Biskinis 2007, Biskinis et al. 2004).

3.2.4.4 Inclination of Compression Stress Field at Ductile Shear Failure Under Cyclic Loading

The method of choice in Eurocode 2 (CEN 2004b) for the design of concrete elements in shear is the "variable strut inclination" model, Eqs. (3.94), (3.95) and (3.97), along with Eqs. (3.96a) and (3.104a). Eurocode 8, conforms to the Eurocode 2 framework and uses Eq. (3.94), that includes a term proportional to cotδ but no V_c term. According to Eurocode 8, columns and walls of DC H (High) buildings, as well as any member of a DC Medium (M) building, may be dimensioned for an angle δ of the compression diagonals as low as $\delta = 22^\circ$ (cot $\delta = 2.5$).The beams of DC H buildings should be dimensioned in shear for $\delta = 45^\circ$ (i.e. with a classical 45° truss and no V_c term).

The data used for the fitting of Eqs. (3.114) have also been utilised in (Biskinis 2007, Biskinis et al. 2004) to compute the value of δ at which the sum of $N(h-x)/2L_s$ and V_{Rs} from Eq. (3.94) is equal to the experimental shear resistance. The outcome for the 300 tests is depicted in Fig. 3.41 as a function of the chord rotation ductility factor, μ, at failure. Figure 3.41 shows a tendency of the angle δ to

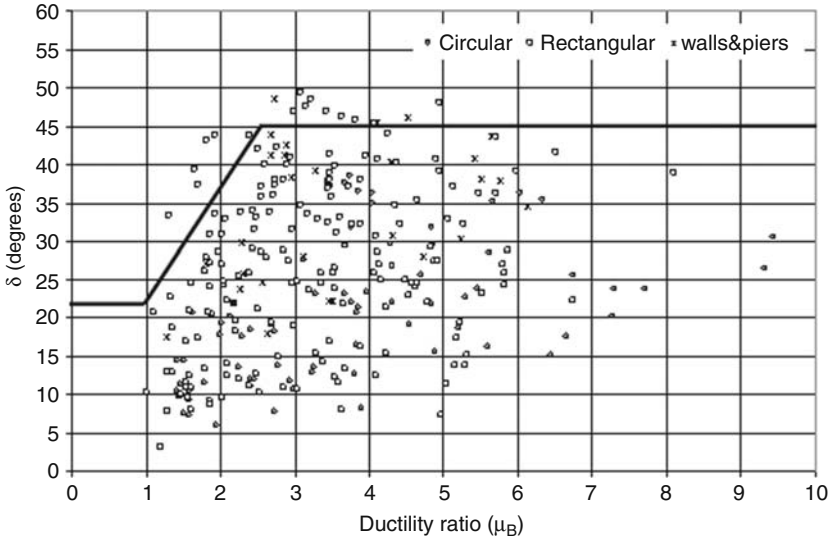

Fig. 3.41 Experimental data on the dependence of the strut inclination δ on chord rotation ductility ratio, for cyclic loading after flexural yielding (Biskinis 2007, Biskinis et al. 2004)

increase on average with increasing μ, from a value well below the Eurocode 2 lower limit of $\delta = 22^\circ$ for $\mu = 1$. However, as important parameters reflected in the V_c term of Eqs. (3.110), (3.113) and (3.114) are missing, the scatter is very large. So, any attempt to fit the angle δ as a function of μ_θ is meaningless. An approximate 5%-fractile line is drawn in Fig. 3.41, extending from the Eurocode 2 lower limit of $\delta = 22^\circ$ for $\mu = 1$, to $\delta = 45^\circ$ for $\mu = 2.5$. This line may be considered to give a very safe-sided estimate of shear strength for design purposes. So, despite the merits of the "variable strut inclination" method for shear design against monotonic loads, a classical 45°-truss model with a V_c term that depends on displacement ductility demand, seems to be a better means for the design of concrete members against diagonal tension failure under cyclic loading after flexural yielding.

3.2.4.5 Degradation with Cyclic Loading of the Diagonal Compression Strength of Walls

Squat shear walls subjected to cyclic loading in the lab or in the field may fail in shear by diagonal compression, often after flexural yielding. Over 50 wall or hollow rectangular piers (all with shear span ratio, L_s/h, less or equal to 2.5) have been found in the literature as having failed by shear compression under cyclic loading (Biskinis 2007, Biskinis et al. 2004). Most of them failed in shear after they had yielded in flexure, but a total of 18 specimens (walls with barbelled or T-section or hollow rectangular piers) failed before flexural yielding. Figure 3.42 shows that the cyclic shear resistance of these walls decreases when their inelastic deformations increase.

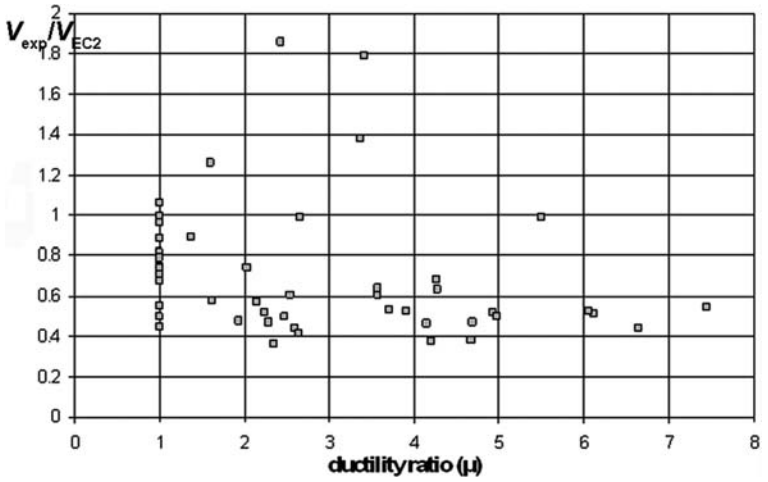

Fig. 3.42 Experimental shear resistance of squat walls for web diagonal compression, as a fraction of the shear resistance from Eqs. (3.97), (3.98) and (3.99), using the concrete strength reduction factor of Eurocode 2 and Model Code 90, Eq. (3.96a)

More important, it is generally much less than the shear resistance of walls in diagonal compression of the web for monotonic, non-seismic actions from Eqs. (3.97), (3.98), (3.99) and (3.96a) (CEN 2004b, CEB 1991). The cyclic shear resistance of these walls is less than the monotonic value in (CEN 2004b, CEB 1991), even when shear failure occurs before flexural yielding ($\mu_\theta = 1$ in Fig. 3.42). It seems therefore, that the Eurocode 2 design rules are not safe for shear compression failure of squat walls under cyclic loading. For this reason in Part 1 of Eurocode 8 the value of $V_{\mathrm{R,max}}$ of ductile walls in DC H buildings is just 40% of the value in Eurocode 2, Eqs. (3.96a) and (3.97). As shown in Fig. 3.42, that value is a 5%-fractile.

A purely empirical model for the cyclic degradation of the shear strength in diagonal compression has been fitted in (Biskinis 2007, Biskinis et al. 2004) to the data that have been used in Fig. 3.42. In addition to ${\mu_\theta}^{\mathrm{pl}} = \mu_\theta - 1$, expressing the effect of inelastic cyclic displacements, statistically significant parameters for the shear strength in cyclic diagonal compression are those included in the V_{c} term of Eqs. (3.114) plus the axial force. Most specimens in the database failed around the value of δ that maximises $V_{\mathrm{R,max}}$ in Eq. (3.97): $\delta = 45^\circ$. So, the model is based on the classical 45° truss. For units MN, m, it gives the cyclic decay of diagonal compression strength as (Biskinis 2007, Biskinis et al. 2004):

$$\begin{aligned} V_{R,\max} = {} & 0.85\left(1 - 0.06\min\left(5;\ \mu_\theta^{pl}\right)\right)\left(1 + 1.8\min\left(0.15;\ \frac{N}{A_c f_c}\right)\right) \\ & (1 + 0.25\max(1.75;\ 100\rho_{tot}))\left(1 - 0.2\min\left(2;\ \frac{L_s}{h}\right)\right) \\ & \sqrt{\min(f_c;\ 100)}\, b_w z \end{aligned} \tag{3.115}$$

The internal lever arm z is taken as $z = 0.8 l_{\mathrm{w}}$ for rectangular walls and $z = d - d_1$ for walls with barbelled or T-section and in hollow rectangular piers.

Equation (3.115) fits the data with a median test-to-prediction ratio of 1.01 and a coefficient of variation of 17.6% (Biskinis 2007). The data fitted include the 18 cyclically loaded walls with barbelled or T-section or hollow rectangular piers failing in shear compression prior to yielding in flexure. Therefore, it may be considered to hold also (with ${\mu_\theta}^{\mathrm{pl}} = 0$) for failure in cyclic shear before flexural yielding.

Equation (3.115) has been adopted in Part 3 of Eurocode 8 (CEN 2005a). Being fully empirical, it applies strictly within the range of parameter values in the fitting:

- L_{s}/h from 0.5 to 2.4 (squat walls),
- $N/A_{\mathrm{c}}f_{\mathrm{c}}$ from 0 to 0.18,
- ρ_{tot} from 0.5 to 3%,
- f_{c} from 16.5 to 137 MPa,
- μ_θ from 1 to 7.5.

3.2.5 Cyclic Behaviour of Squat Members, Controlled by Flexure-Shear Interaction

3.2.5.1 Introduction

Short columns (including captive ones, see Section 2.1.13.4), deep beams and squat walls have low shear span ratio, M/Vh. During earthquakes short columns develop nearly equal and opposite bending moments at their ends. The same holds in short beams, because their end moments due to gravity loads are normally very small. So, the shear span ratio of short columns or beams is equal to $0.5L/h$, where L is the clear length and h the depth of their section. The bending moment diagram of squat walls is affected little by any beams framing into them. So their shear span ratio at the base is between $0.5H_w/l_w$ and $2/3(H_w/l_w)$, where H_w is the total height of the wall.

For given cross-sectional dimensions and longitudinal reinforcement, hence for given moment resistance, the shear force increases with decreasing shear span ratio. Moreover, low shear span ratio elements have a two-dimensional geometry. So it is not possible to distinguish between their end regions, governed by flexure, and the rest of their length, where (the constant) shear force controls the resistance and the behaviour. As a matter of fact, if we ignore that the short length of the member – compared to its depth – invalidates the simple models applicable to prismatic elements, we may be surprised at first sight by some conclusionst. For example, if the usual fan pattern of cracking and of the compression field near the member's end regions extends up to mid-length, $x = L/2$, then, if the corresponding value of the inclination of the compression field at $x = L/2$: $\cot\delta = L/z$ is used for the forces in the chords: $F_t(x) = M(x)/z + 0.5V\cot\delta$ (see Section 3.2.4.2 under *The Variable Strut Inclination Truss of the CEB/FIP Model Code 90 and Eurocode 2*), we get:

- at the mid-section, $x = L/2$: a tensile force in both chords equal to that at the end sections: $F_t = M(x{=}0)/z$,
- at the end sections $x = 0$ and $x = L$: zero force in one chord, instead of the compressive force $F_t = -M(x = L)/z$ expected there on the basis of flexure alone.

So, the stress in the tension longitudinal reinforcement should drop from $\sigma_s = f_y$ at $x = L/2$, to $\sigma_s = 0$ at $x = L$, inducing very high bond demands on the length of the bars between these two sections. Unless another failure mode develops first, splitting cracks may form all-along the corner bars of short concrete members subjected to cycling loading.

Figure 1.2(a) in Section 1.3.1 shows the load-deformation response of an element with $L_s/h = 1.9$ under monotonic loading. Soon after the monotonic ultimate strength is reached, resistance drops drastically. In cyclic loading, hysteresis loops are narrow and have inverted-S shape, with a tendency to tilt and shrink further with cycling. The ultimate deformation is low and the displacement ductility factor

at member failure is not much larger than 1.0. The behaviour is not ductile and is strongly affected (or even governed) by shear.

3.2.5.2 Monotonic Lateral Force Resistance of Squat Members with Flexure-Shear Interaction

As pointed out in Section 3.2.1, if the shear span ratio is low the mechanisms of force transfer by shear or flexure essentially merge into a single one. Diagonal compression in the concrete plays a prime role in this joint mechanism. A good starting point for the understanding of the mechanism of force transfer and of ultimate failure of low shear span ratio elements is the shear resistance model in AIJ (1994), outlined in Section 3.2.4.2 under *The Truss Plus Diagonal Strut Model of the AIJ Guidelines*. That model, though, has certain limitations:

1. the assumption that the diagonal compression strut takes up one-half of the member depth, h, is arbitrary;
2. the effect of axial load is ignored;
3. concrete stresses in the diagonal strut are directly added to those in the compression field of the truss mechanism, although they do not act in the same direction, but at angles ϕ and δ to the member axis, respectively.

An important feature of the AIJ model is that the diagonal compression strut acting between the compression zones at the two end sections resists, via its force component that is transverse to the member axis, a certain part of the shear force (cf. term $N(h–x)/2L_s$ in Eqs. (3.110) and (3.114)). The rest of the shear force is resisted through the familiar truss mechanism comprising:

– the two parallel chords,
– the stirrups, and
– the concrete compression field at an inclination δ to the member axis.

The AIJ model for shear resistance of relatively slender elements without effect of the axial force (Section 3.2.4.2 under *The Truss Plus Diagonal Strut Model of the AIJ Guidelines*) is extended below to squat elements with axial compression:

(a) by taking into account the contribution of the axial load, N, and
(b) by considering that at the two end sections the diagonal strut extends over the neutral axis depth there at flexural yielding (i.e., it is equal to: $x = \xi_y d$, with ξ_y from Section 3.2.2.2 under *Cross-Sections with Rectangular Compression Zone*), in lieu of $0.5h$.

Owing to (b), the strut inclination to the member axis is $\phi = \arctan[(h-x)/2L_s]$. Its width normal to the strut axis is $x \cos\phi$.

As in the AIJ (1994) model, the member is considered to fail in diagonal compression under the action of:

- the normal stress in the diagonal strut, assumed uniform over its width, $x \cos \phi$, even at the end section of the member;
- the inclined compression field of the truss mechanism, considered uniform over the internal lever arm $z = \zeta h$ between the chords and acting at an angle δ to the member axis.

Also as in the AIJ shear model, the difference in the orientation of these two compression fields is neglected. So, their stress magnitudes are added up and the sum is set equal to a fraction n of the uniaxial compressive strength of concrete, f_c (see Eqs. (3.96)).

The assumptions and approximations above give the following, as generalisation of the procedure in Shohara and Kato (1981) – where the truss was a classical Mörsch-Ritter one with $\delta = 45^\circ$ and $n = 1$ – (see Fig. 3.43(a), where $\nu = N/bhf_c$, $\upsilon = V/bhf_c$, $\lambda = L/h = 2L_s/h$, $\zeta = z/h$ and ω_s is the total mechanical longitudinal reinforcement ratio, denoted here as ω_{tot}).

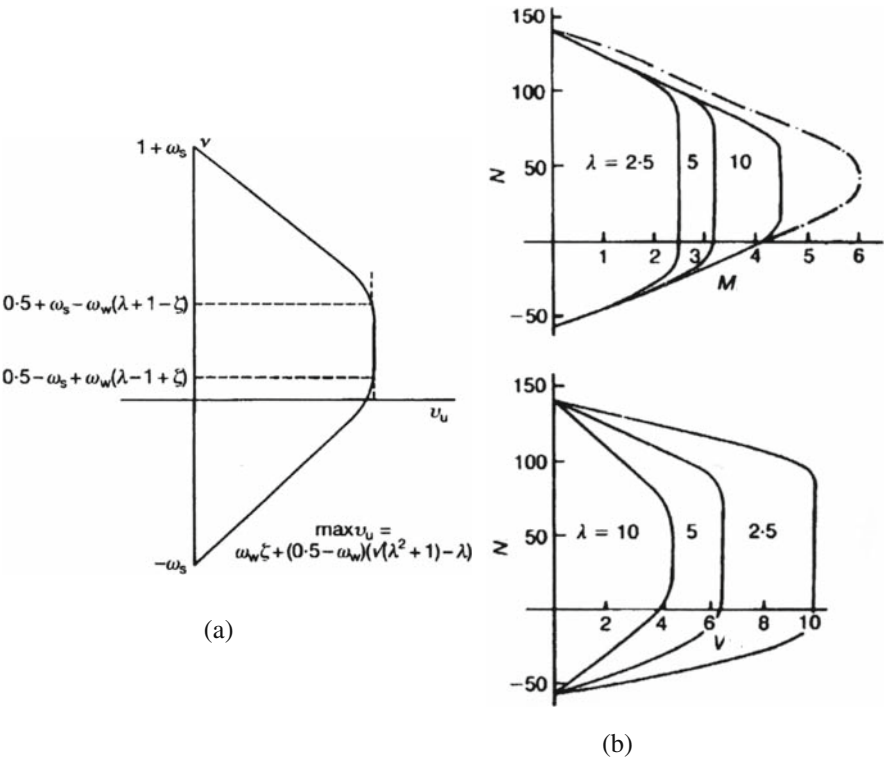

Fig. 3.43 (**a**) Schematic interaction diagram in dimensionless *V-N* space (CEB 1996a); (**b**) application for dimensional *M-N* and *V-N* diagrams of 200 mm square column with four 16 mm bars (CEB 1996a)

1. In the following range of axial forces N (positive for compression):

$$\begin{aligned} N_1 = {} & 0.5bhnf_{\mathrm{c}} - A_{\mathrm{s,tot}} f_{\mathrm{y}} + \rho_{\mathrm{w}} b_{\mathrm{w}} f_{\mathrm{yw}} [\cot\delta(2L_{\mathrm{s}} + (z - 0.5\,h)\cot\delta) - 0.5\,h] \\ & \le N \le N_2 = 0.5bhnf_{\mathrm{c}} + A_{\mathrm{s,tot}} f_{\mathrm{y}} - \rho_{\mathrm{w}} b_{\mathrm{w}} f_{\mathrm{yw}} \\ & [\cot\delta(2L_{\mathrm{s}} - (z - 0.5\,h)\cot\delta) + 0.5\,h] \end{aligned} \tag{3.116}$$

   failure is brittle, taking place by yielding of transverse reinforcement and diagonal concrete crushing, while all the longitudinal reinforcement is still in the elastic range. The shear resistance is independent of the exact value of N between N_1 and N_2 and of the total cross-sectional area of longitudinal reinforcement, $A_{\mathrm{s,tot}}$. It is obtained from Eq. (3.107) using there the value of tan ϕ from Eq. (3.106).
2. In the range of N-values:

$$N_1 \ge N \ge -A_{\mathrm{s,tot}} f_{\mathrm{y}} \tag{3.117}$$

   failure is by diagonal concrete crushing, but it is less brittle than in case 1, as not only the transverse steel but also the tension reinforcement have already yielded. The shear resistance is:

$$V_R = (N + A_{s,tot} f_y)\tan\phi + \rho_w f_{yw} b_w \cot\delta\,(z - (2L_s + z\cot\delta)\tan\phi) \tag{3.118}$$

   where:

$$\tan\phi = \min\left(\sqrt{\left(\frac{L_s}{\eta h}\right)^2 + \frac{1-\eta}{\eta}} - \frac{L_s}{\eta h},\ \frac{h}{2L_s}\right) \tag{3.119}$$

   and

$$\eta = \frac{N + A_{s,tot} f_y - \rho_w f_{yw} b_w (2L_s + z\,\cot\delta)\cot\delta}{b_w h\left(nf_c - \rho_w f_{yw}\left(1 + \cot^2\delta\right)\right)} \tag{3.120}$$

3. In the remaining range of N-values, i.e. for

$$nf_{\mathrm{c}} b_{\mathrm{w}} h + A_{\mathrm{s,tot}} f_{\mathrm{y}} \ge N \ge N_2 \tag{3.121}$$

   failure is again by diagonal concrete crushing with the transverse steel at yielding, but in this case with the compression reinforcement yielding as well. So, it is again less brittle than in case 1. The shear resistance is:

$$V_R = (N - A_{s,tot} f_y)\tan\phi + \rho_w f_{yw} b_w \cot\delta\,(z + (2L_s - z\cot\delta)\tan\phi) \tag{3.122}$$

   The value of tan ϕ is still given by Eq. (3.119), but with the following value of η:

$$\eta = \frac{\left(N - A_{s,tot} f_y\right) + \rho_w f_{yw} b_w \left(2L_s - z \cot\delta\right) \cot\delta}{b_w h \left(n f_c - \rho_w f_{yw} \left(1 + \cot^2\delta\right)\right)} \tag{3.123}$$

The upper limit of $\cot\delta$ is still given by Eq. (3.108b). An inclination of the compression field close to the cracking pattern is: $\cot\delta = L_s/h$.

Case 1 above, of brittle failure and of shear resistance independent of N exists only if $N_2 > N_1$, i.e. only if:

$$\cot\delta \leq \frac{\omega_{tot}}{\omega_w} \frac{h}{2L_s} \tag{3.124}$$

Equations (3.116), (3.117), (3.118), (3.119), (3.120), (3.121), (3.122) and (3.123), supplemented with Eqs. (3.106) and (3.107) where relevant, are essentially analytical expressions of the monotonic ULS resistance of squat columns under skew-symmetric bending, as governed by moment, shear and axial force. In other words, they give the reduction of flexural resistance due to high shear.

Using the relationship $M = VL_s$, Eqs. (3.116), (3.117), (3.118), (3.119), (3.120), (3.121), (3.122) and (3.123) can be converted into interaction diagrams relating the dimensionless moment $\mu = M/bh^2 f_c = (V/bhf_c)(L_s/h)$ to the dimensionless axial force $\nu = N/bhf_c$. When the shear span ratio, L_s/h, increases, such μ–ν interaction diagrams tend asymptotically to the simple bilinear diagram:

$$\mu = 0.5\zeta(\nu + \omega_{\text{tot}}) \qquad \text{for } 0.5n > \nu \geq -\omega_{\text{tot}} \tag{3.125a}$$

$$\mu = 0.5\zeta(n + \omega_{\text{tot}} - \nu) \qquad \text{for } n + \omega_{\text{tot}} \geq \nu \geq 0.5n \tag{3.125b}$$

Equations (3.125) can be derived as interaction relations between dimensionless moment and axial force of a single section at the ULS in bending, assuming:

- for Eq. (3.125a), that the resultant force of the concrete stresses in the compression zone is applied at the location of the compression reinforcement and
- for Eq. (3.125b), that the entire cross-section is under a compressive stress of nf_c.[20]

Figure 3.43(b) presents interaction diagrams derived from the above procedure with $n = 1$ and $\delta = 45^\circ$ (Shohara and Kato 1981).

3.2.5.3 Under What Conditions Does Shear Reduce the Moment Resistance?

The conventional criterion for the characterisation of an element as squat and prone to reduction of its moment resistance owing to shear, is its slenderness, $\lambda = L/h$, or – preferably – its shear span ratio, $M/Vh = L_s/h$. A more rational criterion can

[20] Normally we take $n = 1$ for flexure with axial load without shear.

be based on Eq. (3.124), which is the condition for the existence of the axial-load-range where failure is brittle, Eq. (3.116). Equation (3.124) has been generalised in Biskinis (2007) to members with not just tension and compression reinforcement, but also with "web" reinforcement in-between. Taking for simplicity $\delta = 45^\circ$ as in Shohara and Kato (1981), the generalised criterion is:

$$2\frac{L_s}{h} \leq \frac{\omega_{tot}}{\omega_w} \tag{3.124a}$$

The yield moment of rectangular beams or columns with relatively low shear span ratio, L_s/h, has been compared in Biskinis (2007) with the value calculated from Section 3.2.2.2.[21] Over 300 such members were identified to exhibit reduction of the yield moment owing to shear and low slenderness. Calculation according to Section 3.2.2.2 gives for them a median test-to-prediction ratio of 0.86, distinctly lower than the median test-to-prediction ratio of 1.025 for about 2050 beams or columns that do not exhibit effects of shear on their yield moment (see Section 3.2.2.2 under *Comparison with Experimental Results and Empirical Expressions for the Curvature*). Scrutiny of the experimental results has led to proposed new criteria for members whose moment resistance is reduced by shear:

i. If $2.0 < L_s/h < 3.0$: the axial force N is between the bounds of Eq. (3.116).
ii. If $L_s/h < 2.0$: Eq. (3.124a) is met.

If the member does not satisfy one of these two criteria, its yield moment may be calculated according to Section 3.2.2.2.

The yield moment of the over 300 members found to meet one of these two criteria is slightly underpredicted by the procedure of Section 3.2.5.2, even when applied with $n = 1$ and $\delta = 45^\circ$, i.e. as in Shohara and Kato (1981). The test-to-prediction ratio has a median of 1.085 and a coefficient of variation of 29.1%, to be contrasted with the median of 1.025 and the coefficient of variation of 16.3% of the about 2050 beams/columns without effects of shear (Biskinis 2007).

A more sophisticated alternative to the analysis in Section 3.2.5.2 has also been considered in Biskinis (2007), where:

- the difference in the orientation of the truss (at an angle δ to the member axis) and of the stress in the diagonal strut is taken into account; the principal compressive stress of the combined field is set equal to nf_c
- plane-sections analysis is carried out at the end sections.

It has further been found in Biskinis (2007) that:

(a) If the principal compressive stress of the combined stress field reaches the limit value of nf_c together with yielding of the stirrups but before attainment of the

[21] In squat members whose moment resistance is reduced owing to shear, the yield moment is essentially equal to the moment resistance.

moment resistance of the end section(s) with exceedance of ε_{cu} at the extreme compression fibres, the more sophisticated alternative gives predictions closer to the experimental yield moment than the procedure in Section 3.2.5.2 with $n = 1$ and $\delta = 45^\circ$. In those cases the test-to-prediction ratio of the yield moment has a median of 0.99 and a coefficient of variation of 23.7%.

(b) When the moment resistance of the end section(s) is not attained before failure of the concrete in diagonal compression and yielding of the stirrups, the procedure of Section 3.2.5.2 with $n = 1$ and $\delta = 45^\circ$ gives better prediction: a median of 1.035 for the test-to-prediction ratio and a coefficient of variation of 31.3%.

Among those members meeting criteria (i) and (ii) for dependence of their moment resistance on shear, alternative (a) above has been found to approximately correspond to one of the following two conditions (Biskinis 2007):

$$\nu \geq 0.4; \tag{3.126a}$$

$$\frac{\omega_{tot}}{\omega_w} \leq 2\frac{L_s}{h}\max(2;\ 10\nu) \tag{3.126b}$$

If none of these two conditions is met, the procedure of Section 3.2.5.2 gives better predictions.

3.2.5.4 Degradation with Cyclic Loading of the Resistance of Squat Columns to Shear Compression Failure, After Flexural Yielding

The main problem of squat columns is that, after reaching their shear-dependent flexural capacity (see Section 3.2.5.2), they may fail in shear at relatively low values of the chord rotation, θ. Most often shear failure of squat columns takes place by compression along the diagonal of the element between opposite ends of its end sections.

Close to 40 columns from the literature with shear span ratio, L_s/h, less or equal to 2, have failed under cyclic loading by shear compression after flexural yielding (Biskinis et al. 2004). A purely empirical model for the cyclic degradation of shear strength in members failing by diagonal compression has been fitted to those data. Based on the experimental observations, compression failure is taken to occur along the column diagonal in elevation. Inelastic cyclic displacements are expressed through $\mu_\theta{}^{pl} = \mu_\theta - 1$. For units: MN, m, the cyclic shear resistance is (Biskinis et al. 2004):

$$V_{R,\max} = \frac{4}{7}\left(1 - 0.02\min\left(5;\ \mu_\theta^{pl}\right)\right)\left(1 + 1.35\frac{N}{A_c f_c}\right)(1 + 0.45\cdot 100\rho_{tot})\sqrt{\min(f_c;\ 40)}\ b_w z \sin 2\delta \tag{3.127}$$

where δ is the angle between the diagonal and the axis of the column ($\tan\delta = h/2L_s$). The internal lever arm z is taken as $z = d - d_1$.

Equation (3.127) fits the test results with a median value of the test-to-prediction ratio equal to 1.005 and coefficient of variation of 8.9%. Being almost fully empirical, it applies only in the range of parameter values in the relevant database:

- L_s/h from 1 to 2,
- $N/A_c f_c$ from –0.1 to 0.7,
- ρ_{tot} from 0.7 to 4%,
- f_c from 14.5 to 61 MPa,
- μ_θ from 1.4 to 7.

Equation (3.127) has been adopted for squat columns in Part 3 of Eurocode 8 (CEN 2005a).

3.2.5.5 Diagonal Reinforcement in Squat Columns or Deep Beams

It has been pointed out already that elements with low shear span ratio are nearly two-dimensional. Design of two-dimensional concrete elements for monotonic loads is normally based on Strut-and-Tie Models (STMs). In the STM approach, the internal stress field is idealised as a statically determined truss. Bands of compressive stresses identified with concrete struts are verified in compression. Reinforcement is placed along tensile stress bands considered as ties of the STM.

Let's consider a squat column or a deep beam in skew-symmetric bending, i.e. with equal and opposite design moments at its ends: $M_d = V_{Ed}L/2 = V_{Ed}L_s$ where L and L_s are the total clear length and the shear span, respectively, and V_{Ed} is the design shear associated with M_d. The simplest STM of the member consists of;

- a concrete strut along its diagonal in elevation, connecting the compression zones of its two end sections, and
- a (steel) tie along its other diagonal.

Dimensioning of the diagonal steel tie would give a cross-sectional area, A_{sd}, such that:

$$V_{Ed} = 2A_{sd} f_{yd} \sin\delta \tag{3.128a}$$

$$M_d = zA_{sd} f_{yd} \cos\delta \tag{3.128b}$$

where:

- z is the internal lever arm at the end section(s) and
- δ is the angle between the diagonal reinforcement and the axis of the member:

$$\delta = \arctan(z/L) = \arctan(0.5z/L_s) \tag{3.129}$$

If the loading is cyclic, the strut and the tie would alternate between the two diagonals and the member should be reinforced along both, with a steel tie having cross-sectional area, A_{sd}, satisfying Eqs. (3.128) and (3.129). When the diagonal tie is in compression, it could resist (if effectively restrained laterally against buckling) the full compressive force along the diagonal. The surrounding concrete would be protected from diagonal crushing.

Reinforcement placed along both diagonals of the element in sufficient quantity to prevent shear failure before or after flexural yielding of the end sections greatly enhances the flexure-controlled deformation capacity of the element, no matter whether it is sufficient to take the full design action effects according to Eqs. (3.128). The last term in Eqs. (3.78) shows that, all other parameters being the same, a diagonal reinforcement ratio of 1% increases, on average, by 25% the ultimate chord rotation capacity or by 27.5% its plastic part. The enhancement increases more than proportionally for larger diagonal reinforcement ratios. Moreover, the hysteresis loops of the diagonally reinforced element resemble those of steel in uniaxial tension-compression, i.e. they are broad and stable.

Diagonal reinforcement can easily be placed in deep beams, like coupling beams between coupled walls. It may even be placed fairly easily in squat walls (although there it crosses the base section at mid-length, its main purpose being to prevent sliding shear failure, and it does not enhance much the wall moment resistance). As a matter of fact, in deep coupling beams diagonal reinforcement should preferably be arranged in square column-like elements with dense hoops around them, to prevent buckling of the longitudinal bars and confine the concrete inside (Fig. 3.44). In such cases, only nominal (e.g. the minimum) longitudinal and transverse reinforcement needs to be placed in the coupling beam, as the diagonal one is dimensioned to resist the full design action effects according to Eqs. (3.128).

It is very difficult to place diagonal reinforcement in squat columns, while providing at the same time transverse reinforcement at the density and with a pattern normally necessary for confinement of the concrete core and anti-buckling action. Note that, if the column is squat in both horizontal directions, diagonal reinforce-

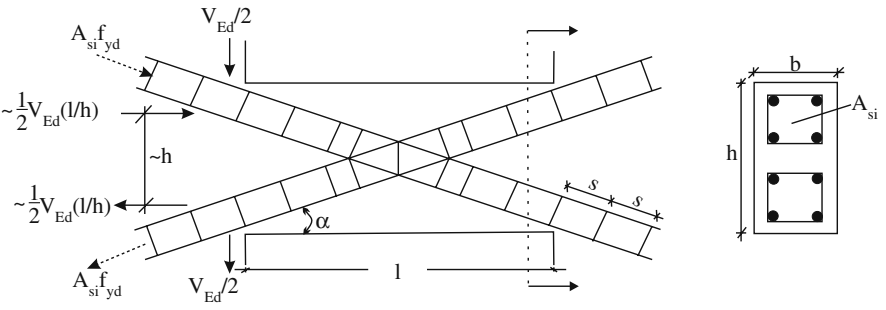

Fig. 3.44 Diagonally reinforced coupling beam (CEN 2004a)

ment should normally be placed along both. This is impracticable. It might be feasible, though, to place diagonal reinforcement in a column which is effectively squat only in one direction (e.g., if beams frame into it at short vertical spacing only within one vertical plane, or if its squatness is due to a concrete or masonry infill in contact with the column, see Fig. 2.12 in Chapter 2).

3.3 Joints in Frames

3.3.1 Force Transfer Mechanisms in Concrete Joints: Bond and Shear

Bending moments in beams due to gravity loading normally have the same sign at opposite faces of their joint with a vertical member. By contrast, beam bending moments due to seismic loading have opposite sign at opposite faces of the joint. Therefore, seismic shear forces are very high in the joint itself. Figure 3.45(a) illustrates the reason for the magnitude of this shear:

- With the joint considered as part of the beam, the change in the beam moment from a (high) negative value to a positive one across the joint produces a vertical shear force, $V_{\mathrm{jv}} = \Sigma M_{\mathrm{b}}/h_{\mathrm{c}} = \Sigma V_{\mathrm{b}} L_{\mathrm{cl}}/2h_{\mathrm{c}}$, where M_{b} and V_{b} denote the beam seismic moments and shears at the face of the joint, L_{cl} the beam clear span and h_{c} the depth of the column.
- With the joint considered as part of the column, the change of the column bending moment from a high value just above the joint to an equally high value with opposite sign just below, produces a horizontal shear force, $V_{\mathrm{jh}} = \Sigma M_{\mathrm{c}}/h_{\mathrm{b}} = \Sigma V_{\mathrm{c}} H_{\mathrm{cl}}/2h_{\mathrm{b}}$, where M_{c} and V_{c} denote column seismic moments and shears above or below the joint, H_{cl} the clear storey height and h_{b} the beam depth.

The joint shear forces produce a nominal shear stress in the concrete of the joint: $v_{\mathrm{j}} = \Sigma M_{\mathrm{c}}/(h_{\mathrm{c}} h_{\mathrm{b}} b_{\mathrm{j}}) = \Sigma M_{\mathrm{b}}/(h_{\mathrm{c}} h_{\mathrm{b}} b_{\mathrm{j}})$, where $(h_{\mathrm{c}} h_{\mathrm{b}} b_{\mathrm{j}})$ is the volume of the joint, with b_{j} its effective width normal to the plane of bending, conventionally taken by seismic design codes (CEN 2004a) as:

$$\text{if } b_{\mathrm{c}} > b_{\mathrm{w}}: \qquad b_j = \min\{b_c; (b_w + 0.5h_c)\}; \tag{3.130a}$$

$$\text{if } b_{\mathrm{c}} \le b_{\mathrm{w}}: \qquad b_j = \min\{b_w; (b_c + 0.5h_c)\} \tag{3.130b}$$

where b_{c} and b_{w} denote the width of the column and the beam, respectively, at right angles to the plane of bending.

Shear stresses are introduced in a joint mainly by bond along the bars of the beam and the column (or wall) around the core of the joint. Because the nominal shear stress in the concrete of the joint is the same, no matter whether it is computed

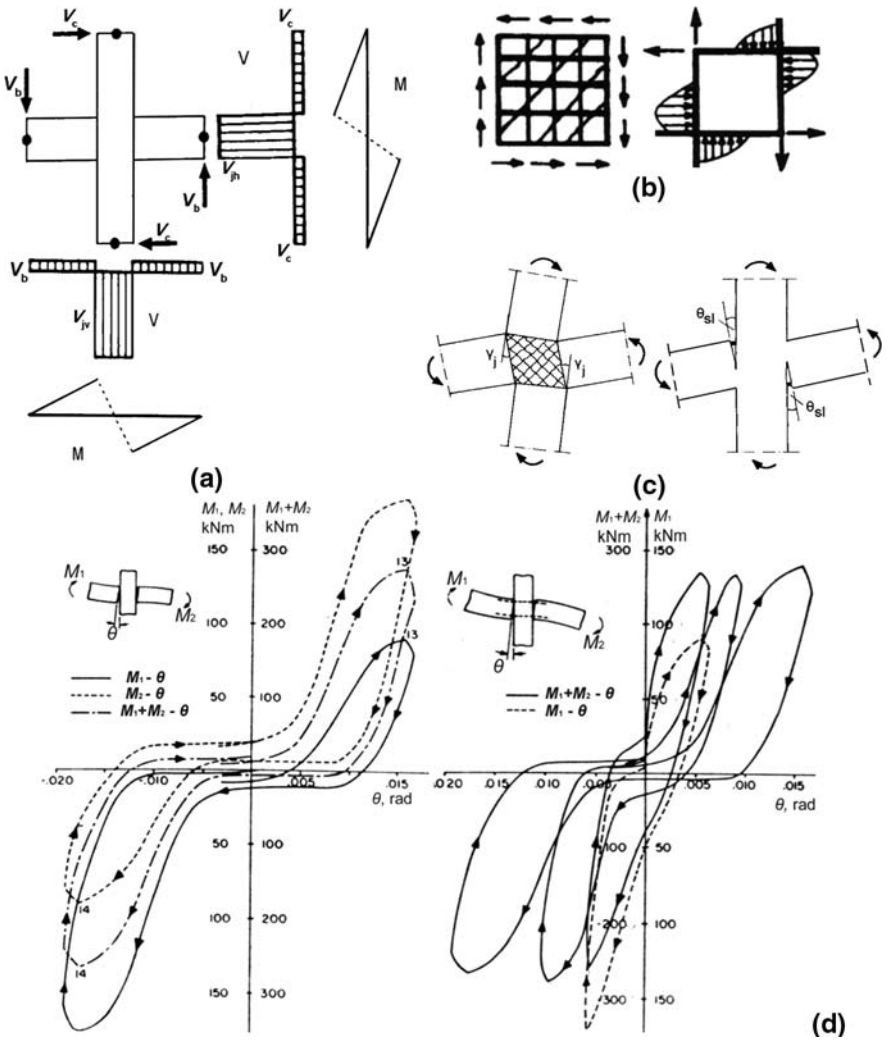

Fig. 3.45 Interior beam-column joint: (**a**) shear forces within the joint; (**b**) shear resistance mechanisms; (**c**) joint deformation; (**d**) experimental loops of moment on joint v fixed-end rotation due to bar slippage within/through joint (adapted from Viwathanatepa et al. 1979)

from the horizontal or the vertical shear force, V_{jh} or V_{jv}, it is more convenient to compute it from the horizontal shear, V_{jh}, which is based on the forces transferred via bond stresses along the top bars of the beam. Note that, even when Eq. (1.4) is not fulfilled, the beams framing into a joint normally yield before the column or the wall. If they don't, the horizontal joint shear is overestimated if computed from the top bars of the beam, and hence is on the safe side for the joint.

So, the joint may be considered as a series system of two (independent) mechanisms of force transfer:

- from the beam and column (or wall) longitudinal bars to the core of the joint, by bond;
- from each side of the joint core to the opposite, through shear (see Fig. 3.45(b)).

This implies that:

- if one of the two force transfer mechanisms fails, the joint fails as well; and
- the overall (shear) deformation of the joint is the sum of the individual deformations of the two mechanisms (see Fig. 3.45(c)).

Force transfer to the joint core by bond along the longitudinal bars passing through the joint or anchored in it causes slippage along these bars. Slippage shows up as fixed-end rotation, θ_{sl}, of the end of the member where the longitudinal bars belong (see Fig. 3.45(c) and (d)). Force transfer through the joint by shear causes an angular distortion (shear strain) of the joint core, γ_j (Fig. 3.45(c)). The total deformation of the joint is an apparent shear deformation, equal to the sum of γ_j and of the fixed-end rotations, θ_{sl}, at the ends of all (four, in an interior joint) members framing into the joint (unless such a fixed-end rotation is incorporated in the chord rotation of the member, see discussion in Section 3.3.2). As shown in Fig. 3.30, the total shear deformation of a frame panel made up of two beams and two columns is equal to the sum of:

- the average apparent shear deformation of the four joints at the corners of the panel; plus
- the average chord rotation at the (four) column ends on either side of the panel, θ_c; plus
- the average chord rotations at the (four) beam ends above and below the panel, θ_b.

It is interesting that, although it adds to $\theta_c + \theta_b$, the angular distortion (shear deformation) of the joint core, γ_j, takes place in the opposite sense with respect to the sum of $\theta_c + \theta_b$ (see Fig. 3.45(c)): the joint diagonal that shortens is the one parallel to the panel diagonal that gets longer during the deformation of the panel. This is consistent with the opposite sign of the joint shears, V_{jv}, and V_{jh}, with respect to those in the members themselves (see Fig. 3.45(a)).

3.3.2 The Bond Mechanism of Force Transfer in Joints

Beams normally yield before the columns. Moreover, compressive stresses in the vertical bars of columns are normally below yield (as cracks at column ends normally are not open through the column depth and the concrete participates fully in

resisting the force of the compressive zone). Therefore, bond stresses are normally higher along the longitudinal bars of beams passing through a joint, than along the column bars. So, the transfer of forces into the joint is normally controlled by the longitudinal bars of the beam.

As the (unusual) example in Fig. 3.21 shows, bond failure along longitudinal bars of beams or columns within the very length of the element manifests itself as a splitting crack along the bar, especially if it is a corner one. Bond failure along the length of the bar within the joint normally manifests itself through partial pull-out of the bar through the joint. The high static indeterminacy of the system of the joint and of the members framing in it limits the magnitude of any pull-out of member longitudinal bars from the joint. Such pull-out manifests itself as a large fixed-end rotation, θ_{sl}, of the end of that member to which the longitudinal bars belong. Witness the resemblance of the end moment-fixed end rotation loops in Fig. 3.45(d) (Viwathanatepa et al. 1979) to the bond-slip loops in Fig. 3.22. They are narrow, have inverted-S shape and degrade with cycling.

The fixed-end rotation, θ_{sl}, at a member end due to partial pull-out of the member's bars from the joint is normally added to the chord rotation of the member itself at that end (see Fig. 3.24 and Eq. (3.42) in Section 3.2.2.3 and 3rd term in Eqs. (3.66) in Section 3.2.3.2) increasing its apparent flexibility (through Eq. (3.68), Section 3.2.3.3). It also increases its apparent deformation capacity (see 2nd term in Eq. (3.72) in Section 3.2.3.4 and terms with a_{sl} in Eqs. (3.78) in Section 3.2.3.5). At the extreme, bond failure along the member's longitudinal bars within the joint may prevent the full yield moment from developing at the end section of the member (see Fig. 3.29 in Section 3.2.2.3 for two field cases).

The problem of bond is more acute at interior joints, where beam longitudinal bars continue into the adjacent span, rather than at exterior ones, where beam bars are anchored with a 90° bend at the far end of the joint. As a matter of fact, taking into account that bond stresses along the part of the beam bars outside the confined joint core are negligible because:

- yielding penetrates into the initial length of the bar into the joint while confinement there is poor, and
- horizontal cracking of the column may take place at the plane of the beam longitudinal bars,

and taking the width of the joint confined core along the depth h_c of the column as: $h_{co} \approx 0.8h_c$, the average bond stress along a beam bar is:

- $\sim d_{bL}f_y/4h_{co} \approx 0.3d_{bL}f_y/h_c$, if the bar reaches its yield stress in tension at one face of the joint and has zero compressive stress at the opposite face,
- $\sim d_{bL}f_y/2h_{co} \approx 0.6d_{bL}f_y/h_c$, if the bar reaches its yield stress in tension at one face of the joint and in compression at the opposite one. This may happen if the crack at the beam section at the face of the column stays open at the top under positive moments (see Fig. 3.7 in Section 3.1.1.1 and point 3 in Section 3.2.2.6). In that case the top bars of the beam bear the full force of the compression zone.

At exterior joints, the average bond stress along beam bars bent by 90° at the far end of the joint is lower: $\sim 0.2 d_{\mathrm{bL}} f_{\mathrm{y}} / h_{\mathrm{c}}$.

For common values of d_{bL} and h_{c} the level of bond stresses estimated above ranges from 5 to 15 MPa, often exceeding the ultimate bond stress under cyclic loading. Test results show, however, that cyclic bond stresses of that magnitude can develop in joints, without causing unduly large pull-through slippage of the beam bars (thanks primarily to lateral confinement at the level of the beam top bars by the transverse beams and the slab, but also to enhancement of bond by compression normal to the bar surface due to the column axial load).

Figure 3.46 demonstrates the effect of the column depth, h_{c}, on the hysteresis loops of shear force v overall deformation of a cross-shaped beam-column subassembly (Kaku and Asakusa 1991). If the column size is small, namely $h_{\mathrm{c}} = 18.8 d_{\mathrm{bL}}$, the overall force-displacement loops are controlled by bond slip within the joint and their shape resembles the loops in Fig. 3.22. However, the system's peak force resistance does not degrade with cycling. Only the reloading stiffness is greatly reduced, giving lower energy dissipation and certain growth of the overall lateral displacements with cycling. For larger column sizes bond slip in the joint does not govern and the overall force-displacement loops are controlled by the flexural behaviour of the beam.

If l (: left) and r (: right) index the two vertical faces of the joint, σ_{s} denotes the stress in the beam bars and h_{co} is the width of the confined core of the joint along the depth h_{c} of the column, the average bond stress along these beam bars is:

$$\tau_b = \frac{\pi d_{bL}^2}{4} \frac{|\sigma_{sl} - \sigma_{sr}|}{\pi d_{bL} h_{co}} = \frac{d_{bL}}{4} \frac{|\sigma_{sl} - \sigma_{sr}|}{h_{co}} \tag{3.131}$$

Bond stresses along the length of the bars outside the confined core are negligible. Plastic hinges are assumed to develop in the beam at both sides of the joint. Let's consider the top flange to be in tension on the left of the joint and in compression on the right (as in Fig. 3.45(a), (b) and (c)). The top flange is normally much stronger than the bottom one, both in tension and in compression and, therefore, its yield force cannot be balanced by the bottom flange unless the bottom bars yield. So, the stresses of the bottom bars are: $\sigma_{\mathrm{s,l}} = -f_{\mathrm{y}}$, $\sigma_{\mathrm{s,r}} = f_{\mathrm{y}}$ and the average bond stress along them at beam plastic hinging is: $\tau_{\mathrm{b}} = 0.5 d_{\mathrm{bL}} f_{\mathrm{y}} / h_{\mathrm{co}}$. Regarding now the top bars, they yield at the plastic hinge of the left beam: $\sigma_{\mathrm{s,l}} = f_{\mathrm{y}}$. At the opposite face of the joint these bars have a compressive stress, $\sigma_{\mathrm{s,r}}$, such that, acting together with the force of the concrete at the top flange, $F_{\mathrm{c,r}}$ (taken negative for compression), they balance the tension force of the bottom bars. These latter bars are forced by the stronger top flange to yield. So, if $A_{\mathrm{s,r1}}$ and $A_{\mathrm{s,r2}}$ denote the cross-sectional area of the top and bottom beam bars on the right of the joint, the compressive stress of the top bars there is:

$$\sigma_{s,r} = -\frac{A_{s,r2}}{A_{s,r1}} f_y - \frac{F_{c,r}}{A_{s,r1}} = -\frac{\rho_2}{\rho_1} f_y \left(1 - \frac{\xi_{eff}}{\omega}\right) \tag{3.132}$$

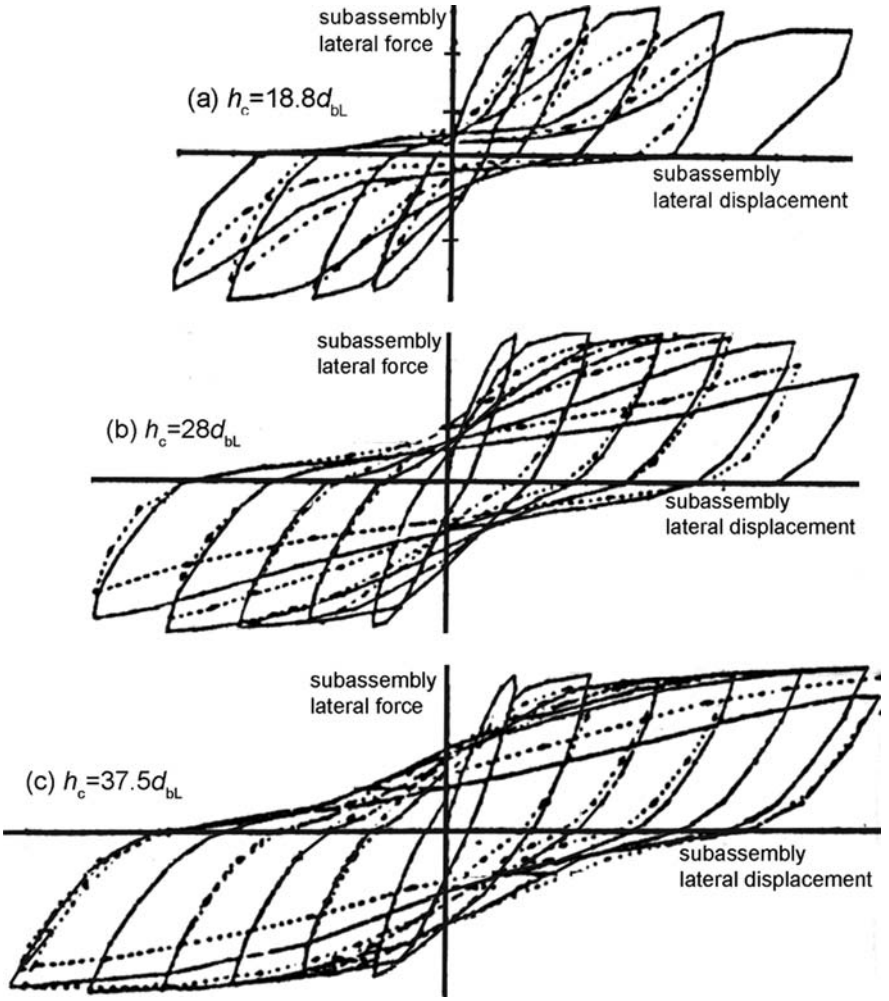

Fig. 3.46 Effect of bond-slip in the joint, as controlled by column size, on overall force-displacement loops of a beam-column subassembly (adapted from Kaku and Asakusa 1991)

where ρ_1 and ρ_2 are the ratios of top and bottom reinforcement at the right of the joint, normalised to the product bd of the beam, ω is: $\omega = \rho_1 f_y / f_c$ and ξ_{eff} is the depth of a fictitious compression zone (normalised to d), such that $F_{c,r} = -bd\xi_{\text{eff}} f_c$. Therefore the average bond stress along the top bars at beam plastic hinging is:

$$\tau_b = \frac{d_{bL}}{4} \frac{f_y}{h_{co}} \left(1 + \frac{\rho_2}{\rho_1} \left(1 - \frac{\xi_{eff}}{\omega}\right)\right) \tag{3.133}$$

and is less than the average bond stress along bottom bars with the same diameter, d_{bL}. However, the bond problem is more acute along the top bars, because bond stresses are not uniform around a bar but are concentrated more on the side facing the joint core. This is the underside of the top bars, where bond conditions are considered "poor" owing to laitance and consolidation of concrete during compaction. All around the bottom bars bond conditions are considered as "good" (see Section 3.1.3.2).

The bond stress demand given by Eq. (3.133) is capped at the ultimate bond stress along these bars. Bond outside the confined joint core is normally neglected, but its enhancement inside the joint core due to confinement by the joint stirrups, the top bars of the transverse beam and all the surrounding concrete is taken into account. It has been pointed out in Section 3.1.3.2 that the maximum steel stress at pull-out (or -through) bond failure may be obtained from Eq. (3.31) with the 1st and 2nd terms inside the bracketed last term replaced by the upper limit value of 2.0. Bond strength is further enhanced by the 3rd term inside the brackets, $0.2p$ (in MPa), owing to the mean normal stress across the horizontal plane of the bar due to the axial load of the column: $p = N/A_c = \nu f_c$ (f_c in MPa). In Section 5.4.1 these considerations are used with Eq. (3.133) to justify the lower limit on the h_c/d_{bL} ratio imposed by Eurocode 8 on beam bars passing through, or anchored at joints.

Notwithstanding the shortfall within the joint of the full anchorage of the yield stress of (top) beam bars in tension at one face of the joint and in compression at the opposite one, there is a real problem only for low h_c/d_{bL} values. The solution is a large column size and/or a small bar diameter. Needless to say, bars of small diameter are more susceptible to buckling and may require very dense stirrups at the end of the beam for its prevention. Fortunately, compressive stresses are lower in beam top bars than in the bottom ones (cf. histories of bar strains in Figs. 3.6 and 3.7) and the slab next to the beam prevents top bar buckling in a horizontal plane.

3.3.3 Force Transfer Within Joints Through the Shear Mechanism

3.3.3.1 Shear Force Demand in Joints

As already pointed out in Section 3.3.1, if there is no pull-out (or -through) of the beam or column bars around the joint core, shear stresses develop within the joint core with a nominal value equal to the ratio of $\Sigma M_c = \Sigma M_b$ to the volume of the joint, $h_c h_b b_j$. Shear failure of the joint, as in the examples of Fig. 3.47, is far more brittle than any failure of plastic hinges around the joint, even in the columns. So, it should be prevented through design and detailing of the joint. To this end, the maximum possible shear force that can develop in the joint is established from capacity design calculations, on the basis of the capacity of the beams or the columns framing into the joint (whichever is weaker) to deliver shear through bond along the outermost beam or column bars passing through the joint.

If the sum of moment resistances of the beams framing into a joint, $\sum M_{Rb}$, is less than that of the columns, $\sum M_{Rc}$, ($\sum M_{Rb} < \sum M_{Rc}$), the shear input in the joint

(a) (b) (c)

Fig. 3.47 Shear failure of exterior joints. (**a**) reinforced joint; (**b**), (**c**): unreinforced joints (See also Colour Plate 10 on page 724)

is governed by the beams. If pull-out (or -through) of the beam top bars does not take place, the maximum possible value of the horizontal shear force in an interior joint, V_{jh}, can be computed as:

- the maximum possible tensile force in the top bars at one face of the joint, $A_{\mathrm{sb1}} f_{\mathrm{y}}$,
- plus the maximum possible compressive force in the top flange at the opposite face,
- minus the shear force V_{c} in the column above the joint.

No matter how it is shared by the concrete and the top reinforcement, the maximum possible compression force in the top flange will be governed by the bottom reinforcement. It will be equal to its maximum possible tensile force, $A_{\mathrm{sb2}} f_{\mathrm{y}}$. So, the horizontal shear force in the joint is (Fardis et al. 2003):

If $\sum M_{\mathrm{Rb}} < \sum M_{\mathrm{Rc}}$:

$$\begin{aligned} V_{jh} &= (A_{sb1} + A_{sb2})\, f_y - V_c = (A_{sb1} + A_{sb2})\, f_y - \frac{\sum M_{Rb}}{H} \frac{L}{L_{cl}} \\ &= \sum M_{Rb} \left(\frac{1}{z_b} - \frac{1}{H} \frac{L}{L_{cl}} \right) \approx (A_{sb1} + A_{sb2})\, f_y \left(1 - \frac{z_b}{H} \frac{L}{L_{cl}} \right) \end{aligned} \tag{3.134}$$

where:

- A_{sb1}, A_{sb2}: cross-sectional area of the beam top reinforcement at one face of the joint and of its bottom reinforcement at the opposite face, respectively;
- V_{c}: column shear at beam plastic hinging;
- H: storey height;
- L, L_{cl}: theoretical and clear beam span, respectively; and
- z_{b} ($\approx h_{\mathrm{jb}}$) = d–d_1: beam internal lever arm.

The larger of the two sums $A_{sb1}+A_{sb2}$ diagonally across the joint should be used in Eq. (3.134). Normally, no such distinction needs to be made at interior joints, as the steel area is the same at both sides. At exterior joints one term in $A_{sb1}+A_{sb2}$ is zero.

The shear force is translated into a nominal shear stress, considered uniform within the joint core:

$$v_j = \frac{V_{jh}}{b_j h_{jc}} \tag{3.135}$$

where:

- h_{jc}: horizontal distance between the outermost layers of column reinforcement in the direction of the horizontal joint shear force, and
- b_j: joint width in the orthogonal horizontal direction, conventionally taken from Eqs. (3.130).

If $\sum M_{Rb} > \sum M_{Rc}$, it is the columns that govern the shear input in the joint. Let's $A_{sc,top}$ and $A_{sc,bot}$ denote the cross-sectional area of vertical bars on one side of the column above or below the joint, respectively.[22] Then the vertical shear force in the joint core is (Fardis et al. 2003):

$$V_{jv} = f_y(A_{sc,top} + A_{sc,bot}) + N_{top} - V_{b,\min}, \tag{3.136}$$

where:

- N_{top}: axial force in the column above; and
- $V_{b,min}$: algebraically minimum (and possibly negative) beam shear force on either side of the joint:

$$V_{b,\min} \approx \frac{\sum M_{Rc}}{L}\frac{H}{H_{cl}} - \max\left(\left[V_{g+\psi q,b}\right]_l ; \left[V_{g+\psi q,b}\right]_r\right) \tag{3.137}$$

where:

- H and H_{cl} are the theoretical and the clear storey height and
- $V_{g+\psi q,b}$ is the shear force at the beam end on the left (index: l) or on the right (index: r) face of the joint, due to the gravity loads acting on the beam concurrently with the seismic action.

$$\sum M_{Rc} \approx f_y(A_{sc,top} + A_{sc,bot})z_c + 0.5h_c\left(N_{top}\left(1-\nu_{top}\right) + N_{bot}\left(1-\nu_{bot}\right)\right) \tag{3.138}$$

[22] Normally column vertical bars are the same above and below the joint: $A_{sc,top} = A_{sc,bot}$, except at the joints of the top floor where $A_{sc,top} = 0$.

with z_c ($\approx h_{jc}$) $\approx 0.9d \approx 0.8h_c$ denoting the internal lever arm of the column and $\nu = N/A_c f_c$.

So, Eq. (3.136) finally gives: If $\sum M_{Rb} > \sum M_{Rc}$:

$$V_{jv} \approx \sum M_{Rc} \left(\frac{1}{z_c} - \frac{1}{L} \frac{H}{H_{cl}} \right) + \frac{1}{2} \left| \left[V_{g+\psi q,b} \right]_l - \left[V_{g+\psi q,b} \right]_r \right| \tag{3.139}$$

The shear stress in the joint core is computed as:

$$v_j = \frac{V_{jv}}{b_j h_{bj}} \tag{3.140}$$

where h_{bj} is the clear depth of the beam between its top and bottom reinforcement.

3.3.3.2 Joint Shear Strength

Diagonal tension cracking of the joint core takes place when the principal tensile stress under the combination of the shear stress, v_j, and of the mean vertical compressive stress in the joint, $v_{top} f_c$, exceeds the tensile strength of concrete, f_{ct}, i.e. when:

$$v_j \geq v_{cr} = f_{ct} \sqrt{1 + \frac{v_{top} f_c}{f_{ct}}} \tag{3.141}$$

According to Priestley (1997) confinement by beam bars bent vertically towards the core of exterior joints increases the shear stress at joint diagonal cracking by 50% over the value in Eq. (3.141).

Diagonal cracking of the joint core seldom has grave consequences, especially if the joint is reinforced with horizontal hoops and/or beams of significant cross-section frame into all four sides of the joint. After cracking, the joint core is called to resist the shear without reaching its ultimate stress in cyclic loading, v_{ju}.

The seismic behaviour of joints has been studied experimentally and analytically since the 1960s. Nevertheless, there is still no universally accepted rational model for the mechanism through which a joint resists cyclic shears. Variations of a rational physical model in Park and Paulay (1975) are still used in certain seismic design codes. According to it a joint resists shear via a combination of two mechanisms (Fig. 3.45(b)):

1. A diagonal concrete strut between the compressive zones of the beams and columns at opposite corners of the joint, contributing to the resistance against the horizontal shear force in the joint, V_{jh}, with the horizontal component of its diagonal force.
2. A truss extending over the entire core of the joint, comprising:

- (any) horizontal hoops in the joint;
- (any) intermediate vertical bars between the column corner bars in planes parallel to that of bending (including column bars contributing to the column moment resistance above and below the joint as distributed "web" reinforcement, ω_v);
- a diagonal compression field in the concrete.

The force in the strut under (1) above is assumed to develop from:

- the concrete forces in the compression zones of the beam and the column at the two ends of the strut, and
- the bond stresses transferred to the joint over the length of the beam bars within the width of the strut itself.

The truss under (2) above takes the rest of the joint shear force, V_{jh}, not resisted by the horizontal component of the strut diagonal force. So, for safe-sided dimensioning of the horizontal joint reinforcement, the horizontal component of the strut force should not be overestimated.

Unless there is bond failure along the beam bars, pushing their compressed end into the joint, the neutral axis depth of the beam is significantly reduced by cycling of the beam moment, as the crack may not fully close (especially at the top flange) owing to accumulation of plastic strains in the reinforcement. Then the compression zone of the beam does not deliver a horizontal force to the diagonal concrete strut, but only a compressive force to the beam reinforcement. The sum of this force and of the tension force at the opposite face of the joint is transferred to the truss and the strut in proportion to their share in the joint width at the level of the beam top reinforcement. So, the width of the diagonal strut is defined by the neutral axis depth of the column at the faces of the joint. According to this reasoning, the force input into the strut directly from the compression zones of the members is reduced during cycling of the moments. By contrast, the force input into the strut by bond increases, as the degradation of bond with cycling pushes the force transfer by bond mainly to that length of the bar within the joint core where bond is enhanced by transverse compression, i.e. the bar length within the strut width. Therefore, despite the deterioration of bond along most of the bar length within the joint core, the strut mechanism remains intact.

Paulay and Priestley (1992) make the assumption that at the face of the joint where the beam is under sagging moment (tension at the bottom) the crack cannot close at the top flange, owing to accumulation of plastic strains in the top reinforcement. This means: $\xi_{eff} = 0$ in Eq. (3.133). Then the horizontal width of the strut at that level is equal to the neutral axis depth of the column above the joint, x_c. So, the beam compression chord does not contribute to the force of the diagonal concrete strut and the horizontal component of the strut diagonal force is equal to:

- the force transferred by bond along the bar length within the strut width, minus
- the column shear force, V_c (appearing also in Eq. (3.134) for V_{jh} and considered to be applied directly to the strut through the compression zone of the column above and affect only its horizontal shear force and not that of the truss).

Moreover, Paulay and Priestley (1992) assume – for simplicity – that the transfer of the total force $(A_{sb1}+A_{sb2})f_y$ by bond takes place uniformly along the total length of the top bars within the joint, h_c. So, the fraction of this force going to the horizontal force of the strut is equal to x_c/h_c. The rest, equal to $(1–x_c/h_c)$, goes to the truss. Therefore, as the truss extends over the full vertical face of the joint, the total area of the horizontal legs of hoops within the joint, A_{sh}, should be dimensioned for a force equal to $(1–x_c/h_c)(A_{sb1}+A_{sb2})f_y$. The value of $\xi_c = x_c/h_c$ may be obtained from Eq. (3.52) in Section 3.2.2.4 under *Curvature at Spalling of the Concrete Cover*, using there: $\omega_1 = \omega_2$, $\omega_v = 0$ (for convenience), $\varepsilon_{co} = 0.002$ and $\varepsilon_{cu} = 0.004$ (for spalling of the extreme concrete fibres at the end section of the column). Then $\xi_c \approx (6/5)\nu$, with both ν and ξ_c normalised to h_c. So the following total area of horizontal hoops should be provided according to this version of the Park and Paulay model.

– At interior joints:

$$A_{sh} f_{yw} \geq (A_{sb1} + A_{sb2})\, f_y \left(1 - \frac{6}{5}\nu\right) \tag{3.142a}$$

where the normalised axial force, ν, is the minimum value in the column above the joint for any combination of the design seismic action with the concurrent gravity loads.

The reinforcement required in exterior joints cannot be obtained by setting $A_{sb2} = 0$ in Eq. (3.142a), because the beam top reinforcement is bent down at the far face of the joint. Then, when the bar is in tension, the bend delivers to the diagonal strut starting there the full diagonal compression force of the strut. The horizontal component of that force is about equal to $f_y A_{sb1} – V_c$. So, very little force is transferred by bond along the part of the top bars outside the strut, to be resisted as horizontal shear by the part of the truss falling between the strut and the face of the joint towards the beam. The horizontal shear force of the truss is governed by the force transferred by bond along the part of the bottom bars outside the strut.[23] The compression zone at the bottom flange of the beam delivers to the lower end of the strut a horizontal force equal to the compression force in the concrete, i.e. to the tension force in the top reinforcement, $A_{sb1}f_y$, minus the force, $A_{sb2}f_y$, in the bottom reinforcement that yields in compression. The difference between:

– the horizontal component of the strut force at its top end, $A_{sb1}f_y – V_c$, and
– the horizontal forces delivered
  - to the lower end of the strut by the beam and the column below: $(A_{sb1}–A_{sb2})f_y – V_c$, and
  - by bond within the strut width at the level of the bottom reinforcement: $(1–x_c/h_c)A_{sb2}f_y$,

[23]The upward bend of the bottom bars at the far face of the joint does not deliver forces to the joint core when these bars are in compression.

is the force transferred by bond along the length of the bottom bars outside the strut width. This force is a horizontal shear force to be resisted by the part of the truss falling between the strut and the exterior face of the joint. This gives:

– At exterior joints:

$$A_{sh} f_{yw} \geq A_{sb2} f_y \left(1 - \frac{6}{5}\nu\right) \tag{3.142b}$$

where now ν is the minimum value of the normalised axial force in the column below the joint, for any combination of the design seismic action with the concurrent gravity loads.

Test results on interior joints have been collected and compiled in Kitayama et al. (1991) as in Fig. 3.48. Figure 3.48 suggests that the joint ultimate shear strength, expressed in terms of the shear stress, v_j, of Eqs. (3.135) and (3.140), increases about linearly with the ratio of horizontal reinforcement within the joint, ρ_{jh}, from a minimum value $v_{ju} \approx 0.15 f_c$ at $\rho_{jh} = 0$ (unreinforced joint) to an upper limit value in the range of $0.24 f_c$–$0.4 f_c$ (with mean value: $v_{ju} \approx 0.32 f_c$) at $\rho_{jh} = 0.4\%$. Above that value of the steel ratio and up to $\rho_{jh} = 2.4\%$, the joint ultimate strength seems to be attained always by diagonal compression in the concrete and to be practically independent of the value of ρ_{jh} and of the axial load ratio in the column, $\nu = N/f_c A_c$ (Kitayama et al. 1991).

The experimental results in Fig. 3.48, along with careful and detailed measurements of the evolution of strains in the horizontal hoops within the joint during the history of cyclic displacements (Kitayama et al. 1991), lead to the following conclusions:

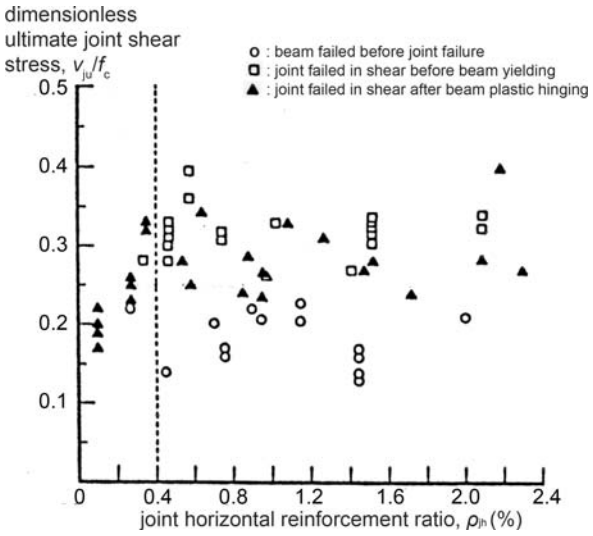

Fig. 3.48 Effect of horizontal reinforcement ratio in interior joint, ρ_{jh}, on joint strength (adapted from Kitayama et al. 1991)

- Cycling of applied loads and displacements causes a gradual degradation of bond along the length of a bar within the joint closer to its end which is in tension, and a concentration of most of the bond transfer near the opposite end of the bar within the joint, where the bar is in compression (the part falling within the strut width).
- The breakdown of bond along the length of the beam bar falling outside the strut width may cause drastic reduction of the contribution of the truss mechanism to the shear resistance of the joint. When this happens the horizontal component of the strut diagonal force resists almost the full horizontal joint shear, V_{jh}. This force is delivered to the strut partly by bond along the length of the beam bars falling within the strut and partly by the compression zone of the beam.
- The joint shear that the strut can resist is governed by the compressive strength of the concrete in its diagonal direction. Any horizontal hoops in the joint affect the contribution of the strut to shear resistance only to the extent they enhance this diagonal compressive strength through confinement. So, attainment of the joint ultimate strength activates not only the hoop legs parallel to the applied shear (i.e. in the plane of bending), considered in the truss mechanism to resist part of the joint shear, but also (and to the same extent) the orthogonal hoop legs (at right angles to the plane of bending). The top and bottom reinforcement of any beams framing into the joint at right angles to the plane of bending play a role similar to these orthogonal hoop legs, confining the core of the joint.
- Yielding of the horizontal reinforcement in the joint caps the confinement of the concrete core and increases tensile strains in the direction(s) normal to the diagonal strut, reducing further the diagonal compressive strength.
- The column axial force level, measured through $\nu = N/A_c f_c$, does not seem to be important, neither for the bond-slip performance of the beam bars, nor for the joint ultimate shear stress, v_{ju}.

Test results in Fig. 3.49 (Kitayama et al. 1991) suggest that confinement on both sides of the joint by a slab at the level of the beam top and/or by a transverse beam significantly increases the joint ultimate shear strength, v_{ju} (to values close to $0.4f_c$). This may explain the scarcity of shear failures at interior joints – even unreinforced ones – in the field in strong earthquakes.

In view of the test results of Figs. 3.48 and 3.49 and the conclusions above that cast doubts about the validity of the truss-and-strut physical model, alternative simple plane stress models have emerged for the shear strength of beam-column joints. For example, the model adopted in Eurocode 8 (CEN 2004a) as alternative to the truss-and-strut model and to Eqs. (3.142) for the calculation of joint horizontal reinforcement assumes a homogeneous stress field in the body of the joint, comprising:

1. the shear stress, v_j, from Eqs. (3.135) or (3.140),
2. the vertical normal stress from the column, $N/A_c = \nu f_c$ (positive for compression), and
3. a smeared horizontal normal stress, such that the concrete core and the joint horizontal reinforcement balance together the zero external horizontal force applied

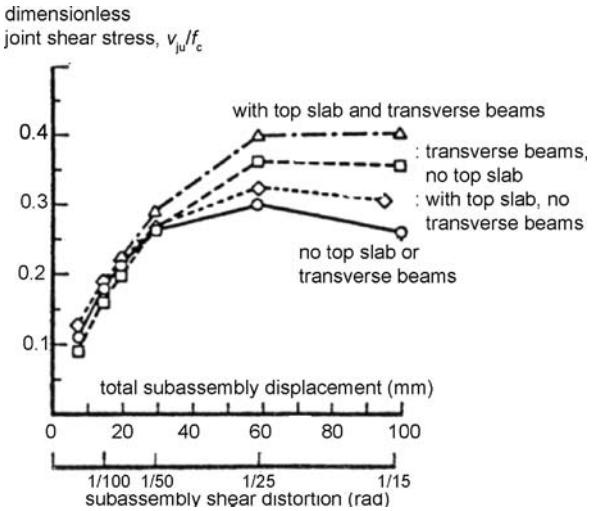

Fig. 3.49 Effect of top slab and/or transverse beam on both sides on the ultimate shear strength of interior joints (adapted from Kitayama et al. 1991)

on the joint by the beams; this normal stress has a limit value of $-\rho_{jh} f_{yw}$ (compression), when the joint horizontal reinforcement is driven to yielding by the dilatancy of the concrete core at imminent failure.

Joint strength criteria in Eurocode 8 are based on the principal stresses, in tension, σ_I, and compression, σ_{II}, under the above system of stresses, 1–3. The joint shear stress at diagonal cracking ($\sigma_I = f_{ct}$) in the presence of horizontal reinforcement is (CEN 2004a):

$$\frac{v_j}{f_c} = \sqrt{\left(\frac{f_{ct}}{f_c} + \nu_{top}\right)\left(\frac{f_{ct}}{f_c} + \frac{\rho_{jh} f_{yw}}{f_c}\right)} \tag{3.143}$$

where ν_{top} is computed from the minimum value of the axial force of the column above the joint under any combination of the design seismic action with the concurrent gravity loads, including the effect of overturning moment on exterior joints. Note that, for $\rho_{jh} = 0$ and ν_{top} between 0 and 0.3, Eq. (3.143) gives values of v_j from $0.1 f_c$ to $0.2 f_c$, in good agreement with the average value of $v_j \approx 0.15 f_c$ suggested for $\rho_{jh} = 0$ by the test results in Fig. 3.48 (Kitayama et al. 1991).

The real threat to the joint is crushing of its core by the diagonal compression. According to the simple plane stress model above, this may take place if σ_{II} reaches the concrete compressive strength, as this is reduced due to the tensile stresses and/or strains in the transverse direction (i.e. that of σ_I). The reduction factor on f_c may be taken the same as factor n from Eq. (3.96a) for diagonal compression in concrete members due to shear. Eurocode 8 (CEN 2004a) neglects for simplicity the – adverse – effect of the horizontal normal stress, $-\rho_{jh} f_{yw}$, on the magnitude of σ_{II}, as well as its (more important) favourable effect on the compressive strength in the

diagonal direction through confinement. So the condition: $\sigma_{II} = -nf_c$ gives (CEN 2004a):

$$\frac{v_{ju}}{f_c} = n\sqrt{1 - \frac{v_{bottom}}{n}} \tag{3.144}$$

where ν is computed from the maximum axial force of the column below the joint under any combination of the design seismic action with the concurren gravity loads.

For common values of ν ($\sim$0.25) Eq. (3.144) gives an ultimate shear stress, v_{ju}, close to $0.4f_c$, at the upper strength limit of interior joints in Figs. 3.48 and 3.49. It does not seem to provide a safety margin against diagonal compression failure, unless the design value $f_{cd} = f_{ck}/\gamma_c$ is used for f_c, with a partial factor for concrete, γ_c, (significantly) higher than 1.0.

An alternative plane stress approach is to apply the variable strut inclination truss model of Section 3.2.4.2 under *The Variable Strut Inclination Truss of the CEB/FIP Model Code 90 and Eurocode 2* to the joint that is already cracked diagonally, owing to a shear stress above the limit of Eq. (3.143). In this analogy the counterpart of the transverse direction of the concrete element of Section 3.2.4.2 under *The Variable Strut Inclination Truss of the CEB/FIP Model Code 90 and Eurocode 2* is the horizontal direction of the joint. Its transverse reinforcement ratio, ρ_w, corresponds to the joint horizontal reinforcement ratio, ρ_{jh}. The counterpart of the vertical direction of the joint is the longitudinal one of the concrete element, but with $M = 0$, $\omega_1 = 0$ and N equal to the axial force of the column (positive for compression). The inclination δ is the angle of the centreline of the diagonal strut in the joint to the vertical direction.

According to the variable strut inclination truss analogy, the shear stress in the joint at yielding of the horizontal reinforcement before failure of the concrete in the diagonal direction may be obtained from Eq. (3.101), adapted as follows to the conditions of the joint:

$$\frac{v_j}{f_c} = \sqrt{v_{top}\frac{\rho_{jh} f_{yw}}{f_c}} \tag{3.145}$$

which coincides with Eq. (3.143) for $f_{ct} = 0$.

Adapted to the conditions of the joint, Eq. (3.99) gives the shear strength of the joint for diagonal concrete failure after yielding of the joint horizontal reinforcement:

$$\frac{v_{ju}}{f_c} = \sqrt{\frac{\rho_{jh} f_{yw}}{f_c}\left(n - \frac{\rho_{jh} f_{yw}}{f_c}\right)} \tag{3.146}$$

The counterpart of Eq. (3.97) for the joint shear at diagonal compression failure is:

$$\frac{v_{ju}}{f_c} = 0.5n \sin 2\delta \tag{3.147}$$

If the amount of horizontal reinforcement is large, namely if $\rho_{\mathrm{jh}} f_{\mathrm{yw}} > 0.5nf_{\mathrm{c}}$, diagonal compression failure will take place before yielding of the joint reinforcement, at the upper limit value of both Eqs. (3.146) and (3.147): $v_{\mathrm{ju}} = 0.5nf_{\mathrm{c}}$. With this value of v_{ju} for $\rho_{\mathrm{jh}} f_{\mathrm{yw}} > 0.5nf_{\mathrm{c}}$, Eq. (3.146) gives a variation of the joint ultimate shear with the strength of the horizontal reinforcement similar to the parabola-cum-horizontal line given for Eq. (3.99) in Fig. 3.40. The mean upper limit: $v_{\mathrm{ju}} \approx 0.32 f_{\mathrm{c}}$ in Fig. 3.48 agrees well with the theoretical upper limit of: $v_{\mathrm{ju}} = 0.5nf_{\mathrm{c}}$. However, although the data in Fig. 3.48 might suggest a parabolic variation up to $\rho_{\mathrm{jh}} = 0.4\%$, the value $\rho_{\mathrm{jh}} = 0.4\%$ is much lower than the theoretical one of $0.5nf_{\mathrm{c}}/f_{\mathrm{yw}}$ giving the peak value of v_{ju} according to Eq. (3.146).

Equation (3.103), adapted to the conditions of the joint gives an ultimate shear stress of:

$$\frac{v_{ju}}{f_c} = \sqrt{v_{top}\left(1 - \frac{v_{top}}{n}\right)} \tag{3.148}$$

which is not supported at all by the experimental data.

The shear strain in the joint core, γ_{ju}, at the ultimate shear stress, v_{ju}, is in the order of 0.005 rad (0.5%), i.e., very small compared to the total shear distortion of a system of ductile beams and columns at failure of the joint.